Natural Resources Canada   Ressources naturelles Canada

GEOLOGICAL SURVEY OF CANADA
OPEN FILE 8637

Piston cores and supporting high-resolution seismic data, CCGS Hudson Expedition 2015018, Scotian Slope, offshore Nova Scotia, Canada

K.A. Jenner, D.C. Campbell, J.M. Barnett, J. Higgins, and A. Normandeau

2022

Canada

ISSN 2816-7155
ISBN 978-0-660-44154-2
Catalogue No. M183-2/8637E-PDF

GEOLOGICAL SURVEY OF CANADA
OPEN FILE 8637

Piston cores and supporting high-resolution seismic data, CCGS Hudson Expedition 2015018, Scotian Slope, offshore Nova Scotia, Canada

K.A. Jenner[1], D.C. Campbell[1], J.M. Barnett[2], J. Higgins[1], and A. Normandeau[1]

[1]Geological Survey of Canada, 1 Challenger Drive, P.O. Box 1006, Dartmouth, Nova Scotia
[2]Environmental Science Program, Dalhousie University, 6299 South Street, Halifax, Nova Scotia

2022

Permanent link: https://doi.org/10.4095/330088

This publication is available for free download through GEOSCAN (https://geoscan.nrcan.gc.ca/).

Recommended citation

Jenner, K.A., Campbell, D.C., Barnett, J.M., Higgins, J., and Normandeau, A., 2022. Piston cores and supporting high-resolution seismic data, CCGS Hudson Expedition 2015018, Scotian Slope, offshore Nova Scotia, Canada; Geological Survey of Canada, Open File 8637, 167 p. https://doi.org/10.4095/330088

Publications in this series have not been edited; they are released as submitted by the author.

Contents

Preface

This Open File report summarizes a set of 26 piston cores, collected during CCGS Hudson Expedition 2015018, from the continental slope of Nova Scotia, Canada, in water depths between 1520 m and 2648 m. It provides down-core lithostratigraphy, physical properties measurements, core photography and core X-radiography, in addition to high-resolution sub-bottom profiler data over the core sites, grain size data and limited portable X-ray fluorescence (pXRF) data. Preliminary along-slope correlation between cores and radiocarbon dates are also included. Further information on these cores is available through the Expedition Database at https://ed.gdr.nrcan.gc.ca/index_e.php

Acknowledgments

We thank Kate Jarrett, Kevin MacKillop, Lori Campbell, Owen Brown, Emily MacLean, Linda Fan and Simon Poirier for assistance with core splitting at sea. Makeala MacIntyre and Ryan Carver-Rose completed the core processing and core data compilation at the GSC(A) Core Processing Laboratory. Grain size analyses were led by Owen Brown with assistance from Alexis Imperial and Logan Robertson. We also thank Kate Jarrett for assistance with core subsampling. The Open File was internally reviewed by Robbie Bennet.

List of Tables

All tables appear at the end of this report.

List of Figures

All figures appear at the end of this report.

1.0 Introduction

The twenty-six piston cores presented in this study were collected during CCGS Hudson cruise 2015018, to the Scotian Slope, between the eastern edge of Northeast Channel and the eastern edge of Logan Canyon, extending from the shelf break to the continental rise, in water depths ranging from 1520 m to 2648 m (Figure 1.1; Table 1.1). The piston cores were collected as part of a joint mission between the Geological Survey of Canada (GSC) and the Nova Scotia Department of Energy (NSDE) to investigate and sample seabed hydrocarbon seep features along the continental slope of Nova Scotia (Campbell and MacDonald, 2016). Since the majority of cores were taken in undisturbed stratigraphy they provided an opportunity to expand our knowledge of the late Quaternary stratigraphy of the Scotian Slope. This study, therefore, builds upon previous late Quaternary lithostratigraphy research across the margin (Hill, 1984; Piper and Skene, 1998; Piper, 2001; Hundert and Piper, 2008; Jenner et al., 2010) and within specific geographic and morphologic regions of the margin (Mosher et al., 1989; Mosher et al., 1994; Gauley, 2001; Hundert, 2003). It includes several radiocarbon-dated legacy cores to provide an updated lithostratigraphic correlation within the existing stratigraphic framework. Multibeam bathymetry, 3.5 and 12 kHz sub-bottom profiler data and Huntec Deep Tow seismic reflection data provide context for the core locations (Campbell and MacDonald, 2016).

2.0 Methods

2.1 Shipboard Operations

Piston core and sub-bottom profile records presented in this report were collected in June and July 2015 during CCGS Hudson Expedition 2015018 (Campbell and MacDonald, 2016). Core samples were acquired using the AGC Long Corer. Multibeam data were collected using the Reson Seabat 7160 pole-mounted system. A Knudsen 3260 echo sounder collected sub-bottom profiler data and Deep Tow System (DTS) data were collected using NRCan's AGC #3 DTS.

Core samples were processed on board as described below by Campbell and MacDonald (2016). Core sections were split longitudinally from the surface and down the core as soon as possible after being collected. The plastic liner was cut longitudinally using the Geological Survey of Canada (Atlantic) (GSC(A)) Duits splitter and the sediment itself was split longitudinally by pulling a piece of fine wire through the sediment along cuts in the plastic core liner. The two core halves were designated as 'archive' and 'working'. Each half was labelled with an up arrow, cruise number, sample number and section information. Metre tape was placed along the length of the split core section to indicate down-core depth.

The two halves were separated to undergo different analyses. The archive half was photographed, measured for spectral reflectance and described visually. The working half was measured for physical properties (velocity, shear strength, bulk density and water content) before the core began to dry. Both core halves were covered with plastic wrap, sealed in labelled plastic core sleeving, placed in labelled plastic D-tubes and stored at 4°C in a refrigerated container until their return to the GSC(A).

2.1.1 Core Photography

The archive half of the core was photographed using a Nikon D300 12.3 megapixel digital camera. Overlapping digital photographs were taken at two scales. The first image covered a 30 cm interval with a 5 cm overlap and the second image covered a 90 cm interval with a 25 cm overlap. The images were saved in raw, tiff and jpeg formats.

2.1.2 Reflectance Spectrophotometry

High accuracy measurements of spectral reflectance from the split core surface were made over wavelengths of 400 nm to 700 nm using the Konica Minolta Spectrophotometer CM-2600d. Tristimulus values X, Y and Z were derived from colour reflectance spectra according to the Commission Internationale de l'Eclairage (CIE) method. The L*a*b* system (CIELAB) represents coordinates in 3 dimensional space where L* is the vertical axis representing lightness and a* b* are horizontal radii representing chromaticity. The L* value ranges from zero (black) to 100 (white). The a* value represents green (-) to red (+) and the b* value represents blue (-) to yellow (+). Munsell® colour is calculated but there is no international standard for converting Tristimulus values to Munsell® Hue, Value, Chroma (HVC) notation.

A zero calibration was performed to compensate for the effects of any change in the optical system and changes in ambient and internal temperature. A white calibration was completed using a white ceramic calibration cap to set the maximum reflectance to 100%. Zero calibrations were performed daily and white calibrations were performed at least once daily. Prior to spectral reflectance measurements the core was carefully covered with Glad® Cling Wrap taking care to minimize the presence of air bubbles between the sediment and the plastic wrap. Measurements on the CM-2600d were taken by hand every 5 cm and interfaced with a computer using SpectraMagicTM NX software.

2.1.3 Sample Description

Written descriptions for sediment cores include: 1) sample condition (e.g. cracks, disturbance, oxidation), 2) sample consistency (e.g. soft, hard, firm), 3) reaction to hydrochloric acid which indicates the presence of calcium carbonate, 4) colour (based on the Munsell® soil colour charts), and 5) visual core description consisting of colour, texture, grain size, bedding, contacts, bedforms, structures, presence of organic material, bioturbation and any other visible feature.

2.2 Discrete Core Measurements

2.2.1 Discrete Velocity

The discrete velocimeter has four transducer probes that were carefully inserted into the split core section to measure pressure (or compressional) wave velocity in both longitudinal and transverse directions to the axis of the core. Longitudinal and transverse velocity measurements were taken at a standard 10 cm interval; because the sediment was being probed, measurements were only taken in sediments that did not drain. Daily calibrations were completed to determine the p-wave travel time delay inherent in the system (i.e. electronics); the delay was calculated for each pair of transducers by measuring the distance between them, determining what the travel time should be in distilled water of known temperature, and then comparing this to an actual measurement of the travel time in distilled water at the known temperature. Each measured p-wave travel time was corrected for the travel-time delay and then the p-wave velocity was calculated.

2.2.2 Discrete Shear Strength

Shear strength measurements were made using a motorized miniature vane shear apparatus. A four bladed vane was inserted into the split surface of the sediment core to a constant depth and rotated at a constant rate of 90°/min until sediment failure. Measurements were taken only in undrained and undisturbed soft sediments.

The difference in rotational strain between the top and bottom of a linear spring (deflection angle) was measured and the torque required to shear the cylindrical surface around the vane was calculated. Each vane has a vane-blade constant dictated by the geometry of the blade, and each spring has a spring constant that relates the deflection angle to the torque. Peak and remoulded shear strength values were calculated according to ASTM Method D4648. Routine calibration of the system is not necessary. Peak shear strength measurements were taken at a standard 10 cm interval and two to three measurements of remoulded shear strength were taken per section.

2.2.3 Constant Volume Sampling

Constant volume samples were taken using a stainless steel cylindrical sampler of known volume. The sampler, which was lightly greased with vegetable oil spray to minimize friction, was gently inserted into the sediment at a constant rate to avoid compression of the sediment. The sampler, with the sediment inside, was then carefully removed from the core and the sample was trimmed using a wire saw. The sediment sample was extruded from the cylinder, stored in a glass bottle of known weight and then sealed to prevent desiccation. The samples were stored in a refrigerated container at 4ºC until their return to the GSC(A) where they were weighed, dried at 105ºC for 24 hours and weighed again. Bulk density and water content values were then calculated according to ASTM Method D2216-98.

2.3 Core Processing at the GSC(A)

(modified from Weitzman et al., 2014)

All split core halves were brought to the GSC(A) Core Processing Laboratory for non-destructive core X-radiography and Multi Sensor Core Logger (MSCL) measurements. X-radiography was completed and then the cores were run through the split core MSCL for measurement of magnetic susceptibility and reflectance spectrophotometry at a standard 1 cm down-core resolution.

2.3.1 Multi Sensor Core Logger (MSCL)

The MSCL is designed to push sections of core past an array of sensors; in the case of the split core MSCL, the sensors are mounted on an arm that moves up and down so that the sensors make contact with the split core surface. At the GSC(A), the split core MSCL is integrated with magnetic susceptibility and reflectance spectrophotometry sensors and measurements are taken at a 1 cm down-core resolution.

2.3.1.1 Magnetic Susceptibility (MS)

A Bartington point sensor (MS2E) measures the magnetic susceptibility of the sediment. It is mounted to minimize the effects of magnetic or metallic components of the MSCL system. An oscillator circuit in the sensor produces a low intensity non-saturating, alternating magnetic field. Changes in the oscillator frequency caused by material that has a magnetic susceptibility is measured and converted into magnetic susceptibility values. The sensor is zeroed in air before each measurement, when the sensor arm is in its highest position above the core.

2.3.1.2 Reflectance Spectrophotometry

Split core MSCL reflectance spectrophotometry follows the same protocol as that for onboard/handheld measurements, including using the same spectrophotometer model. The only difference is that the spectrophotometer is mounted on the motorized sensor arm and incorporated into the MSCL for higher resolution measurements.

2.3.2 X-radiography

Both the working and the archive halves of the core samples were X-radiographed together. Core samples were laid side by side on a Picker Clinix Radiographic table and were exposed to X-rays from above using a Universal HE425 X-ray system. X-radiographs were acquired on cassettes loaded in a drawer mounted underneath the table top. Full lengths of core sections were captured by taking a series of overlapping X-ray images. These cassettes were then digitized by a Konica Minolta Regius 110 Computed Radiography system and stored on a computer that runs Konica

Minolta ImagePilot software for viewing the digital X-ray images. When required, jpegs and DICOM images were exported from the ImagePilot software for broader accessibility and usage.

2.3.3 Core Data Compilation

MSCL data, spectral reflectance, shear strength and constant volume data for individual cores were compiled as Excel workbooks. Each workbook consists of individual worksheets containing the original unedited physical property datasets and a worksheet of the compiled physical property dataset. The compiled dataset was imported into Kaleidagraph and poor quality data were masked. The edited, good quality, data were saved as a tab delimited text file and plotted. A graphic of the lithology, MSCL data, spectral reflectance data, and discrete onboard and laboratory physical property data were compiled in a CorelDRAW letter size core plot summary (CPS) file. Lithologies in the CPS were interpreted using core descriptions, core photography, X-radiography, MSCL data, discrete core measurements and limited pXRF data.

2.3.4 Portable X-ray Fluorescence (pXRF) Spectrometry

An Olympus Innov-X Delta Premium 6000 spectrometer, mounted on the vertical motorized arm of the MSCL, is configured for analyzing split cores to facilitate high resolution down-core elemental data. Generally, the instrument is capable of measuring many elements from Mg through U, however, elements are not all measured simultaneously. Down-core resolution and measurement times of the instrument are user-defined. In this study, pXRF data were collected at a 1 cm down-core resolution using Soil Mode with 30 second dwell times for each of beams 1, 2 and 3.

Because there are a number of sources of error that are inherent when taking pXRF measurements on marine core samples (i.e. matrix effects, water content, sample inhomogeneity, uneven split-core surface) it is widely accepted that these pXRF measurements are semi-quantitative. All pXRF data herein are presented as elemental ratios. The pXRF data maximum extents for accompanying core plot summaries are: *Ca/Ti* 0 to 80; *K/Rb* 0 to 400; *Zr/Rb* 0 to 12; *Sr/Ca* 0.0001 to 1 and *Th/Rb* -2 to 4.

2.3.5 Grain Size Measurements

All samples were dried and washed at 63 µm. The < 63 µm fraction (mud) was freeze dried prior to analysis. Laser diffraction analyses using the Beckman Coulter Laser LS-230 were completed separately on the < 63 µm fraction and the > 63 µm to < 1000 µm fraction. Manual sieving at ¼ phi intervals was completed on the > 1000 µ fraction. All data were then merged at 1/5th phi midpoint intervals and converted to microns using in-house Particle Sizing System (PSS) software. End-member modelling analysis (EMMA) were then completed using the open-source R package EMMAgeo software tool to quantify process-related grain size subpopulations within mixed sediment after Dietze and Dietze (2019).

2.4 Radiocarbon Dating

Radiocarbon dating was carried out on a total of nine samples at the Keck AMS Laboratory at the University of California at Irvine. Four dates were from shells; the remaining five dates were from planktic foraminifers with one of these samples also containing benthic and agglutinated foraminifers (Table 2.1).

Dates reported on core plot summaries and in the text are conventional radiocarbon ages which have been calibrated with the online software Calib 7.1 using the Marine13 calibration curve of Reimer et al. (2013) with a ΔR of 0 (Table 2.1).

3.0 Results, Core Summaries and Acoustic Stratigraphic Setting

Piston and trigger weight cores in this study are presented within four areas based on their geographic setting: 1) Logan Canyon to Bonnecamps Canyon (cores 029, 028, 027,025, 024, 023, 022 and 021), 2) the region surrounding Dawson Canyon and Verrill Canyon (cores 020, 019, 018, 017 and 016), 3) the area surrounding Mohican Channel (cores 015, 014, 013, 012, 011, 010 and 009), and 4) the slope just east of Northeast Channel (cores 008, 006, 005, 004, 003, and 001) (Figure 1.1).

Lithofacies are distinguished on the CPS using a combination of MSCL data, core photography and X-radiography, discrete core measurements and the colour a* trace. Generally, the a* values and associated lithofacies are as follows: grey mud -2.0 to +1.0, grey brown mud 1.0 to +2.0, brown mud +2.0 to +3.5, red brown mud +3.5 to +6.0, red orange mud +6.0 to +10.5, brick red sandy mud ‘d’ (brm‘d’) +5.75 to +11.25, brick red sandy mud ‘b’ (brm‘b’) +3.5 to +7.5, olive brown mud +1.5 to +3.5 (at the tops of cores).

3.1 Logan Canyon to Bonnecamps Canyon

2015018 029 piston core

43.270203 N; -60.05894 W; 1620 m WD; Just west of Logan Canyon; 546 cm (opened). The target is 35 m east of a distinct acoustic wipeout (Figure 3.1).

The base of the core to 470 cm (Figures 3.2, 3.3a and 3.4a) consists of brown mud with a moderate degree of ice-rafted detritus (IRD) and vague bedding. A gradational contact separates brown mud from overlying massive to vaguely laminated red orange mud. IRD occurs throughout this interval but is coarser and more abundant toward the basal contact. Red orange mud is frequently interrupted by < 9 cm thick massive brown mud beds with moderate amounts of fine to coarse IRD and gradational upper and lower contacts. The colour a* trace for this red orange and interbedded brown mud interval is distinctly ‘scalloped’ and correlates well with a similar looking colour a* trace in core 025 between 415 cm and 65 cm. A sharp contact at 140 cm separates red orange mud and interbedded brown mud from overlying brm‘d’ to 128 cm. Brm‘d’ is a massive, sandy to pebbly mud characterized by strong a* values. A distinct colour change separates underlying brm‘d’ from tan-coloured, carbonate-rich Heinrich event 1 (H1). The top of H1, at 123 cm, is defined by an absence of coarse sand and granules and a distinct colour change to brown mud. Brown mud with a low degree of granule-sized IRD continues to 87 cm. Brm‘b’ occurs between 87 cm and 82 cm and is characterized by a strong colour a* trace and sharp upper and lower contacts. X-radiography shows that it consists of coarse sandy mud with granules. Brown, moderately to extensively bioturbated mud continues to 28 cm where it is overlain by moderately bioturbated olive brown mud to the top of the core (Figures 3.3b and 3.4b).

2015018 028 piston core

43.39115 N; -59.809085 W; 1679 m WD; Just east of Logan Canyon; 786 cm (opened). The target is near the Annapolis G-24 well as a calibration site for geomicrobiology research (Figure 3.5).

The base of the core to 765 cm consists of grey brown mud with a low degree of fine IRD and vague bedding (Figures 3.6a and 3.7a). A sharp contact, based on colour and X-radiography, separates underlying grey brown mud from overlying vaguely laminated red orange mud, containing a low degree of IRD and thin brown sandy mud beds. A whole round subsample was taken between 758 cm and 738 cm. The colour a* trace for this red orange mud and interbedded brown mud sequence has a distinct 'scalloped' shape which is tentatively correlated to a similar looking a* trace in core 027. Brm'd' occurs between 432 cm and 419 cm and is characterized by strong colour a* values, a moderate degree of fine IRD and a distinct upper contact, based on colour. The overlying tan-coloured, carbonate-rich H1 continues to 413 cm and contains a low degree of coarse sand. A distinct contact separates H1 from overlying brown mud. Brown mud contains a high degree of granule-sized IRD and continues to 340 cm but is separated by brm'b' between 360 cm and 353 cm. Bioturbated brown mud with isolated, granule-sized IRD occurs between 340 cm and 166 cm. At 166 cm brown mud is gradationally overlain by bioturbated olive brown mud to the top of the core (Figures 3.6b and 3.7b). Thin sections of representative lithofacies from 2015018 028 are presented in Figure 3.8.

2015018 027 piston core

43.227075 N; -60.051148 W; 1671 m WD; Just west of Logan Canyon; 502.5 cm (opened). The target is a large seabed mound which coincides with an elliptical depression on the seabed (Figure 3.9).

The base of the core to 355 cm consists of massive red brown mud with a relatively high shear strength, interpreted to be a mass transport deposit (MTD) mud block (Figures 3.10a and 3.11a).

A whole round subsample was taken between 471 cm and 451 cm. A sharp contact, based on colour and shear strength, separates the underlying MTD mud block from overlying weakly stratified brown mud with moderate to high amounts of fine to coarse IRD. Brown mud, characterized by lower colour a* values, continues to 300 cm. A distinct change in colour a* values distinguishes brown mud from overlying red brown mud which continues to 212 cm. Red brown mud contains a low degree of fine IRD and weak stratification to 260 cm and becomes massive with sandy lenses, isolated fine IRD and numerous shell fragments to 212 cm. IRD-rich brown mud occurs between 212 cm and 202 cm. A sequence of weakly stratified, IRD-rich red orange and interbedded red brown muds occurs between 202 cm and 56 cm. This sequence shows a less well-defined yet distinctive colour a* trace similar to the 'scalloped' a* trace of core 028. A distinct contact separates this sequence, in core 027, from overlying fine IRD-rich and moderately bioturbated olive brown mud to the top of the core (Figures 3.10b and 3.11b).

2015018 025 piston core

43.282571 N; -59.876886 W; 1854 m WD; Just west of Logan Canyon; 645 cm (opened). The acoustic target is where an interpreted deep fault comes near the surface (Figure 3.12).

The base of the core to 509 cm consists of red brown mud with a low degree of fine IRD and vague bedding (Figures 3.13a and 3.14a). A whole round subsample was taken from 626 cm to 606 cm, just below a distinctive sandy, red orange mud bed. Vaguely laminated brown mud with fine to coarse IRD, frequent sand lenses and isolated shell fragments continues to 415 cm. At 495 cm an intact bivalve returned an age of 21.2 cal ka (Table 2.1). A well-defined sequence of red orange and interbedded red brown muds gradationally overlies brown mud at 415 cm and continues to 65 cm. Generally, the red orange mud intervals are thicker, contain a higher degree of fine IRD and appear weakly laminated to thin bedded, in X-radiography, when compared to red brown mud intervals. The interbedded nature of red orange and red brown muds creates a ‘scalloped’ colour a* trace which is tentatively correlated to core 2015018 029 between 470 cm and 140 cm. At 65 cm a gradational contact separates this underlying red orange mud sequence from overlying extensively bioturbated olive brown mud which continues to the top of the core (Figures 3.13b and 3.14b).

2015018 024 piston core

43.340303 N; -59.958476 W; 1540 m WD; Just west of Logan Canyon; 607.5 cm (opened). The acoustic target is where a deep fault comes near the seabed (Figure 3.15)

The base of the core to 526 cm consists of fine IRD-rich sandy grey brown mud with vague bedding (Figures 3.16a and 3.17a). Two whole round subsamples were taken between 588 cm and 563 cm. A sequence of predominantly IRD-rich red orange mud with thin brown mud interbeds occurs between 526 cm and 35 cm. It is characterized by a distinctive ‘scalloped’ colour a* trace which can be correlated to core 029 between 470 cm and 140 cm (here the sequence is thinner than in core 024) and with less certainty to core 028. In core 024 red orange gravelly mud is the predominant lithology within this sequence; brown IRD-rich mud beds are thinner and infrequent. At 35 cm, red orange gravelly mud is gradationally overlain by extensively bioturbated olive brown mud to the top of the core (Figures 3.16b and 3.17b).

2015018 023 piston core

43.013181 N; -60.213841 W; 2342 m WD; Just east of Bonnecamps Canyon; 615 cm (opened). The target is acoustically stratified sediment which shows gassy wipeouts (Figure 3.18). Core 023 is a duplicate of core 022.

The base of the core to 482 cm consists predominately of vaguely laminated red orange mud with thin interbeds (< 8 cm) of IRD-rich brown mud (Figures 3.19a and 3.20a). A whole round subsample was taken between 594 cm and 574 cm. At 482 cm, there is a distinct colour change into IRD-rich brown mud which continues to 432 cm. This brown mud has relatively low colour a* values which can be correlated to cores 022 (between 435 cm and 380 cm) and 021 (between 485 cm and 431 cm). At 432 cm and continuing to the top of the core is the 'scalloped' colour a* trace comprised of red orange and interbedded red brown and brown muds, all with intermittent IRD, which correlates well to cores 022 and 021. This sequence is overlain by a thin, faint brm'd' (14 cm to 12 cm) and H1 (12 cm to 10 cm). Massive olive brown mud continues to the top of the core (Figures 3.19b and 3.20b).

2015018 022 piston core

43.013106 N; -60.213735 W; 2342 m WD; Just east of Bonnecamps Canyon; 691 cm (opened). The target is acoustically stratified sediment which shows gassy wipeouts (Figure 3.18).

The base of the core to 435 cm consists of predominately vaguely laminated, sandy red orange mud with rare IRD-rich brown interbeds (< 10 cm) and infrequent, yet distinctive, black mottling (Figures 3.21a and 3.22a). A whole round subsample was taken between 663 cm and 643 cm. At

533 cm, planktic foraminifers returned an age of 22.4 cal ka (Table 2.1). Above red orange mud, beginning at 435 cm, there is a gradational colour change into IRD-rich massive brown mud which continues to 380 cm. This brown mud interval has distinctive, comparatively low colour a* values which can be correlated to cores 023 (between 482 cm and 432 cm) and 021 (between 485 cm and 431 cm). Above 380 cm to the top of the core is red orange mud and interbedded red brown mud and brown mud with the unique 'scalloped' colour a* trace which correlates to cores 023 and 021. Within this interval, toward the basal contact, vaguely laminated red orange mud predominates. Toward the top of this same interval, IRD-rich red brown mud predominates. This sequence is overlain by a thin, faint brm'd' and H1. Brm'd', H1 and brm'b' are well preserved in the trigger weight core (Figures 3.21b and 3.22b). Sandy olive brown mud continues to the top of the core. Down-core pXRF analyses are presented in Figure 3.23.

2015018 021 piston core

43.080551 N; -59.9134 W; 2320 m WD; Between Bonnecamps Canyon and Logan Canyon; 723.5 cm (opened). The target is on the flank of a diapir (acoustically hummocky and gassy looking) (Figure 3.24).

The base of the core to 578 cm consists of homogeneous red orange and olive grey MTD mud blocks with relatively high shear strengths (Figures 3.25a and 3.26a). A whole round subsample was taken within the MTD between 701 cm and 781 cm. The top of the MTD forms a sharp contact with overlying vaguely laminated red orange mud which continues to 485 cm. IRD-rich massive brown mud overlies red orange mud and continues to 431 cm. This brown mud has distinctive lower colour a* values which can be correlated to cores 023 (between 482 cm and 432 cm) and 022 (between 435 cm and 380 cm). Above 431 cm to 25 cm, red orange and interbedded red brown and brown muds create the ‘scalloped’ colour a* trace which can be correlated to cores 023 and 022. Near the base of this interval, vaguely laminated red orange mud predominates; toward the middle, a section of IRD-rich red brown mud and brown mud occurs (between 318 cm and 248 cm); toward the top, vaguely laminated red orange sandy mud with interbedded red brown mud and brown mud predominates. Bioturbated olive brown mud continues to 5 cm where it is capped by orange brown mud (Figures 3.25b and 3.26b).

3.2 Dawson Canyon and Verrill Canyon

2015018 020 piston core

43.03667 N; -60.929335 W; 1520 m WD; Between Dawson Canyon and Bonnecamps Canyon; 687.5 cm (opened). The acoustic target is a deep seated fault that comes close to the seafloor (Figure 3.27).

The base of the core to 480 cm consists of weakly bioturbated brown and red brown muds with moderate IRD and a single IRD-rich red orange mud bed (Figures 3.28a and 3.29a). A whole round subsample was taken in between 662.5 cm and 643 cm. At 562 cm an intact gastropod returned an age of 22.1 cal ka (Table 2.1). A distinct contact, at 480 cm, separates these lower brown and red brown muds from an overlying finer brown mud interval with weak sand laminae. Massive, bioturbated brown mud with a low degree of IRD continues to 251 cm and contains four distinct and vaguely laminated grey brown mud beds between 465 cm and 333 cm. A distinct colour contact separates this brown mud interval from overlying red orange mud. A correlation can be made between this core and core 019 on the basis of the red orange mud interval colour a* trace. In core 020, this interval begins at 251 cm and continues to 16 cm and in core 019 the same interval begins at 355 cm. Near the base of this interval, in core 020, red orange mud contains gravelly IRD, isolated shell fragments and thin layers of brown IRD-rich mud to 122 cm. Above 122 cm to 22 cm, red orange mud is sandy with rare, vague laminations and a single IRD-rich brown mud bed between 68 cm and 58 cm. A lens of brick red sandy mud between 22 cm and 20 cm with an overlying lighter brown mud is tentatively interpreted to be brm'd' and H1, however the top part of the core is considerably disturbed. Sandy red brown mud continues from about 16 cm to the top of the core (Figures 3.28b and 3.29b). Down-core pXRF analyses are presented in Figure 3.30.

2015018 019 piston core

43.035063 N; -60.932885 W; 1522 m WD; Between Dawson Canyon and Bonnecamps Canyon; 665.5 cm (opened). The acoustic target is a deep seated fault that comes close to the seafloor (Figure 3.27).

The base of the core to 638 cm consists of coarse IRD-rich red brown mud with a thin bed (< 2 cm thick) of red orange mud (Figures 3.31a and 3.32a). A whole round subsample was taken between 638 cm and 618 cm. From 618 cm to 523 cm, coarse sandy brown mud with moderate IRD predominates with a grey brown weakly laminated mud between 564 cm and 546 cm. Above 523 cm to 496 cm, the core consists of IRD-rich red brown mud. A sharp contact at 496 cm separates this red brown mud from overlying brown and grey brown muds which continue to 355 cm. Here, brown mud is predominately massive with some coarse IRD-rich interbeds; grey brown mud beds are thinner (< 4 cm thick) and devoid of IRD. Between 355 cm and 125 cm, red orange IRD-rich mud predominates with thinner (< 20 cm) IRD-rich brown mud interbeds. The red orange mud a* trace correlates well with core 020. A correlation can also be made to the red orange mud in core 018 but in this latter core the red orange mud interval is thinner. Brm'd' and overlying H1 occur between 125 cm and 107 cm and are overlain by slightly bioturbated IRD-rich olive brown mud to 86 cm. IRD-rich brm'b' occurs between 86 cm and 75 cm and is overlain by bioturbated olive brown mud to the top of the core (Figures 3.31b and 3.32b).

2015018 018 piston core

42.775798 N; -61.259595 W; 2084 m WD; Just west of Verrill Canyon; 812 cm (opened). The acoustic target is on the crest of a diapir (Figure 3.33).

The base of the core to 713 cm consists of red brown mud with a moderate degree of IRD (Figures 3.34a and 3.35a). A whole round sample was taken between 788 cm and 769 cm. Between 713 cm and 566 cm the core is characterized by weakly laminated red orange mud with thin brown mud beds near the top of the interval. Both red orange mud and brown mud contain a low degree of fine, disseminated IRD. Bedding is defined by black organic specs and dark grey lenses which may not always be associated with bioturbation. Above red orange mud, between 566 cm and 452 cm, weakly laminated red brown mud predominates with brown mud interbeds throughout and a well-sorted, angled sand bed at 468 cm to 466 cm. Brown mud occurs between 452 cm and 188 cm. Here, sandy laminated brown mud intervals containing isolated, well sorted very fine sand beds, are separated by more massive brown mud beds, a few of which contain a low degree of IRD. Red orange mud with a moderate to high degree of IRD and a distinct colour a* trace occurs between 188 cm and 108 cm. This younger red orange mud interval correlates to the expanded red orange mud interval in cores 019 and 020 and to the thinner younger red orange mud interval in cores 014 and 015. Olive brown mud containing brm‘d’, H1 and brm‘b’ continues from 108 cm to 4 cm and is overlain by a thin orange brown mud (Figures 3.34b and 3.35b).

2015018 017 piston core

42.771301 N; -61.266595 W; 2187 m WD; Just west of Verrill Canyon; 25 cm (opened). The acoustic target is a reflective depression on the margin of a diapir (Figure 3.36).

The base of the core to 19 cm consists of IRD-rich sandy olive brown mud (Figures 3.37a and 3.38a). A distinct contact separates olive brown mud from overlying tentatively interpreted brm‘b’ which continues to 12 cm. Massive, bioturbated olive brown mud continues to the top of the core (Figures 3.37b and 3.38b).

2015018 016 piston core

42.774881 N; -61.234878 W; 2233 m WD; Just west of Verrill Canyon; 683 cm (opened). The acoustic target is on the flank of a diapir (hummocky and gassy looking) (Figure 3.39).

The base of the core to 425 cm consists of interbedded sandy red orange and sandy brown muds, interpreted as stratified MTD blocks on the basis of slightly higher shear strengths and angled bedding (Figures 3.40 and 3.41). A whole round subsample was taken between 654 cm and 634 cm. The top of the MTD forms a sharp contact with overlying host sediments which comprise interbedded brown sandy mud and red orange sandy mud to 367 cm. Red brown coarse sandy mud with fine IRD continues to 352 cm and is overlain by brm‘d’ and H1. H1 continues to 339 cm and is separated from brm‘b’ by red brown sandy mud with isolated, coarse IRD to 305 cm. Brm‘b’ continues to 298 cm. Both brick red muds contain a low degree of granule-sized IRD and are characterized by a strong colour a* trace. Red brown mud with a low degree of coarse IRD continues to 290 cm. Above 290 cm, and continuing to 215 cm, red brown mud is vaguely laminated and contains circular to elongated features (< 2 cm diameter) interpreted as unique-looking bioturbation from the X-radiography. Burrow homogenized brown mud continues from 215 cm to 50 cm and is overlain by extensively bioturbated olive brown mud to the top of the core.

3.3 Mohican Channel and Surrounding Area

2015018 015 piston core

42.402196 N; -62.389195 W; 2178 m WD; Just east of Mohican Channel; 784.5 cm (opened). The acoustic target is a depression which shows an acoustic wipeout (Figure 3.42).

The base of the core to 730 cm consists of IRD-rich grey brown mud (Figures 3.43a and 3.44a). A whole round subsample was taken between 760 cm and 742 cm. Above 730 cm and continuing to 390 cm is an interval of red orange mud with thinner red brown mud and brown mud interbeds, all containing a low degree of IRD. The interbedded red orange, red brown and brown muds form a distinctive colour a* trace which correlates well with cores 012, 013 and 014. Brown sandy mud with infrequent IRD continues from the top of this interval to 277 cm and contains a distinctive light grey brown mud with a low degree of IRD. Red orange mud with disseminated IRD occurs between 277 cm and 170 cm. This younger red orange mud correlates to core 013 (between 61 cm and the top of the core) and to core 014 (between 185 cm and 91 cm). Tentative brm‘d’, H1 and brm‘b’ occur at the top of the younger red orange mud but they are thin and near the break between core sections. Bioturbated olive brown mud overlies brm‘b’ and continues to 4 cm where it is overlain by orange brown mud (Figures 3.43b and 3.44b).

2015018 014 piston core

42.321323 N; -62.462953 W; 2328 m WD; Just east of Mohican Channel; 804 cm (opened). The acoustic target is a grassy terrace (Figure 3.45).

The base of the core, to 729 cm, consists of grey brown sandy mud with a low degree of fine IRD and vague laminae (Figures 3.46a and 3.47a). A whole round subsample was taken between 788 cm and 768 cm. Red brown mud, with infrequent IRD beds, continues to 600 cm. Planktic foraminifers, between 722 cm and 719 cm, returned an age of 29.5 cal ka (Table 2.1). Above 600 cm and continuing to 291 cm, weakly laminated red orange mud, containing disseminated IRD, is interbedded with red brown and brown mud beds. This red brown mud, brown mud and red orange mud sequence forms a distinctive colour a* trace which correlates to core 015 (between 730 cm and 390 cm) and to core 013 (between 712 cm and 191 cm). Planktic foraminifers, from 599 cm to 595 cm, returned an age of 25.9 cal ka (Table 2.1). Brown mud gradationally overlies red orange mud at 291 cm and continues to 185 cm. Between 185 cm and 91 cm, a younger red orange mud with a low degree of disseminated IRD can be correlated to cores 013 and 015. Bioturbated olive brown mud continues to 9 cm where it is overlain by orange brown mud to the top of the core (Figures 3.46b and 3.47b).

2015018 013 piston core

42.360211 N; -62.465481 W; 2208 m WD; Just east of Mohican Channel; 902 cm (opened). The acoustic target is a shallow fault (Figure 3.48).

The base of the core to 810 cm consists predominantly of red brown sandy mud with a moderate degree of IRD. A whole round subsample was taken between 882 cm and 862 cm (Figures 3.49a and 3.50a). Above 810 cm, predominantly massive grey brown mud, with a low degree of IRD, is interbedded with faintly laminated grey brown mud to 712 cm. Red brown mud, with fine IRD, overlies grey brown mud to 635 cm. Above 635 cm, and continuing to 191 cm, red orange mud is interbedded with red brown mud and brown mud. This sequence has a distinct colour a* trace which is well correlated to cores 014 (between 729 cm and 291 cm) and 015 (between 730 cm and 390 cm). A low degree of IRD occurs within this sequence from 635 cm to 440 cm. At 435 cm, a small bivalve returned an age of 25.3 cal ka (Table 2.1). Bioturbated brown mud, with a few thin brown mud interbeds containing fine IRD, begins at 191 cm and continues to 60 cm. Red orange mud, with a low degree of fine to coarse IRD, continues to 7 cm where it is overlain by olive brown mud to the top of the core (Figures 3.49b and 3.50b). The base of this younger red orange mud is well correlated with cores 014 and 015. Grain size data are presented in Figure 3.51; pXRF data are shown in Figure 3.52.

2015018 012 piston core

42.321158 N; -62.467133 W; 2324 m WD; Just east of Mohican Channel; 927.5 cm (opened). The acoustic target is a terrace with acoustic wipeouts (Figure 3.48).

The base of the core to 658 cm consists of massive grey brown mud with intervals of fine IRD and rare red brown mud interbeds (Figures 3.53a and 3.54a). A whole round subsample was taken between 909 cm and 889 cm. Red brown mud, with mostly fine IRD, overlies grey brown mud to 496 cm. Above 496 cm and continuing to 114 cm is a faintly laminated, red orange mud interval punctuated with brown mud beds, both containing a low degree of disseminated IRD. This red orange and brown mud sequence has a distinct colour a* trace which is well correlated to cores 013 (between 712 cm and 191 cm), 014 (between 729 cm and 291 cm) and 015 (between 730 cm and 390 cm). Brown sandy mud, with intermittent fine IRD, overlies the red orange mud sequence and continues to 42 cm. It is gradationally overlain by olive brown mud. At 20 cm there is a distinct contact into overlying bioturbated, red orange mud. The core is capped by 12 cm of bioturbated, olive brown mud with fine IRD (Figures 3.53b and 3.54b).

2015018 011 piston core

42.270058 N; -62.93806 W; 2327 m WD; Just west of Mohican Channel; 404.5 cm (opened). The acoustic target is a shallow fault on a ridge crest (Figure 3.55).

The base of the core to 38 cm consists of an MTD comprised of distinct grey and red brown stratified mud blocks (Figures 3.56a and 3.57a). The interpretation of an MTD is further supported by relatively higher shear strengths which sharply decrease near the top of the MTD. Interbedded, bioturbated red brown mud and olive brown mud overly the MTD and are capped by 2 cm of orange brown mud (Figures 3.56b and 3.57b).

2015018 010 piston core

42.304891 N; -62.843611 W; 2257 m WD; Just west of Mohican Channel; 537 cm (opened). The acoustic target is a hummocky to stratified ridge crest (Figure 3.58).

The base of the core to 380 cm consists of stratified olive grey, blue grey and red mud blocks with elevated shear strengths, interpreted as an MTD (Figures 3.59a and 3.60a). A whole round subsample was taken between 501 cm and 481 cm. The upper contact of the MTD with overlying sediments is sharp. Red brown, predominantly massive mud overlies the MTD to 314 cm and is sharply overlain by an interpreted brm'b'. The top of brm'b' is gradational into predominantly brown muds which contain numerous clean fine sand beds to 215 cm. Sand beds are up to 2 cm thick and are separated by up to 20 cm of brown mud. Brown mud becomes bioturbated at ~210 cm and continues to 150 cm. It is gradationally overlain by extensively bioturbated olive brown mud to 5 cm (Figures 3.59b and 3.60b). Orange brown mud caps the top of the core.

2015018 009 piston core

42.30861 N; -62.836325 W; 2284 m WD; Just west of Mohican Channel; 473 cm (opened). The acoustic target is a fault scarp and MTD (Figure 3.61).

The base of the core to 301 cm consists of an MTD comprised of a basal folded mud block with an overlying stratified mud block and matrix-supported mudclast conglomerate (Figures 3.62a and 3.63a). A whole round subsample was taken between 452 cm and 428 cm. A sharp contact separates the underlying MTD from overlying massive grey mud beds (< 12 cm thick) separated by fine grey sand beds and laminae (< 2 cm thick). Sandy laminae end at 194 cm but grey mud continues to 130 cm where it is gradationally overlain by olive brown mud. Bioturbation begins within grey mud at 235 cm and increases to the top of the core (Figures 3.62b and 3.63b). The core is capped by 4 cm of orange brown mud.

3.4 Northeast Channel to Mohican Channel

2015018 008 piston core

42.097695 N; -63.693831 W; 2360 m WD; Between Northeast Channel and Mohican Channel; 1028.5 cm (opened). The acoustic target is on the top of a mound on the seabed (Figure 3.64).

The base of the core to 1002 cm consists predominately of massive IRD-rich red brown mud (Figures 3.65a and 3.66a). A whole round subsample was taken between 1025 cm and 1005 cm. From 1002 cm to 972 cm, the core consists of vaguely laminated red orange mud with two thin interbeds (< 12 cm thick) of massive IRD-rich brown mud. Massive IRD-rich red brown mud continues from 972 cm to 935 cm. An intact gastropod at 934.5 cm returned an age of 26.3 cal ka (Table 2.1). A sharp contact separates this IRD-rich mud from overlying distinctly interlaminated and interbedded red brown mud and very fine sand to 691 cm. Planktic foraminifers, between 696 cm and 693 cm, returned an age of 25.0 cal ka (Table 2.1). A sequence of interlaminated grey brown mud and very fine sand beds, each < 1 cm thick, occurs between 691 cm and 427 cm. This interval also contains several red brown mud beds, < 4 cm thick, numerous sandy blebs and intervals of microfaulting between 570 cm and 480 cm. At 427 cm, red brown mud sharply overlies grey brown mud and continues to 222 cm. Here, two interlaminated fine sand and mud intervals (< 24 cm thick) are separated by massive red brown mud intervals with isolated IRD (<

75 cm thick). The distinctive younger red orange mud and brown mud sequence, which can be correlated elsewhere along the margin, overlies red brown mud at 222 cm and continues to 116 cm. Brm‘d’ and overlying H1 are interpreted to occur between 112 cm and 102 cm but the colour is vague. Bioturbated olive brown mud continues to the top of the core (Figures 3.65b and 3.66b). Down-core pXRF analyses are presented in Figure 3.67.

2015018 006 piston core

41.92713 N; -63.71642 W; 2648 m WD; Between Northeast Channel and Mohican Channel; 597 cm (opened). The acoustic target is a pockmark on the crest of a buried salt diapir (Figure 3.68).

The base of the core to 420 cm consists of well laminated red brown mud with microfaulting, gas expansion along bedding and distinctive grey to black discolouration interpreted to be a result of fluid migration (Figures 3.69a and 3.70a). A whole round subsample was taken between 585 cm and 561 cm. From 420 cm to 318 cm, the core consists of laminated grey mud with two interbeds (< 14 cm thick) of weakly laminated and bioturbated grey brown mud. From the base of this interval to 340 cm, grey mud displays gas expansion along siltier laminae and some dark grey discolouration. Between 318 cm and 270 cm, grey mud is distinctly interlaminated with very fine sand, rare ripple cross-laminae and sand lenses. At 270 cm, vaguely laminated grey brown mud, with some bioturbation and disseminated fine IRD, sharply overlies grey mud and continues to 202 cm. A sharp contact separates grey brown mud from the overlying red orange mud and brown mud sequence identified elsewhere along the margin. Brm‘d’ and overlying H1 occur between 32 cm and 23 cm. Bioturbated olive brown mud continues to the top of the core (Figures 3.69b and 3.70b). Down-core pXRF analyses are presented in Figure 3.71.

2015018 005 piston core

42.304856 N; -63.888131 W; 1837 m WD; Between Northeast Channel and Mohican Channel; 785.0 cm (opened). The target is an area of an acoustic wipeout (Figure 3.72).

The base of the core to 570 cm consists predominately of well laminated grey brown mud with occasional granule-sized IRD-rich mud beds (Figures 3.73a and 3.74a). A whole round subsample was taken between 765 cm and 739 cm. Sediments from the base of the core to 625 cm appear to have been affected by fluid migration and display associated grey to black mottling and pull-apart structures along bedding. Laminated red brown mud with disseminated IRD and weak bioturbation begins at 570 cm and continues to 495 cm. Laminated grey mud with isolated sand lenses gradationally overlies red brown mud at 495 cm and continues to 403 cm. A second interval of laminated grey brown mud overlies grey mud and continues to 338 cm. Ripple cross-laminated red orange mud occurs between 338 cm and 318 cm. Distinctly laminated red brown mud containing some ripple laminae and rare, IRD-rich beds (< 10 cm) continues to 50 cm. Weak bioturbation occurs toward the top of this interval. A distinct contact separates red brown mud from overlying IRD-rich red orange mud, which continues to 12 cm. Olive brown mud, with a low degree of IRD, continues to the top of the core (Figures 3.73b and 3.74b).

2015018 004 piston core

42.310676 N; -63.886528 W; 1763 m WD; Between Northeast Channel and Mohican Channel; 745.5 cm (opened). The acoustic target is an area of an acoustic wipeout (Figure 3.75).

The base of the core to 465 cm consists of distinctly parallel and wavy interlaminated very fine sand and grey brown mud with two, thin gravelly red brown mud beds between 512 cm and 497 cm (Figures 3.76a and 3.77a). Ripple cross-laminae, isolated sand lenses, mudclasts and rare microfaulting are also present. A sharp contact at 465 cm separates underlying laminated grey brown mud from overlying IRD-rich grey brown mud and red orange mud to 407 cm. Unlike other red orange muds, this red orange mud has a weaker colour a* trace. Above 407 cm to 74 cm is a second interval of distinctly interlaminated and occasionally bioturbated or ripple cross-laminated grey brown mud and very fine sand with microfaulting at 360 cm and 295 cm. Within this laminated grey brown mud interval are thin IRD-rich red brown mud beds, isolated mudclasts and rare sandy lenses. Bioturbated, IRD-rich red brown mud, red orange mud and olive brown mud occur from 74 cm to the top of the core (Figures 3.76b and 3.77b). A tentative correlation can be made between this younger red orange mud and the red orange mud near the top of core 001 on the basis of the colour a* trace.

2015018 003 piston core

42.052693 N; -64.700206 W; 2016 m WD; Between Northeast Channel and Mohican Channel; 566 cm (opened). The acoustic target is a fault associated with a diapir that comes near the seabed (Figure 3.78)

The base of the core to 356 cm consists of distinctly laminated grey brown mud with infrequent ripple cross-lamination, mudclasts, sand lenses and beds (< 20 cm) containing fine IRD (Figures 3.79a and 3.80a). A whole round subsample was taken between 546 cm and 521 cm. The upper contact of grey brown mud with overlying massive, red brown IRD-rich mud is sharp. Red brown mud continues to 320 cm and is sharply overlain by stratified and folded, laminated red brown mud blocks, to 112 cm, interpreted as a localized MTD. Between 112 cm and 95 cm is an IRD-rich olive brown mud containing mottled red mud, tentatively interpreted as brm 'b'. Bioturbated olive brown mud continues to 5 cm (Figures 3.79b and 3.80b). A distinct contact separates olive brown mud from orange brown mud at the top of the core.

2015018 001 piston core

42.112938 N; -64.40527 W; 2082 m WD; Between Northeast Channel and Mohican Channel; 834 cm (opened). The acoustic target is above a salt diapir where faults cut amplitude anomalies and come near the surface (Figure 3.81)

The base of the core to 705 cm consists of laminated and microfaulted grey brown mud with rare granule-sized IRD-rich mud beds (Figures 3.82a and 3.83a). Grey to black sediment discolouration is tentatively interpreted as fluid migration. A whole round subsample was taken between 805 cm and 780 cm. Above 705 cm, and continuing to 645 cm, grey brown mud is predominantly IRD-rich and contains mudclasts, sandy laminae and lenses and two red orange mud beds. A sharp contact separates grey brown mud from overlying laminated grey mud, which continues to 603 cm. Between 603 cm and 557 cm red brown mud, with a moderate degree of fine IRD, grades into red orange mud with coarser IRD. Above red orange mud at 557 cm, and continuing to 197 cm, is a distinctly laminated brown mud with occasional massive IRD-rich red brown mud intervals. Within an IRD-rich red brown mud bed, between 417 and 414 cm, planktic foraminifers returned an age of 21.8 cal ka (Table 2.1). At 197 cm, a sharp contact separates laminated brown mud from overlying massive red brown mud containing fine to medium IRD.

The younger red orange IRD-rich mud, identified in most cores across the margin, begins at 86 cm and continues to 23 cm. This interval in core 001 is especially well correlated to core 008 between 222 cm and 116 cm and to core 004 between 60 cm and 25 cm. Moderately bioturbated olive brown mud continues to the top of the core (Figures 3.82b and 3.83b).

4.0 Scotian Slope Lithostratigraphic Correlation

The Scotian Slope lithostratigraphic correlation (Figure 4.1) is based on late Quaternary lithofacies previously identified across the margin (Hill, 1984; Piper and Skene, 1998; Jenner et al., 2007; Hundert and Piper, 2008; Jenner et al., 2010). Predominantly massive and colour laminated grey muds with laminated fine sand intervals and, less commonly, IRD-rich beds have been identified in cores east of Logan Canyon to Northeast Channel (Jenner et al., 2010). The top of the grey mud facies is constrained by radiocarbon dates of 20.7 cal ka and 22.0 cal ka, recalibrated from core 99036 012 of Jenner et al. (2007) (Figure 1.1; Table 2.1). A succession of brown muds with texturally laminated intervals and more massive intervals containing IRD, overlies grey mud. Massive grey and brown muds containing IRD are interpreted as ice-margin plume fallout from ice crossing the Scotian Shelf (Mosher et al., 1989). Silty and sandy laminated intervals are interpreted as turbidite deposits sourced from glacial meltwater when ice was on the outer shelf (Hill et al., 1984; Mosher et al., 1989). Younger, laminated red brown muds, with more massive intervals containing IRD, record both plume and iceberg discharge from the Gulf of St. Lawrence (Piper and Skene, 1998).

Two brick red sandy mud beds – brm‘d’ and brm‘b’ – occur near the top of brown and interbedded red brown mud and are interpreted as episodes of ice-rafted discharge from the Gulf of St. Lawrence between 17.0 cal ka and 15.9 cal ka (recalibrated from Piper & Skene, 1998). Thin sections of brm‘b’ taken from cores 2015018 028 and 2015018 016 (Figure 4.2) show a subtle but visible fining of grain size within brm‘b’ from Logan Canyon west to Verrill Canyon. A distinctive light tan carbonate-rich bed overlying brm‘d’ is interpreted as Heinrich event 1 (H1), deposited at 16.5 cal ka (recalibrated from Piper & Skene, 1998) from ice rafting and meltwater plumes sourced in Hudson Strait. Holocene bioturbated olive-grey mud overlies the brick red sandy muds. Lithofacies beneath brm‘d’ dated at > 17.1 cal ka (recalibrated from Piper and Skene, 1998) are the focus of this discussion.

Two new lithofacies – grey brown mud and red orange mud (Figures 3.2 and 4.1) - have been included in the 2015018 core interpretations. Grey brown mud occurs in cores west of Verrill Canyon to just east of Northeast Channel. New radiocarbon age control from this study places grey brown mud generally at > 23 cal ka (Figure 4.1), although there is less certainty with the timing and correlation of grey brown mud west of Mohican Channel. On the basis of the colour a* trace and an improved understanding of the timing of lithofacies deposition, previously interpreted grey mud in core 99036 038 (Jenner et al., 2010) has been reinterpreted as grey brown mud (Figure 4.1). Red orange mud appears brighter in 2015018 cores when compared with red brown mud lithofacies identified in cores from previous cruises. Because 2015018 cores targeted underlying gas seeps, a brighter lithofacies colour could indicate a chemical alteration from upward percolating fluids. However, according to Imperial et al. (in prep.) this red orange mud lithofacies primarily results from an improved core photography and lighting system. Nevertheless, it is has been kept as a separate lithofacies for 2015018 cores on the basis of a brighter red colour when compared to red brown mud.

Cores selected for Figure 4.1 include representative, stratigraphic cores from cruise 2015018 taken from west to east across the Scotian Slope, in addition to two cores from cruise 2002046 and a single core from cruise 99036 which provide both age control and coverage between the 2015018 stratigraphic cores. New radiocarbon dates refine our understanding of the timing of lithofacies deposition across the margin and highlight depositional changes between Logan Canyon and Northeast Channel. Some of these depositional changes, presented below, may also be influenced by the morphological disparity between the canyoned region of the margin, from Logan Canyon to Mohican Channel, and the relatively canyon-free region between Mohican Channel and Northeast Channel.

Piston cores from just east of Logan Canyon to Bonnecamps Canyon (029, 028, 027, 025, 024, 023, 022 and 021) contain a distinctive 'scalloped' colour a* trace in red orange mud beneath brm'd' and H1 (see example in Figure 3.3a between 470 cm and 140 cm). This red orange mud lithofacies is interbedded with comparatively thinner red brown and brown muds. The most prominent brown mud interval is characterized by a sharp, left shift in the colour a* trace and is most pronounced in cores 021 (Figure 3.25a – 485 cm to 431 cm), 022 (Figure 3.21a - 435 cm to 380 cm; Figure 4.1) and 023 (Figure 3.19a - 482 cm to 432 cm). Eastward, toward Logan Canyon, an age of 21.2 cal ka in core 2015018 025 marks the onset of this brown mud deposition (Figure 4.1; Table 2.1). To the west, in core 020, brown mud deposition begins at 22.1 cal ka.

West of Bonnecamps Canyon to Mohican Channel, the brown mud interval thickens and separates red orange mud into an older unit and a younger unit (Figure 4.1). Older red orange mud contains more red brown mud and brown mud interbeds when compared to younger red orange mud. From Logan Canyon to just west of Verrill Canyon, most piston cores bottom out within older red orange mud but in core 2015018 013, just east of Mohican Channel, older red orange mud is 5 m thick. West of Mohican Channel to Northeast Channel, older red orange mud correlation is speculative, due to a weaker colour a* trace, and is not extended west of 2018015

013 on Figure 4.1. An age of 22.5 cal ka within grey mud from core 2002046 029 (Jenner et al. 2010) (Figure 4.1), west of Mohican Channel, is contemporaneous with older red orange mud deposition further east. Hundert and Piper (2008) recognize a similar contemporaneous deposition of grey mud in core 2002046 033 and suggest that calving embayments on the Scotian Shelf, west of Mohican Channel, provided a separate shelf-edge proximal supply of grey mud which diluted red orange mud plumes, travelling westward along the margin, from Laurentian Channel. A radiocarbon age of 21.8 cal ka is interpreted to mark the end of older red orange mud deposition in core 2015018 001 and is consistent with similar ages for the onset of overlying brown mud deposition, mentioned above, for cores 2015018 025 and 020 (Figure 4.1). However, Piper and DeWolfe (2003) demonstrate the existence of a discrete calving iceberg outlet in the vicinity of 2015018 001 which may have been the source of older red orange mud in this core.

Younger red orange mud thins progressively westward from Logan Canyon to Mohican Channel (piston cores 020 and 018 and 013). West of Verrill Canyon, the thickness is more variable, partly because of a less well-defined red orange mud in the colour a* trace in 2002046 cores (Figure 4.1). This may be due to a reduced spectrophotometer sampling density in 2002046 cores (5 cm sampling interval) versus more recent 2015018 cores (1 cm sampling interval). Younger red orange mud deposition across the margin is bracketed by a deeper, underlying 20.9 cal ka age (2002046 033) and an overlying 17.1 cal ka age at the base of brm'd' (recalibrated from Piper and Skene, 1998) which overlies 'red brown mud turbidites' on the Scotian margin, described by Piper and Skene (1998).

Grain size data from piston core 2015018 013 (Figure 3.51), which includes the aforementioned younger and older red orange mud intervals, suggests that variable processes were active during deposition. Three end members in 2015018 013 explain more than 85% of the variance – EM 1 (poorly sorted silt to pebble-sized sediment), EM 2 (primary mode at 20 µm) and EM 3 (clay to fine silt). Prior to the onset of older red orange mud deposition, grainsize is dominated by silt in the grey brown and red brown units (EM 3), punctuated by poorly sorted sediment in the IRD-rich beds (EM 1). At the onset of older red orange mud deposition (712 cm), ice-rafted sediments predominate (EM 1). A thin interval of silt deposition (EM 3) including a very fine sand component (EM 2), between 595 cm to 555 cm, corresponds to massive mud interbedded with vague sandy laminae in X-radiography. Above 450 cm (~25 cal ka) to 258 cm, mud deposition predominates with a fairly equal distribution between EM 3 and EM 2. X-radiography shows this interval to be mostly massive mud with isolated fine pebbles and rare sand laminae. Overlying brown mud deposition, between 258 cm and 220 cm, is characterized by silt and very fine sand (EM 2) associated with distinctive sand/silt turbidites in core. Brown mud between 220 cm and 60 cm contains massive clay and silt of EM 2 and EM 3, with rare intervals of silt to pebble-sized IRD of EM 1. The younger red orange mud, at the top of the core (beginning at 60 cm), contains IRD with EM 1 predominating.

From this variability in down-core grain size data, broad-stroke depositional processes can be interpreted for core 2015018 013. Glacial ice reached the upper southwestern Scotian Slope at 28 cal ka (Hundert and Piper, 2008). Basal grey brown, red brown and red orange muds, in core 013, which are older than 25.3 cal ka, are interpreted to represent plume deposition interrupted by ice-rafted input, probably from calving ice along the Scotian Shelf. Above ~25 cal ka, to ~17 cal ka, ice-rafted deposition is less common. Here, plume deposits are interrupted by fine, sandy turbidity current deposits and infrequent fine IRD which suggests a change from predominantly proximal, deglacial ice-margin deposition to gravity process-driven sedimentation and along-slope plume deposition.

5.0 References

Campbell, D. C. and MacDonald, A. W. A. 2016. CCGS Hudson Expedition 2015-018 Geological investigation of potential seabed seeps along the Scotian Slope, June 25 - July 9, 2015. Geological Survey of Canada, Open File 8116, 75 p. https://doi.org/10.4095/299390

Dietze, E. and Dietze, M. 2019. Grain-size distribution unmixing using the R package EMMAgeo. E&G Quaternary Science Journal, 68, 29-46. https://doi.org/10.5194/egqsj-68-29-2019

Gauley, B-J.L. 2001. Lithostratigraphy and sediment failure on the central Scotian Slope. M.Sc. thesis, Dalhousie University, Halifax, Nova Scotia, Canada, 214 pp.

Hill, P.R. 1984. Sedimentary facies of the Nova Scotian upper and middle continental slope, offshore eastern Canada. Sedimentology, 31, 293-309.

Hundert, T. 2003. Western Scotian Slope stratigraphy: insights into late Quaternary deglaciation of the western Scotian Shelf, eastern Canada. M.Sc. thesis, Dalhousie University, Halifax, Nova Scotia, Canada, 154 pp.

Hundert, T. and Piper, D.J.W. 2008. Late Quaternary sedimentation on the southwestern Scotian Slope, eastern Canada: relationship to glaciation. Canadian Journal of Earth Sciences, 45, 267-285.

Imperial, A., Jenner, K.A., Campbell, D.C., Piper, D.J.W. and Desiage, P.-A. In preparation. Effects of fluid migration on surficial sediments on the Scotian Slope, Canada. Geological Survey of Canada, Open File 8854.

Jenner, K.A., Piper, D.J.W., Campbell, D.C. and Mosher, D.C. 2007. Lithofacies and origin of late Quaternary mass transport deposits in submarine canyons, central Scotian Slope, Canada. Sedimentology, 54, 19-38. https://doi.org/10.1111/j.1365-3091.2006.00819.x

Jenner, K.A., Piper, D.J.W., Campbell, D.C. and Mosher, D.C. 2010. Piston cores and supporting high-resolution seismic data, Scotian Slope, Eastern Canada: data and interpretations. Geological Survey of Canada, Open File 6558, 297 p., 1 DVD. https://doi.org/10.4095/286078

Mosher, D.C., Moran, K. and Hiscott, R.N. 1994. Late Quaternary sediment, sediment mass flow processes and slope stability on the Scotian Slope, Canada. Sedimentology, 41, 1039-1061.

Mosher, D.C., Piper, D.W.J., Vilks, G.V., Asku, A.E. and Fader, G.B. 1989. Evidence for Wisconsinan glaciations in the Verrill Canyon area, Scotian Slope. Quaternary Research, 31, 27-40.

Piper, D. J.W., 2001. Geological framework of sediment instability on the Scotian Slope: studies to 1999. Geological Survey of Canada, Open File 3920, 202 p. https://doi.org/10.4095/212710

Piper, D.J.W. and DeWolfe, M. 2003.Pertographic evidence from the eastern Canadian margin of shelf-crossing glaciations. Quaternary International, 99, 99-113. https://doi.org/10.1016/S1040-6182(02)00115-5

Piper, D.J.W. and Skene, K.I. 1998. Latest Pleistocene ice-rafting events on the Scotian Margin (eastern Canada) and their relationship to Heinrich events. Paleoceanography, 13, 205-214.

Reimer, P.J., Bard, E., Bayliss, A., Beck, J.W., Blackwell, P.G., Ramsey, C.B., Buck, C.E., Cheng, H., Edwards, R.L., Friedrich, M., Grootes, P.M., Guilderson, T.P., Haflidason, H., Hajdas, I., Hatté, C., Heaton, T.J., Hoffmann, D.L., Hogg, A.G., Hughen, K.A., Kaiser, K.F., Kromer, B., Manning, S.W., Niu, M., Reimer, R.W., Richards, D.A., Scott, E.M., Southon, J.R., Staff, R.A., Turney, C.S.M. and van der Plicht, J. 2013. IntCal13 and Marine13 radiocarbon age calibration curves 0-50,000 years cal BP. Radiocarbon, 55, 1869-1887.

Weitzman, J.; Ledger, S.; Stacey, C. D.; Strathdee, G.; Piper, D. J. W.; Jarrett, K. A. and Higgins, J. 2014. Logs of short push cores, deep-water margin of Flemish Cap and the eastern Grand Banks of Newfoundland. Geological Survey of Canada, Open File 7148, 389 p. https://doi:10.4095/293871

6.0 Tables and Figures

Table 1.1. Cores used in this study.

Expedition	Core	Latitude (north)	Longitude (west)	Water depth (m)	Split core length (cm) pc	twc
2015018	001	42.112938	-64.405270	2082	834.0	207.0
2015018	003	42.052693	-64.700206	2016	566.0	171.0
2015018	004	42.310676	-63.886528	1763	745.5	30.5
2015018	005	42.304856	-63.888131	1837	785.0	182.0
2015018	006	41.927130	-63.716420	2648	597.0	204.0
2015018	008	42.097695	-63.693831	2360	1028.5	203.0
2015018	009	42.308610	-62.836325	2284	473.0	140.0
2015018	010	42.304891	-62.843611	2257	537.0	206.0
2015018	011	42.270058	-62.938060	2327	404.5	50.5
2015018	012	42.321158	-62.467133	2324	927.5	44.0
2015018	013	42.360211	-62.465481	2208	902.0	156.0
2015018	014	42.321323	-62.462953	2328	804.0	216.0
2015018	015	42.402196	-62.389195	2178	784.5	180.0
2015018	016	42.774881	-61.234878	2233	683.0	no twc
2015018	017	42.771301	-61.266595	2187	25.0	22.0
2015018	018	42.775798	-61.259595	2084	812.0	22.5
2015018	019	43.035063	-60.932885	1522	665.5	29.0
2015018	020	43.036670	-60.929335	1520	687.5	26.0
2015018	021	43.080551	-59.913400	2320	723.5	127.0
2015018	022	43.013106	-60.213735	2342	691.0	198.0
2015018	023	43.013181	-60.213841	2342	615.0	42.0
2015018	024	43.340303	-59.958476	1540	607.5	70.0
2015018	025	43.282571	-59.876886	1854	645.0	42.0
2015018	027	43.227075	-60.051148	1671	502.5	33.0
2015018	028	43.391150	-59.809085	1679	786.0	33.0
2015018	029	43.270203	-60.058940	1620	546.0	39.0
2002046	029	42.682745	-63.954616	860	1174.5	175.0
2002046	033	42.507880	-64.288700	1270	1106.5	28.0
99036	012	43.182098	-60.019753	1800	1042.0	no twc
99036	038	42.591420	-61.799521	2030	1044.5	48.0

Table 2.1. Radiocarbon dates.

Expedition number	Core	Latitude	Longitude	Water depth (m)	Top depth (cm)	Bottom depth (cm)	Material dated	Species where known	Weight dated (mg)	Laboratory Number	Conventional radiocarbon age (years BP)	±	Minimum (1σ)	Maximum (1σ)	Minimum (2σ)	Maximum (2σ)	**Median**	Reference
2015018	PC001	42.112938	-64.405270	2082	414	417	PF, BF, some AF		1.3	UCIAMS-198690 [1]	18400	100	21,640	21,930	21,491	22,111	**21,796**	this research
2015018	PC008	42.097695	-63.693831	2360	693	696	PF	*N. pachyderma* (s)	7	UCIAMS-198691 [1]	21120	60	24857	25179	24615	25256	**24,995**	this research
2015018	PC008	42.097695	-63.693831	2360	934.5	934.5	intact gastropod	*Nautica clausa*	260.5	UCIAMS-198698 [1]	22460	70	26119	26359	26036	26507	**26,248**	this research
2015018	PC013	42.360211	-62.465481	2208	435	435	tiny bivalve; broken	*Portlandia*	11.1	UCIAMS-198699 [1]	21360	70	25189	25427	25081	25534	**25,309**	this research
2015018	PC014	42.321323	-62.462953	2328	595	599	PF	*N. pachyderma* (s)	12.5	UCIAMS-198695 [1]	22060	70	25,845	25,991	25,775	26,068	**25,920**	this research
2015018	PC014	42.321323	-62.462953	2328	719	722	PF	*N. pachyderma* (s)	12.5	UCIAMS-198695 [1]	25840	100	29355	29667	29179	29855	**29,516**	this research
2015018	PC020	43.036670	-60.929335	1520	562	562	intact gastropod	*Nautica clausa*	333.3	UCIAMS-198700 [1]	18635	45	21,979	22,205	21,886	22,289	**22,094**	this research
2015018	PC022	43.013106	-60.213735	2342	530	533	PF	*N. pachyderma* (s)	11.5	UCIAMS-198697 [1]	18960	60	22,367	22,489	22,299	22,571	**22,430**	this research
2015018	PC025	43.282571	-59.876886	1854	495	495	intact bivalve	*Yoldiella sp.*	42.4	UCIAMS-198701 [1]	17935	45	21,059	21,288	20,956	21,392	**21,174**	this research
Legacy Cores																		
99036	PC012	43.182098	-60.019753	1800	989	990	bivalve fragments		10	TO-8773 [2]	17,620	160	20,554	20,970	20,346	21,235	**20,770**	Jenner et al. (2007)
99036	PC012	43.182098	-60.019753	1800	1035	1036	pelecypod valve		22	TO-8495 [2]	18,630	210	21,860	22,335	21,548	22,494	**22,072**	Jenner et a. (2007)
99036	PC038	42.591420	-61.799521	2030	863	875	PF	*N. pachyderma* (s)	13.7	UTRIL - 9547 [2]	23,710	260	27,354	27,723	27,095	27,906	**27,530**	Gauley (2001)
2002046	PC029	42.682745	-63.954616	860	900	904	PF		NA	UCIAMS-68912 [1]	19,010	110	22,360	22,577	22,237	22,770	**22,473**	Jenner et al. (2010)
2002046	PC033	42.507880	-64.288700	1270	1085	1086	single mollusca	*Nuculanidae*	NA	NOSAMS-39338 [3]	17,800	95	20,832	21,144	20,696	21,311	**20,933**	Hundert and Piper (2008)

Radiocarbon dates were converted to calibrated years BP using the online software Calib 7.1, $\Delta R = 0$ and the Marine 13 calibration curve of Reimer et al. (2013).

[1] sample dated at the KECK AMS Laboratory at the University of California at Irvine

[2] sample dated at the Isotrace Laboratory at the Univeristy of Toronto

[3] sample dated at the National Ocean Sciences Accelerated Mass Spectrometry facility at Woods Hole Oceanographic Institution

PF - planktic foraminifers

BF - benthic foraminifers

AF - agglutinated foraminifers

(s) - sinistral

PC - piston core

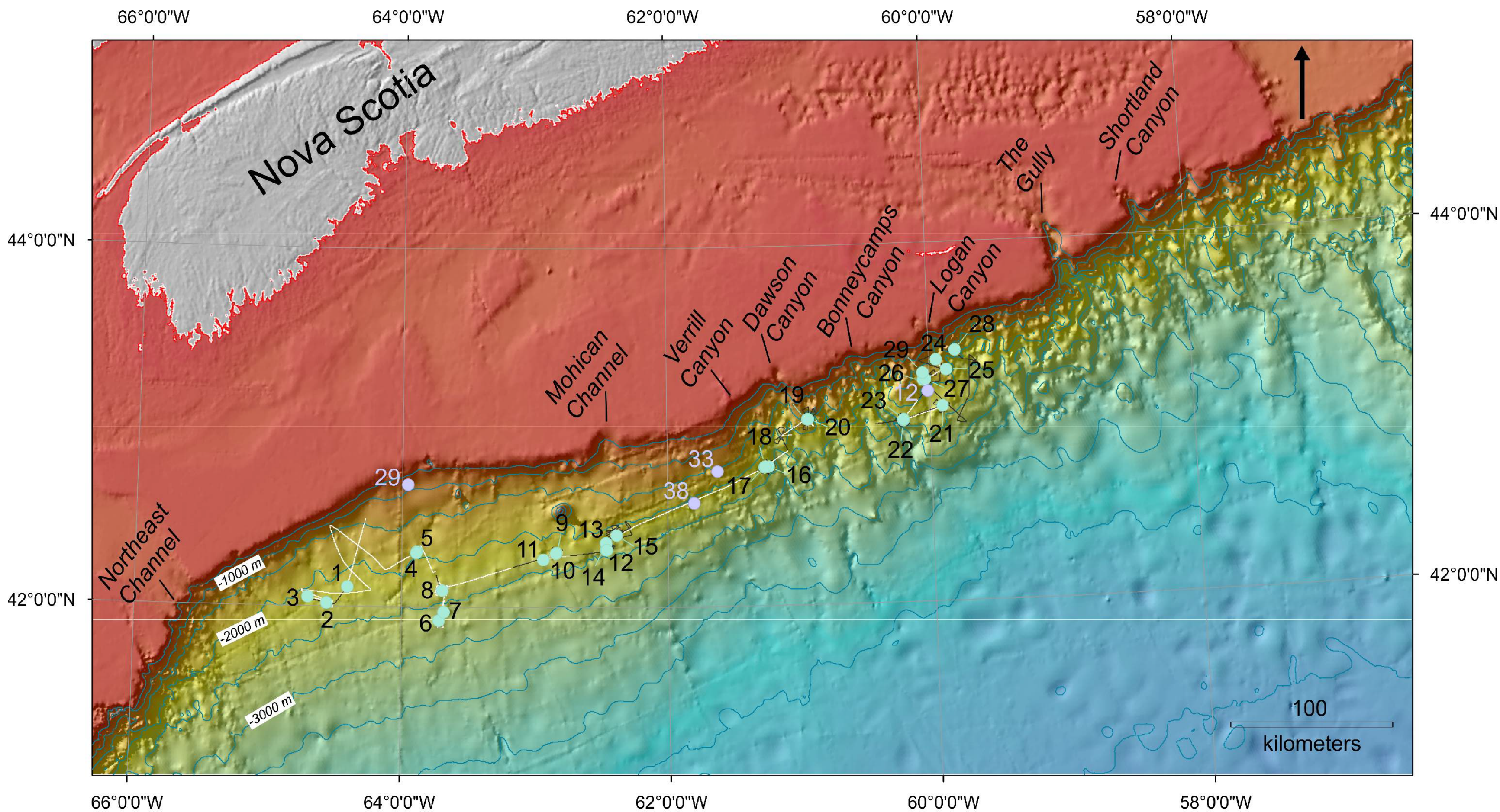

Figure 1.1. Regional map of the Scotian Slope showing 2015018 core locations (teal circles), legacy core locations (lilac circles), 2015018 Knudsen 3.5 kHz coverage (white lines) and 2015018 Huntec DTS coverage (black lines) (after Campbell and MacDonald, 2016). Bathymetric contour interval is 500 m.

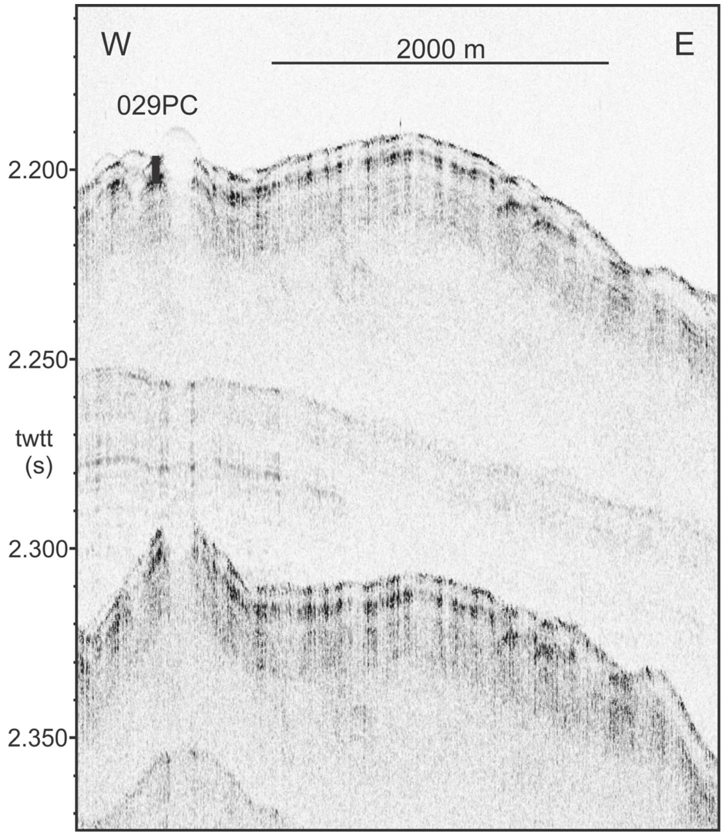

Figure 3.1. High resolution sub-bottom profile showing the acoustic stratigraphy and position of core 2015018 029 (Campbell and MacDonald, 2016).

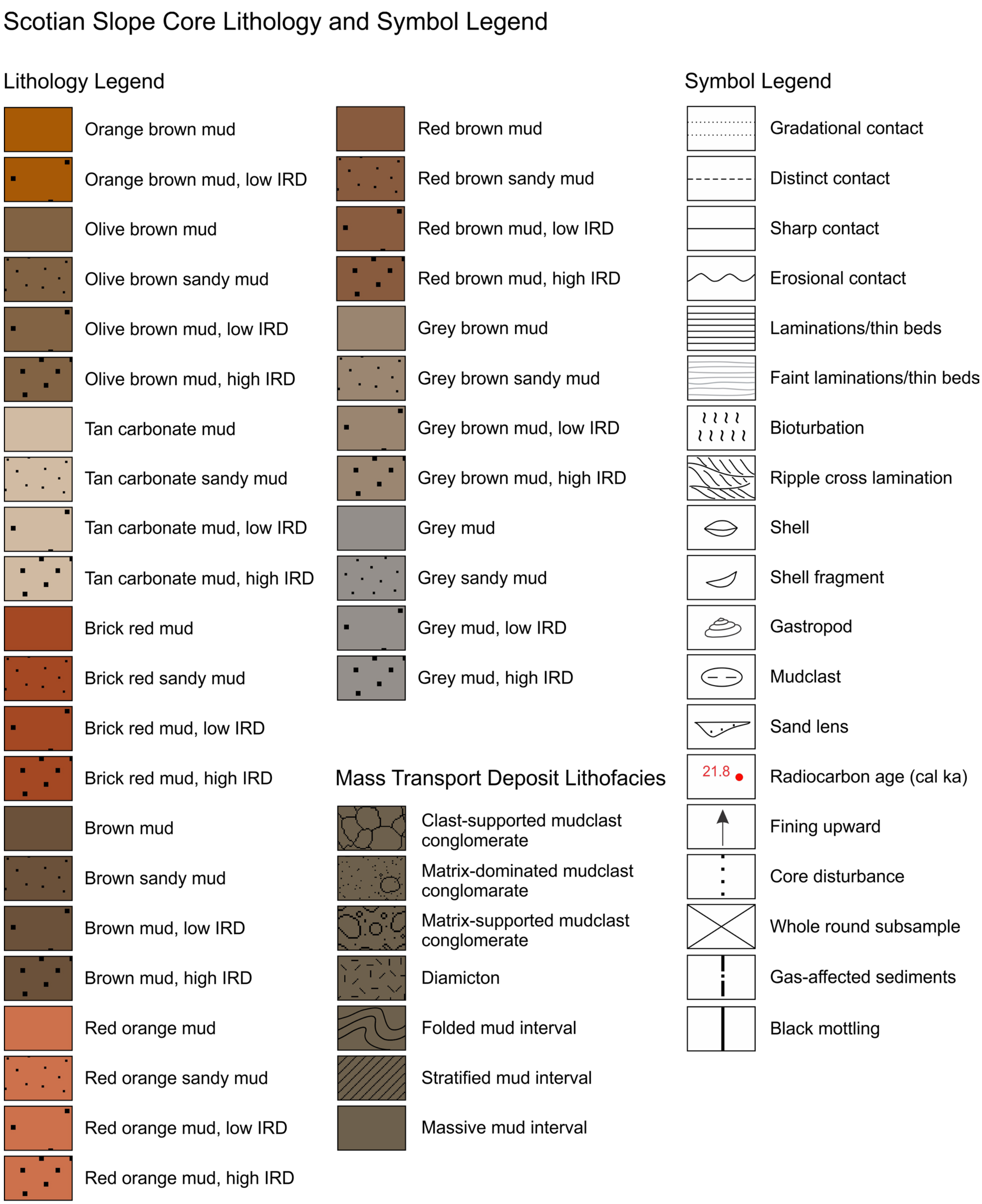

Figure 3.2. Core plot summary legend.

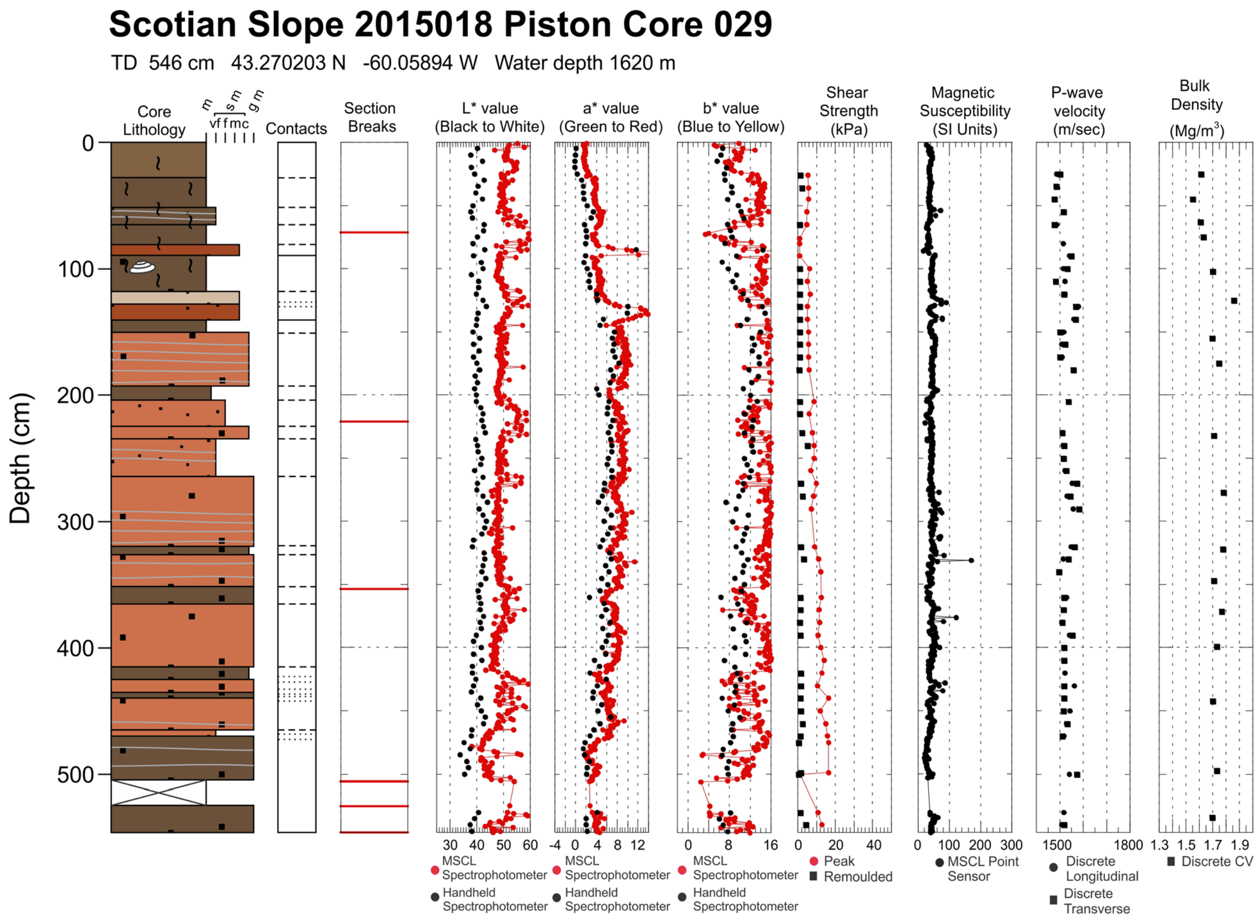

Figure 3.3a. Core plot summary for piston core 2015018 029.

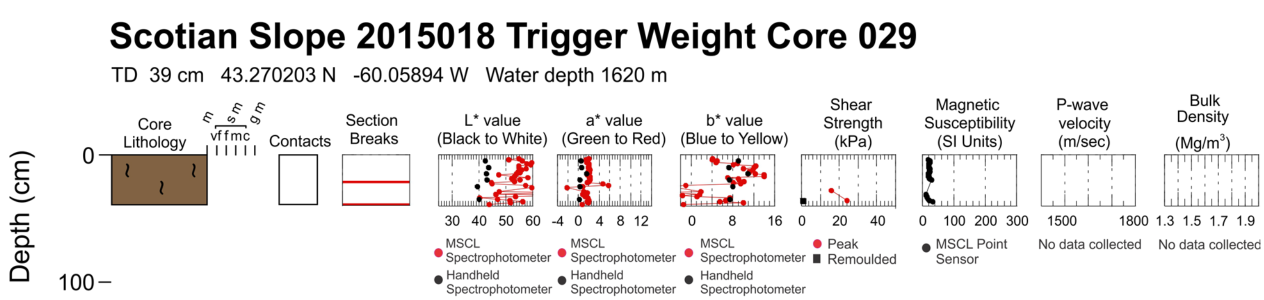

Figure 3.3b. Core plot summary for trigger weight core 2015018 029.

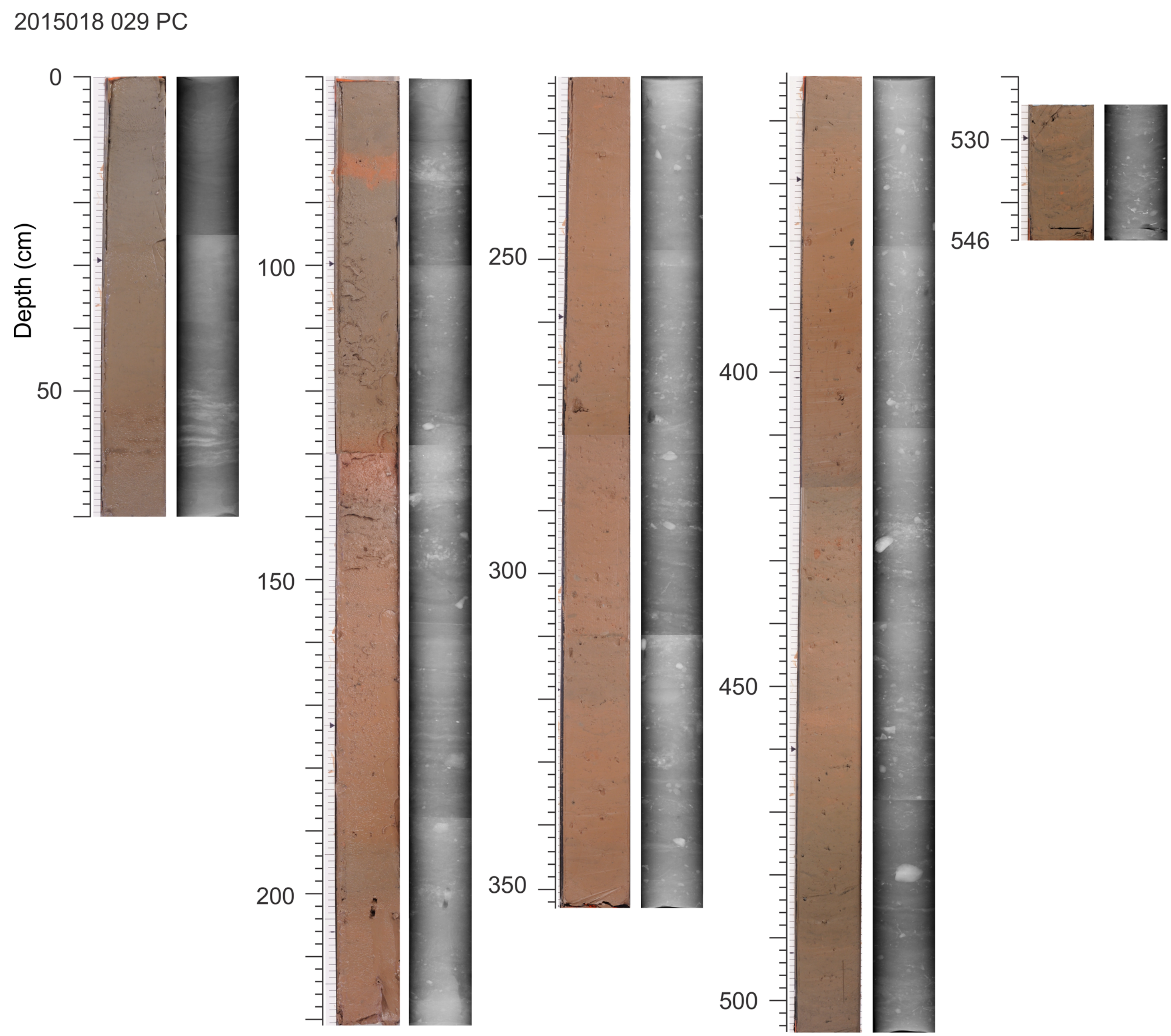

Figure 3.4a. Photography and X-radiography compilation for piston core 2015018 029.

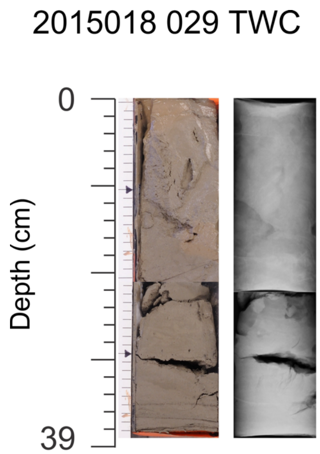

Figure 3.4b. Photography and X-radiography compilation for trigger weight core 2015018 029.

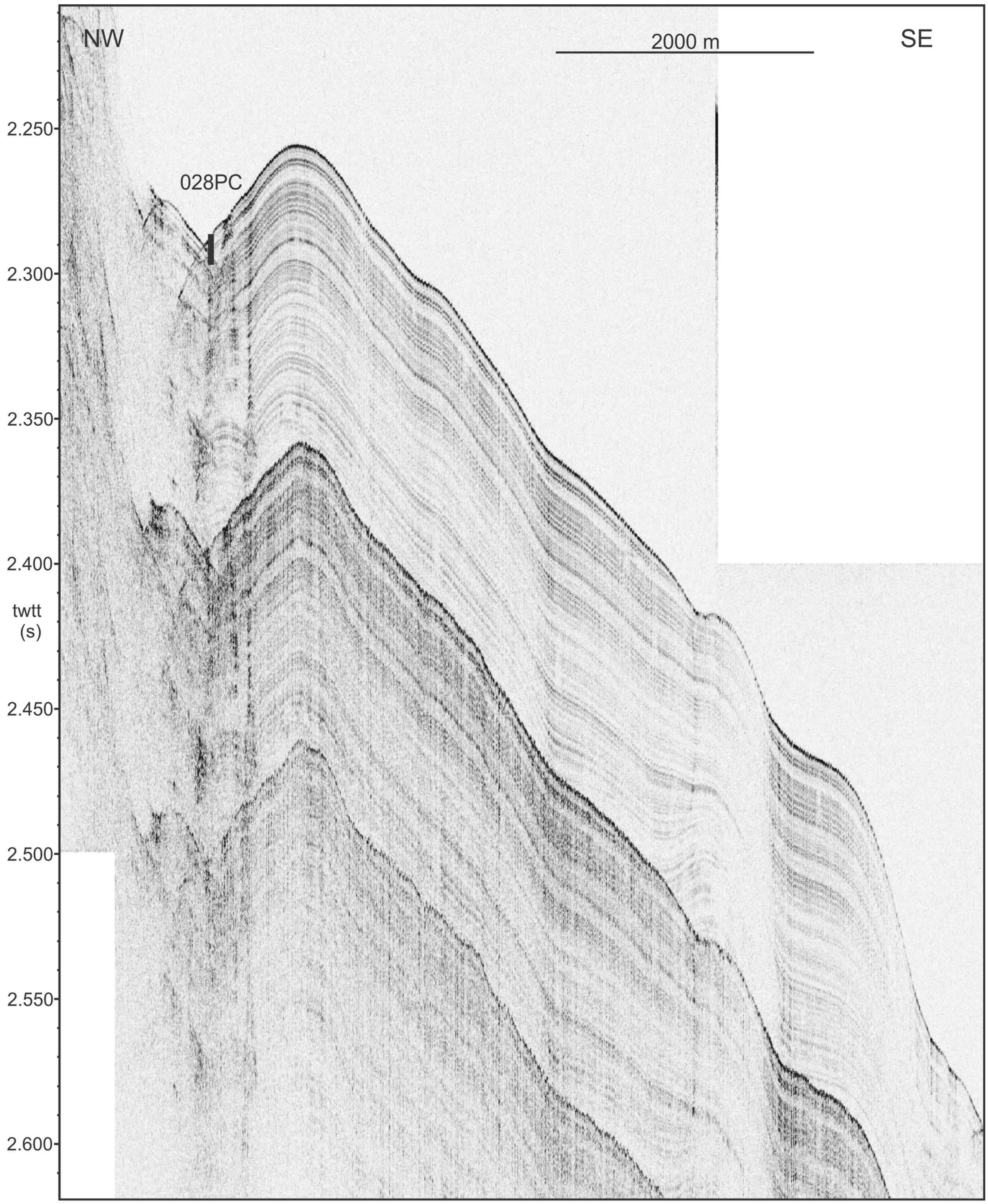

Figure 3.5. High resolution sub-bottom profile showing the acoustic stratigraphy and position of core 2015018 028 (Campbell and MacDonald, 2016).

Scotian Slope 2015018 Piston Core 028

TD 786 cm 43.39115 N -59.809085 W Water depth 1679 m

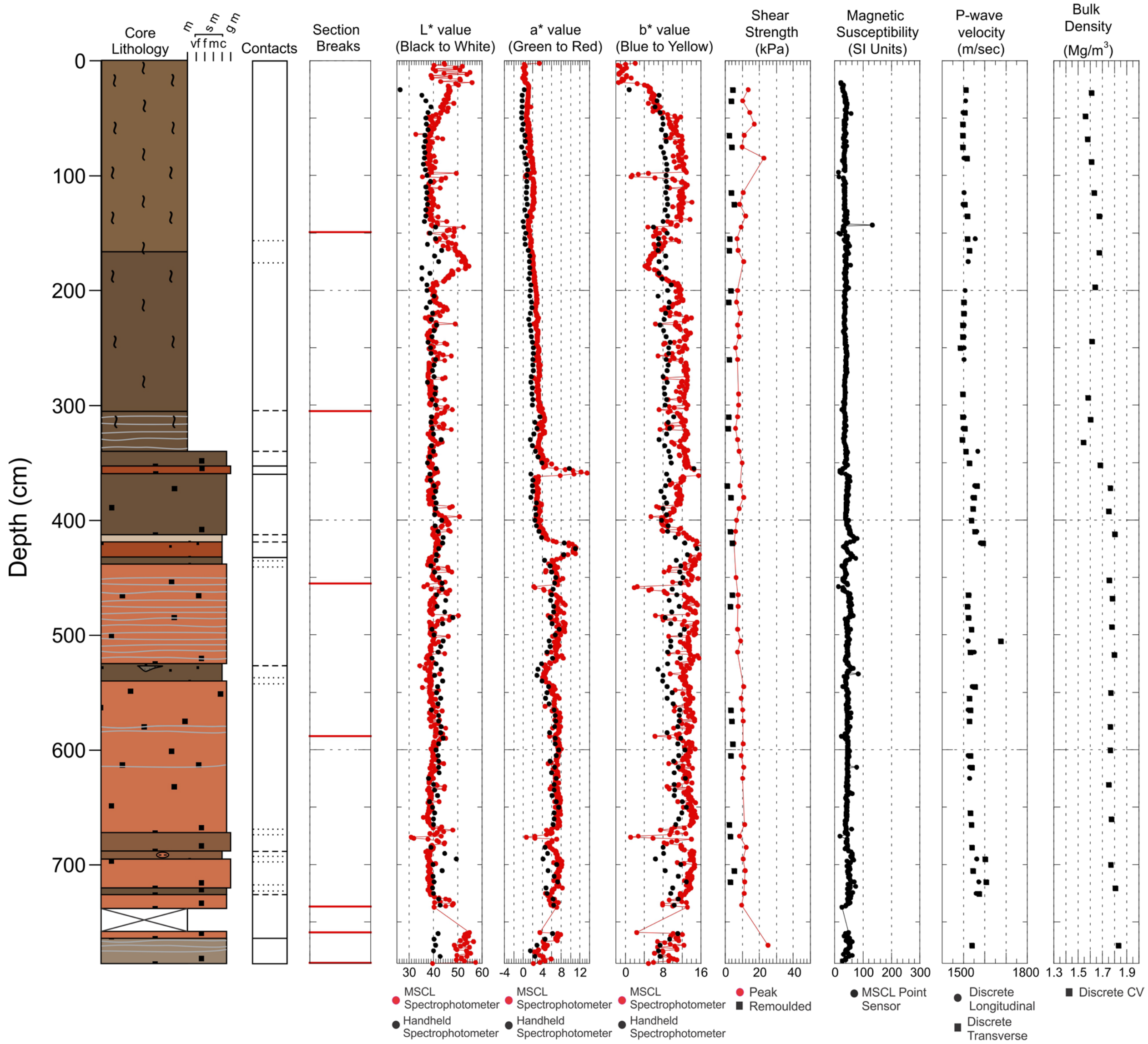

Figure 3.6a. Core plot summary for piston core 2015018 028.

Scotian Slope 2015018 Trigger Weight Core 028

TD 33 cm 43.39115 N -59.809085 W Water depth 1679 m

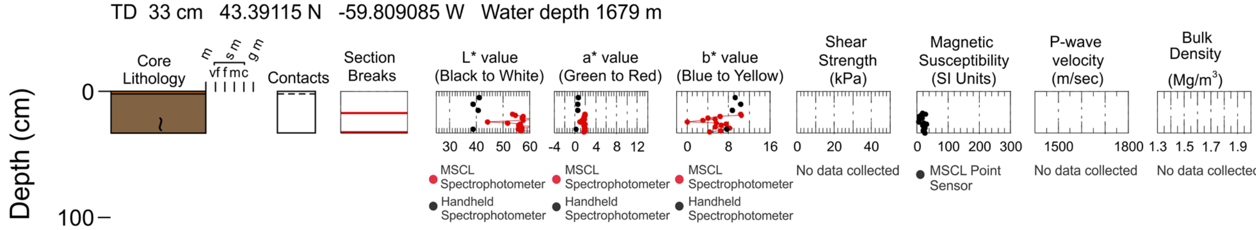

Note: 0-16 cm of 028 TWC was split on board and taken for geomicrobiology research at the University of Calgary. No X-radiography or additional GSC(A) analyses exist for this interval.

Figure 3.6b. Core plot summary for trigger weight core 2015018 028.

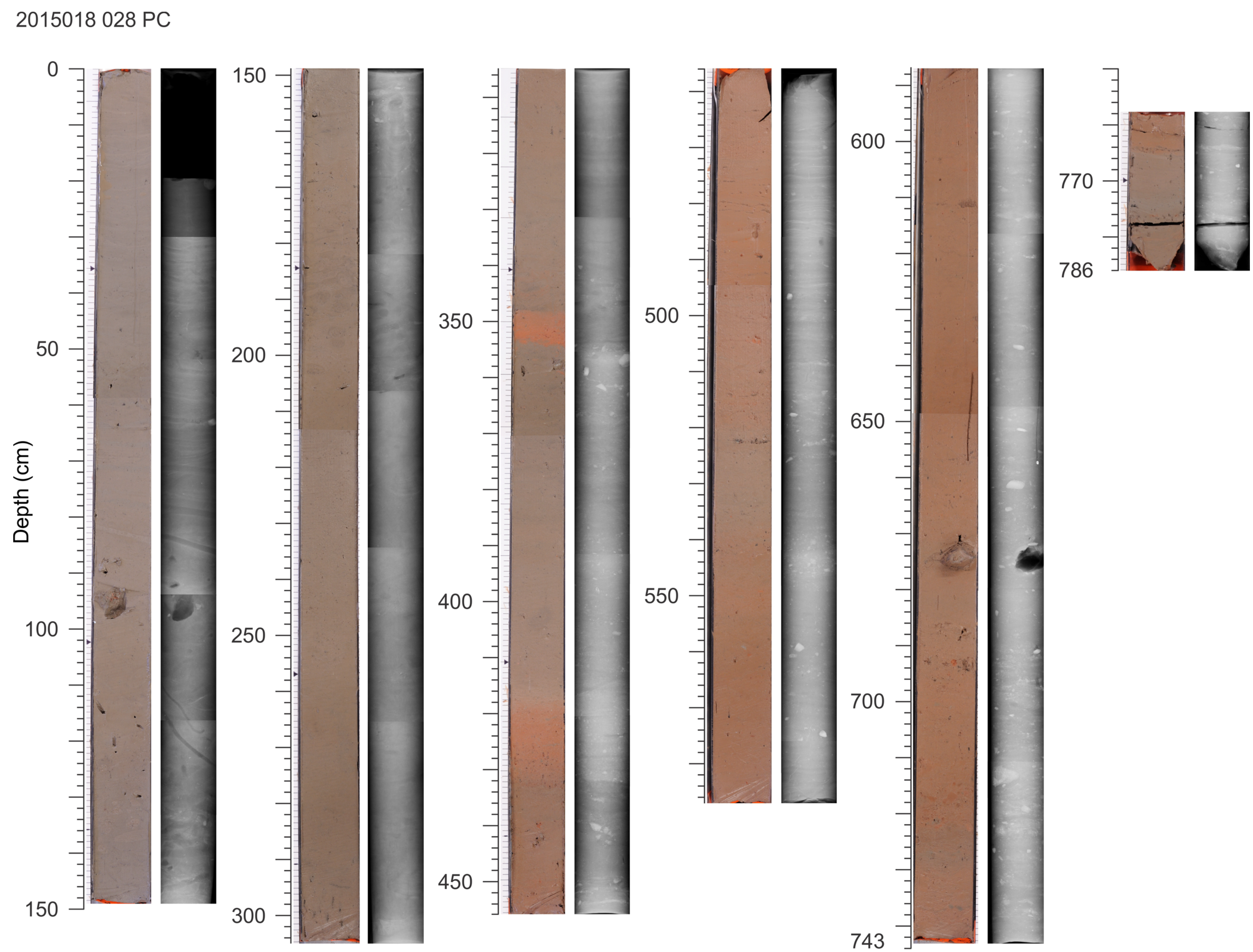

Figure 3.7a. Photography and X-radiography compilation for piston core 2015018 028.

2015018 028 TWC

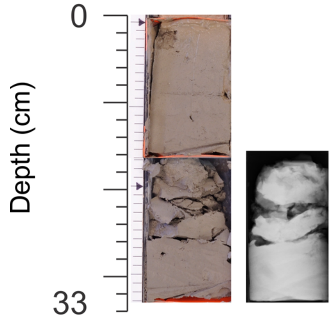

Note: 0-16 cm was taken for geomicrobiology research at the University of Calgary (no X-radiography).

Figure 3.7b. Photography and X-radiography compilation for trigger weight core 2015018 028.

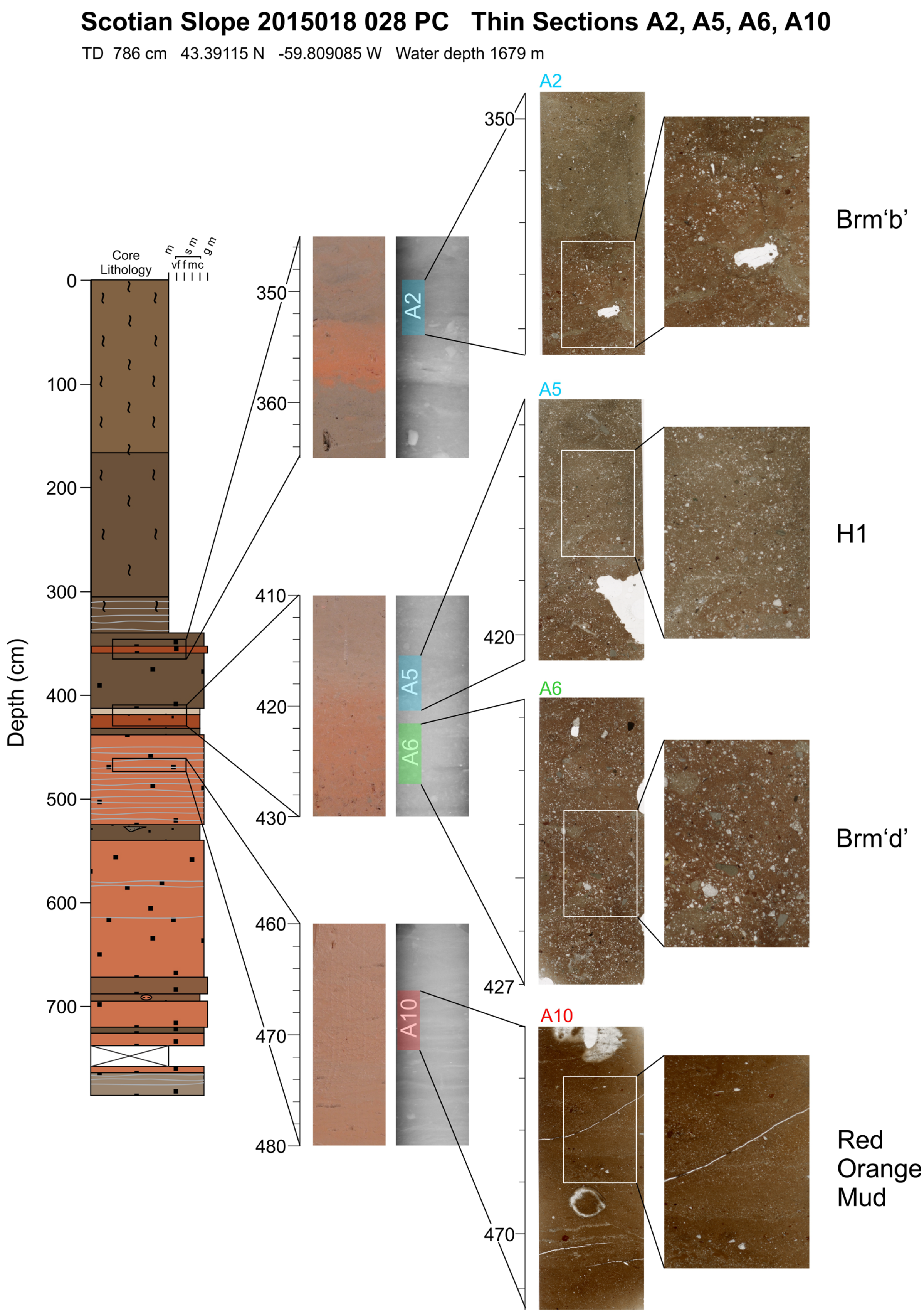

Figure 3.8. Thin section summary for representative lithofacies of piston core 2015018 028.

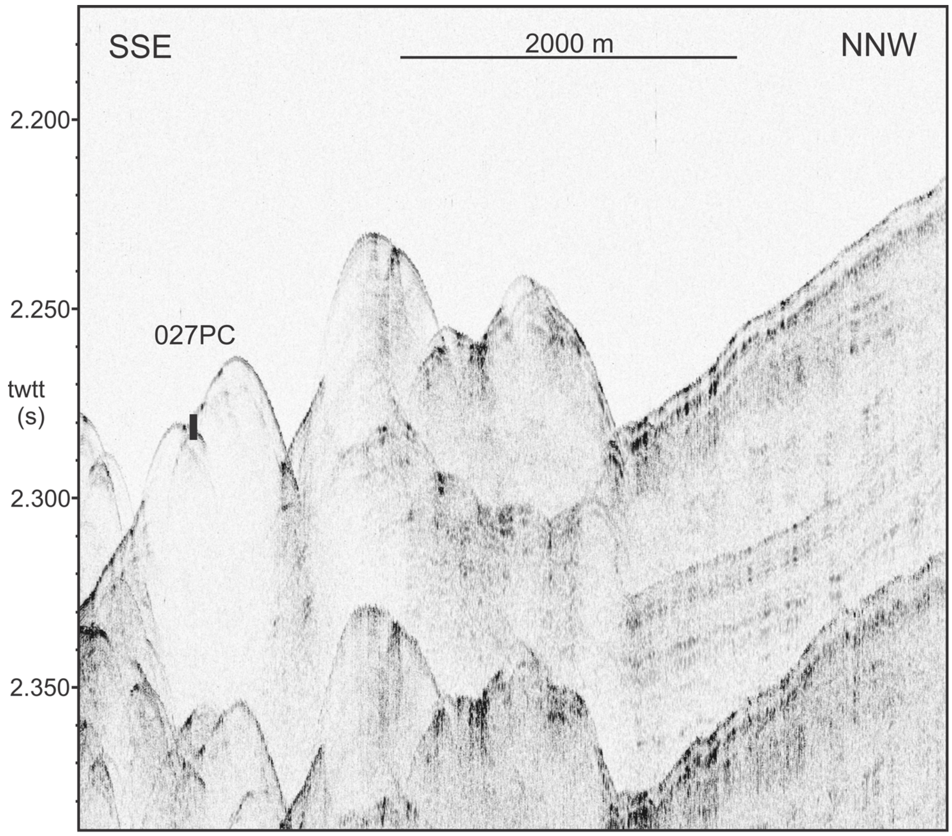

Figure 3.9. High resolution sub-bottom profile showing the acoustic stratigraphy and position of core 2015018 027 (Campbell and MacDonald, 2016).

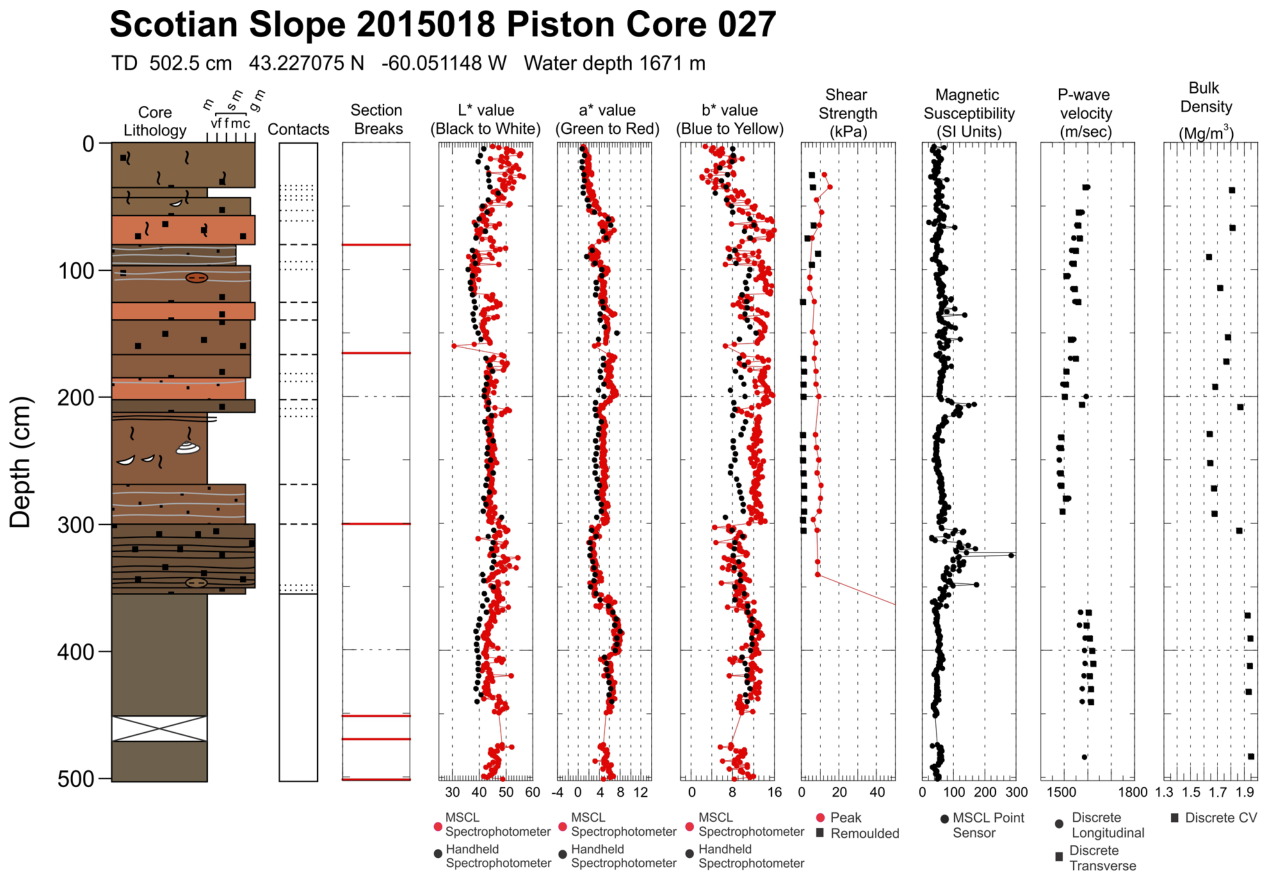

Figure 3.10a. Core plot summary for piston core 2015018 027.

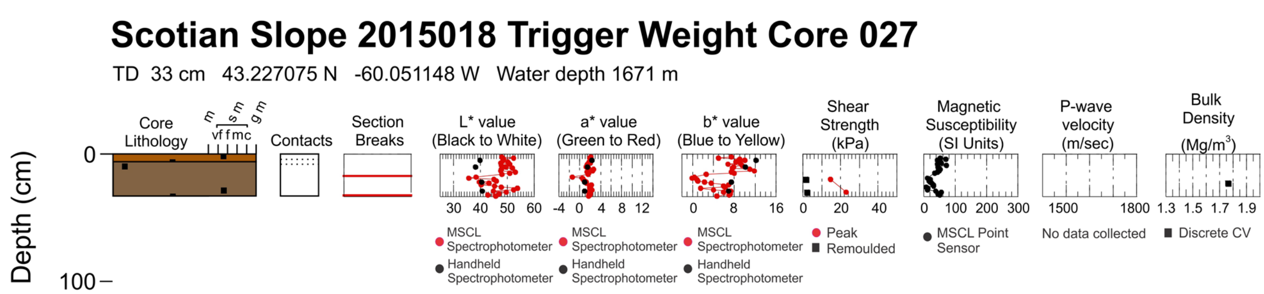

Figure 3.10b. Core plot summary for trigger weight core 2015018 027.

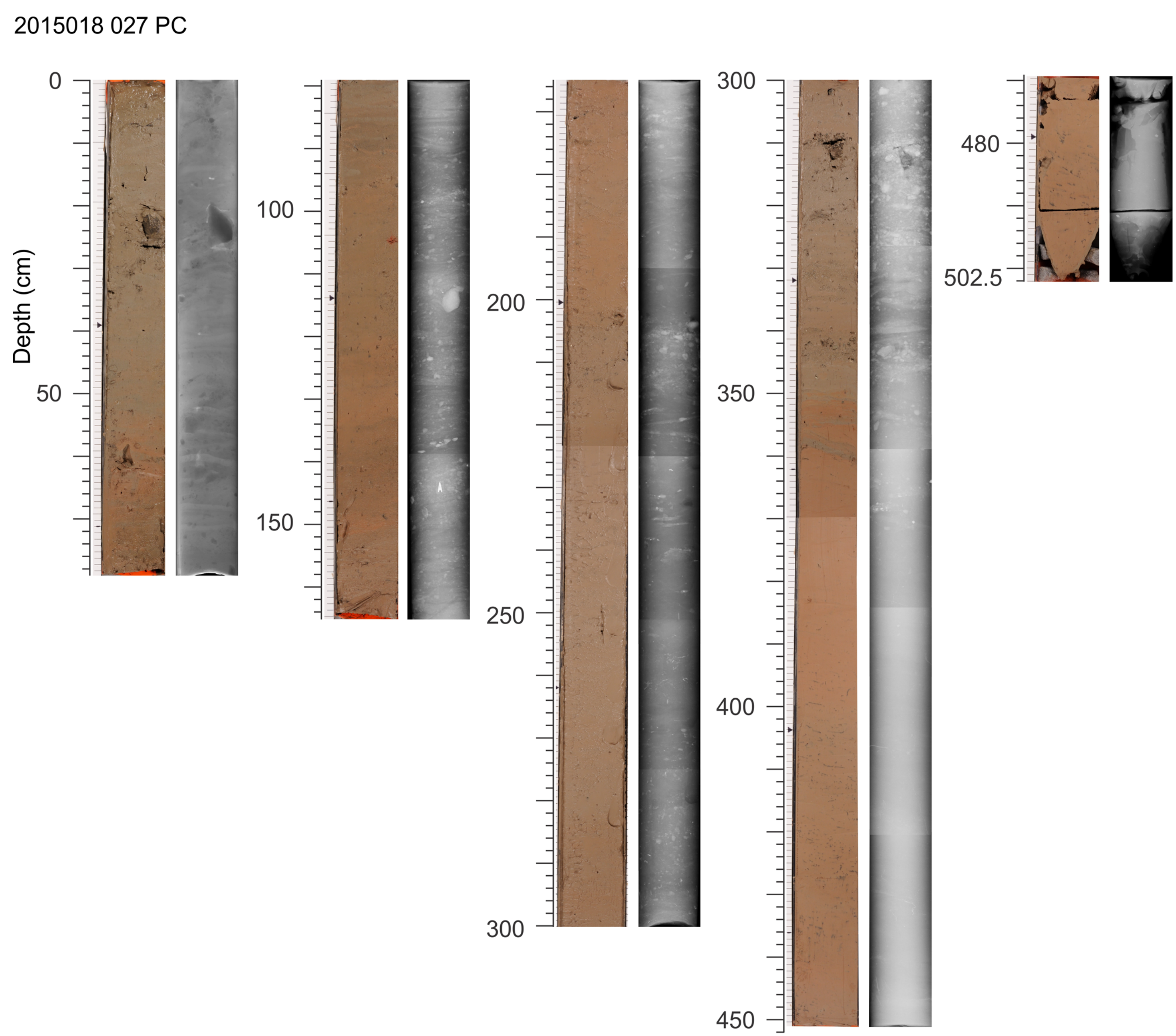

Figure 3.11a. Photography and X-radiography compilation for piston core 2015018 027.

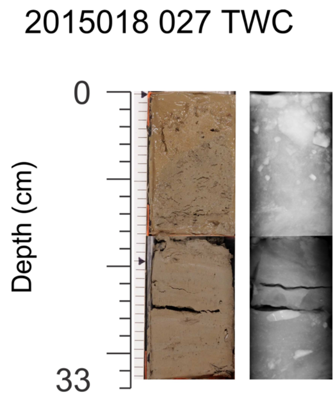

Figure 3.11b. Photography and X-radiography compilation for trigger weight core 2015018 027.

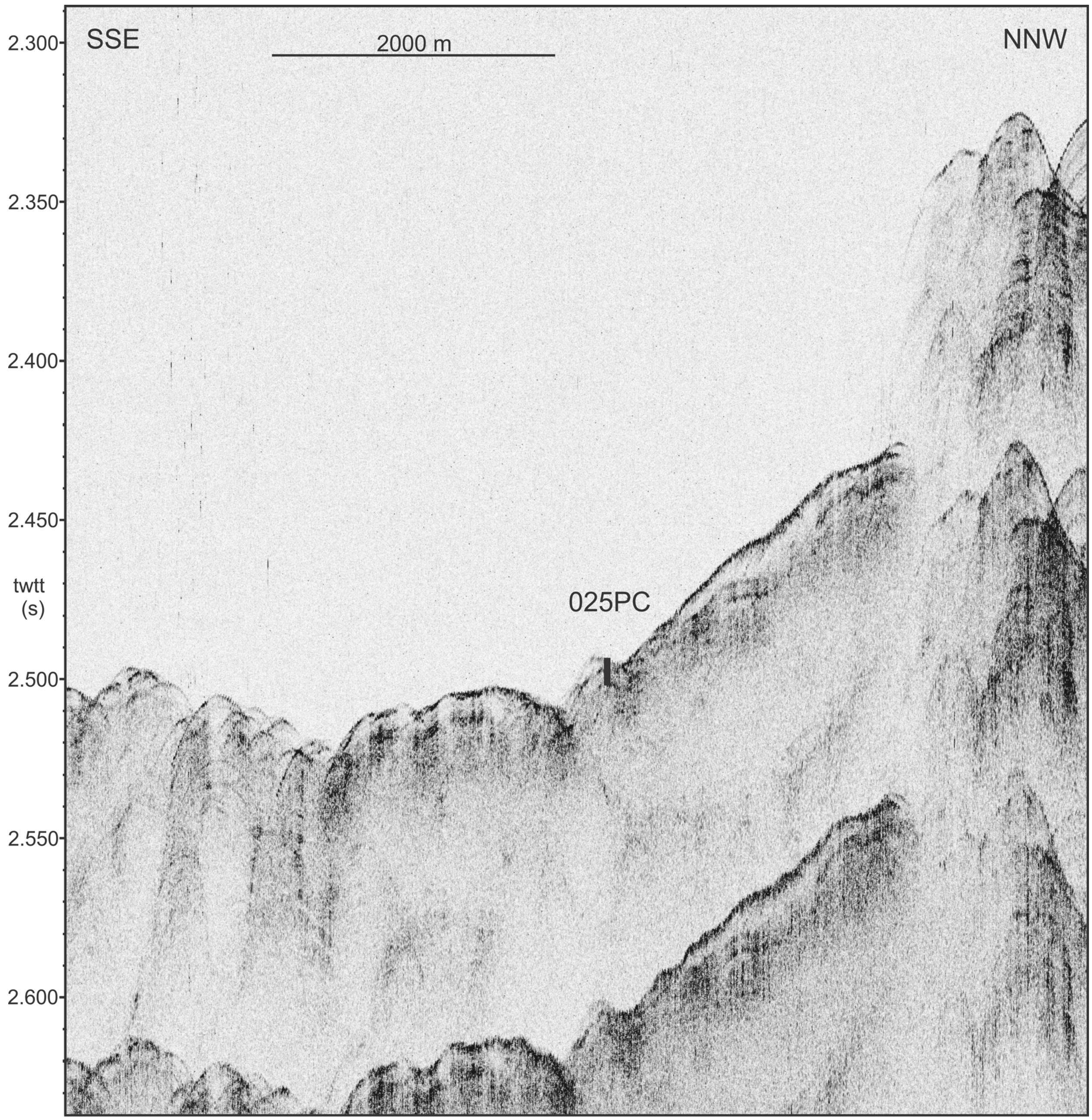

Figure 3.12. High resolution sub-bottom profile showing the acoustic stratigraphy and position of core 2015018 025 (Campbell and MacDonald, 2016).

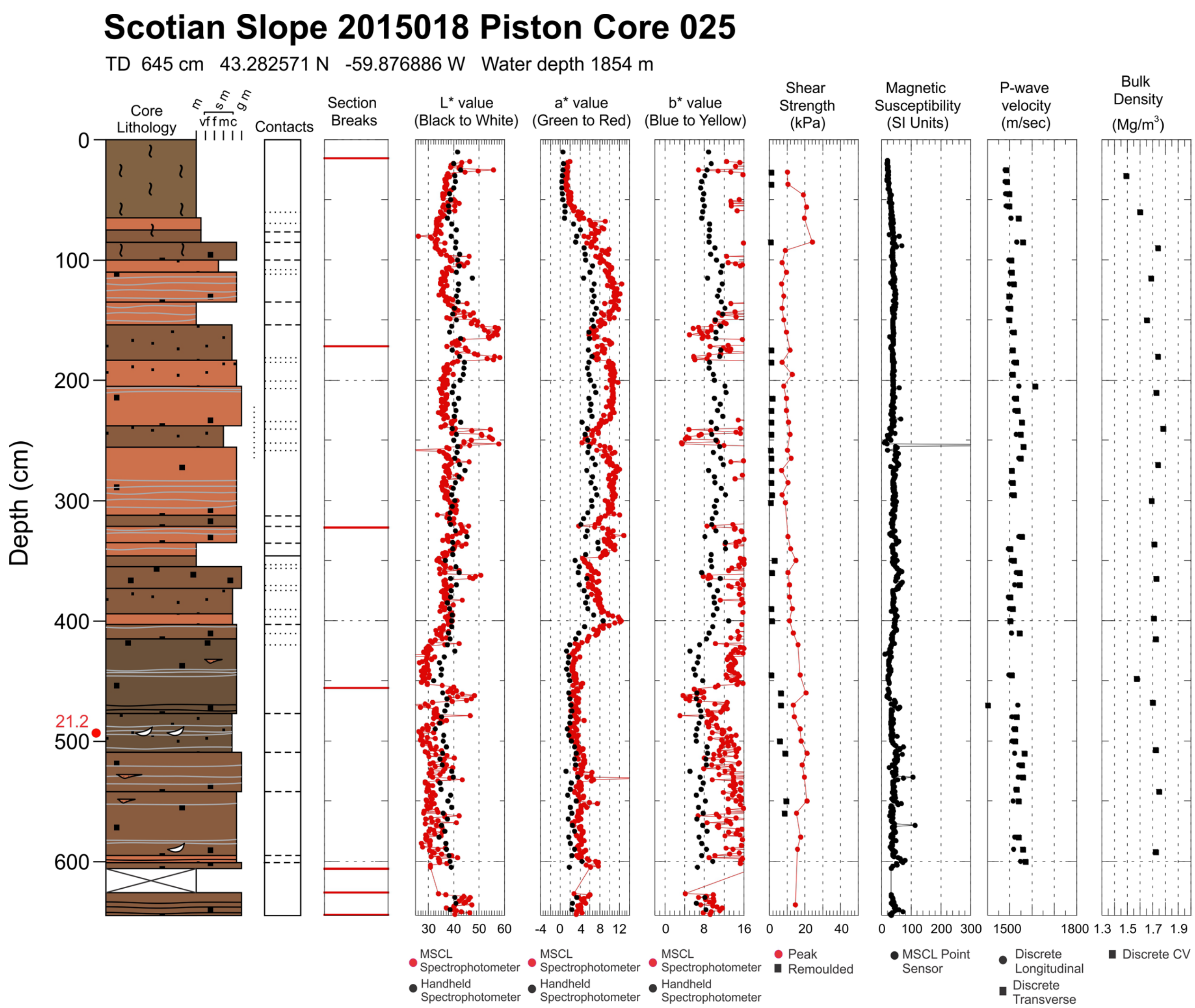

Figure 3.13a. Core plot summary for piston core 2015018 025.

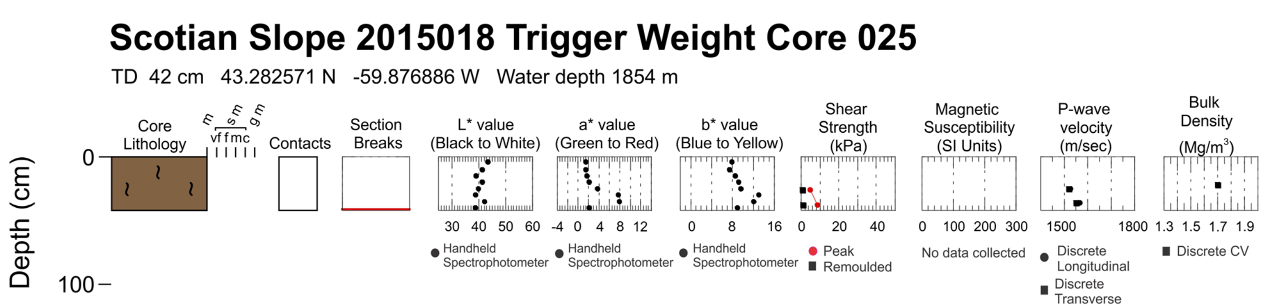

Figure 3.13b. Core plot summary for trigger weight core 2015018 025.

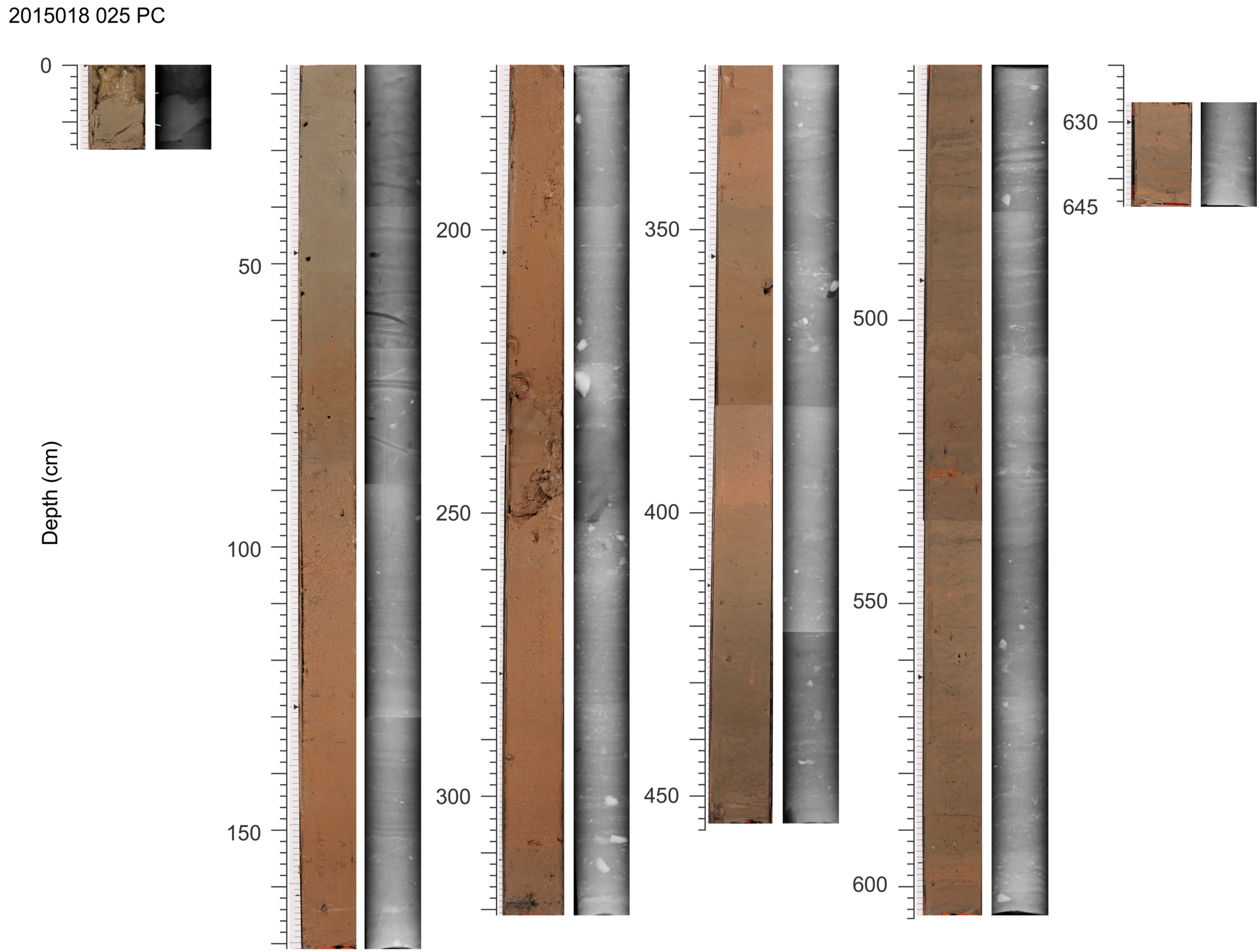

Figure 3.14a. Photography and X-radiography compilation for piston core 2015018 025.

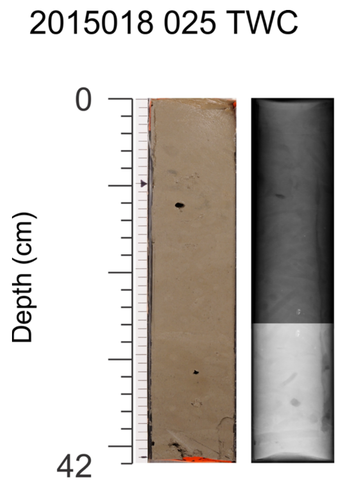

Figure 3.14b. Photography and X-radiography compilation for trigger weight core 2015018 025.

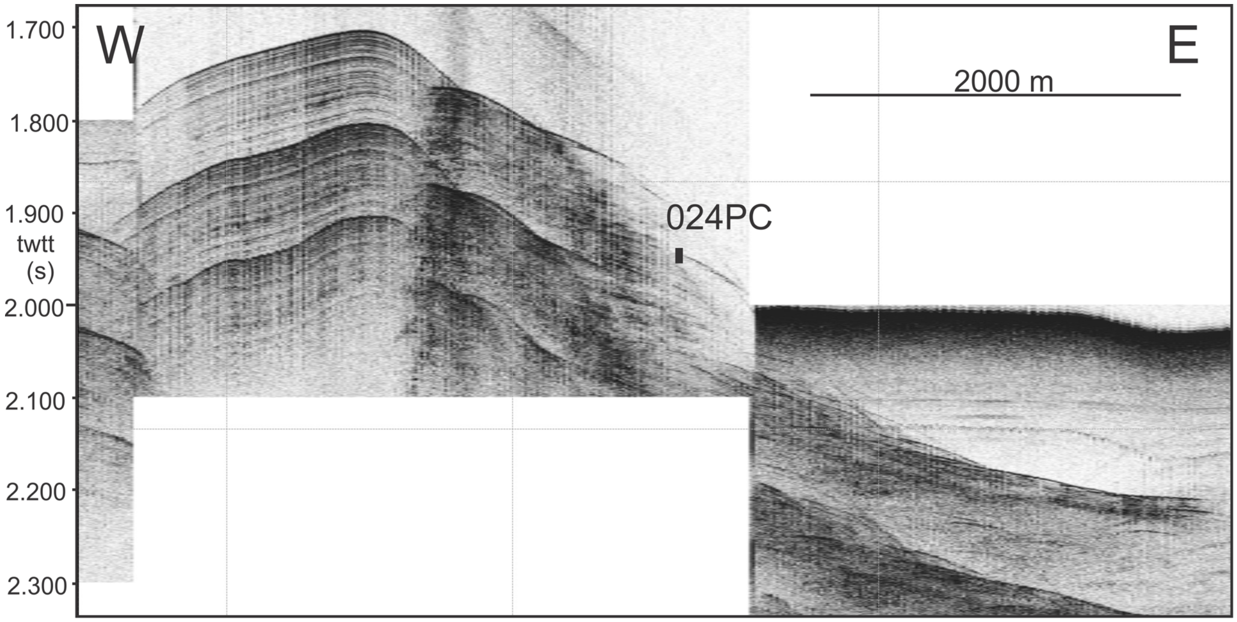

Figure 3.15. High resolution sub-bottom profile showing the acoustic stratigraphy and position of core 2015018 024 (Campbell and MacDonald, 2016).

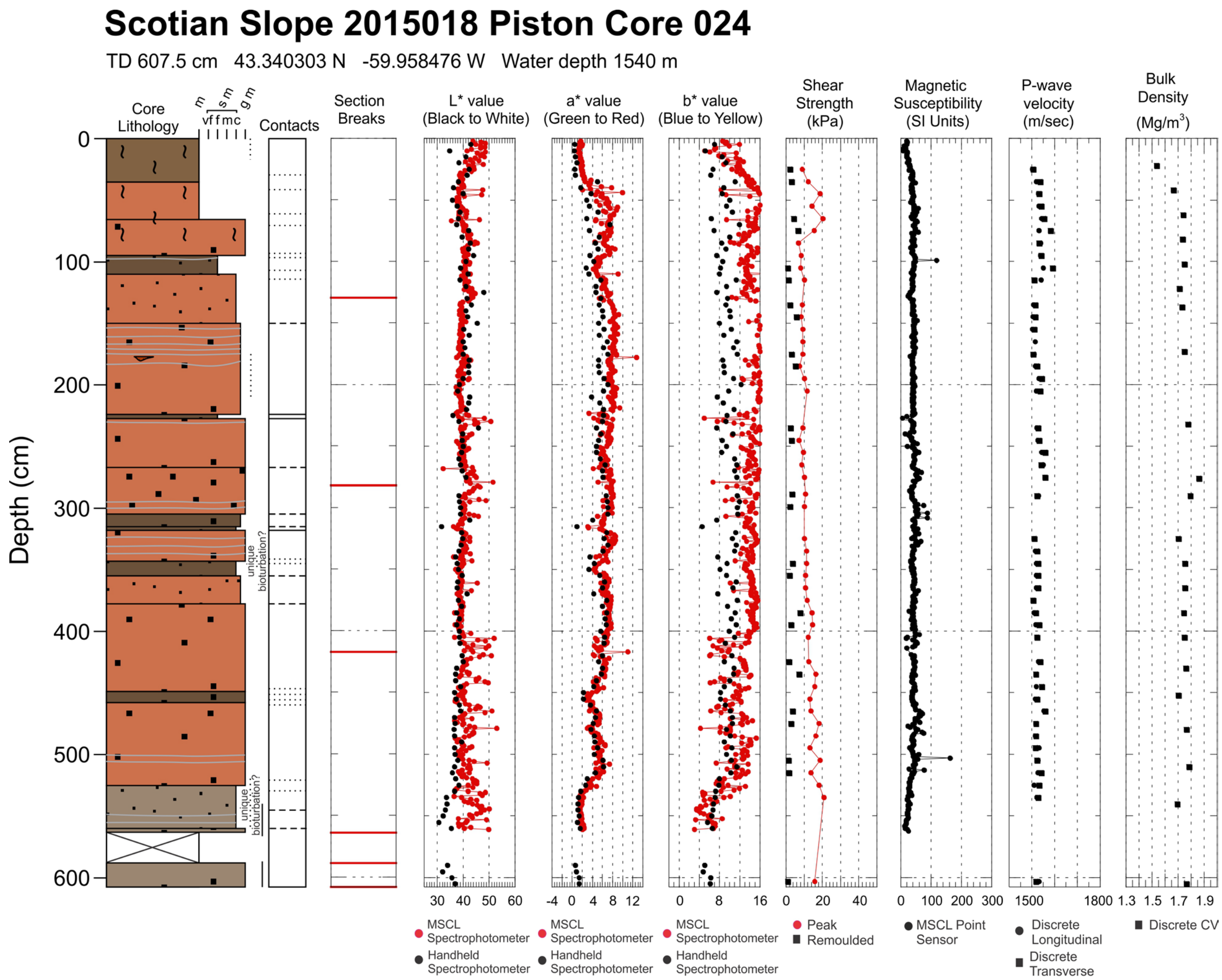

Figure 3.16a. Core plot summary for piston core 2015018 024.

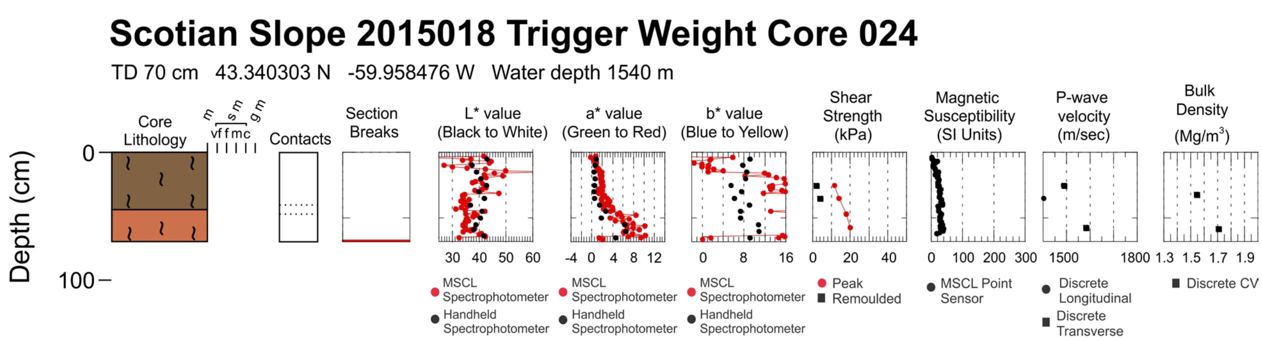

Figure 3.16b. Core plot summary for trigger weight core 2015018 024.

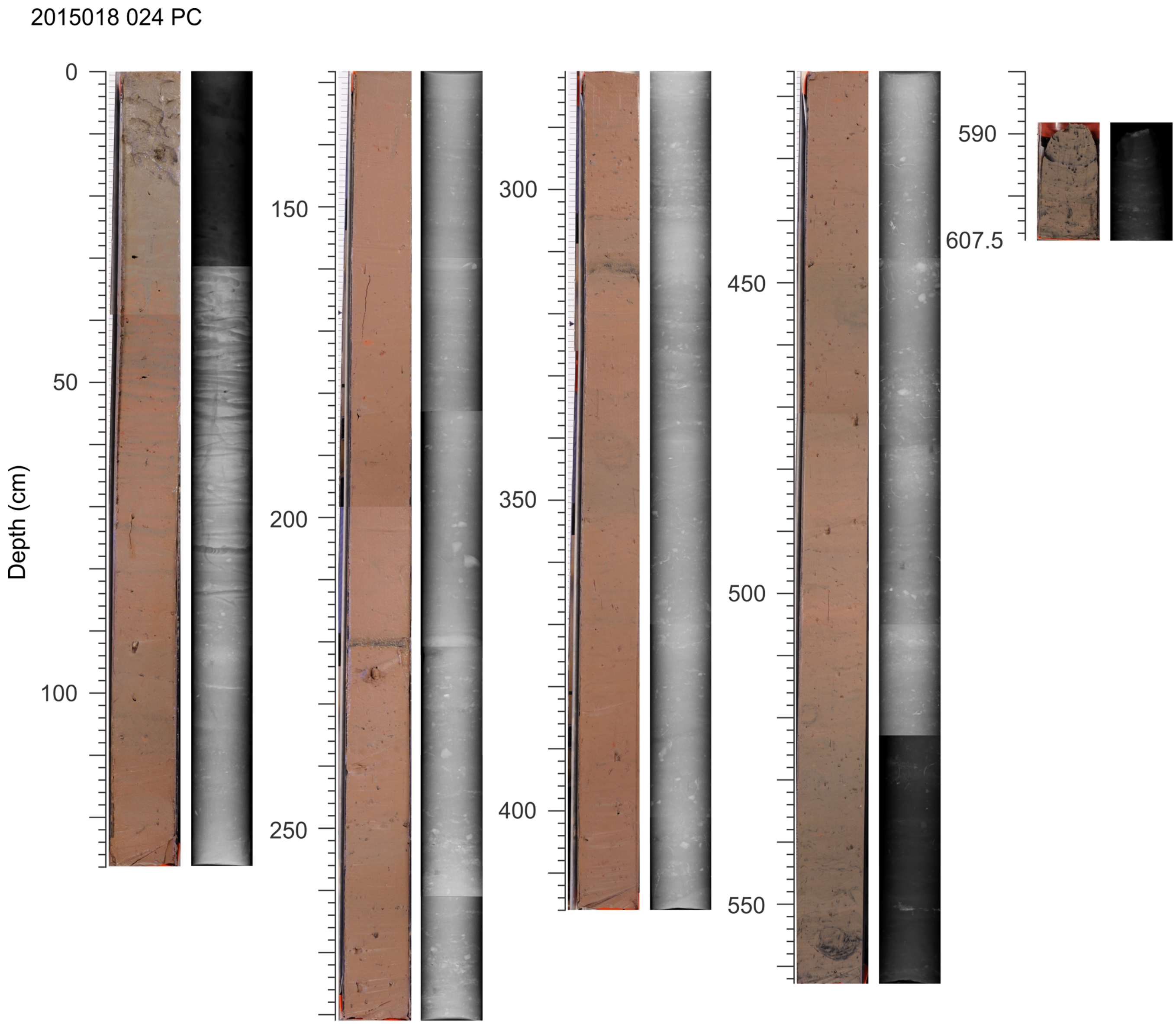

Figure 3.17a. Photography and X-radiography compilation for piston core 2015018 024.

2015018 024 TWC

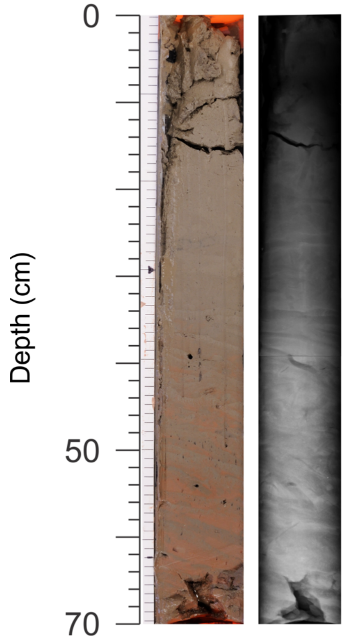

Figure 3.17b. Photography and X-radiography compilation for trigger weight core 2015018 024.

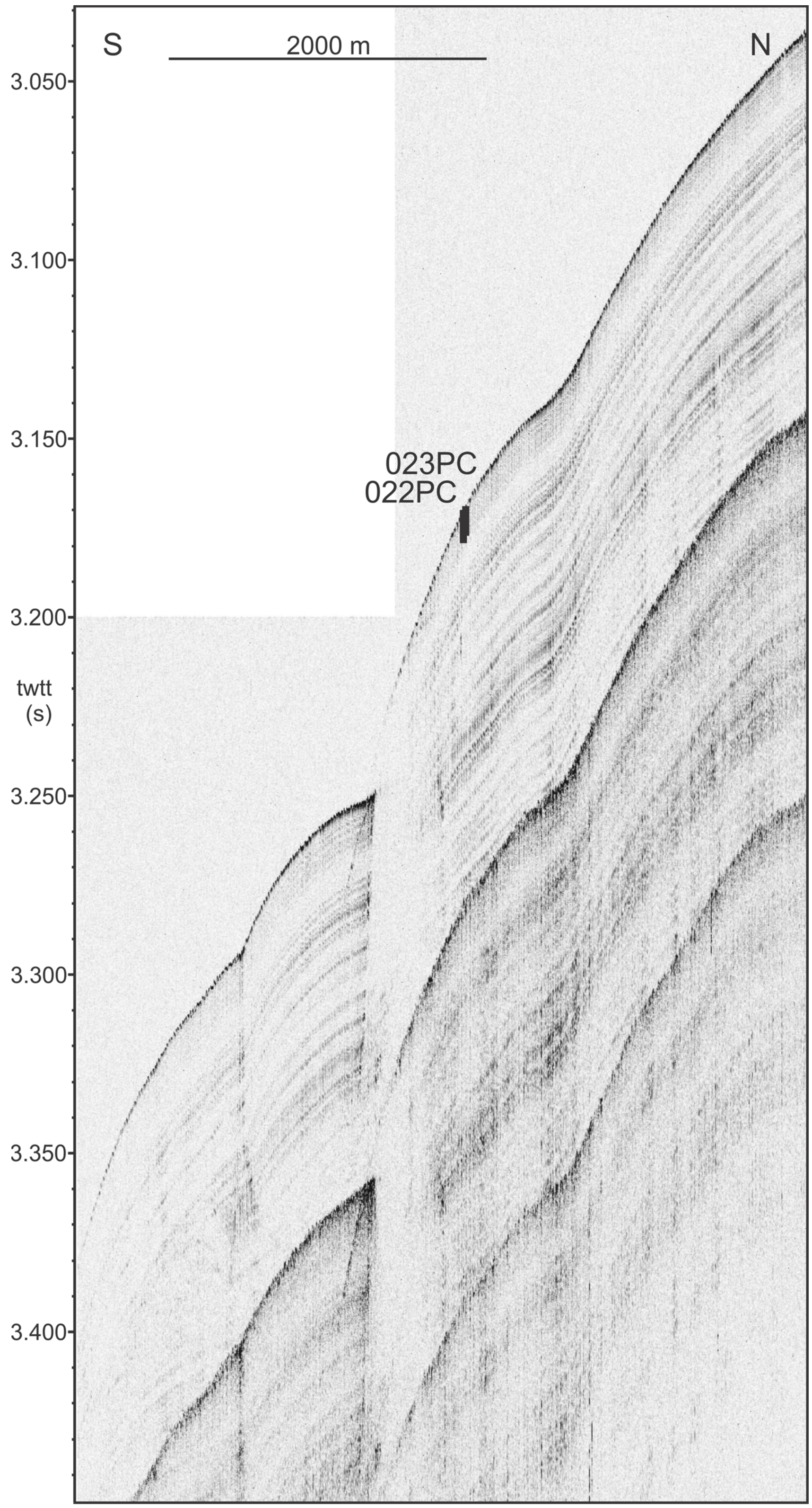

Figure 3.18. High resolution sub-bottom profile showing the acoustic stratigraphy and position of cores 2015018 022 and 2015018 023 (Campbell and MacDonald, 2016).

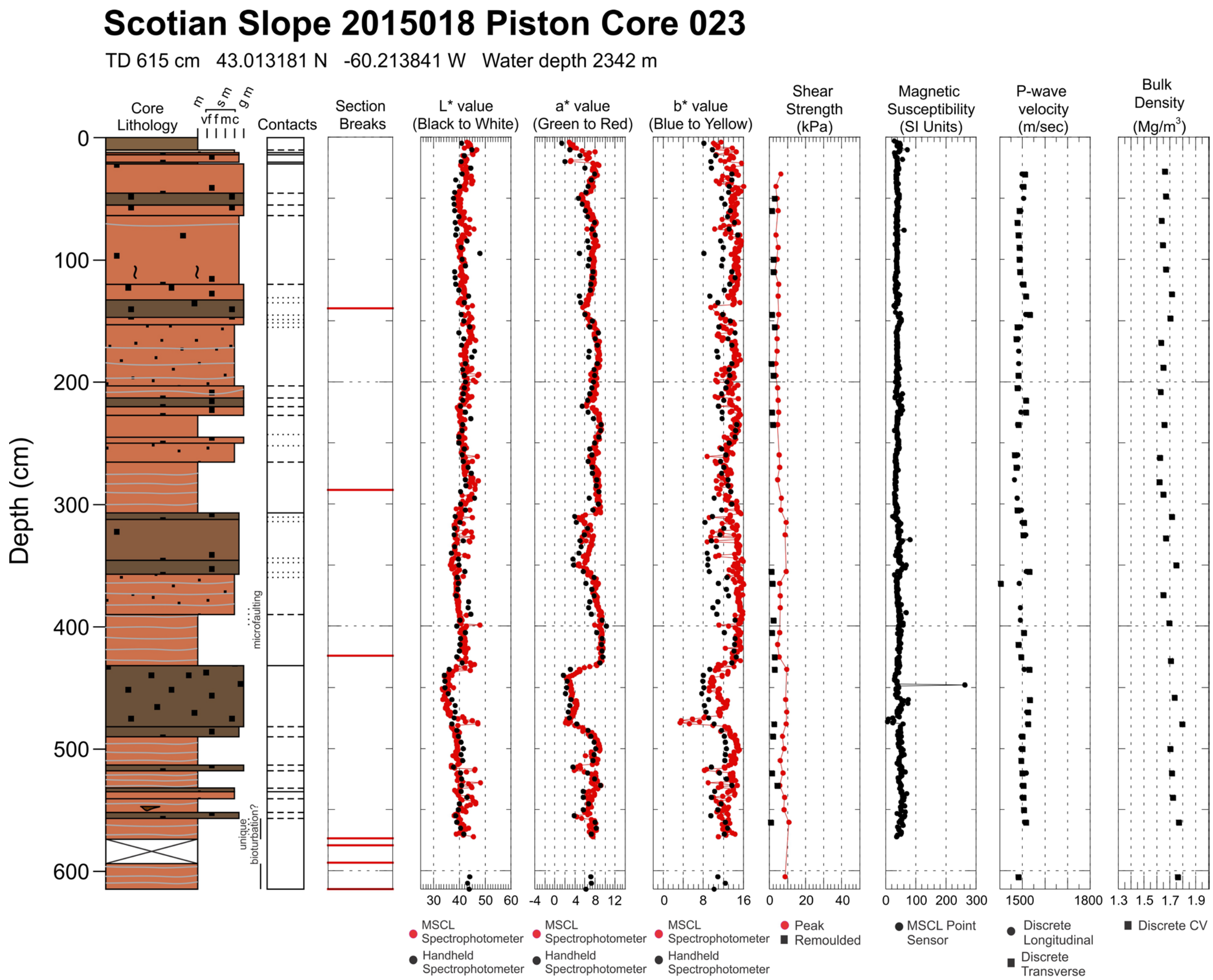

Figure 3.19a. Core plot summary for piston core 2015018 023.

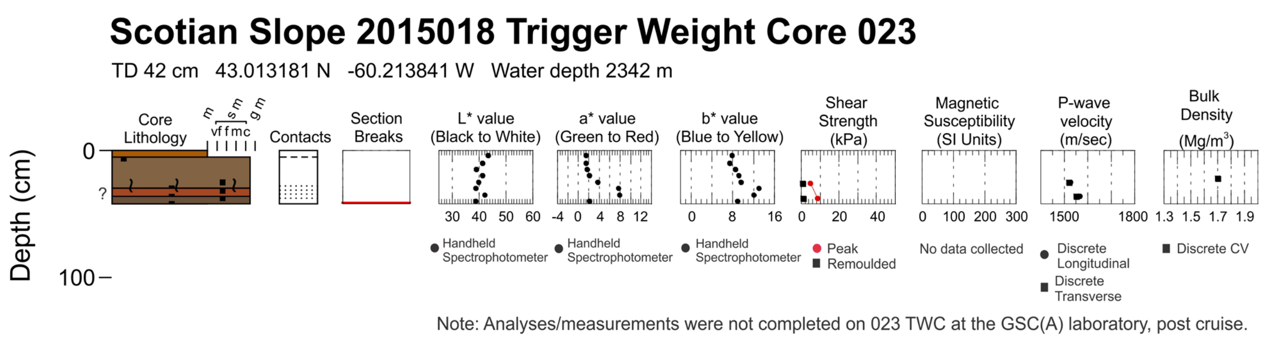

Figure 3.19b. Core plot summary for trigger weight core 2015018 023.

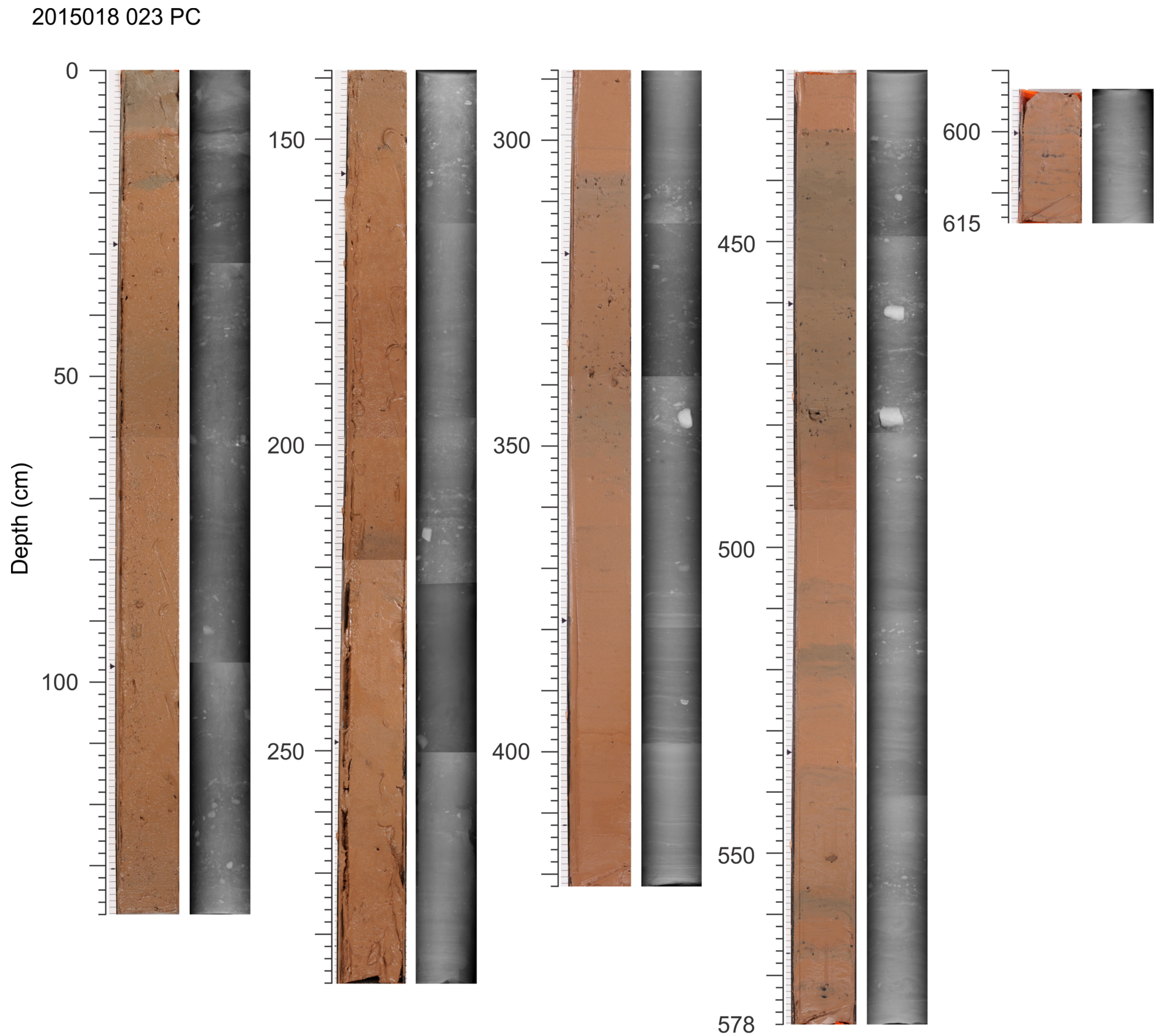

Figure 3.20a. Photography and X-radiography compilation for piston core 2015018 023.

2015018 023 TWC

Figure 3.20b. Photography and X-radiography compilation for trigger weight core 2015018 023.

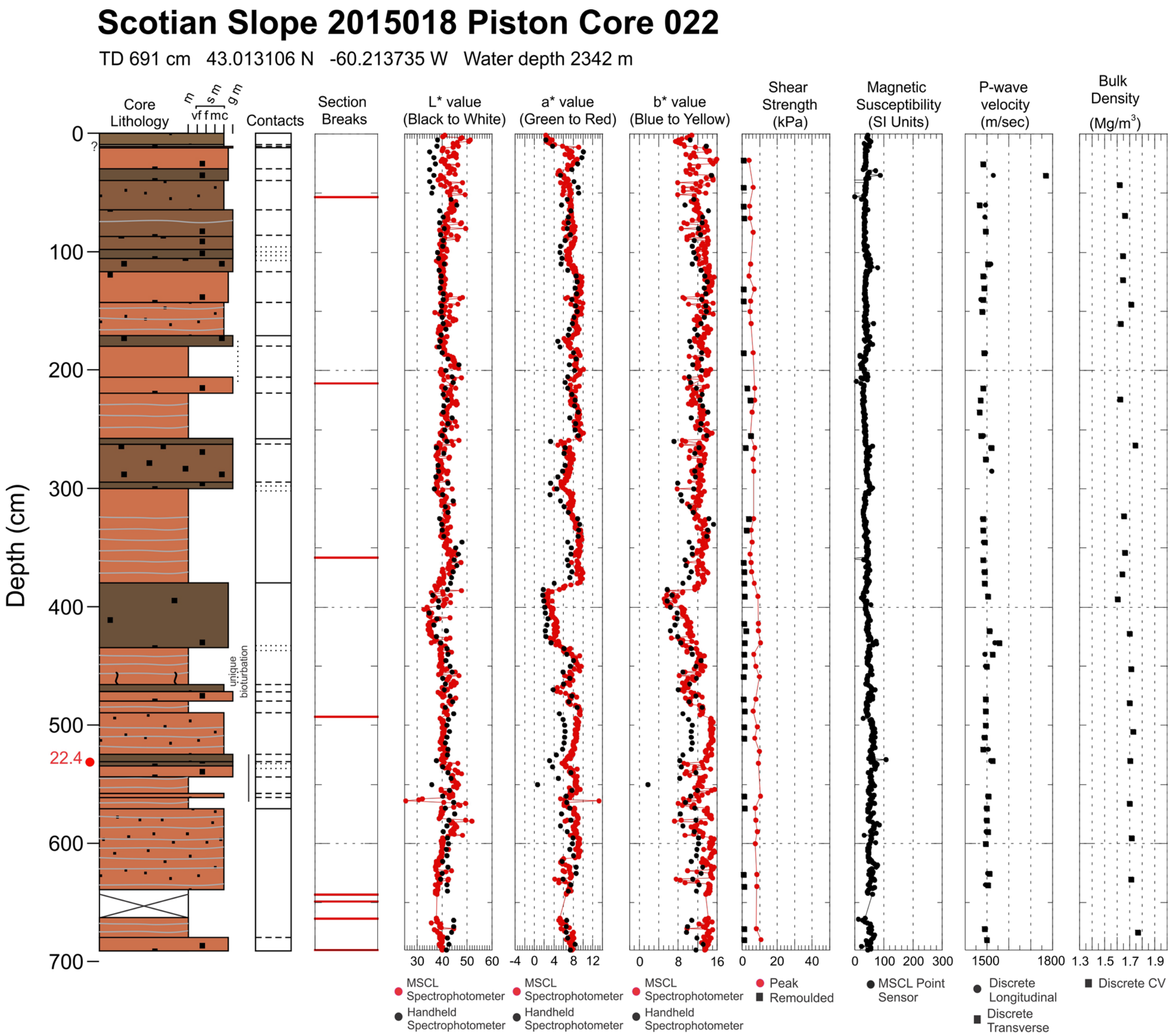

Figure 3.21a. Core plot summary for piston core 2015018 022.

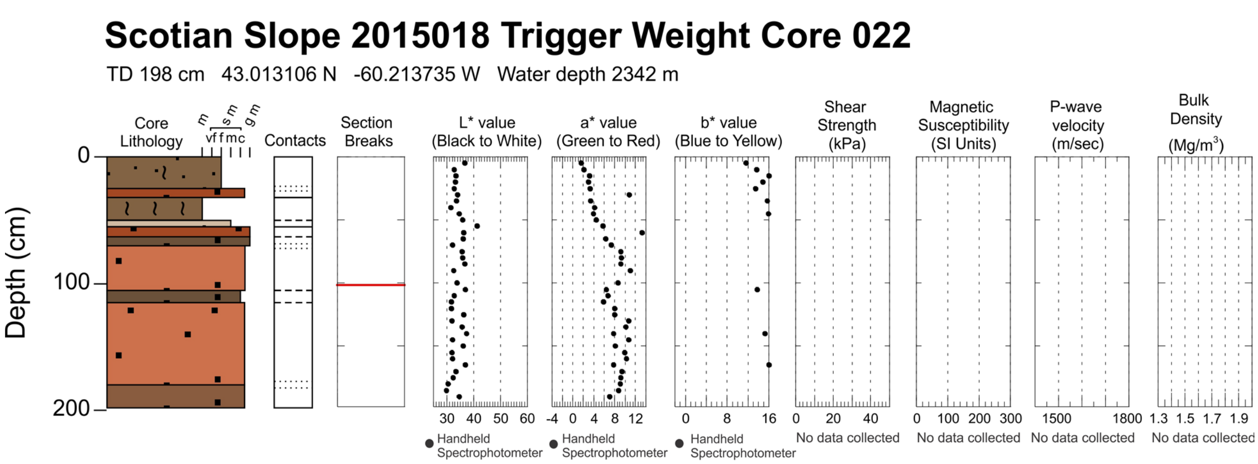

Note: 0-198 cm of 022 TWC was split on board and taken for geomicrobiology research at the University of Calgary. No X-radiography or additional GSC(A) analyses exist for this core.

Figure 3.21b. Core plot summary for trigger weight core 2015018 022.

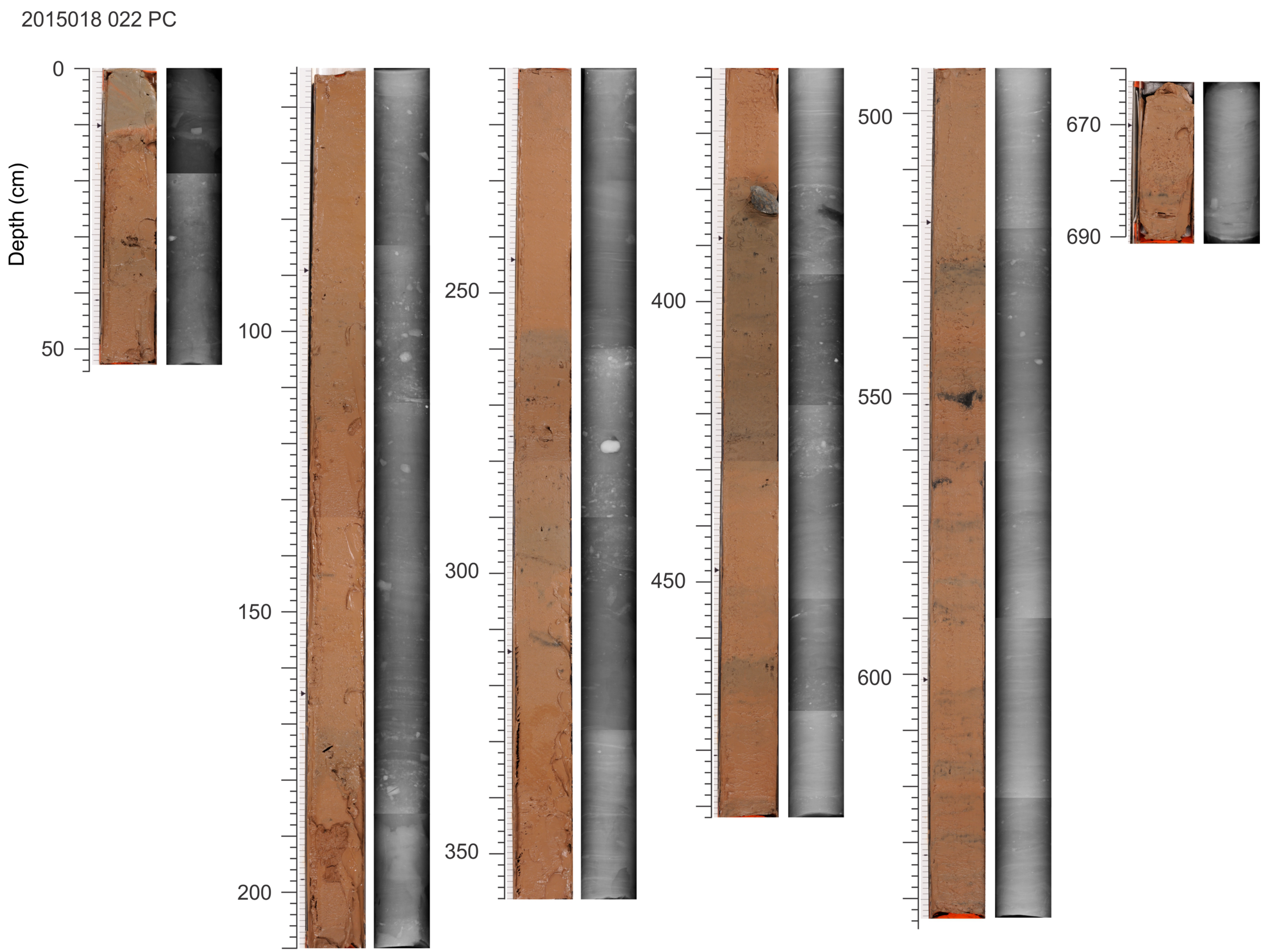

Figure 3.22a. Photography and X-radiography compilation for piston core 2015018 022.

2015018 022 TWC

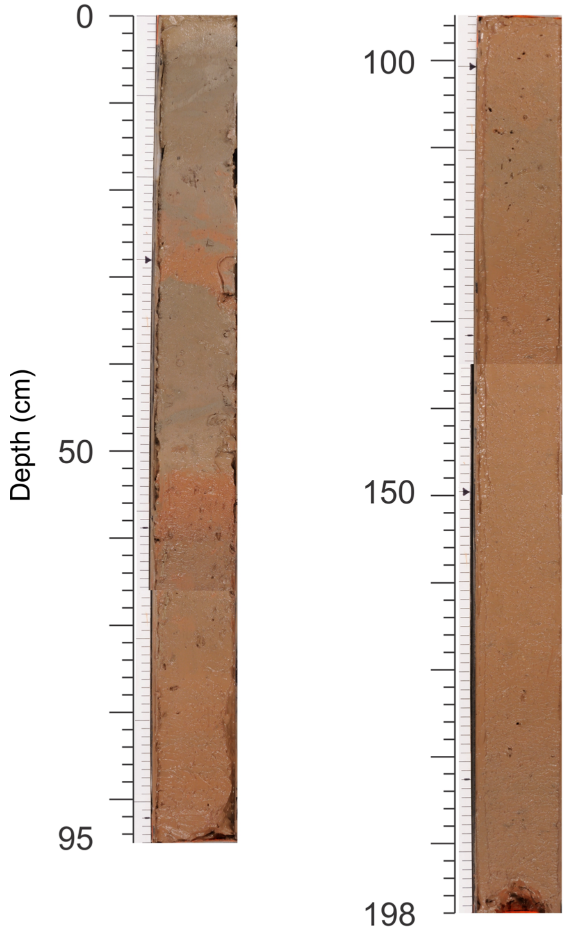

Note: 0-198 cm was taken for geomicrobiology research at the University of Calgary (no X-radiography).

Figure 3.22b. Photography compilation for trigger weight core 2015018 022.

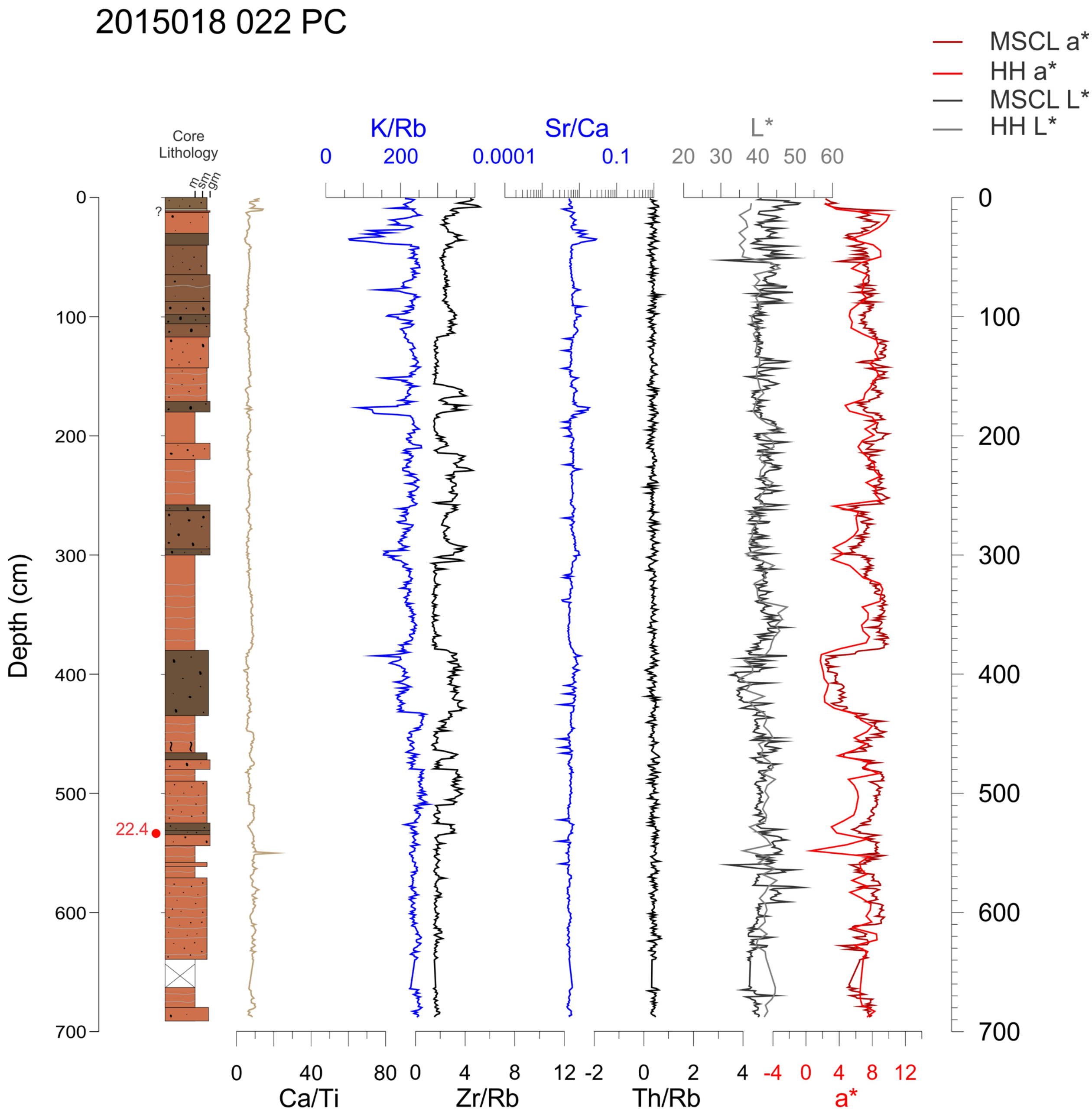

Figure 3.23. Down-core pXRF analyses for piston core 2015018 022. MSCL - Multi Sensor Core Logger; HH - handheld spectrophotometry.

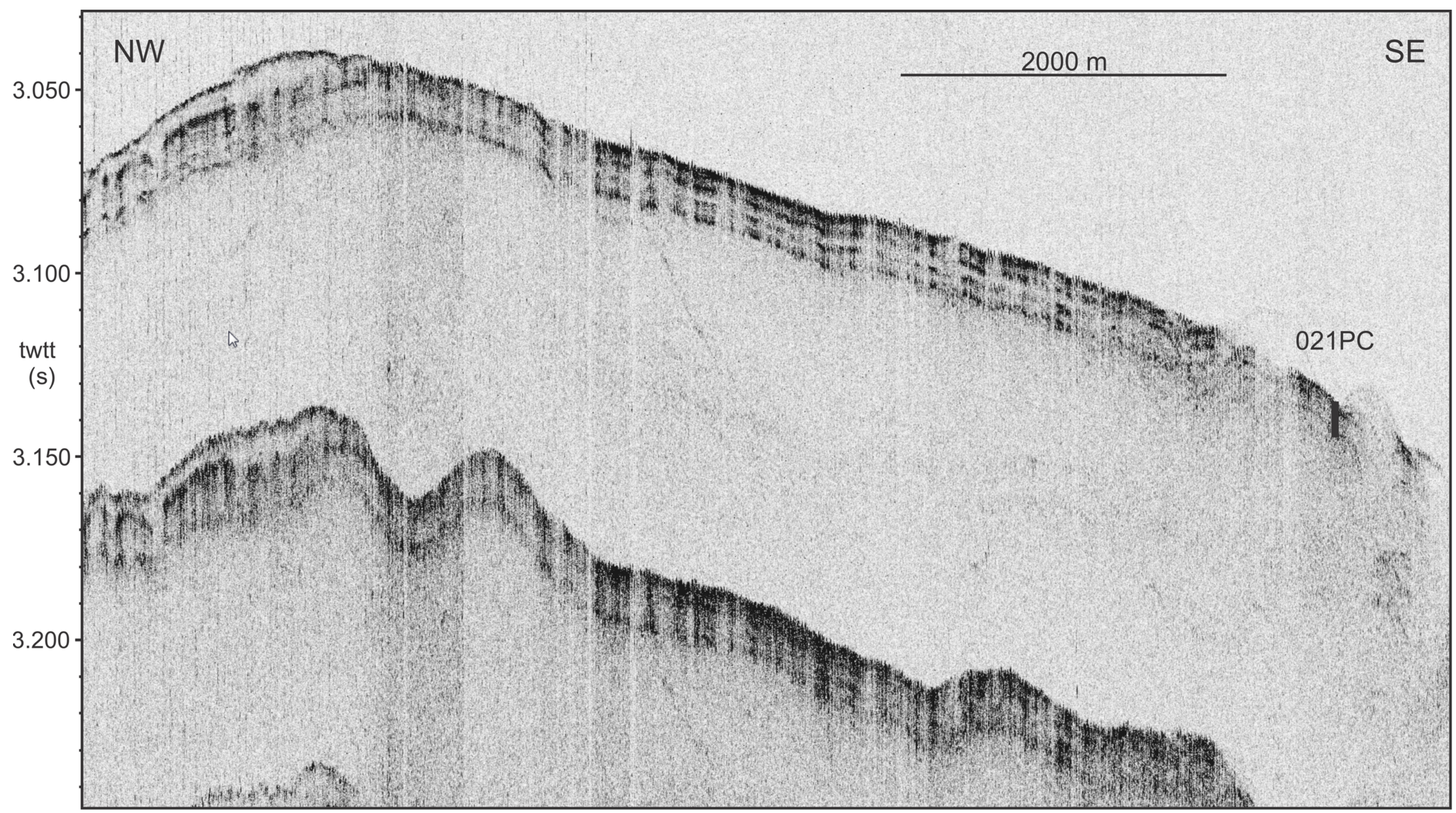

Figure 3.24. High resolution sub-bottom profile showing the acoustic stratigraphy and position of core 2015018 021 (Campbell and MacDonald, 2016).

Scotian Slope 2015018 Piston Core 021

TD 723.5 cm 43.080551 N -59.9134 W Water depth 2320 m

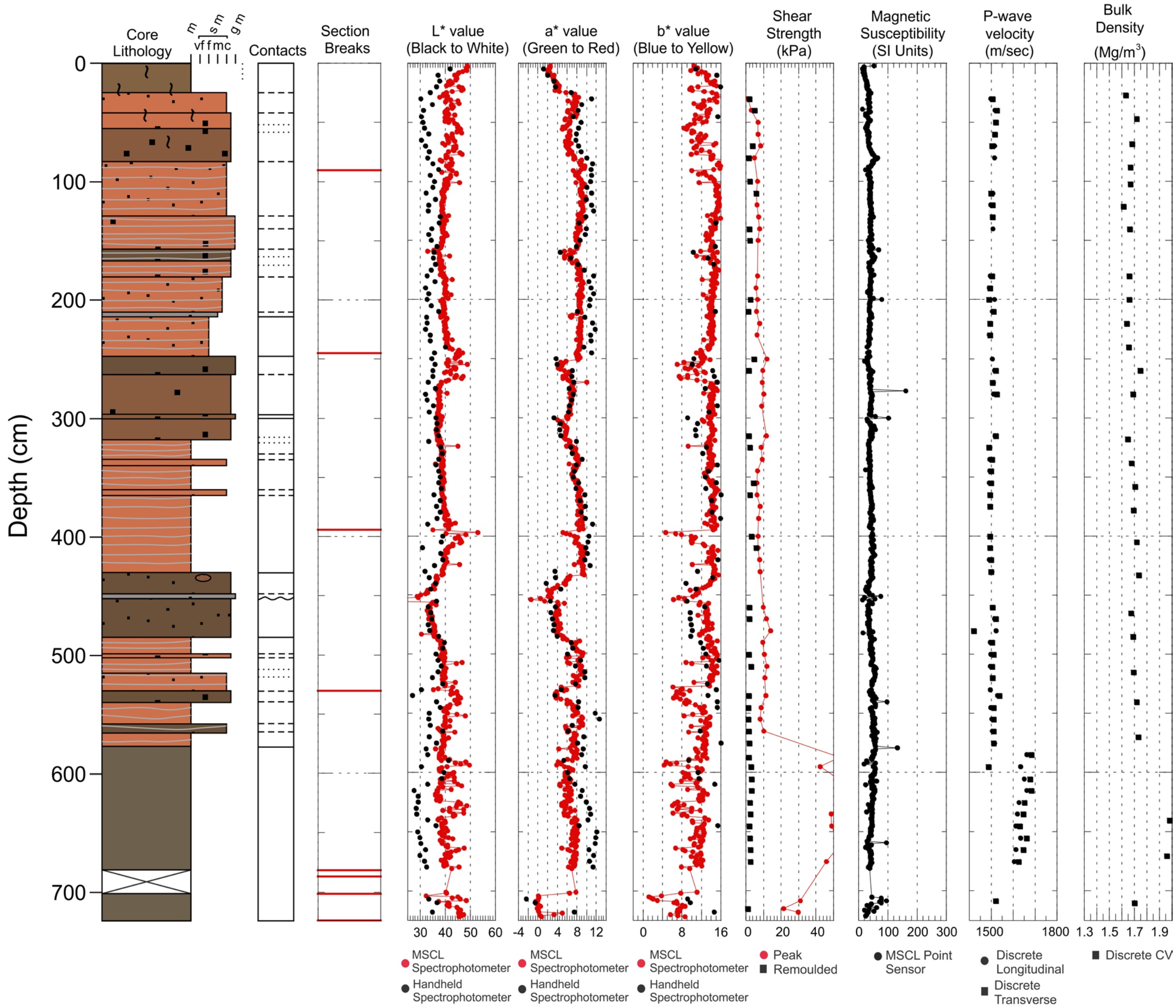

Figure 3.25a. Core plot summary for piston core 2015018 021.

Scotian Slope 2015018 Trigger Weight Core 021

TD 127 cm 43.080551 N -59.9134 W Water depth 2320 m

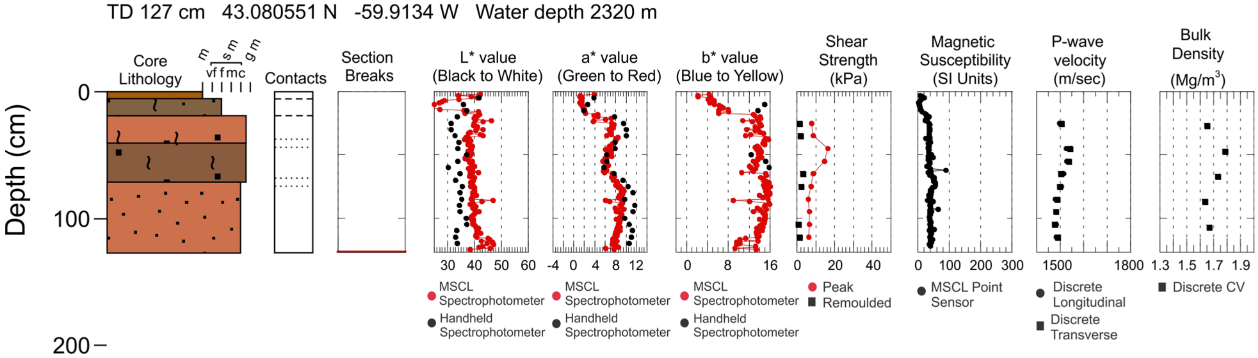

Figure 3.25b. Core plot summary for trigger weight core 2015018 021.

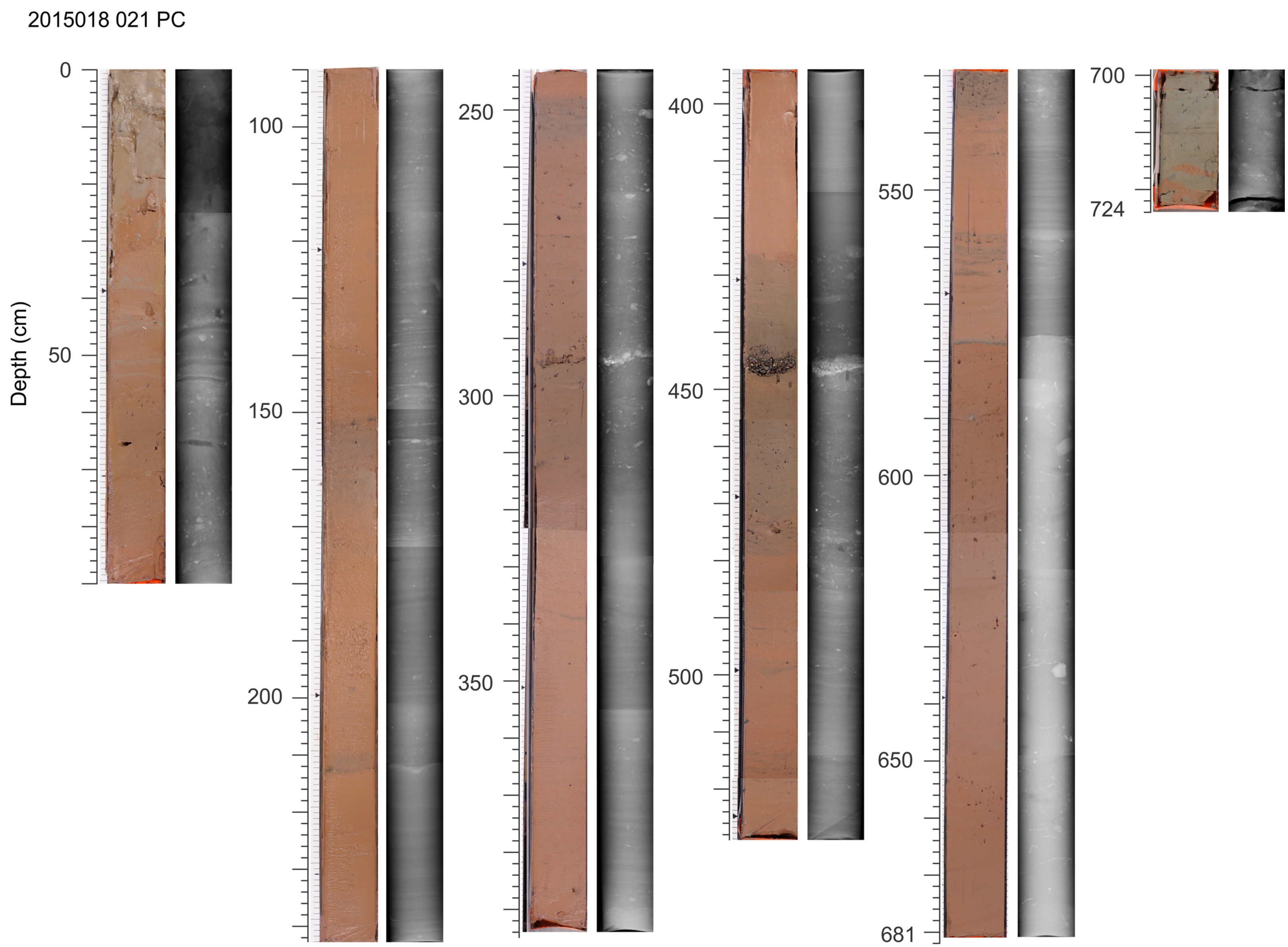

Figure 3.26a. Photography and X-radiography compilation for piston core 2015018 021.

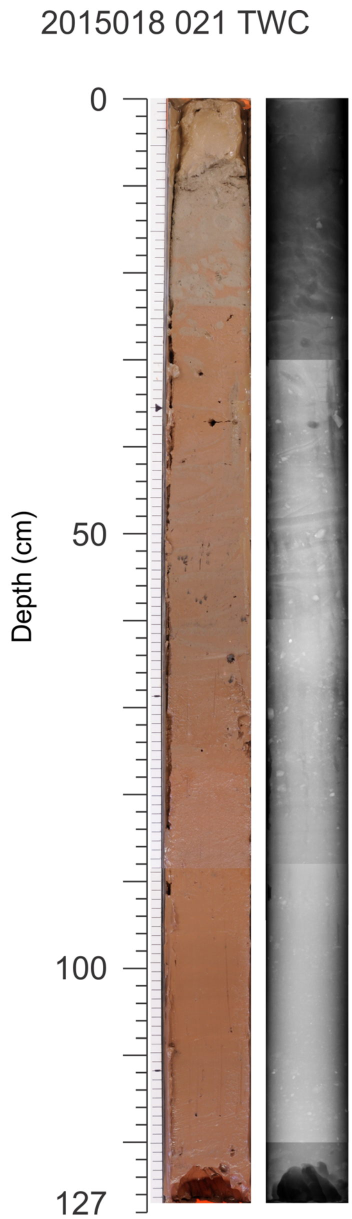

Figure 3.26b. Photography and X-radiography compilation for trigger weight core 2015018 021.

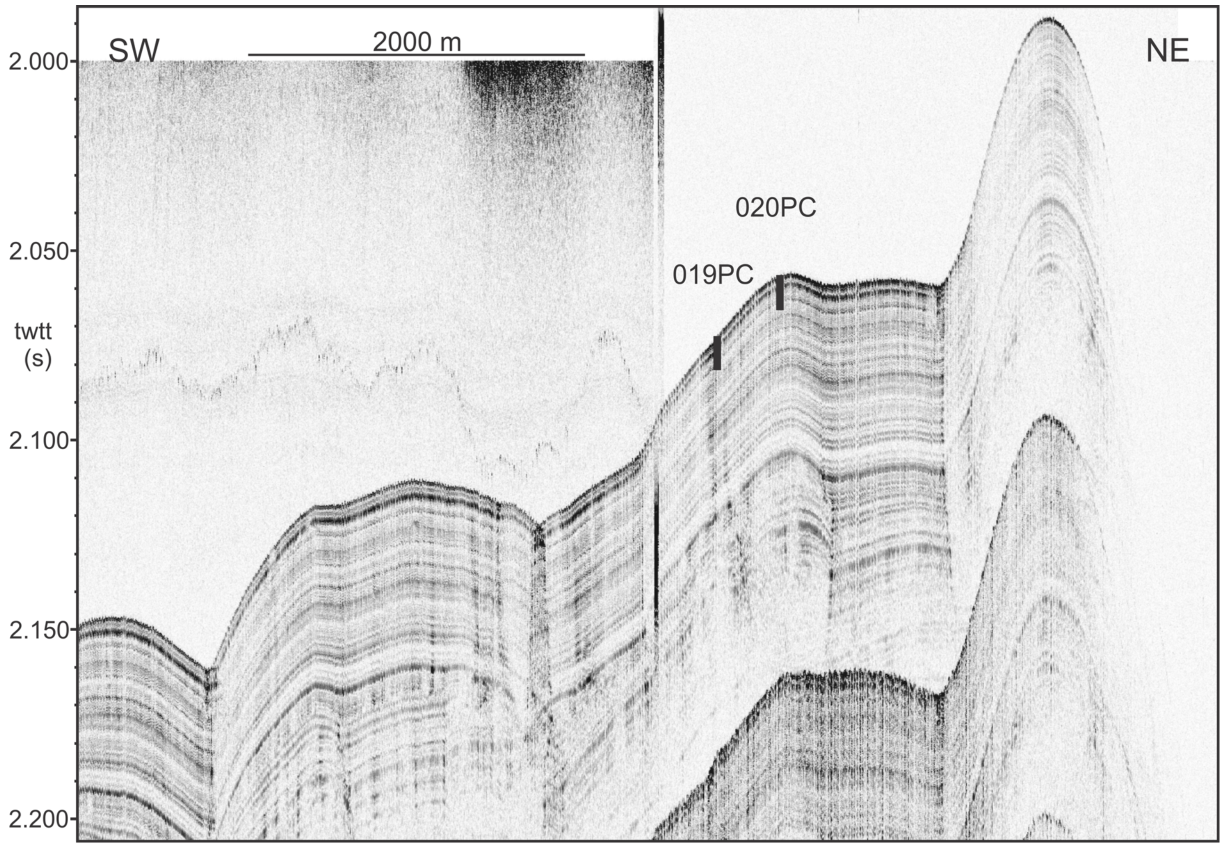

Figure 3.27. High resolution sub-bottom profile showing the acoustic stratigraphy and position of cores 2015018 019 and 2015018 020 (Campbell and MacDonald, 2016).

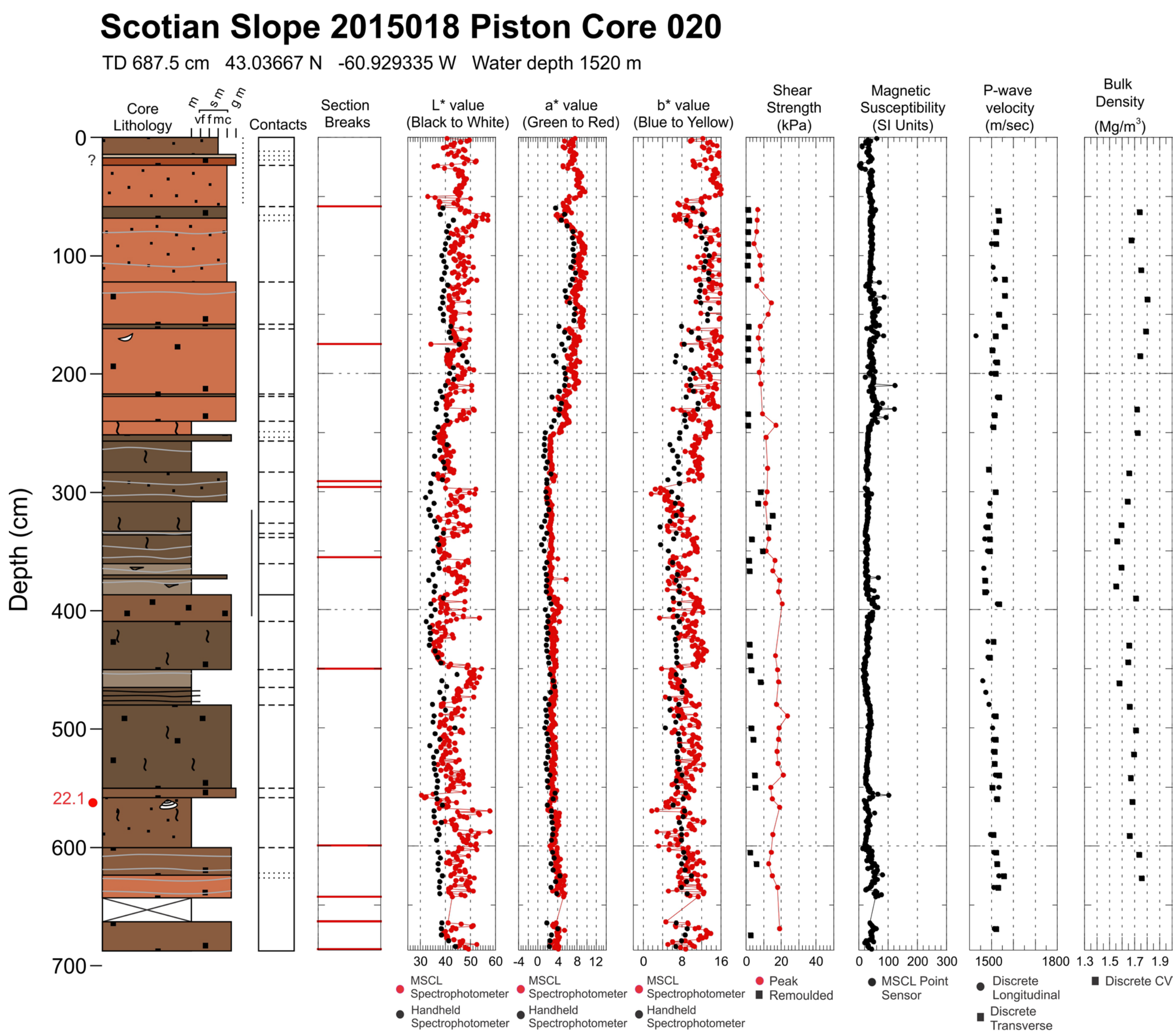

Figure 3.28a. Core plot summary for piston core 2015018 020.

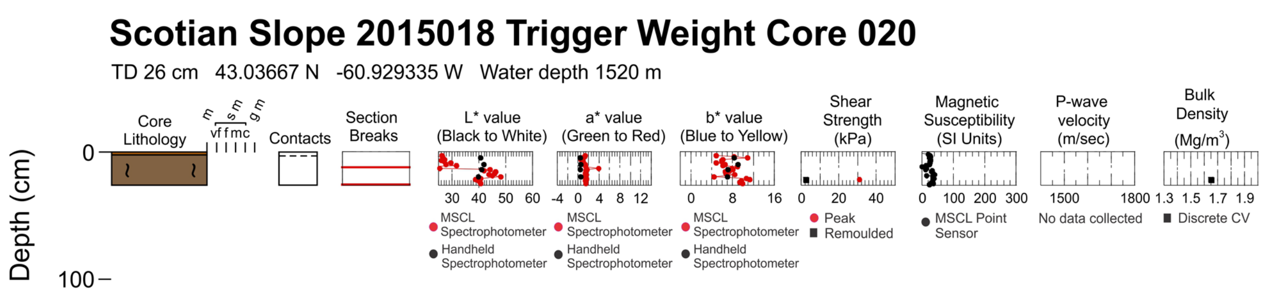

Figure 3.28b. Core plot summary for trigger weight core 2015018 020.

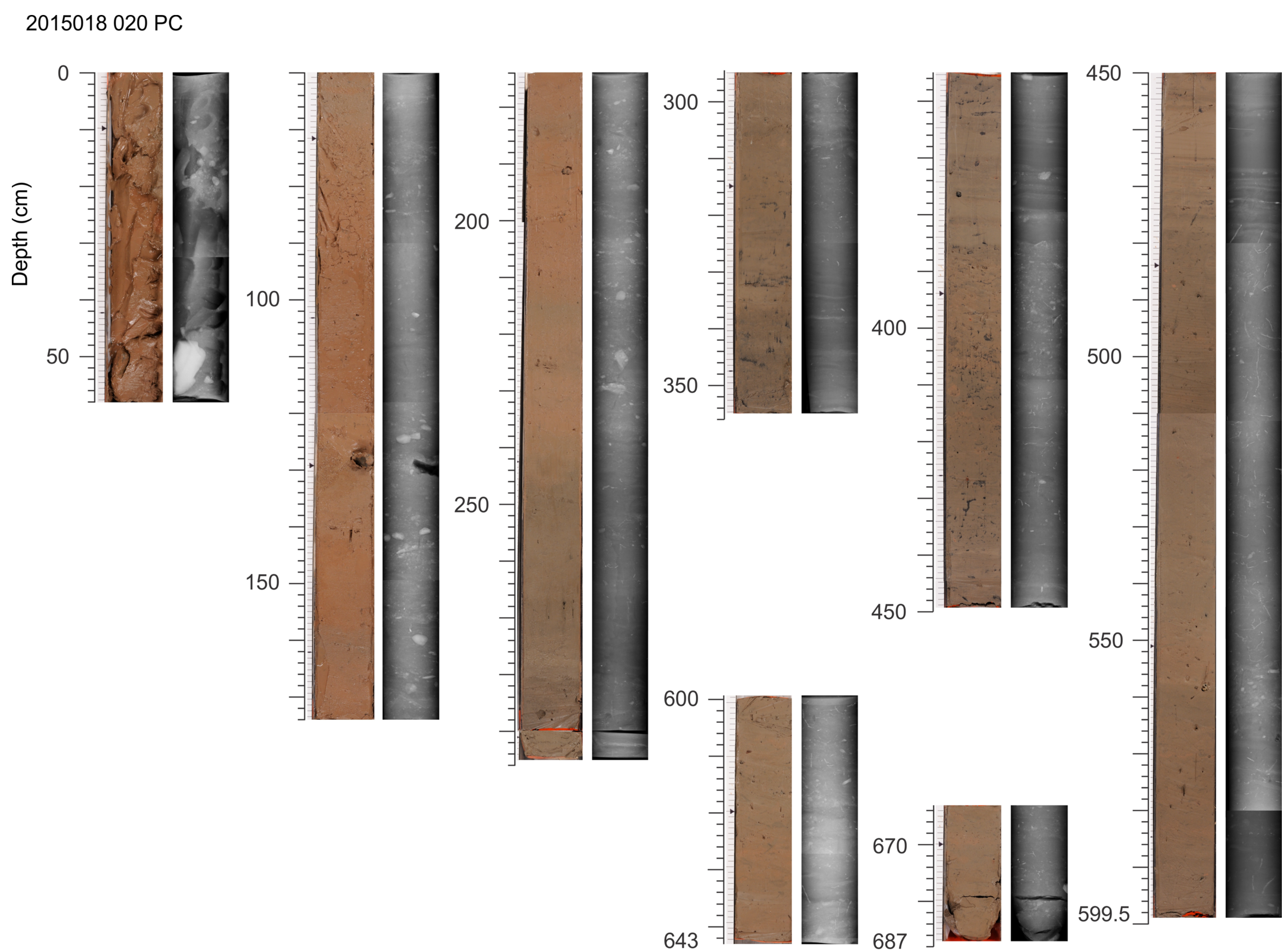

Figure 3.29a. Photography and X-radiography compilation for piston core 2015018 020.

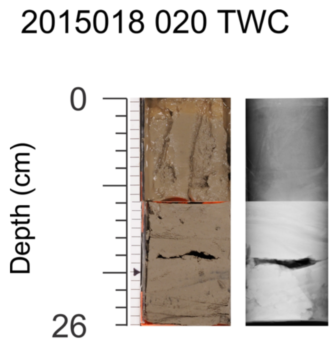

Figure 3.29b. Photography and X-radiography compilation for trigger weight core 2015018 020.

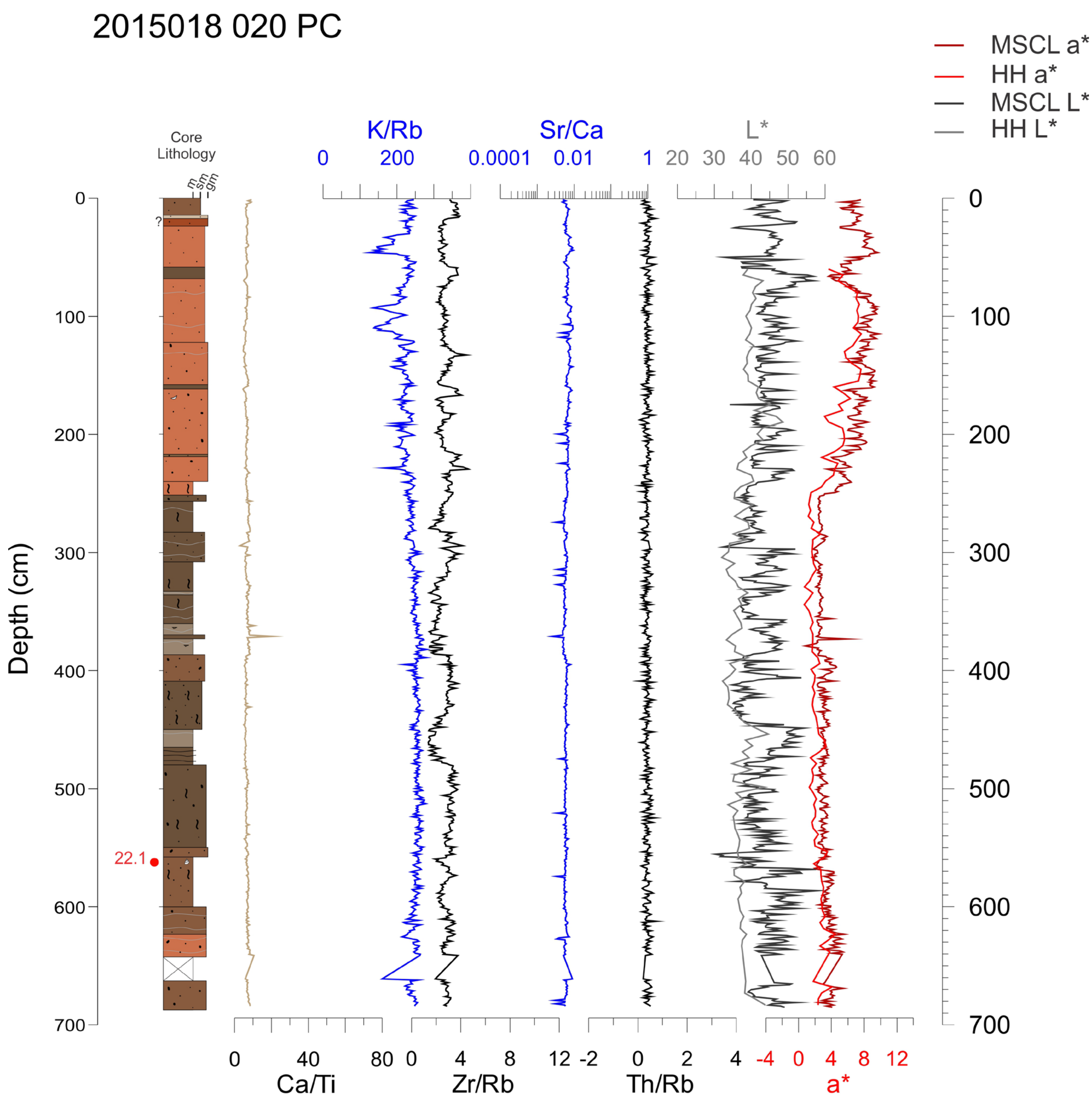

Figure 3.30 Down-core pXRF analyses for piston core 2015018 020. MSCL - Multi Sensor Core Logger; HH - handheld spectrophotometry.

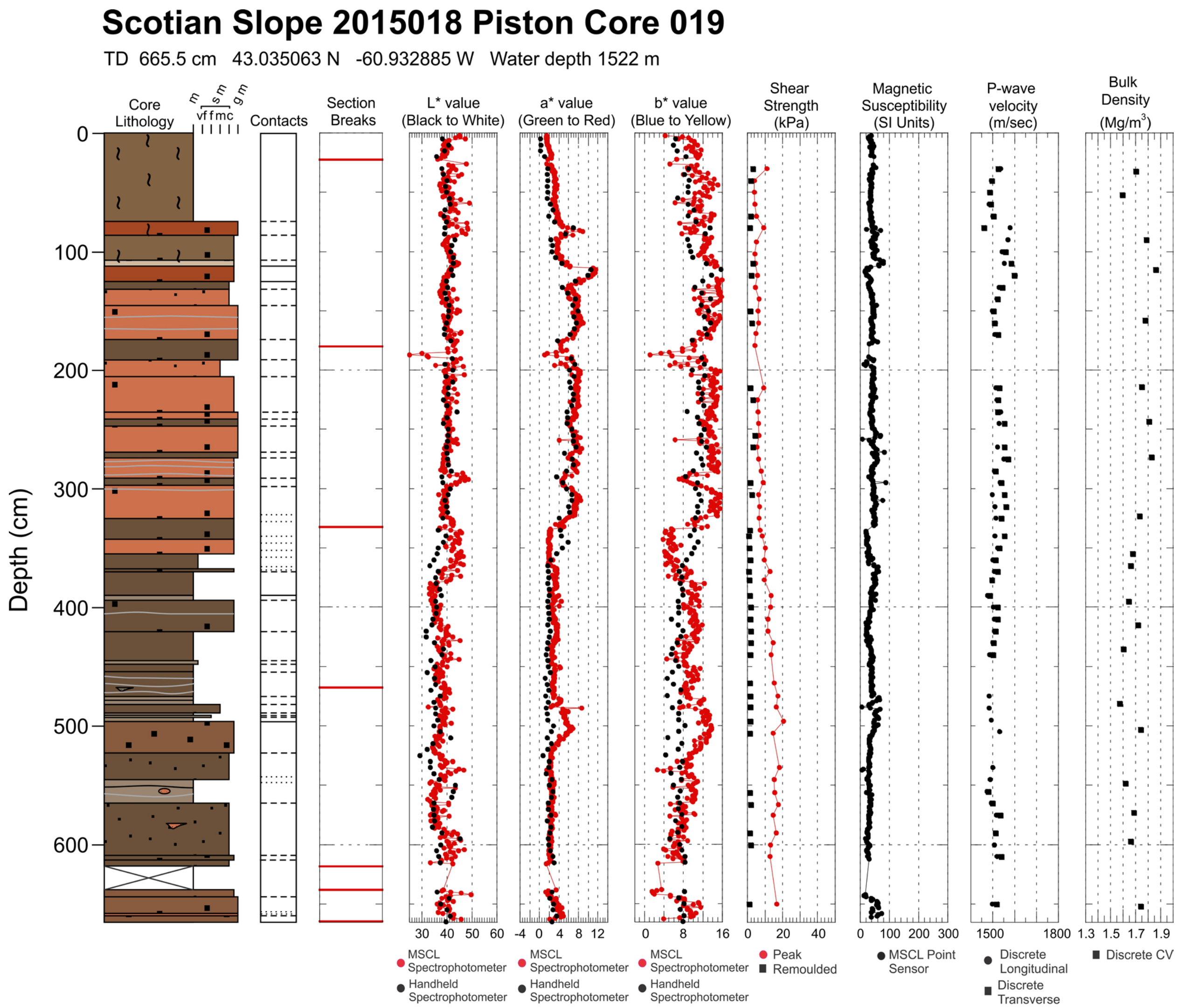

Figure 3.31a. Core plot summary for piston core 2015018 019.

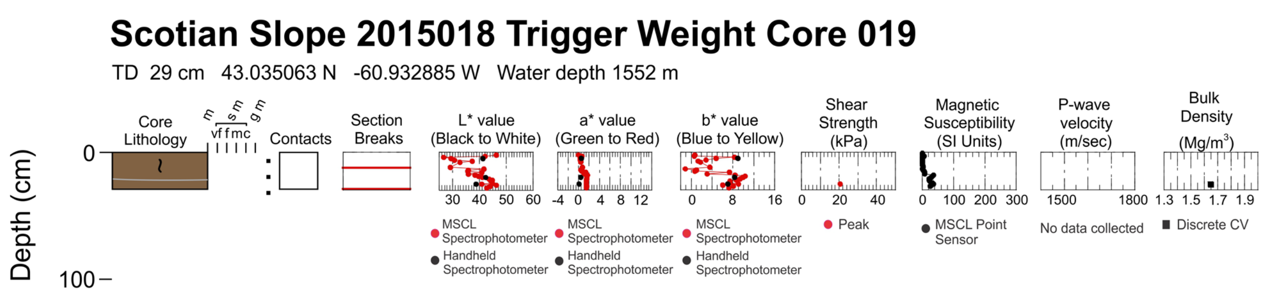

Figure 3.31b. Core plot summary for trigger weight core 2015018 019.

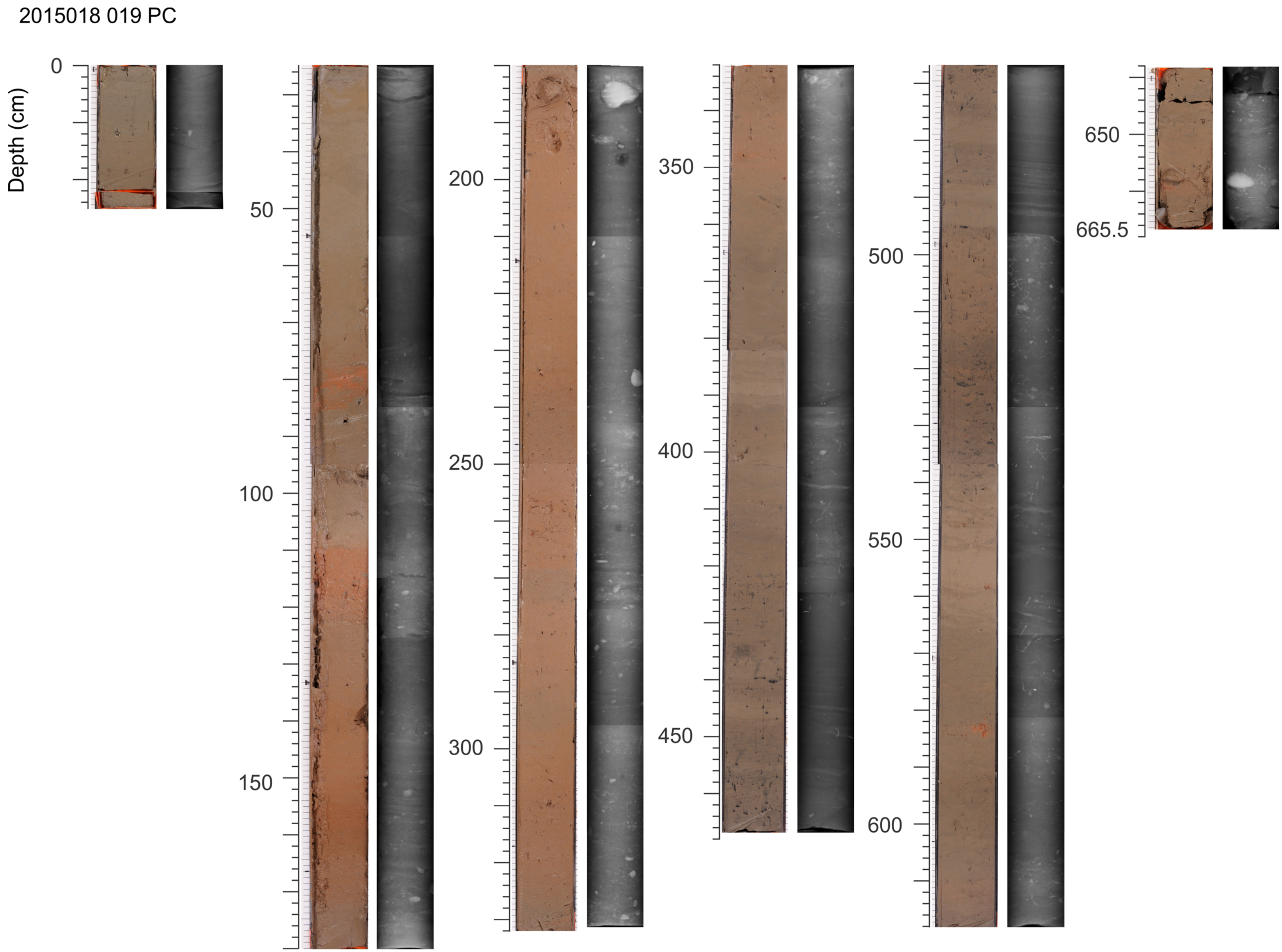

Figure 3.32a. Photography and X-radiography compilation for piston core 2015018 019.

2015018 019 TWC

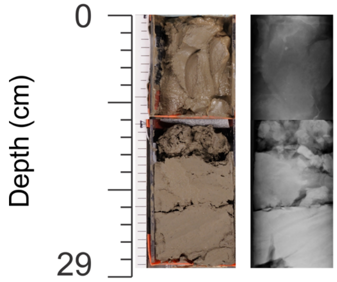

Figure 3.32b. Photography and X-radiography compilation for trigger weight core 2015018 019.

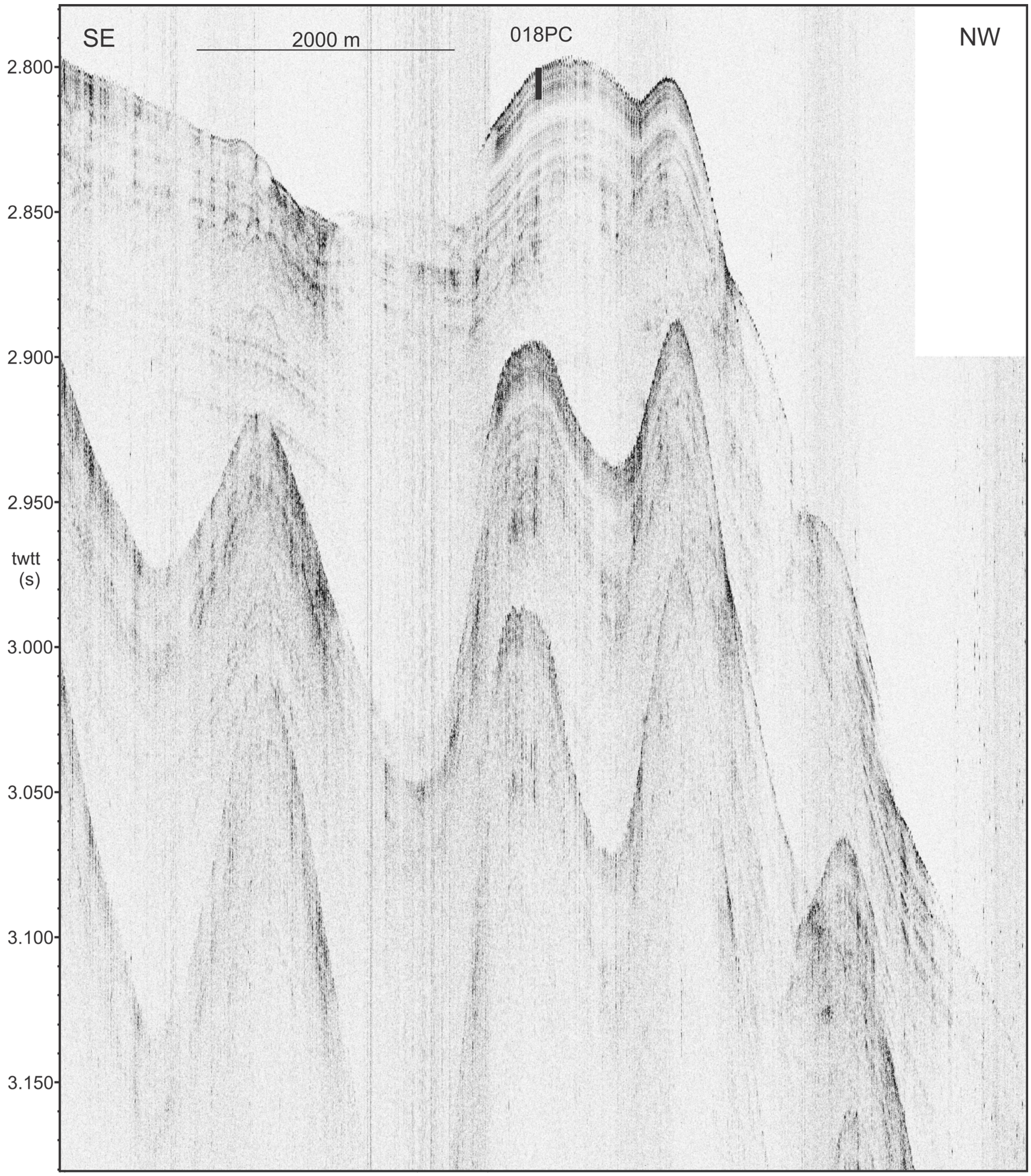

Figure 3.33. High resolution sub-bottom profile showing the acoustic stratigraphy and position of core 2015018 018 (Campbell and MacDonald, 2016).

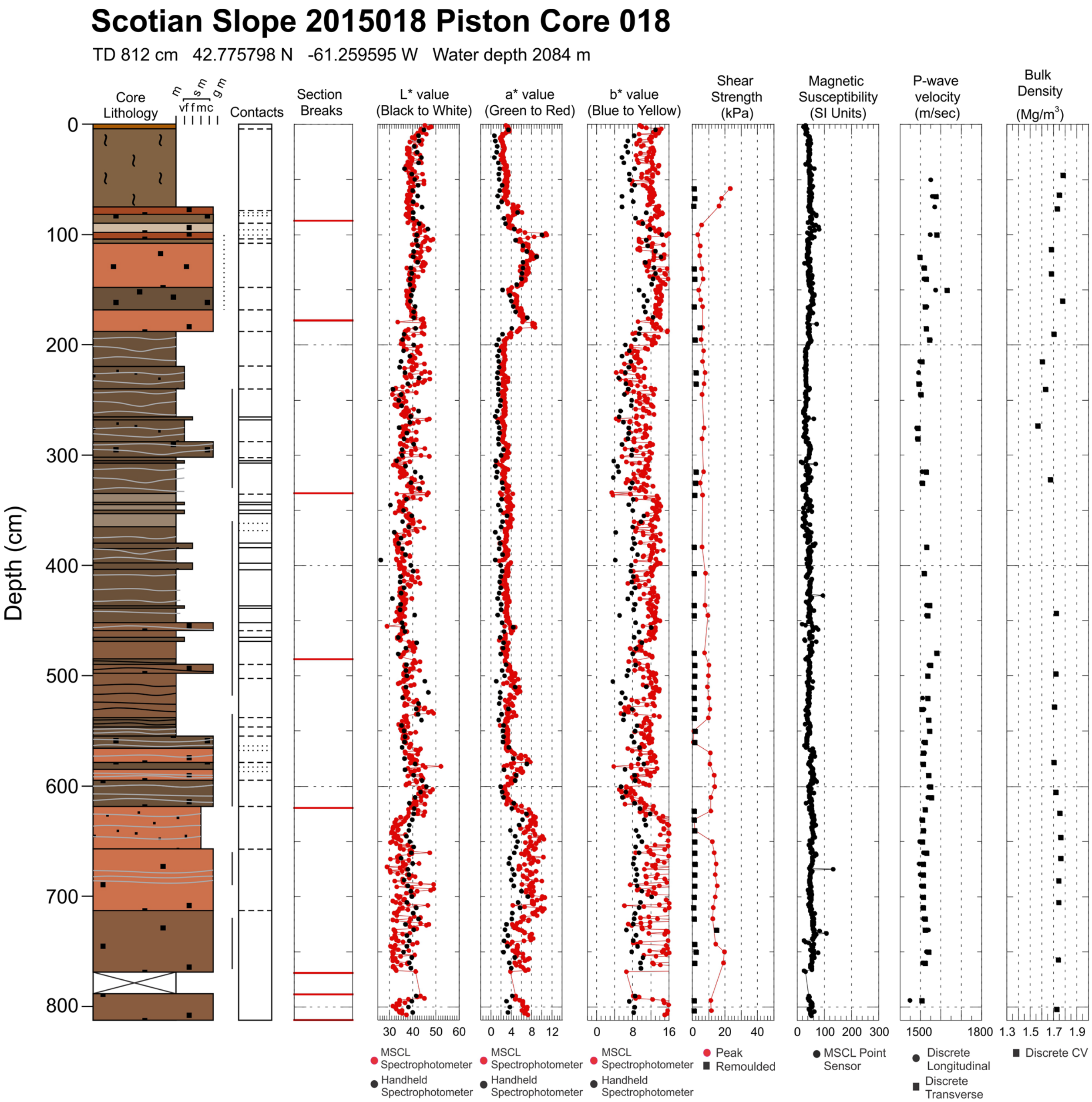

Figure 3.34a. Core plot summary for piston core 2015018 018.

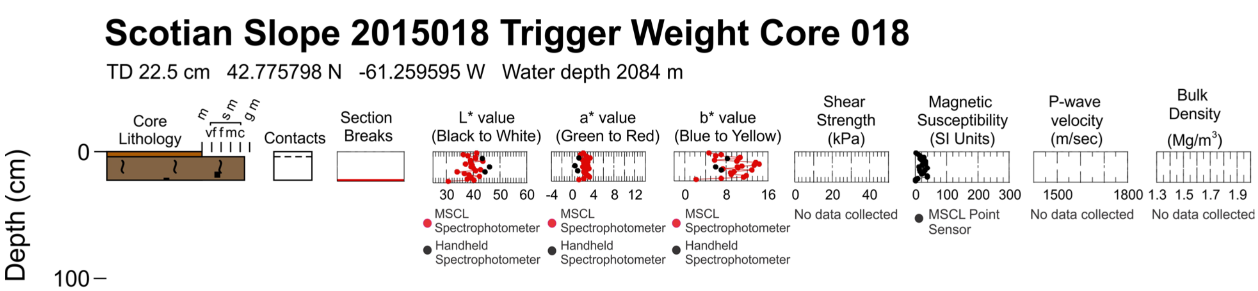

Figure 3.34b. Core plot summary for trigger weight core 2015018 018.

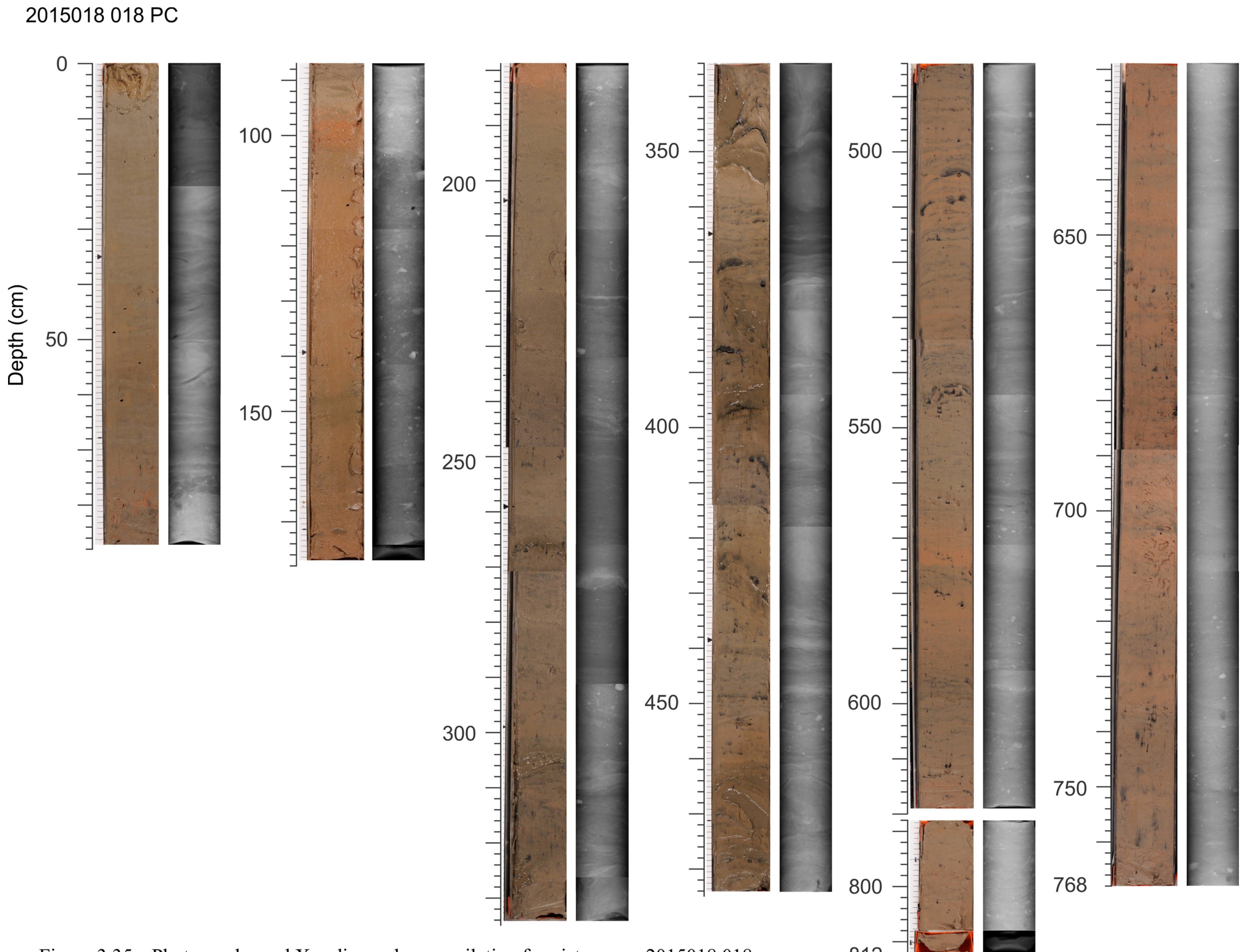

Figure 3.35a. Photography and X-radiography compilation for piston core 2015018 018.

2015018 018 TWC

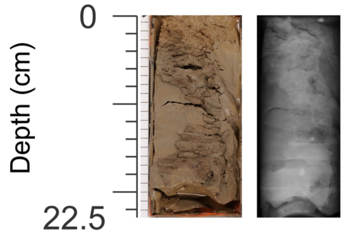

Figure 3.35b. Photography and X-radiography compilation for trigger weight core 2015018 018.

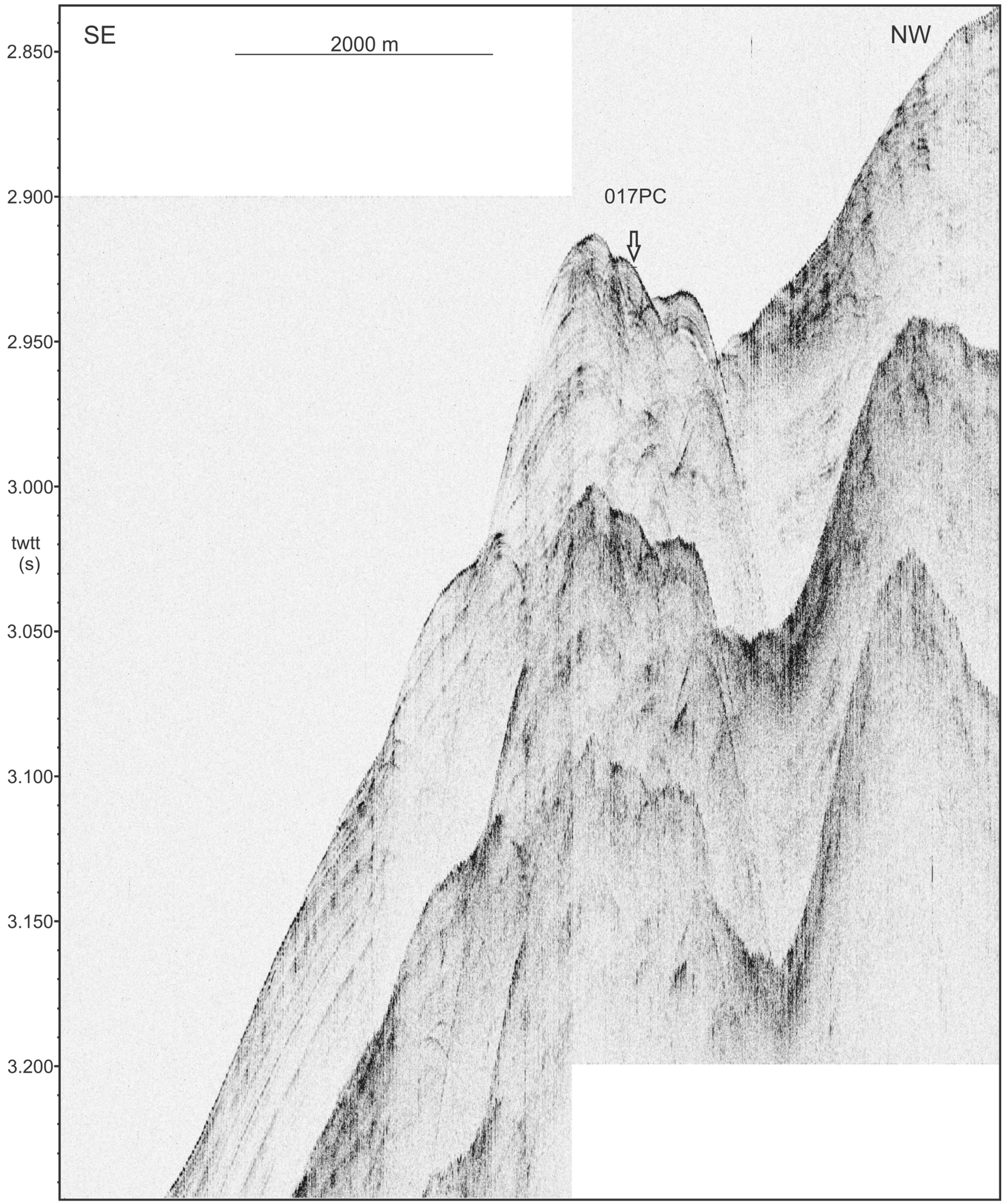

Figure 3.36. High resolution sub-bottom profile showing the acoustic stratigraphy and position of core 2015018 017 (Campbell and MacDonald, 2016).

Scotian Slope 2015018 Piston Core 017

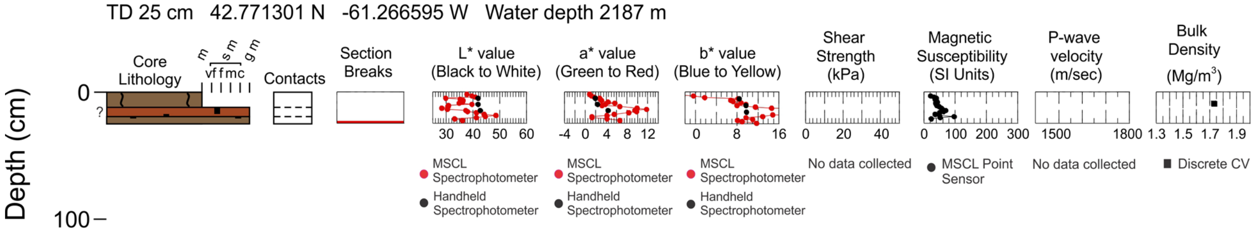

Figure 3.37a. Core plot summary for piston core 2015018 017.

Scotian Slope 2015018 Trigger Weight Core 017

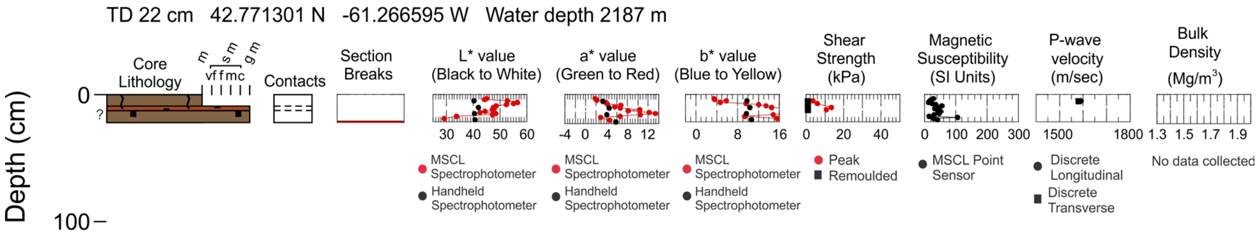

Figure 3.37b. Core plot summary for trigger weight core 2015018 017.

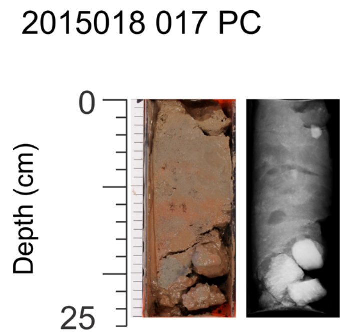

Figure 3.38a. Photography and X-radiography compilation for piston core 2015018 017.

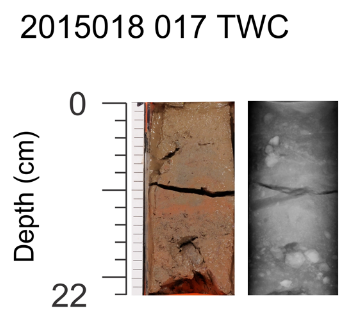

Figure 3.38b. Photography and X-radiography compilation for trigger weight core 2015018 017.

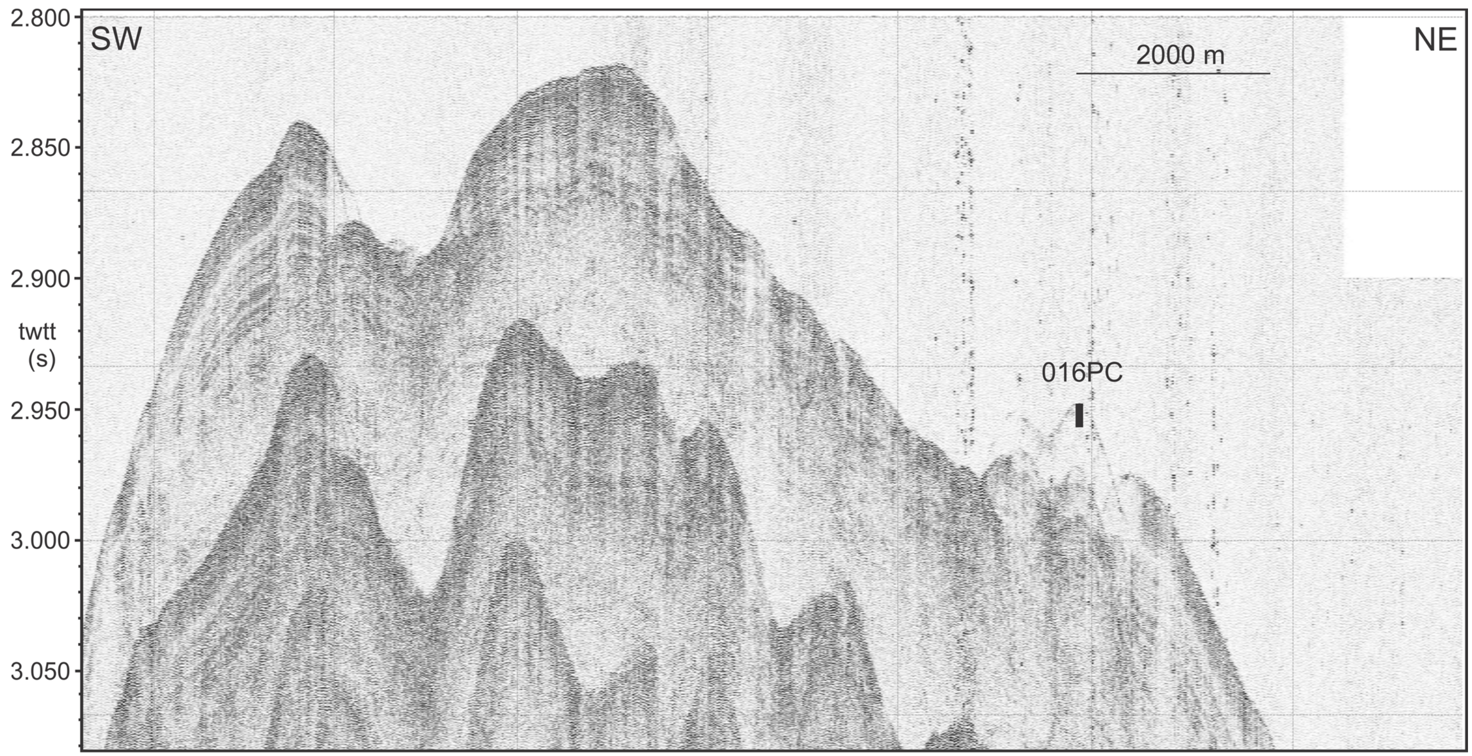

Figure 3.39. High resolution sub-bottom profile showing the acoustic stratigraphy and position of core 2015018 016 (Campbell and MacDonald, 2016).

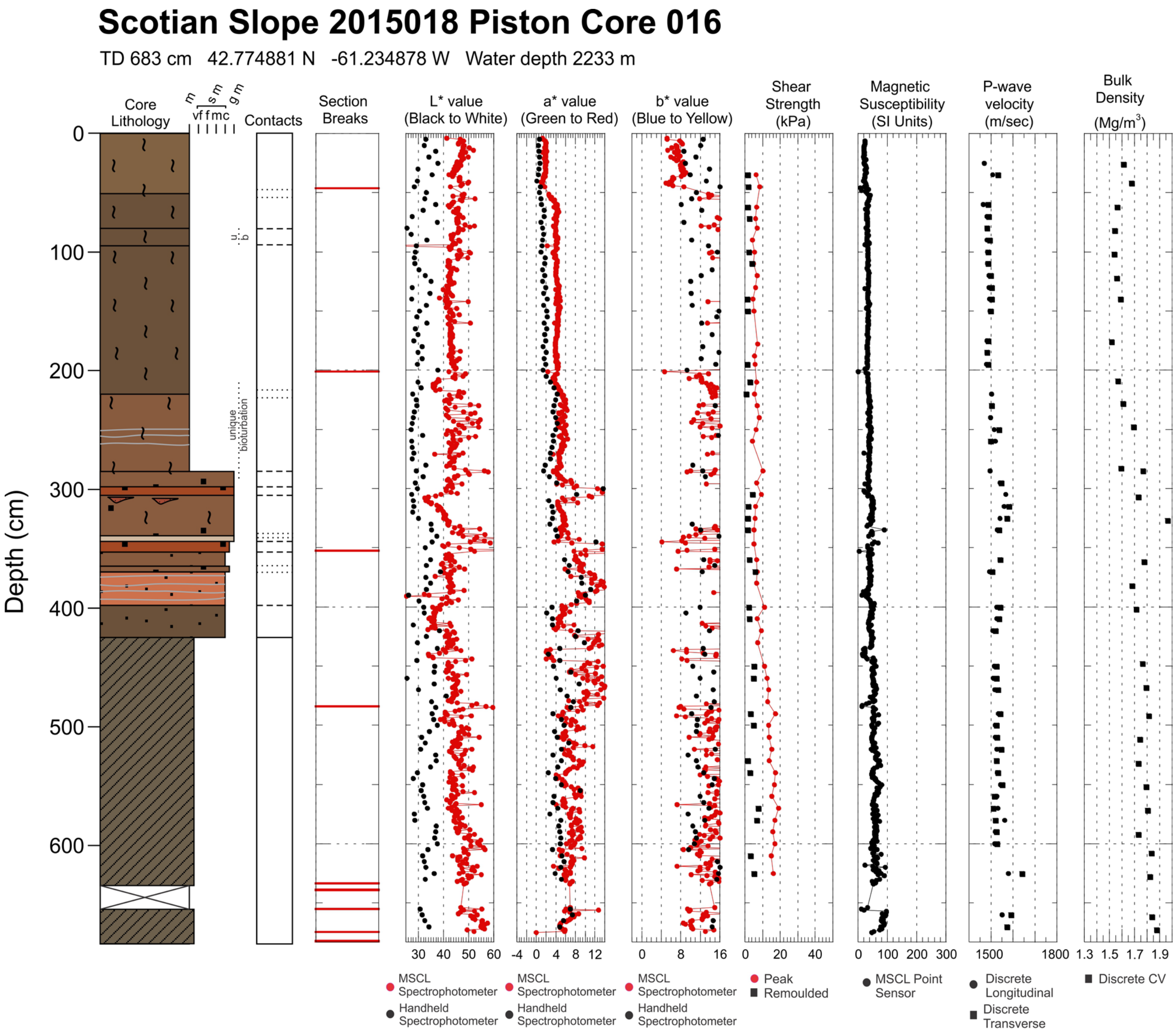

Figure 3.40. Core plot summary for piston core 2015018 016.

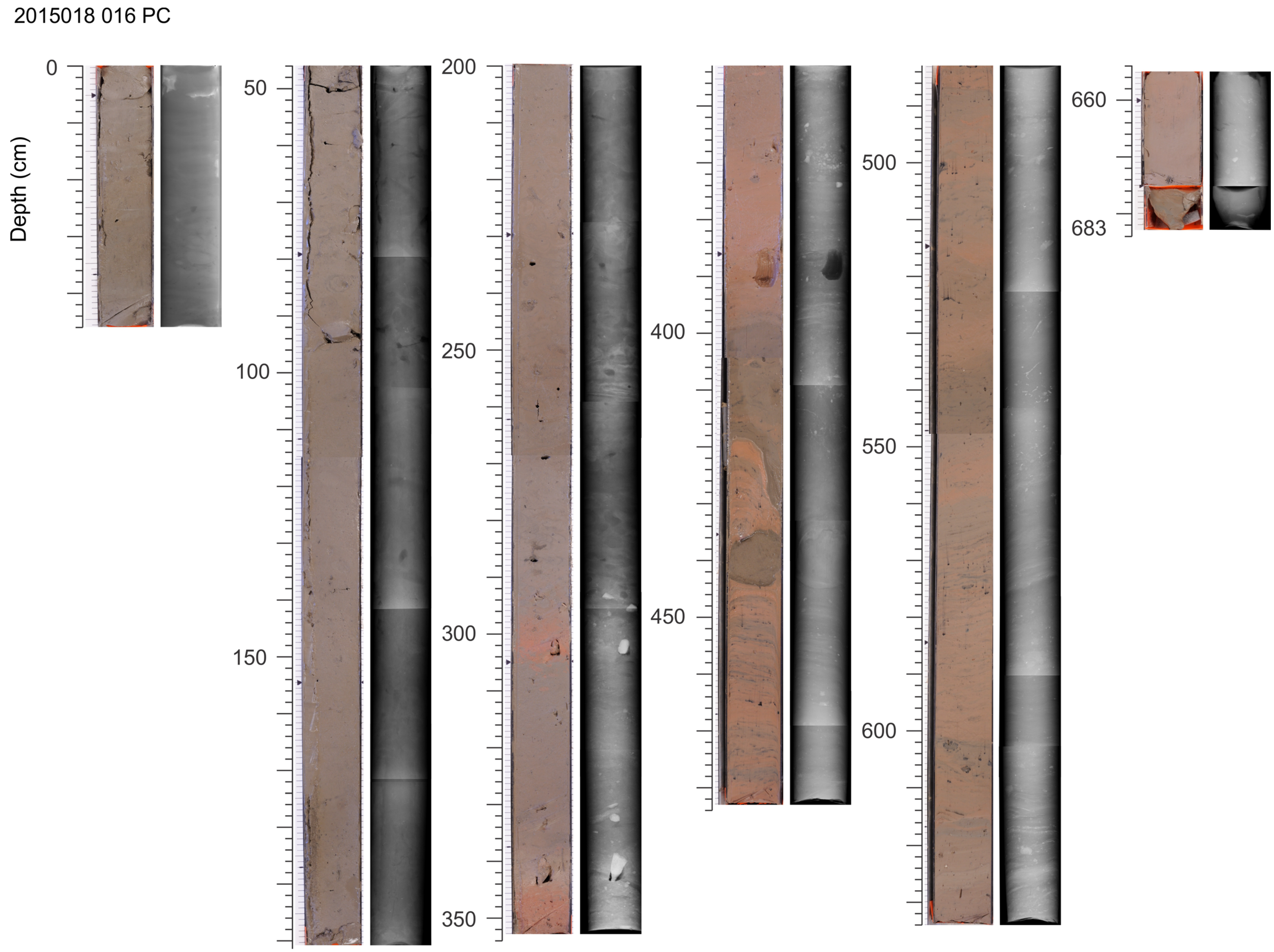

Figure 3.41. Photography and X-radiography compilation for piston core 2015018 016.

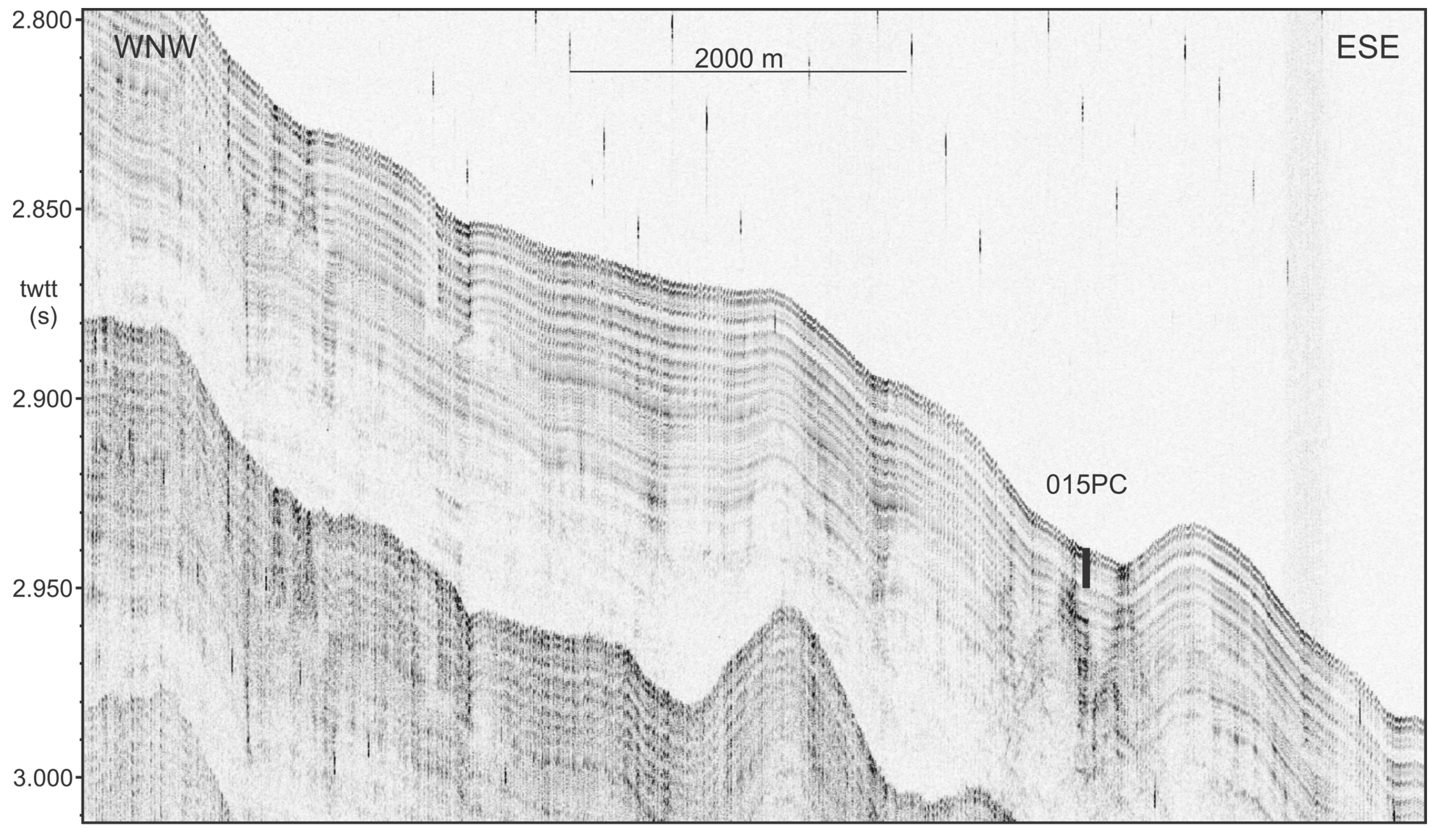

Figure 3.42. High resolution sub-bottom profile showing the acoustic stratigraphy and position of core 2015018 015 (Campbell and MacDonald, 2016).

Scotian Slope 2015018 Piston Core 015

TD 784.5 cm   42.402196 N   -62.389195 W   Water depth 2178 m

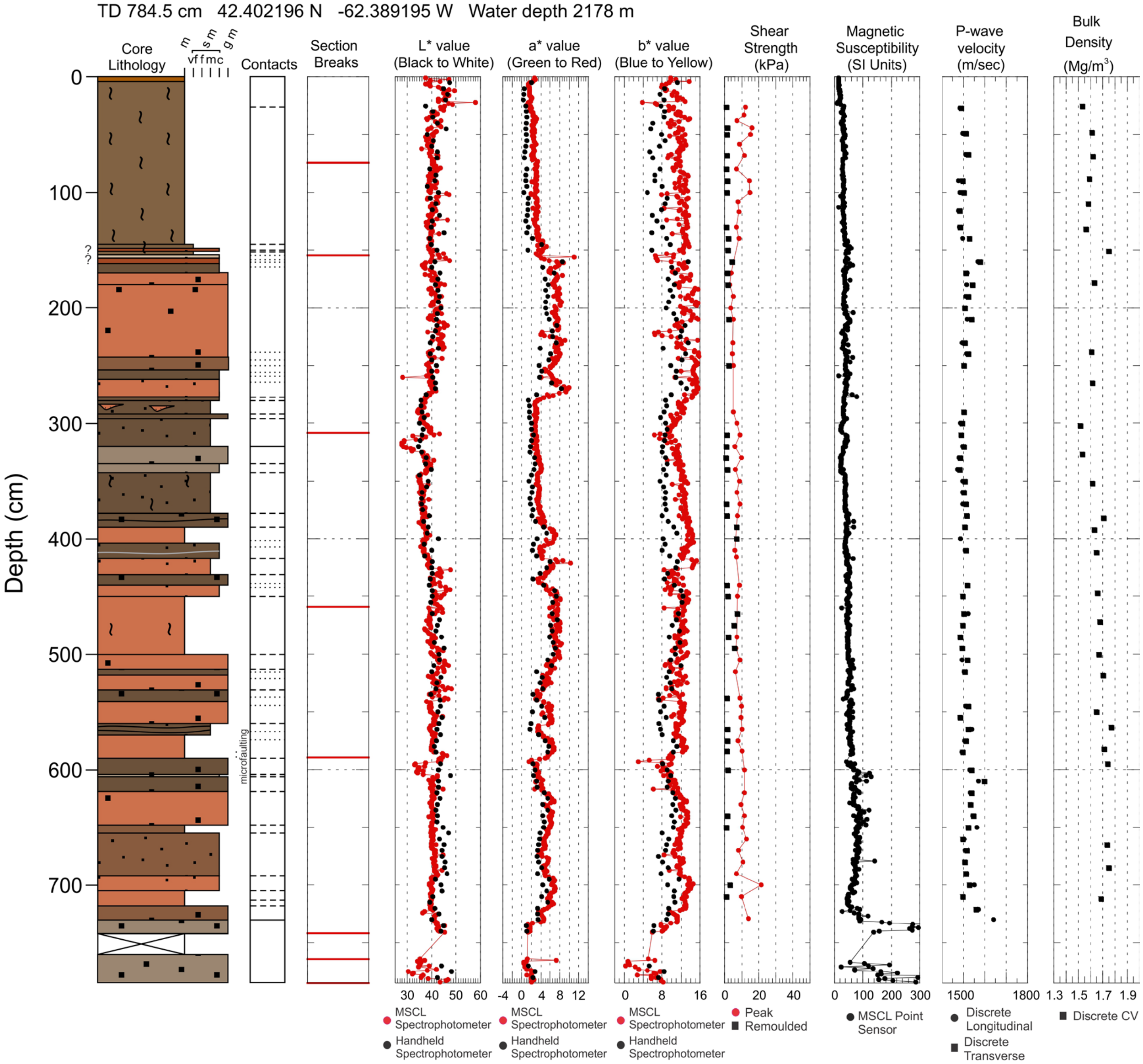

Figure 3.43a. Core plot summary for piston core 2015018 015.

Scotian Slope 2015018 Trigger Weight Core 015

TD 180 cm   42.402196 N   -62.389195 W   Water depth 2178 m

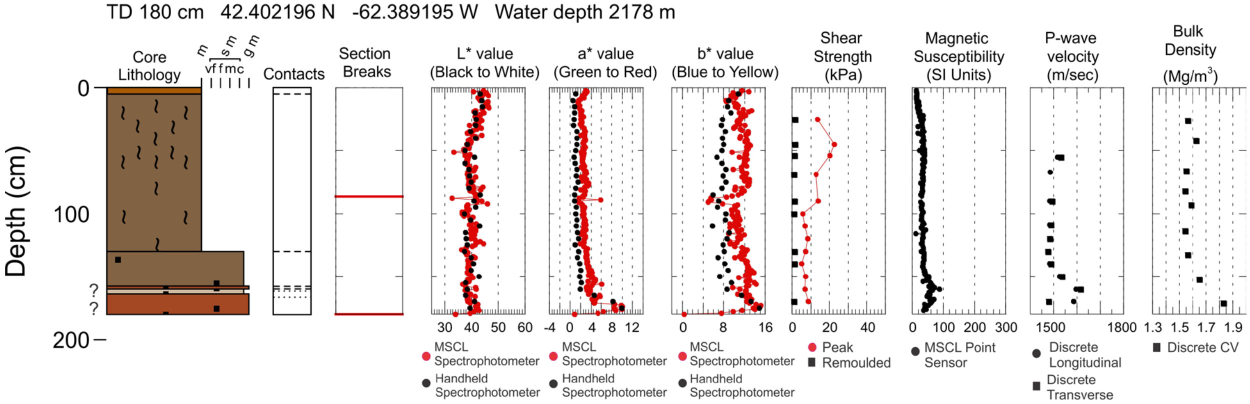

Figure 3.43b. Core plot summary for trigger weight core 2015018 015.

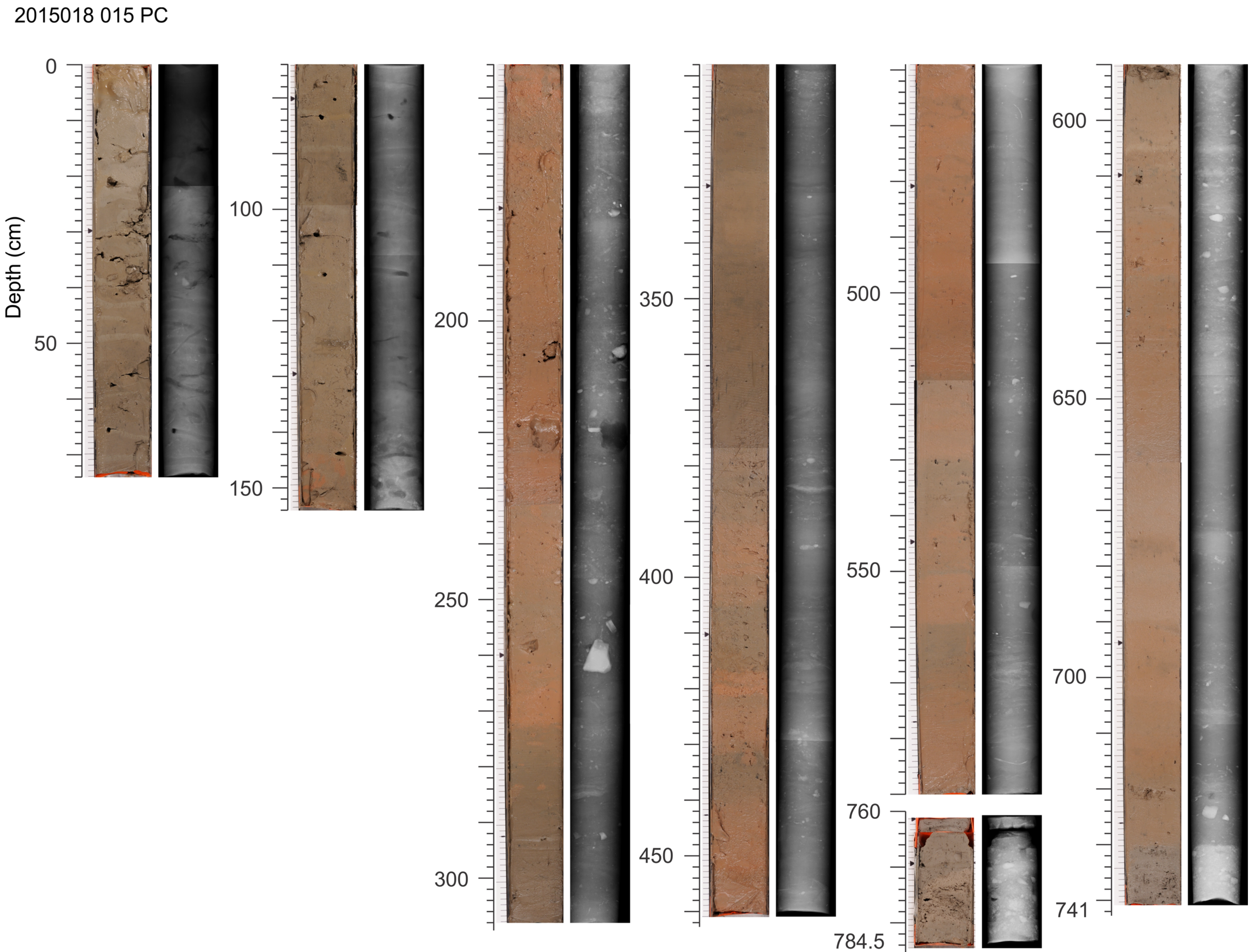

Figure 3.44a. Photography and X-radiography compilation for piston core 2015018 015.

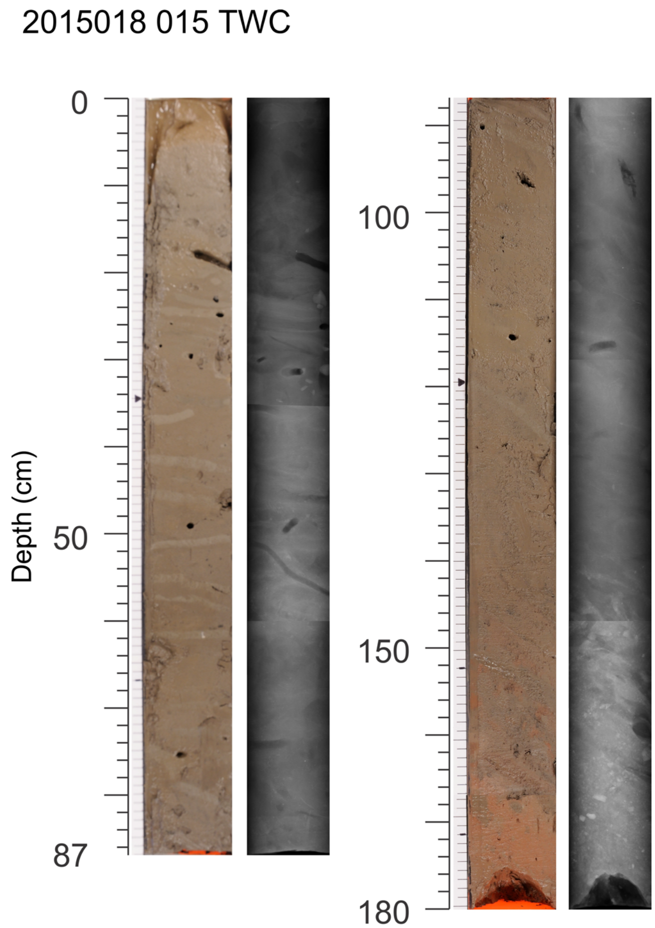

Figure 3.44b. Photography and X-radiography compilation for trigger weight core 2015018 015.

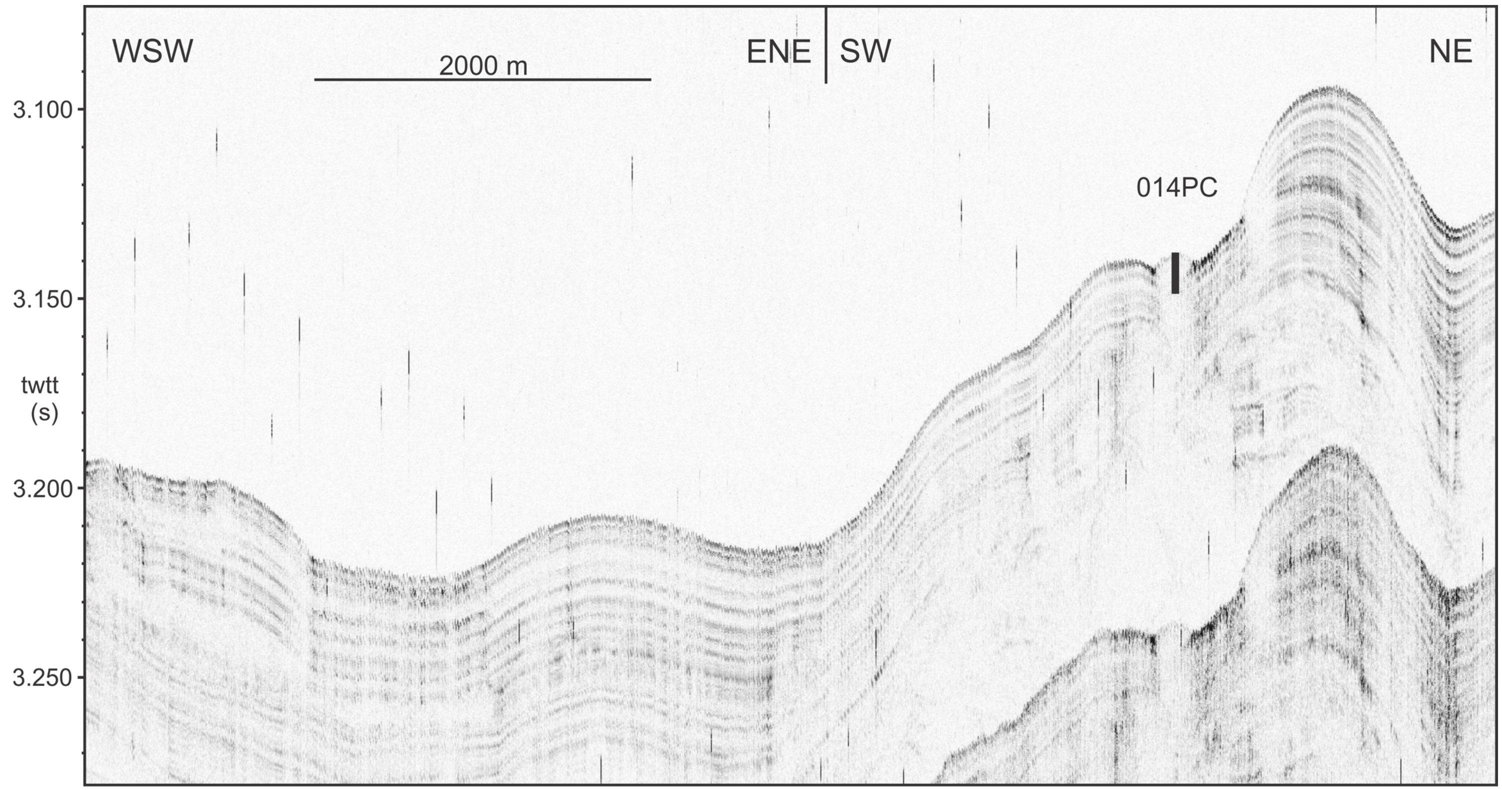

Figure 3.45. High resolution sub-bottom profile showing the acoustic stratigraphy and position of core 2015018 014 (Campbell and MacDonald, 2016).

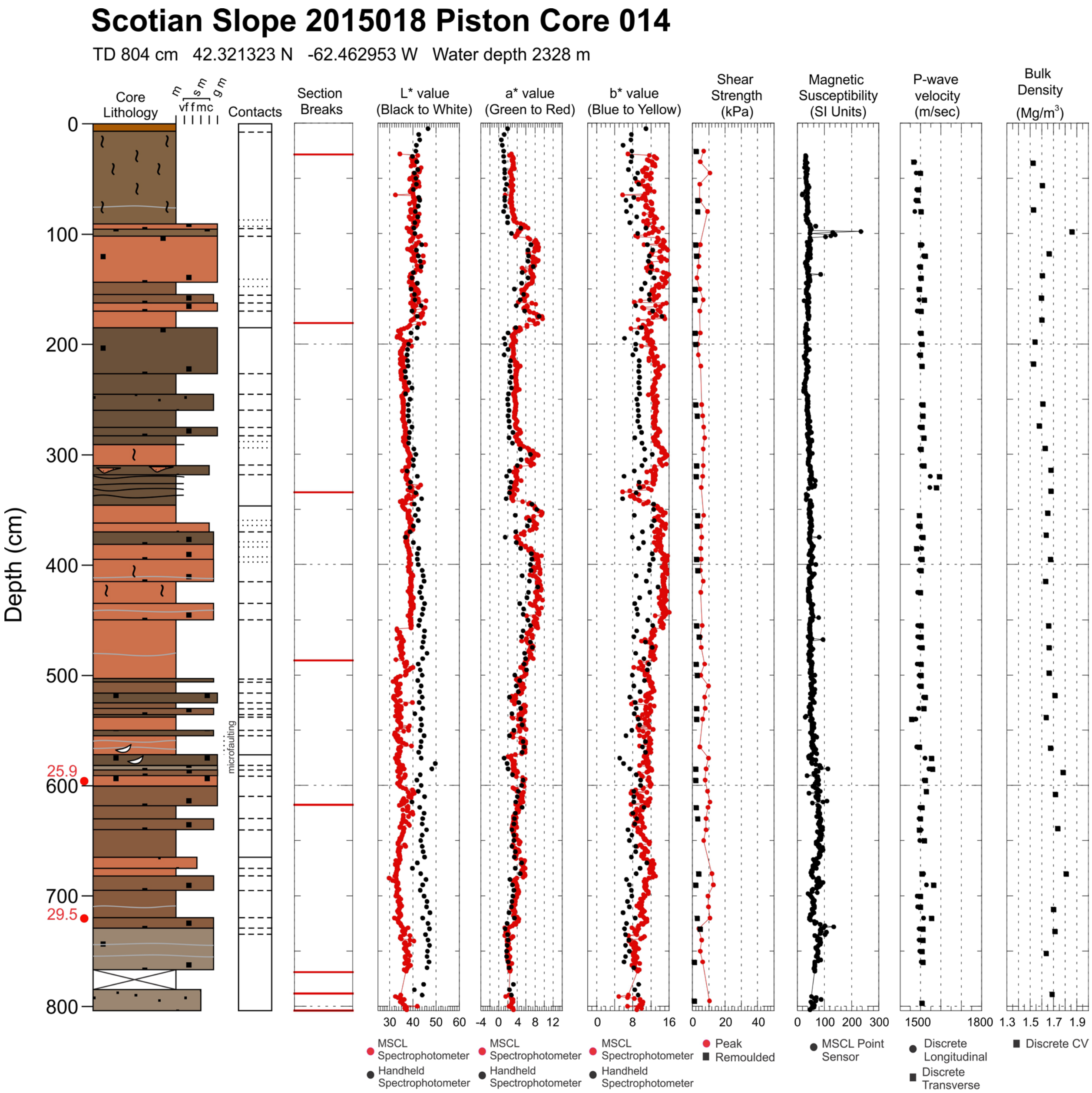

Figure 3.46a. Core plot summary for piston core 2015018 014.

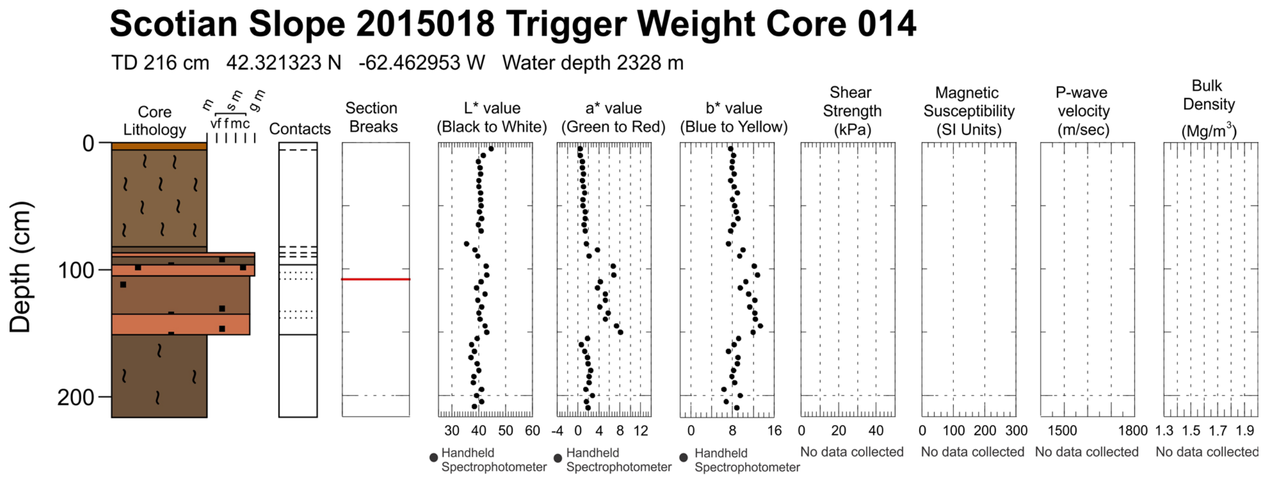

Note: 0-216 cm of 014 TWC was split on board and taken for geomicrobiology research at the University of Calgary. No X-radiography or additional GSC(A) analyses exist for this core.

Figure 3.46b. Core plot summary for trigger weight core 2015018 014.

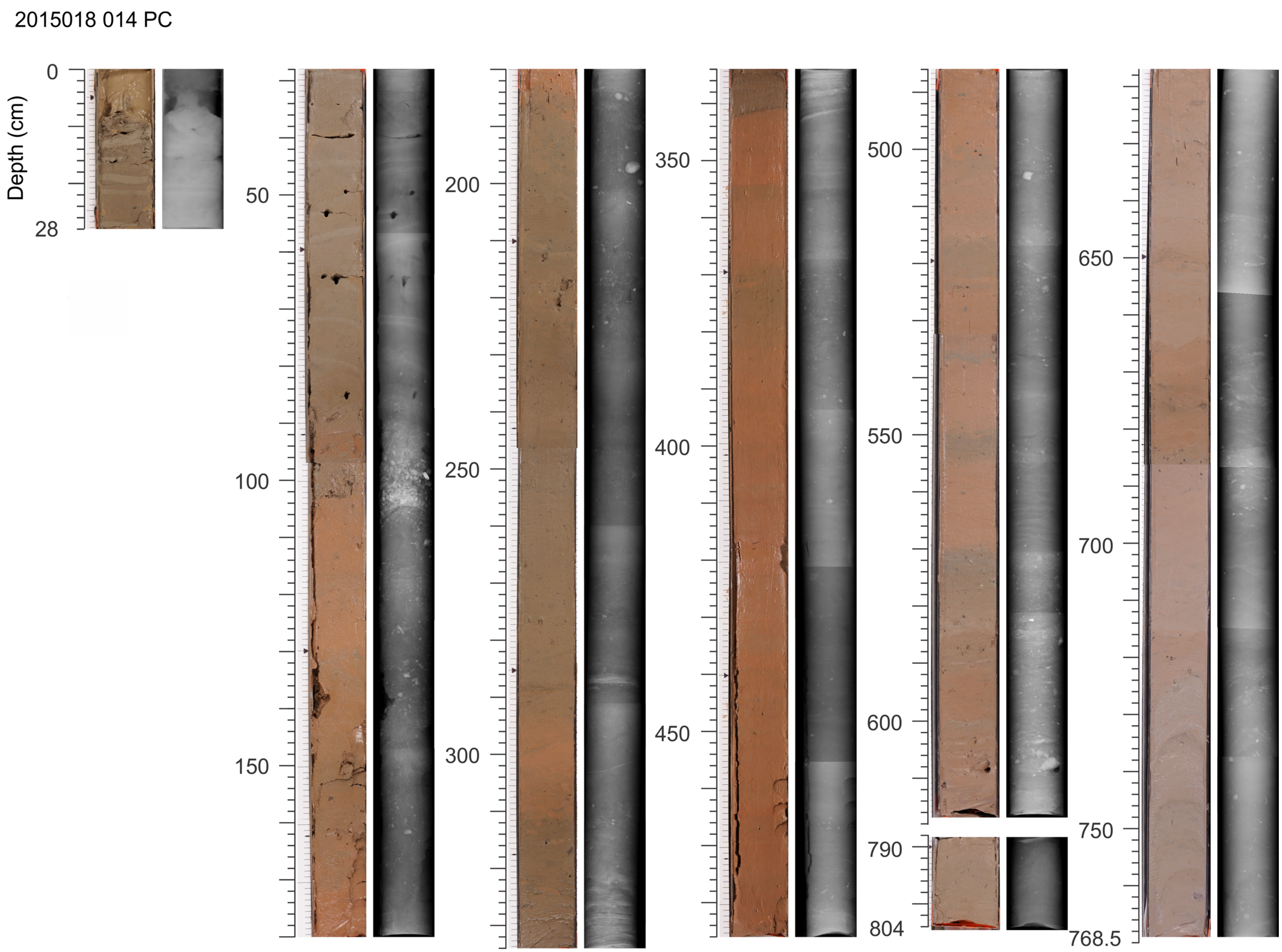

Figure 3.47a. Photography and X-radiography compilation for piston core 2015018 014.

2015018 014 TWC

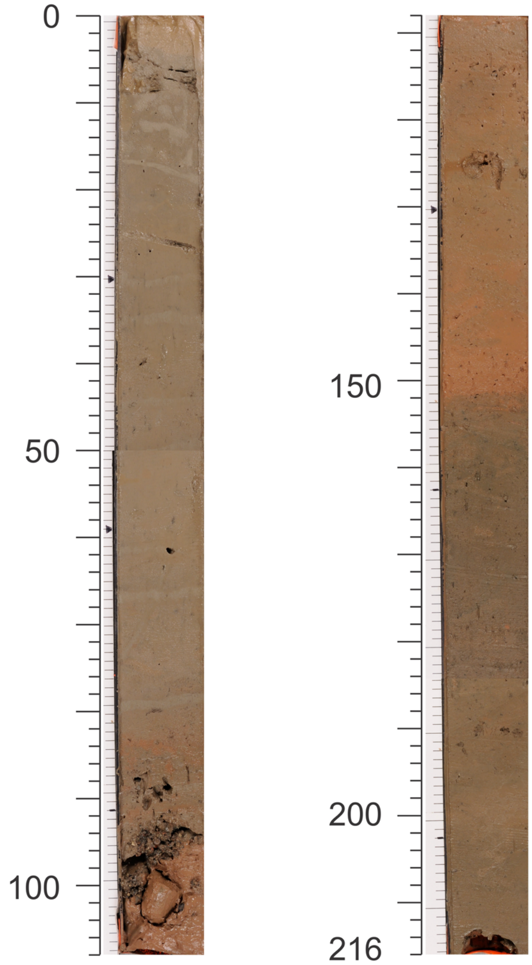

Note: 0-216 cm was taken for geomicrobiology
research at the University of Calgary
(no X-radiography).

Figure 3.47b. Photography compilation for trigger weight core 2015018 014.

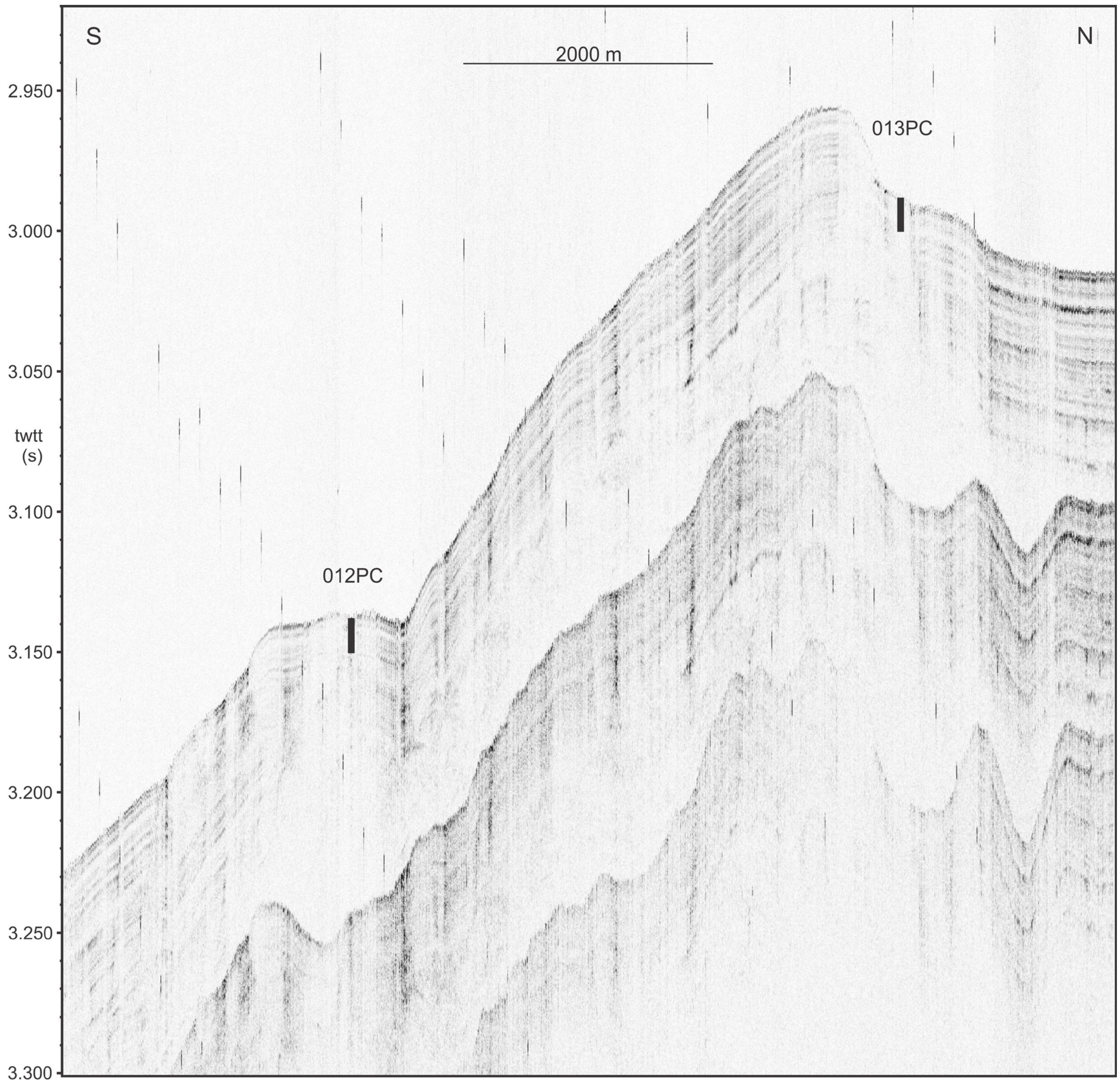

Figure 3.48. High resolution sub-bottom profile showing the acoustic stratigraphy and position of cores 2015018 012 and 2015018 013 (Campbell and MacDonald, 2016).

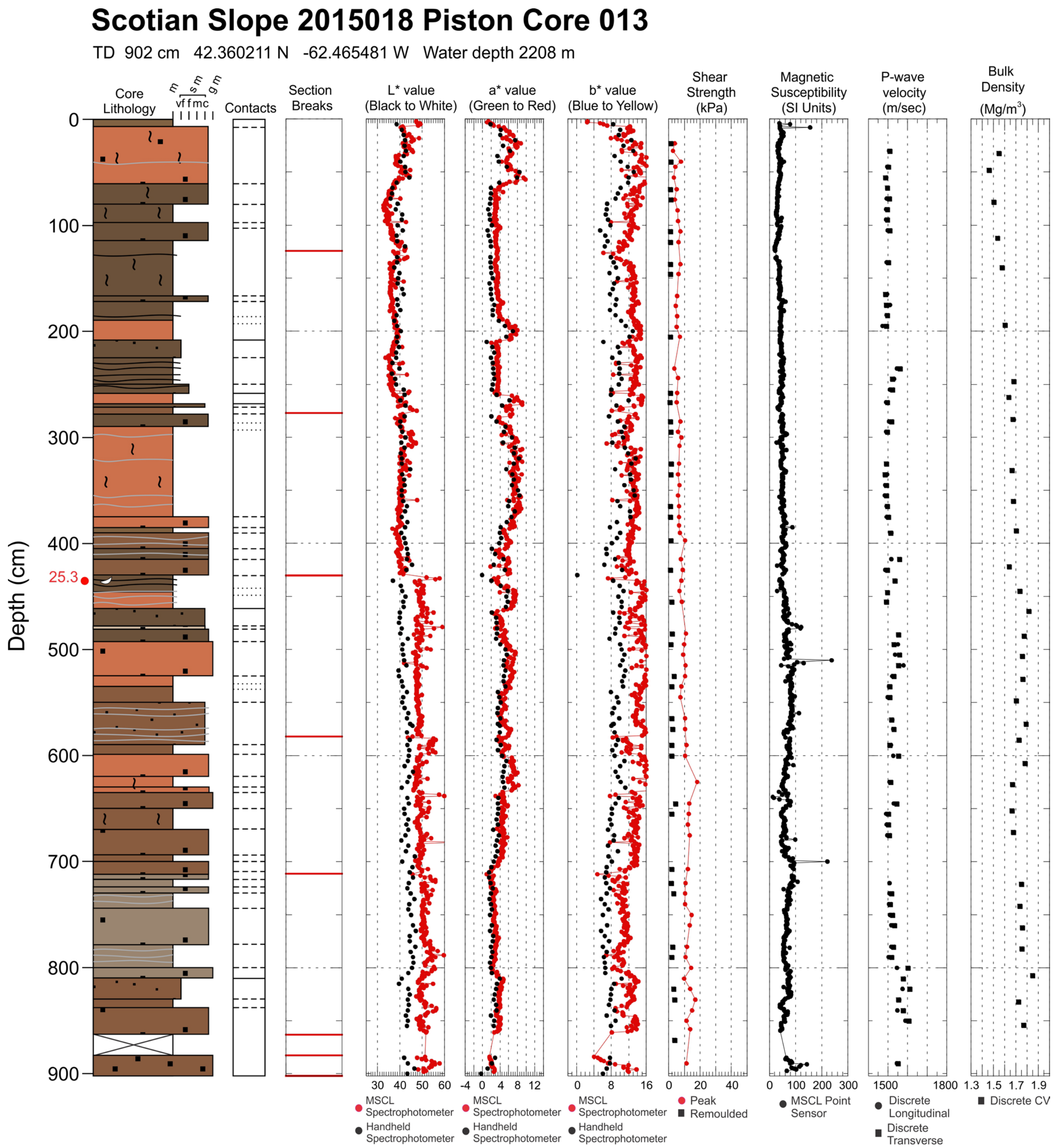

Figure 3.49a. Core plot summary for piston core 2015018 013.

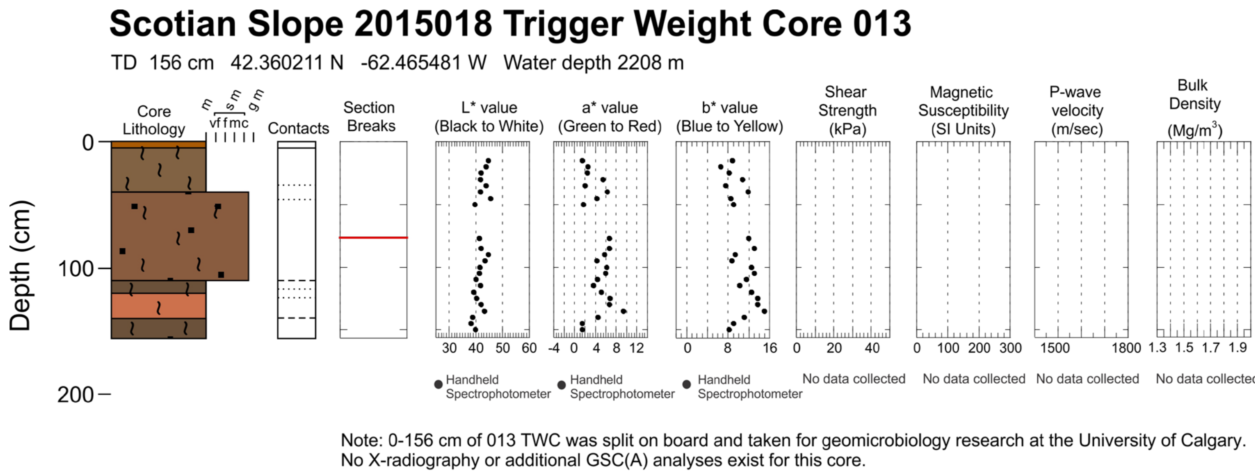

Figure 3.49b. Core plot summary for trigger weight core 2015018 013.

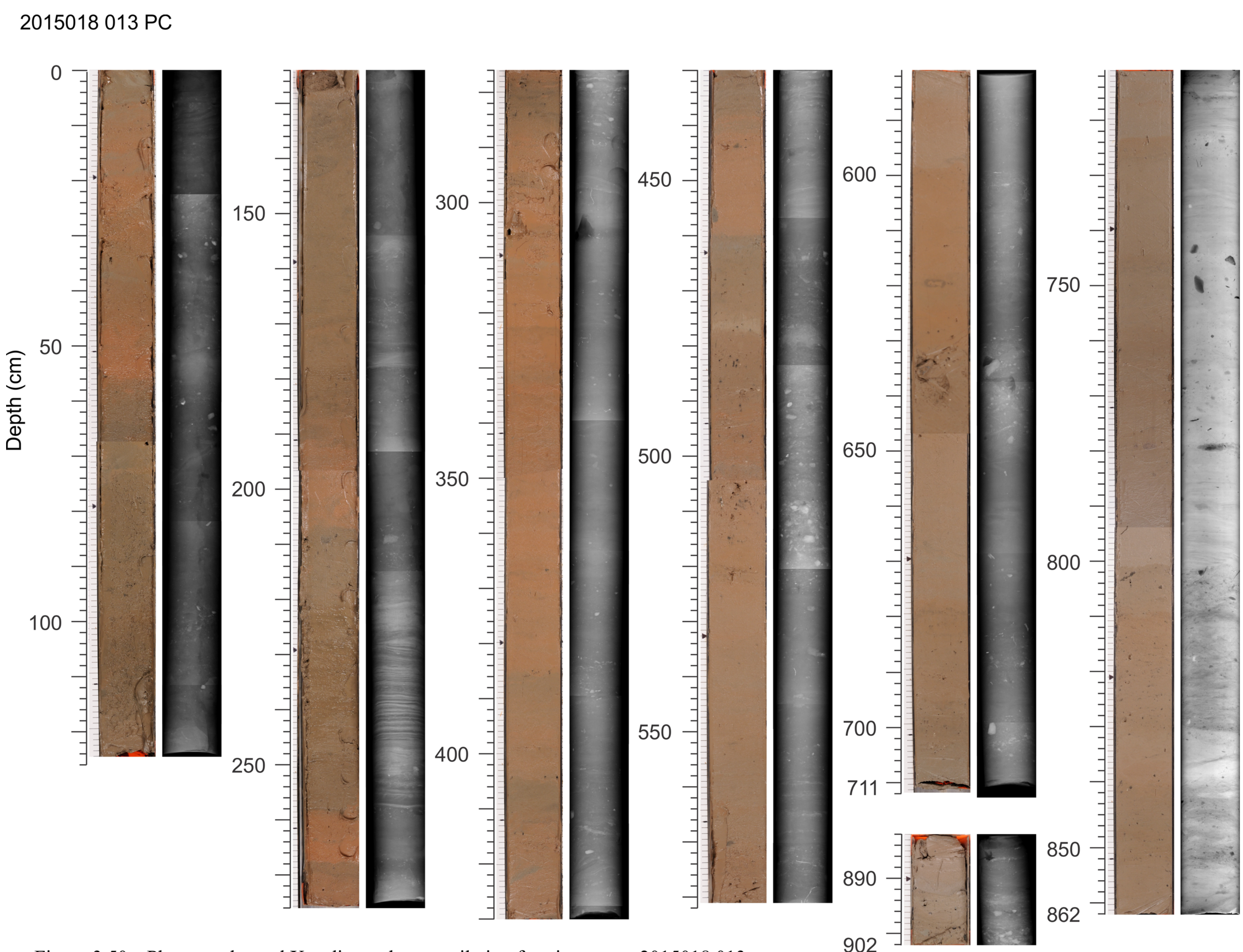

Figure 3.50a. Photography and X-radiography compilation for piston core 2015018 013.

2015018 013 TWC

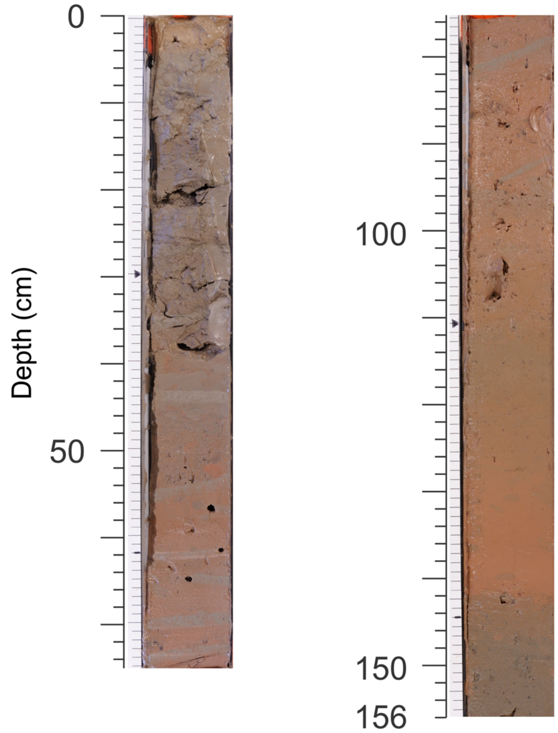

Note: 0-156 cm was taken for geomicrobiology research at the University of Calgary (no X-radiography).

Figure 3.50b. Photography compilation for trigger weight core 2015018 013.

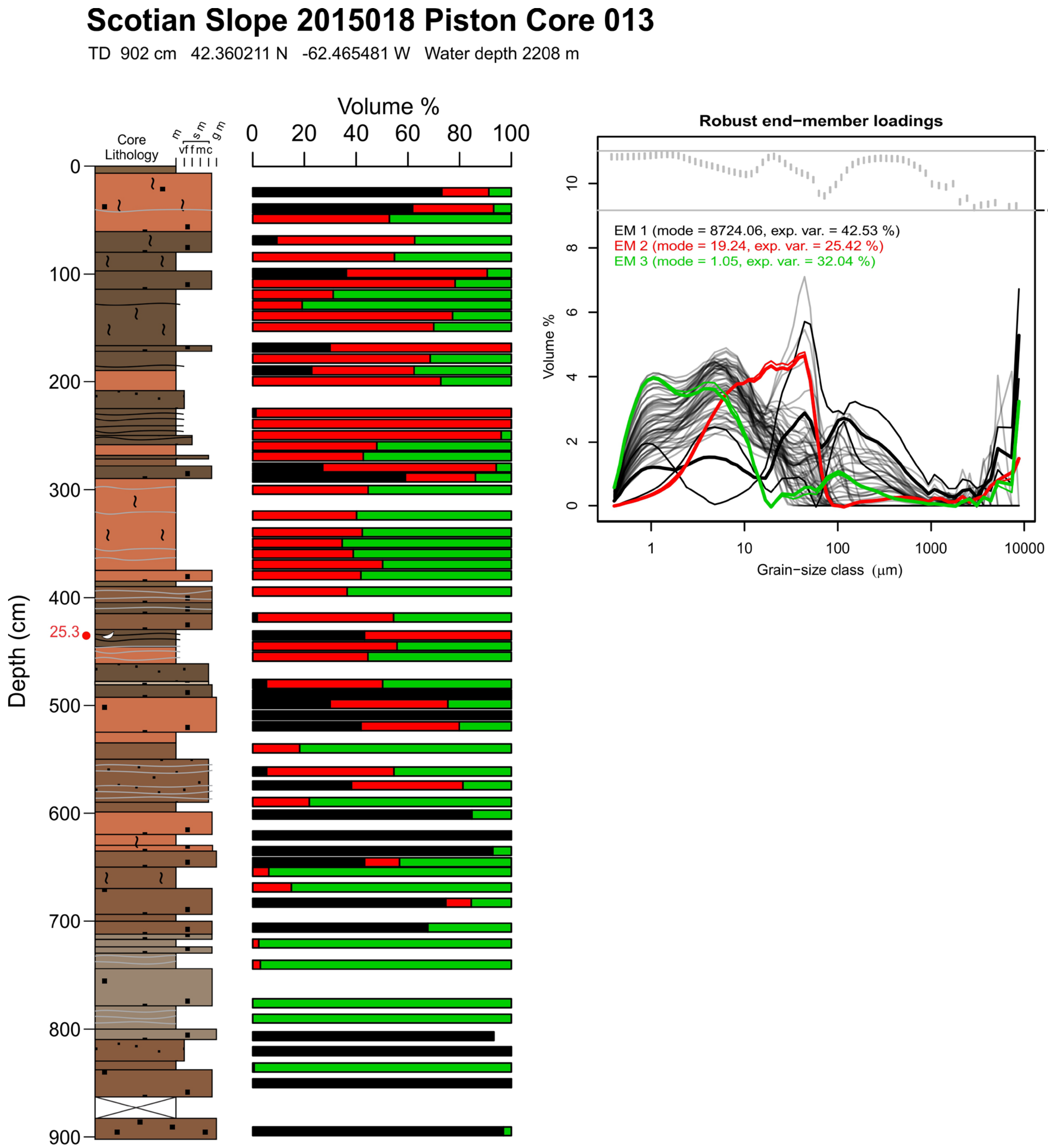

Figure 3.51. Down-core grain size end-member modelling analysis (EMMA) for piston core 2015018 013 using the open-source R package EMMAgeo software. Three end-member subpopulations are represented.

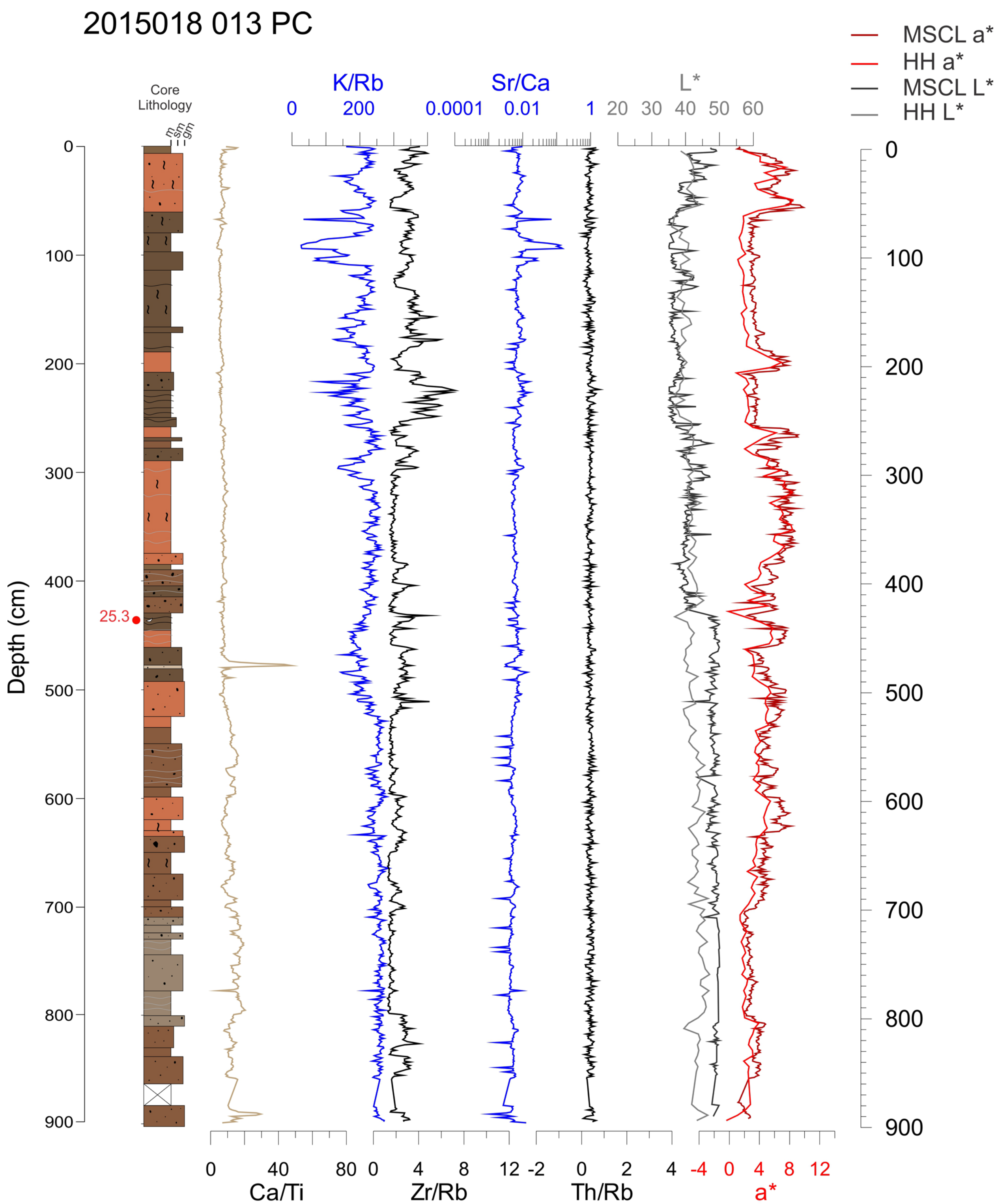

Figure 3.52. Down-core pXRF analyses for piston core 2015018 013. MSCL - Multi Sensor Core Logger; HH - handheld spectrophotometry.

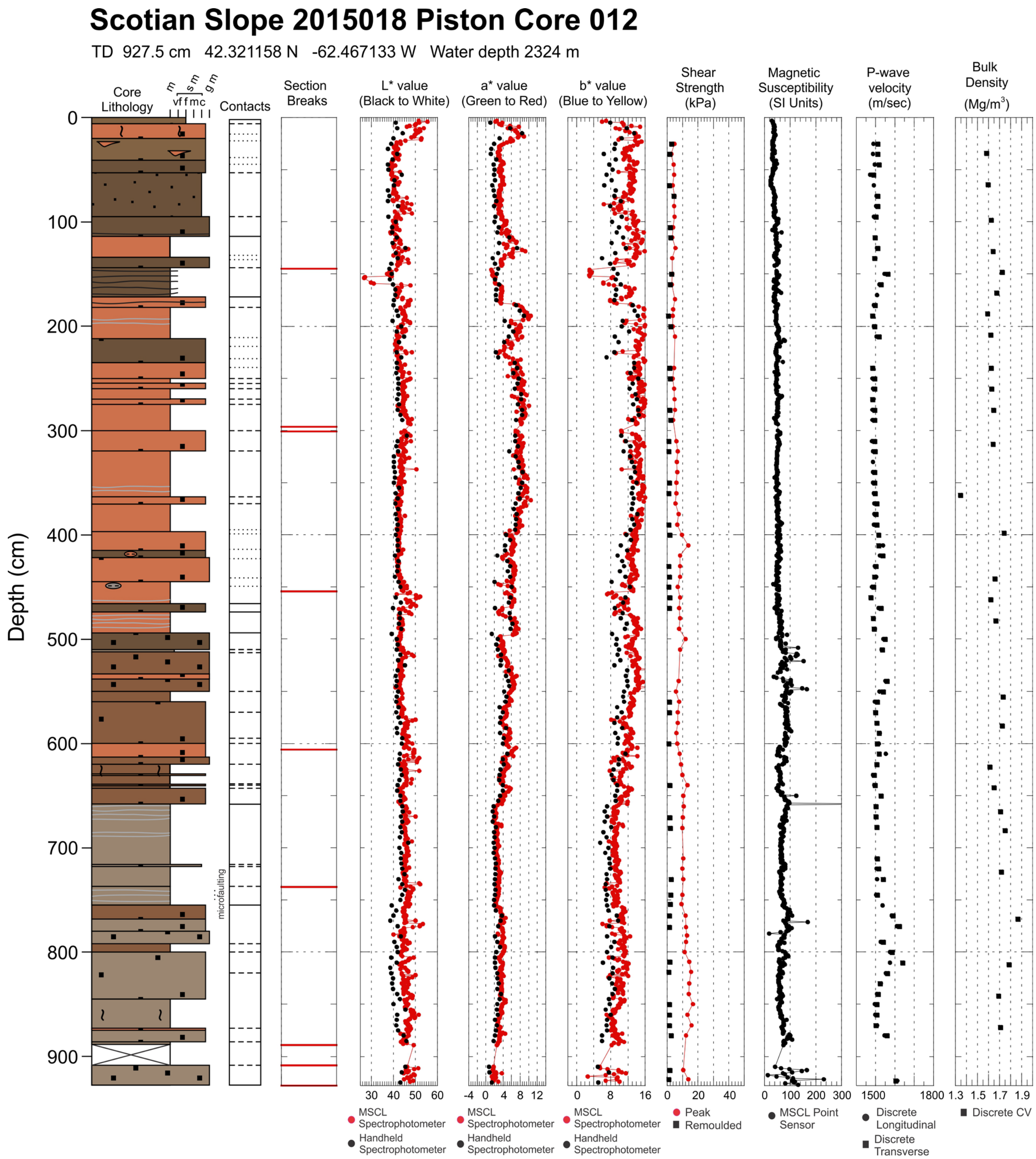

Figure 3.53a. Core plot summary for piston core 2015018 012.

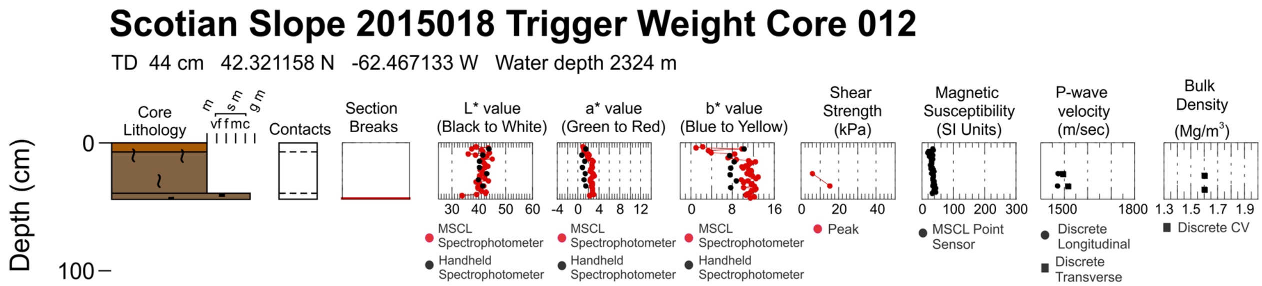

Figure 3.53b. Core plot summary for trigger weight core 2015018 012.

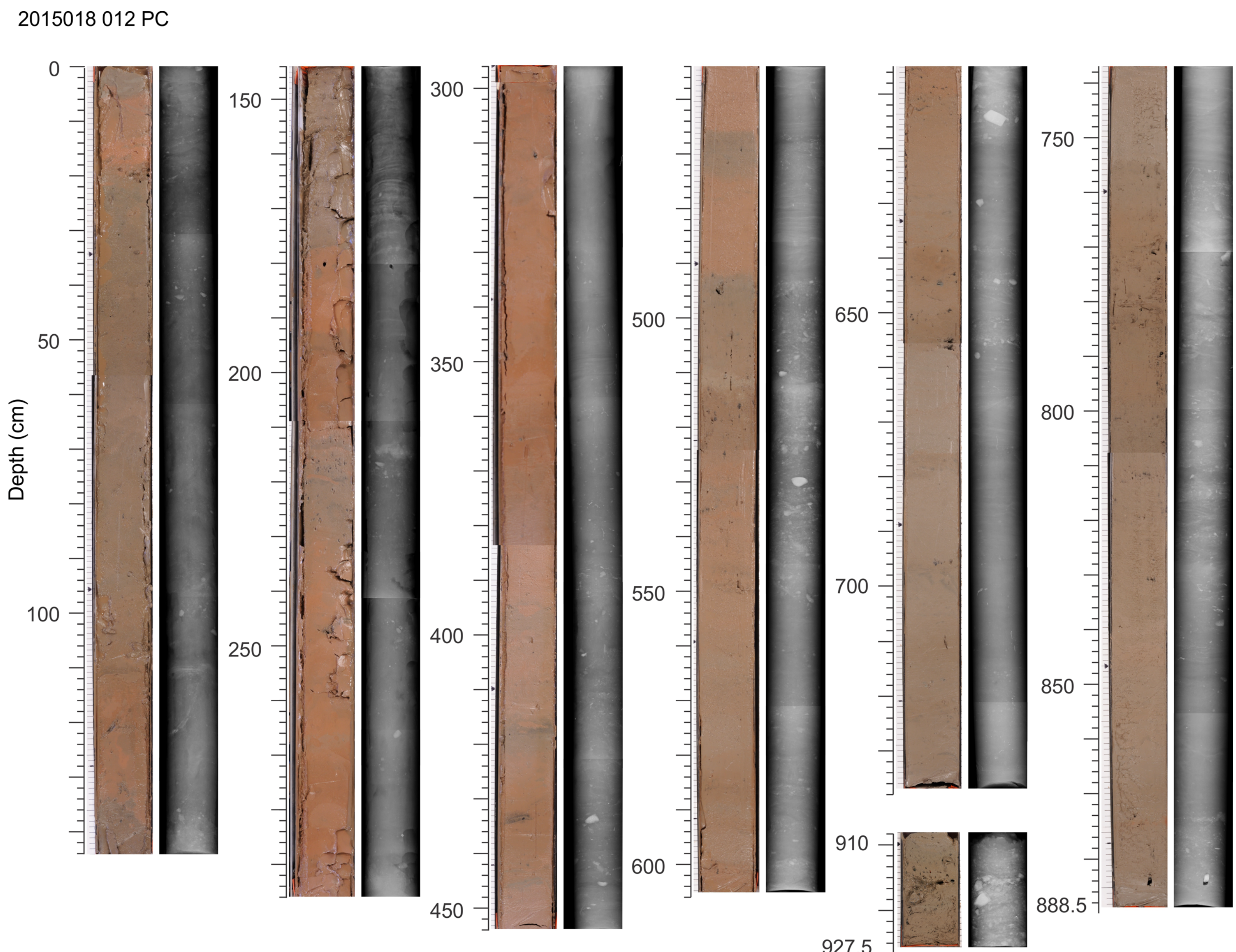

Figure 3.54a. Photography and X-radiography compilation for piston core 2015018 012.

2015018 012 TWC

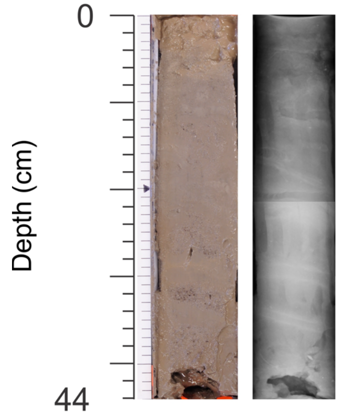

Figure 3.54b. Photography and X-radiography compilation for trigger weight core 2015018 012.

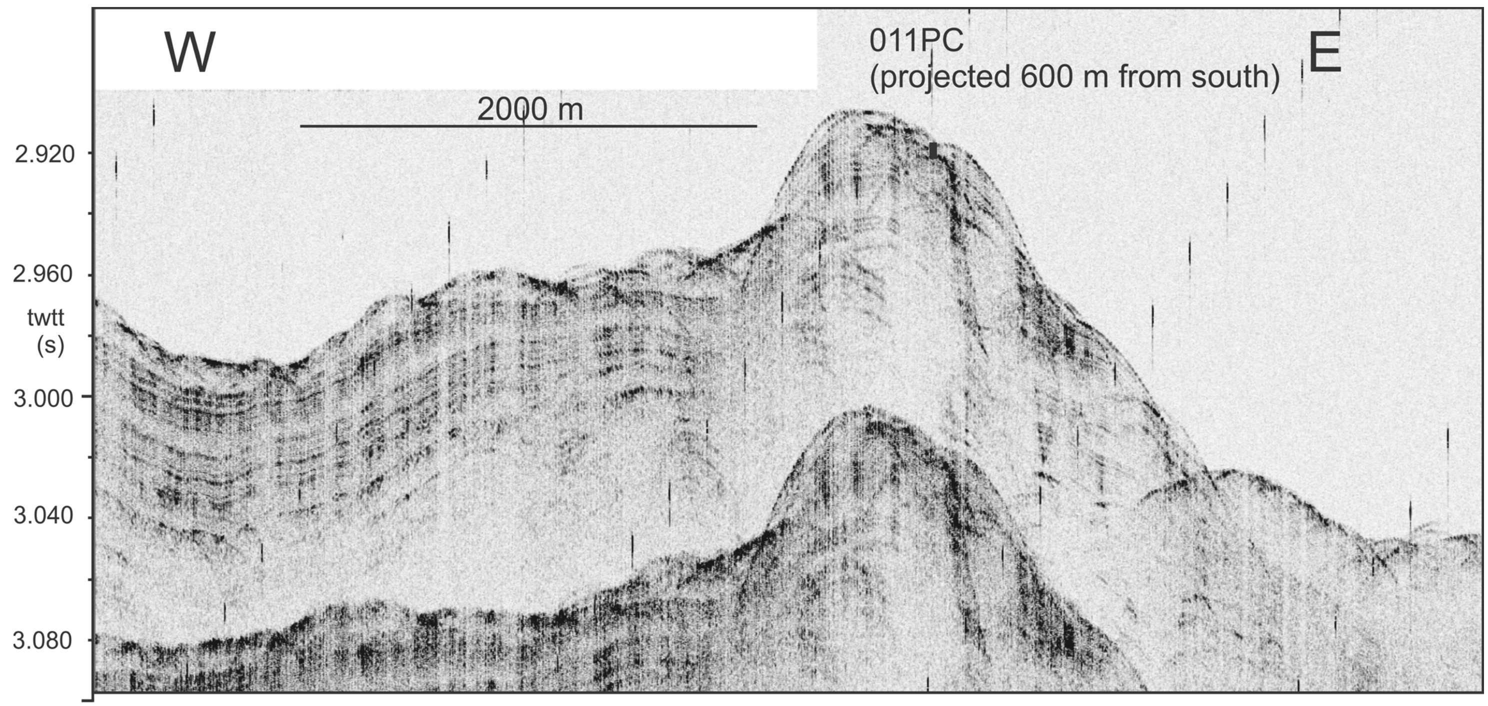

Figure 3.55. High resolution sub-bottom profile showing the acoustic stratigraphy and position of core 2015018 011 (Campbell and MacDonald, 2016).

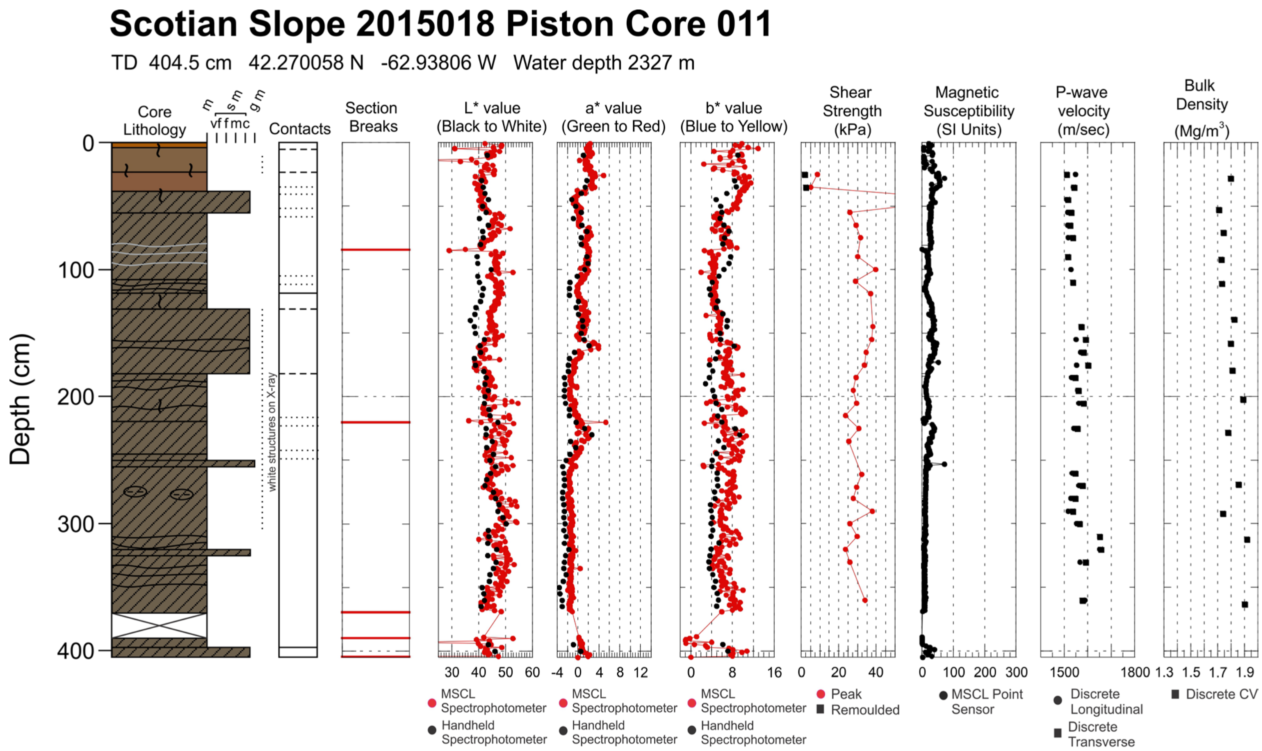

Figure 3.56a. Core plot summary for piston core 2015018 011.

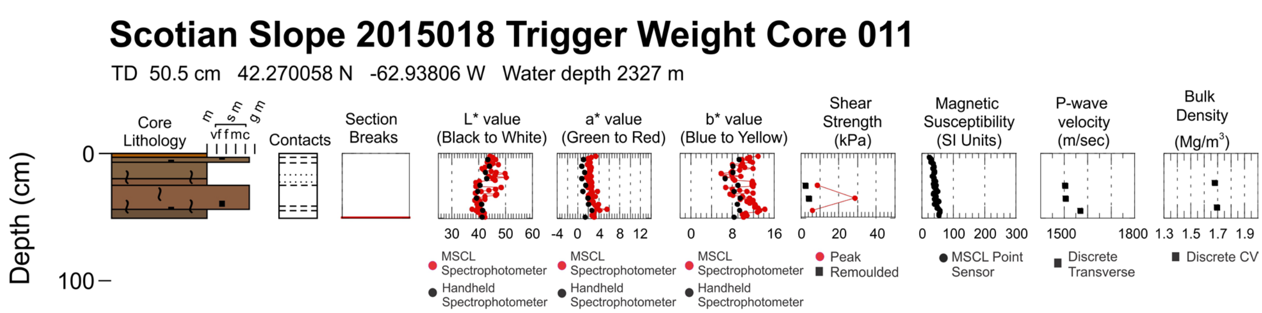

Figure 3.56b. Core plot summary for trigger weight core 2015018 011.

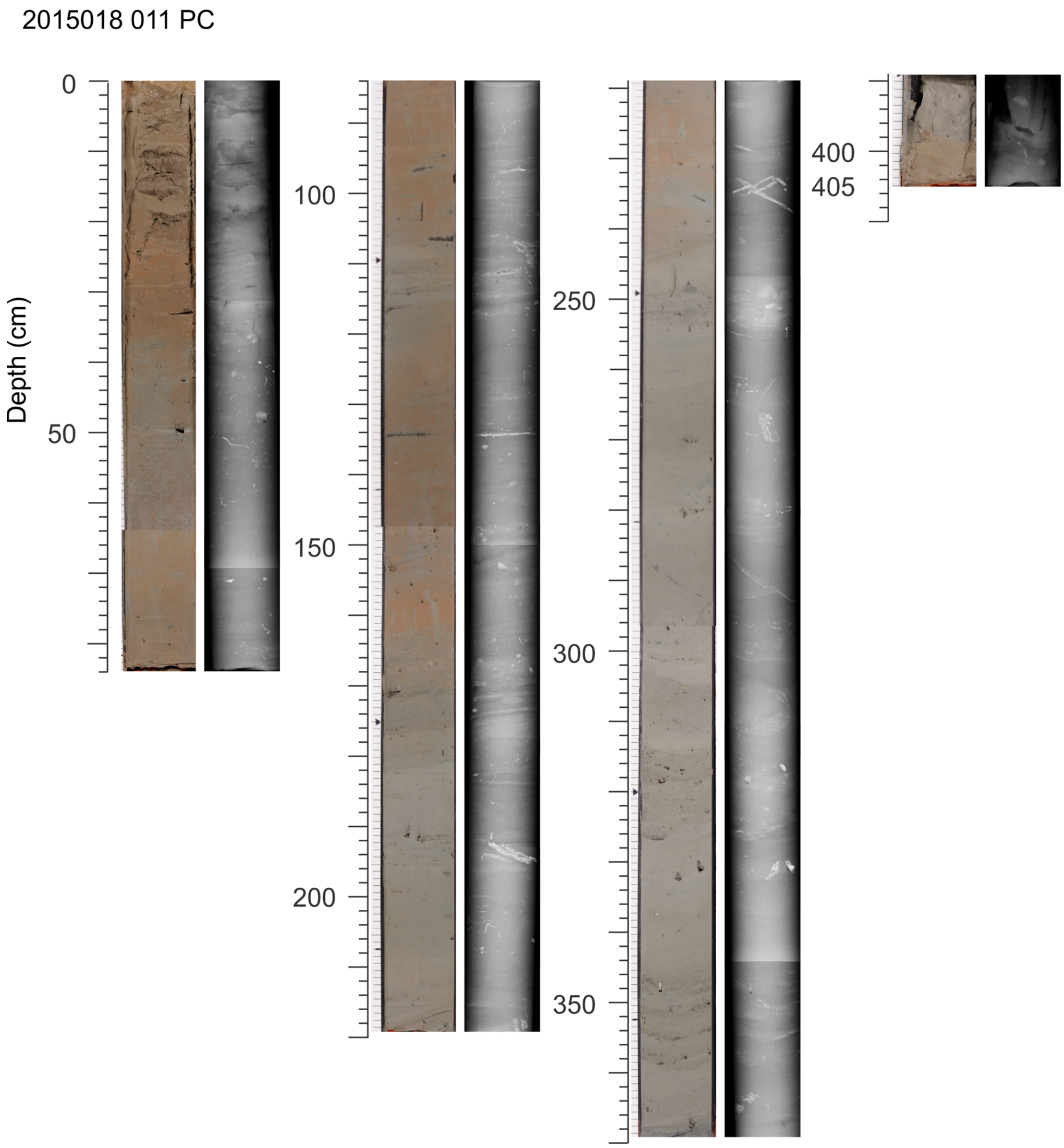

Figure 3.57a. Photography and X-radiography compilation for piston core 2015018 011.

2015018 011 TWC

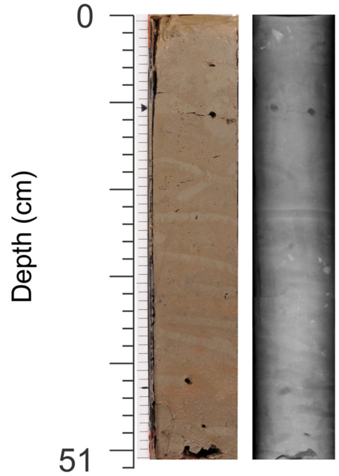

Figure 3.57b. Photography and X-radiography compilation for trigger weight core 2015018 011.

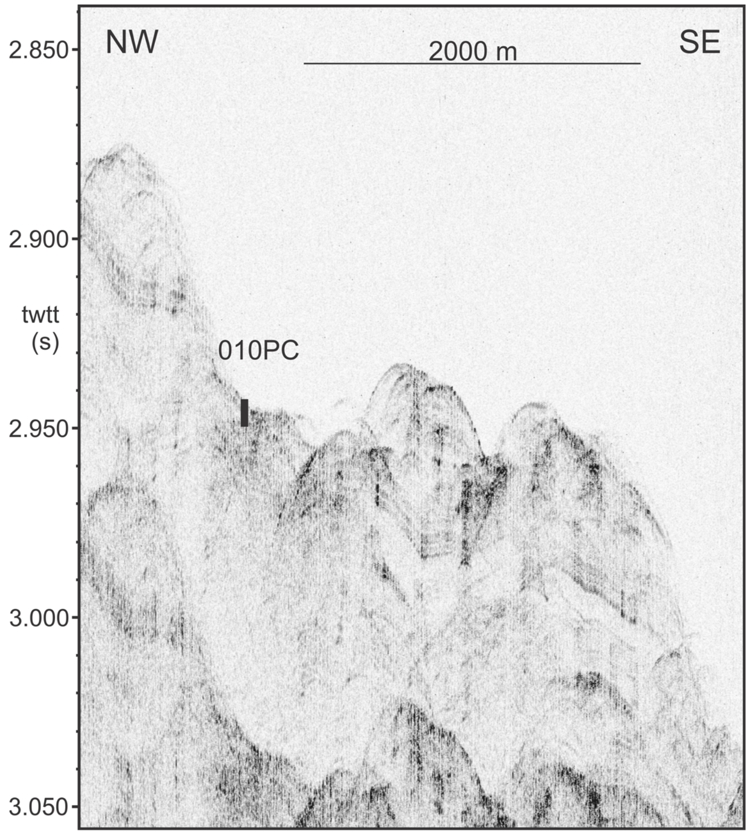

Figure 3.58. High resolution sub-bottom profile showing the acoustic stratigraphy and position of core 2015018 010 (Campbell and MacDonald, 2016).

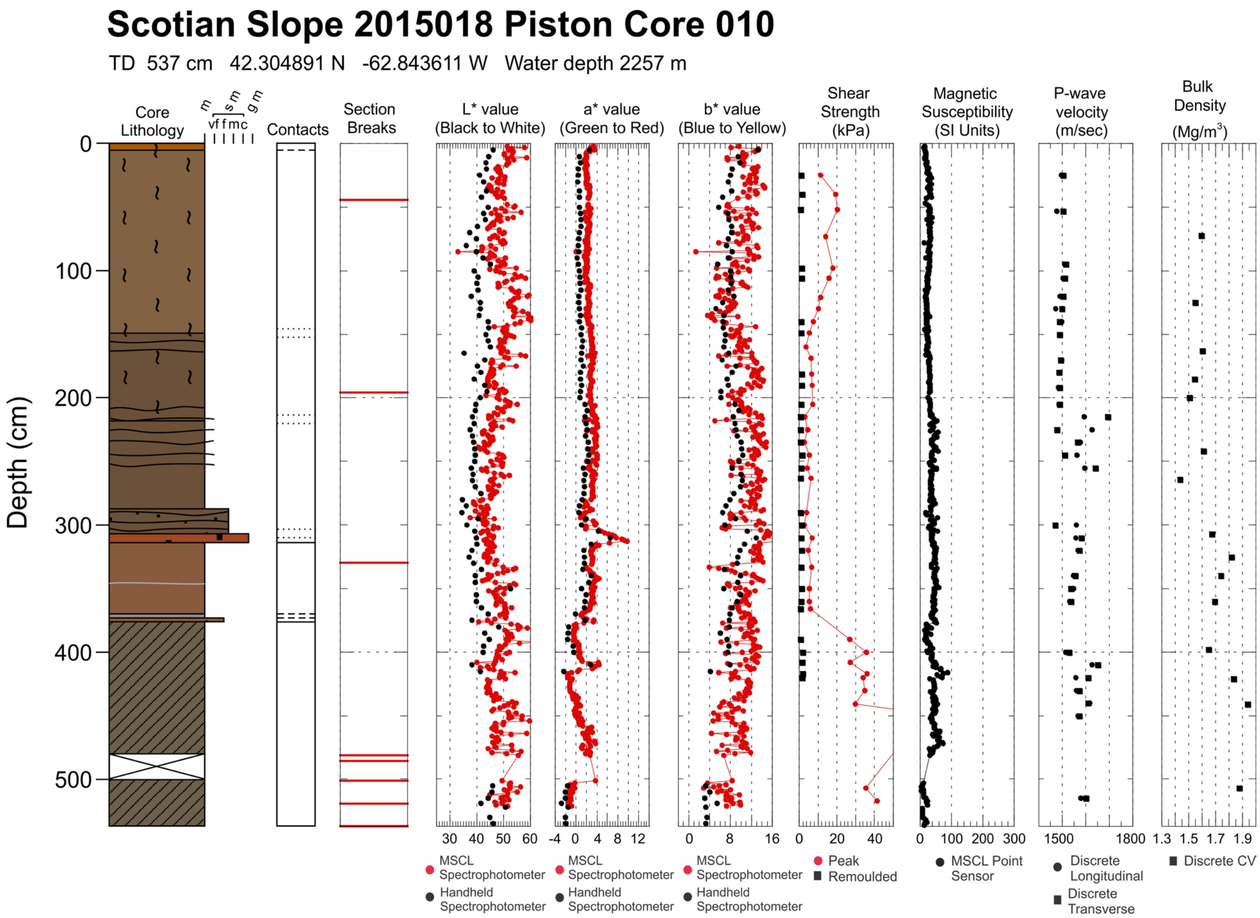

Figure 3.59a. Core plot summary for piston core 2015018 010.

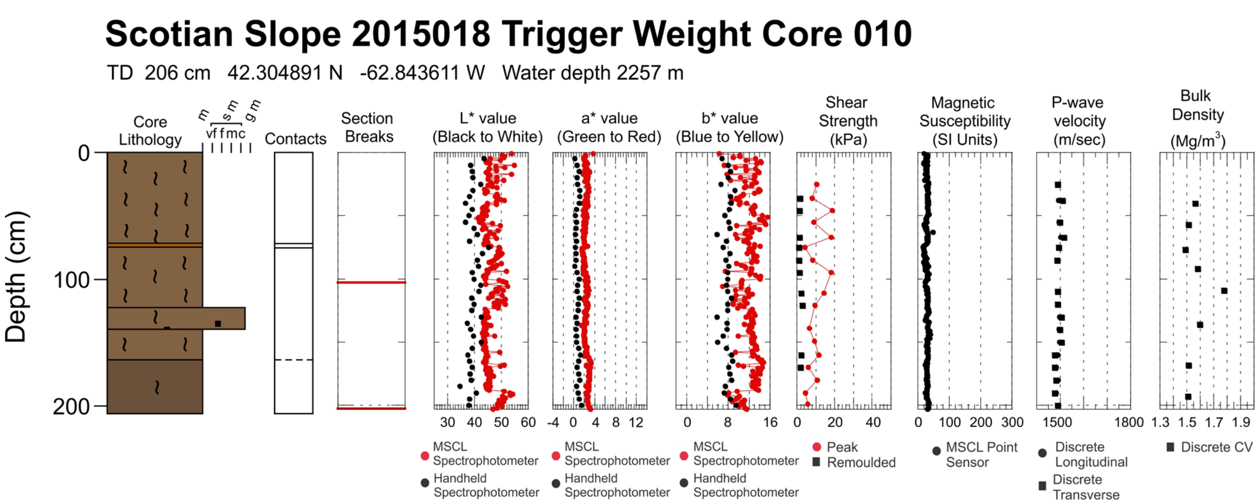

Figure 3.59b. Core plot summary for trigger weight core 2015018 010.

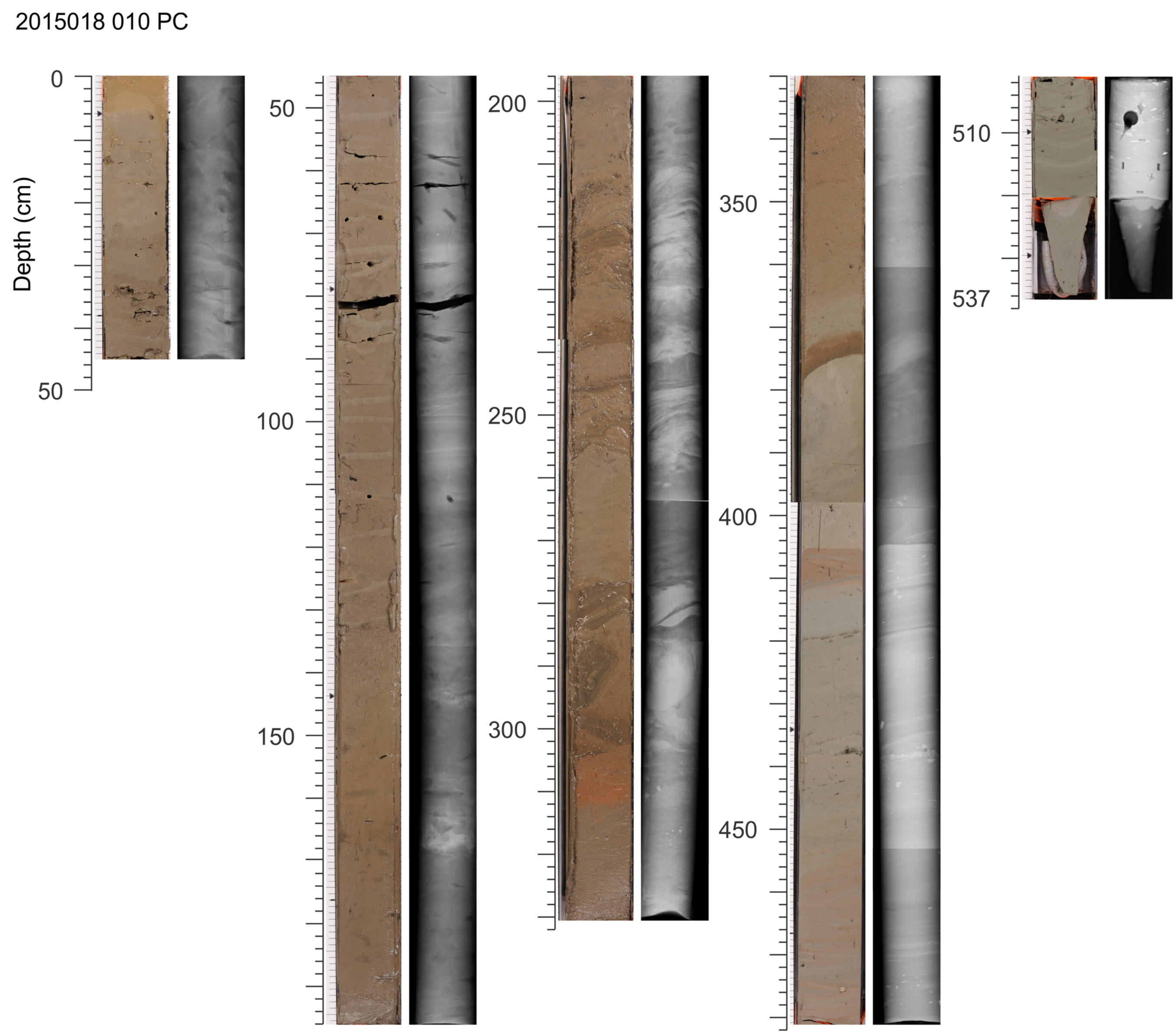

Figure 3.60a. Photography and X-radiography compilation for piston core 2015018 010.

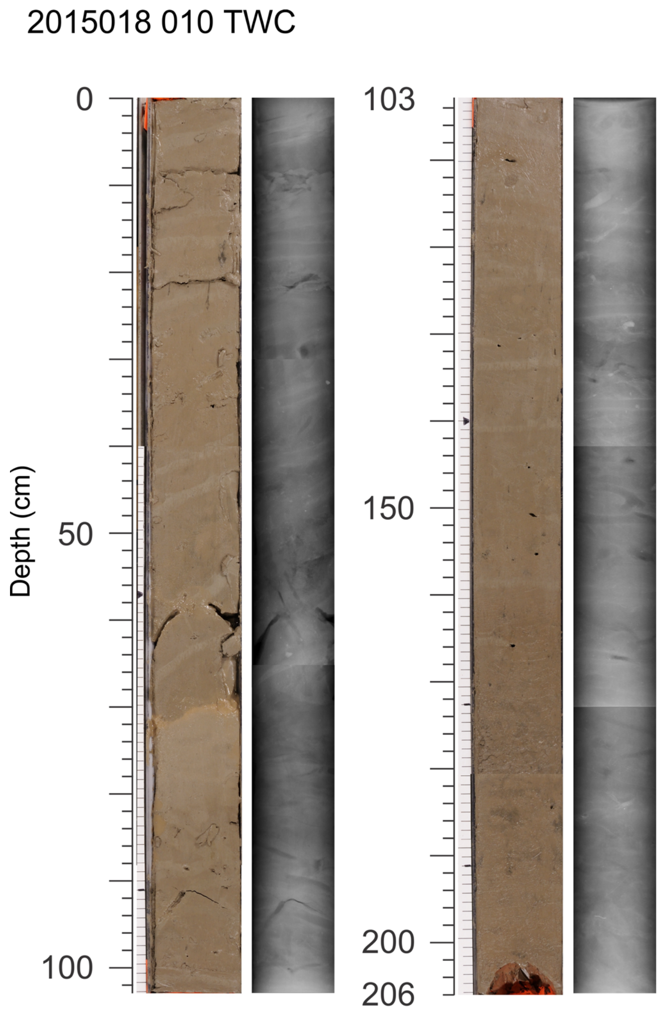

Figure 3.60b. Photography and X-radiography compilation for trigger weight core 2015018 010.

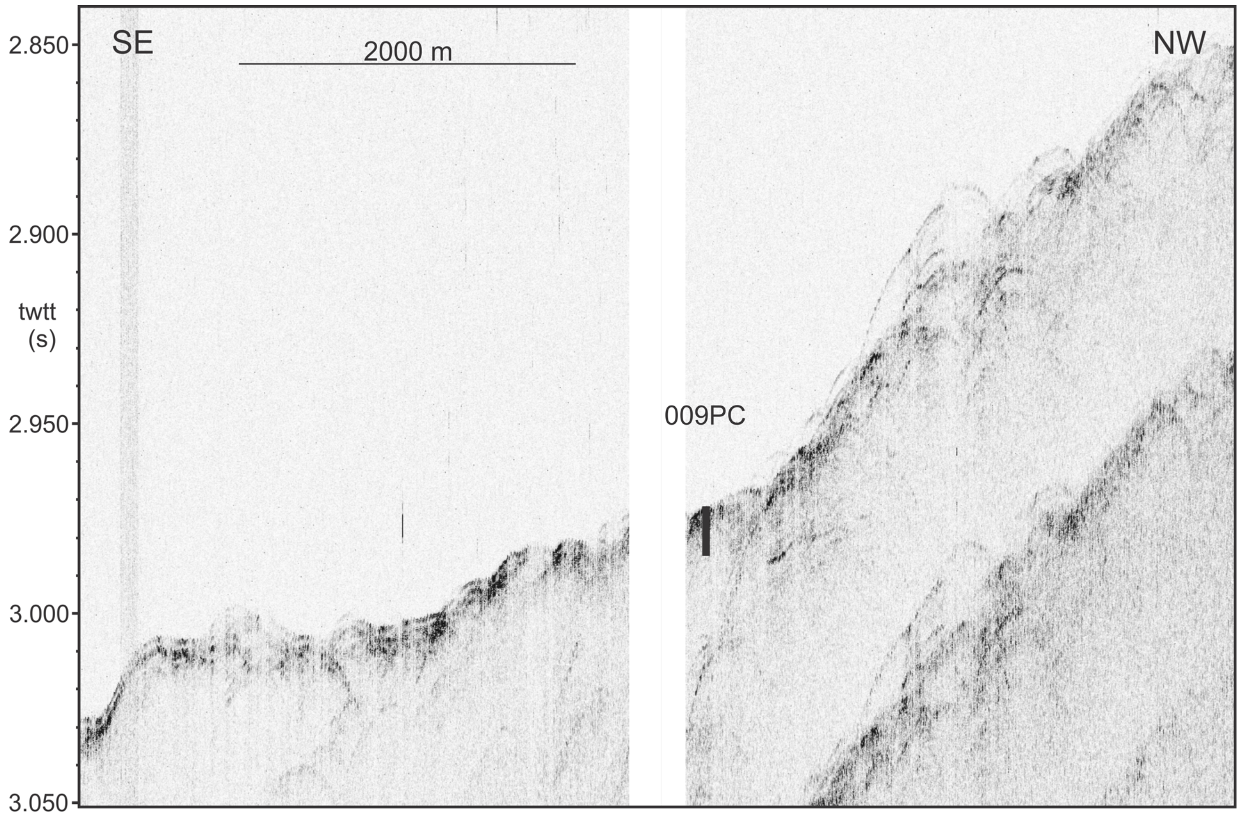

Figure 3.61. High resolution sub-bottom profile showing the acoustic stratigraphy and position of core 2015018 009 (Campbell and MacDonald, 2016).

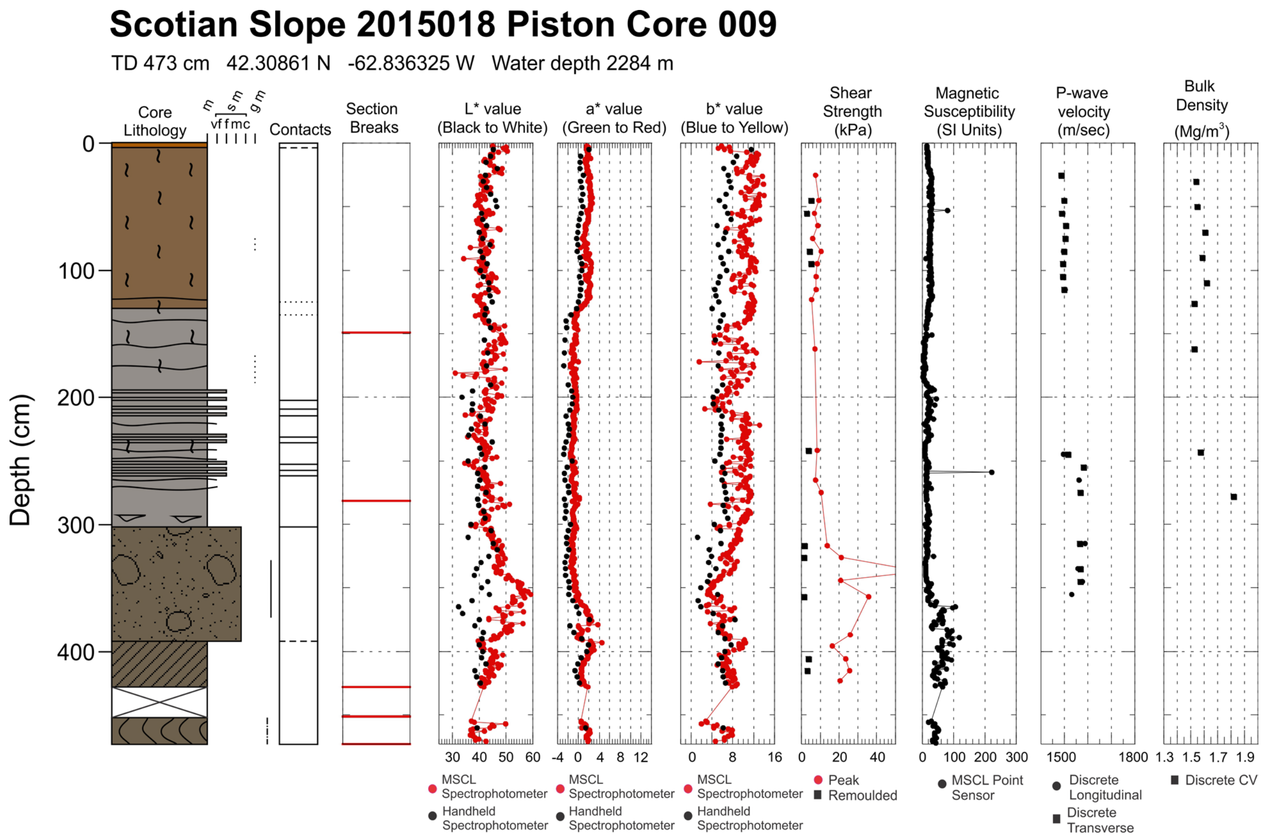

Figure 3.62a. Core plot summary for piston core 2015018 009.

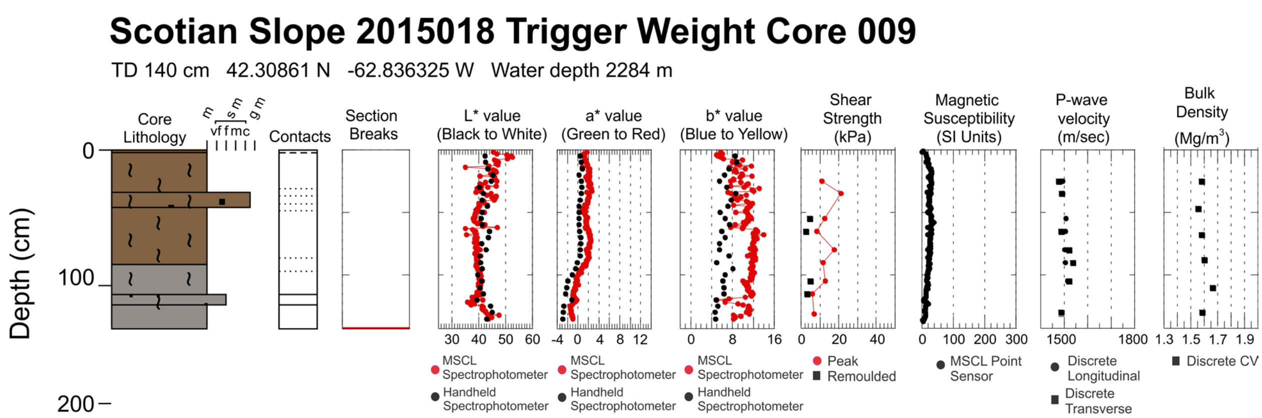

Figure 3.62b. Core plot summary for trigger weight core 2015018 009.

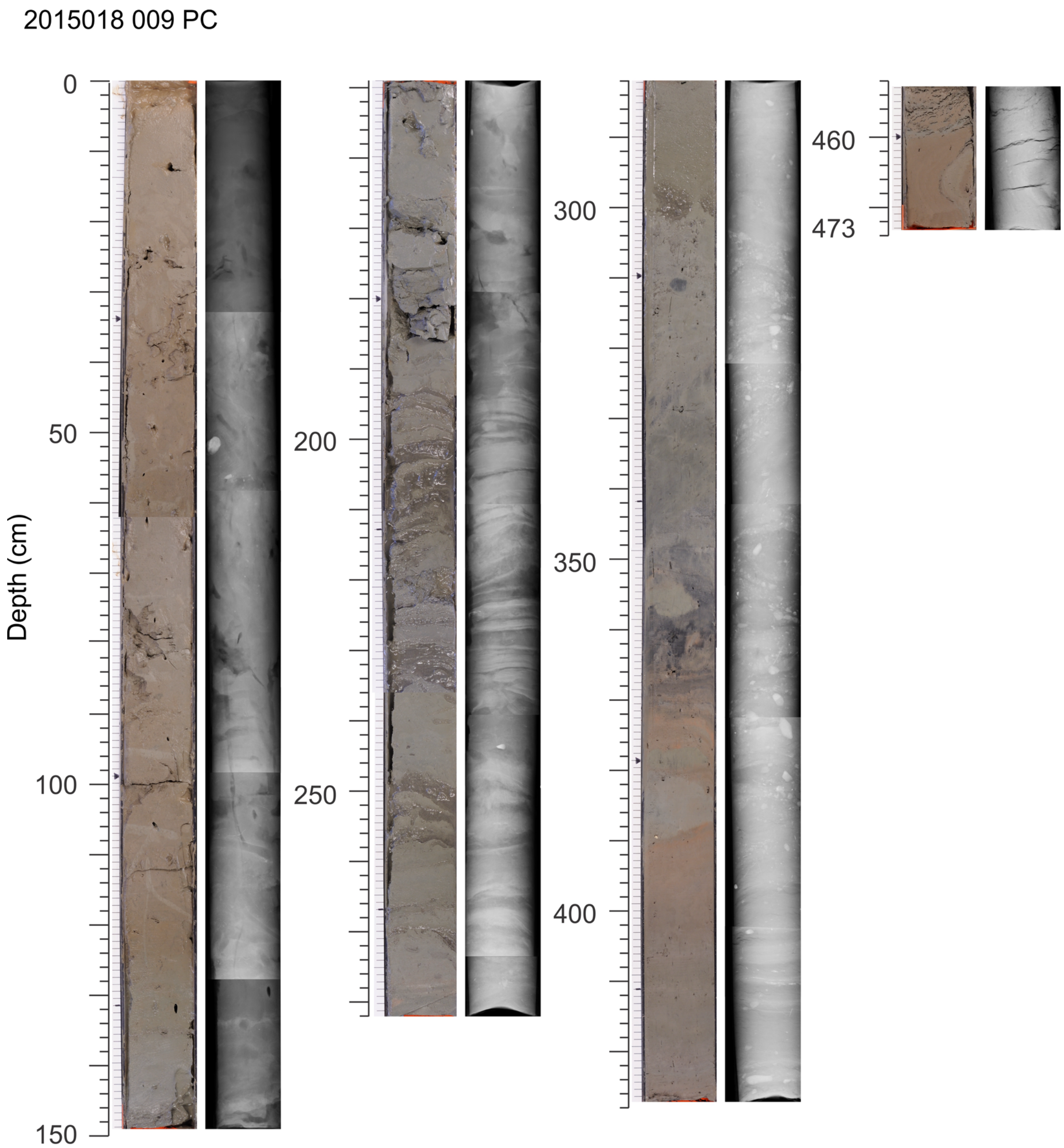

Figure 3.63a. Photography and X-radiography compilation for piston core 2015018 009.

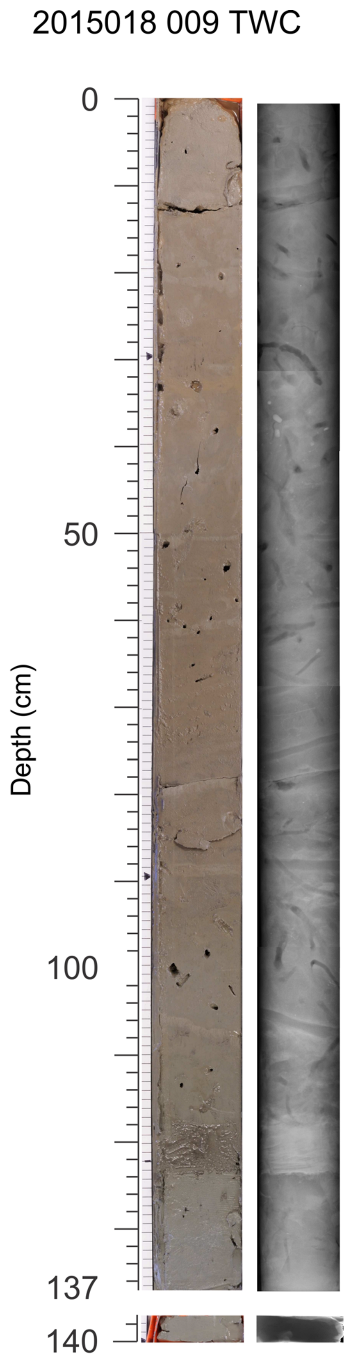

Figure 3.63b. Photography and X-radiography compilation for trigger weight core 2015018 009.

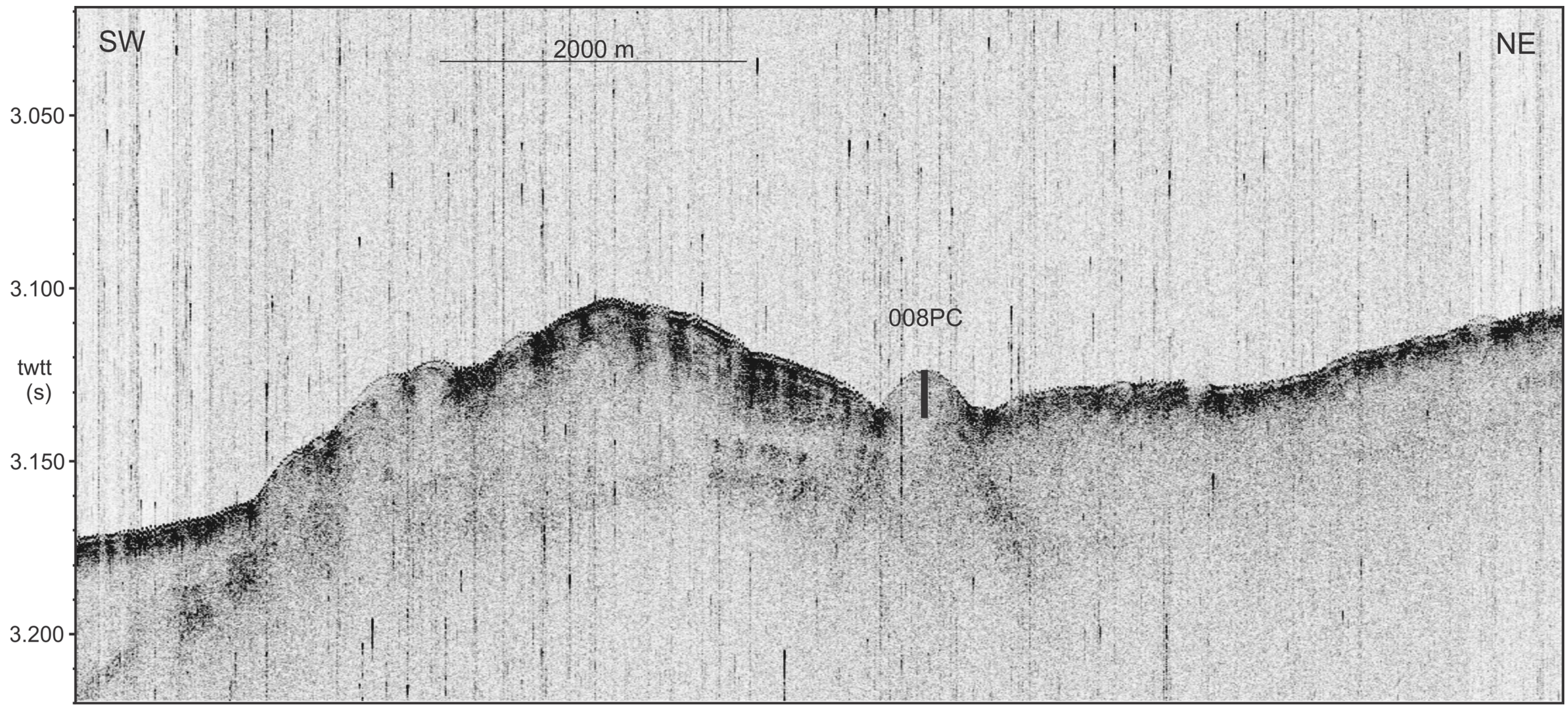

Figure 3.64. High resolution sub-bottom profile showing the acoustic stratigraphy and position of core 2015018 008 (Campbell and MacDonald, 2016).

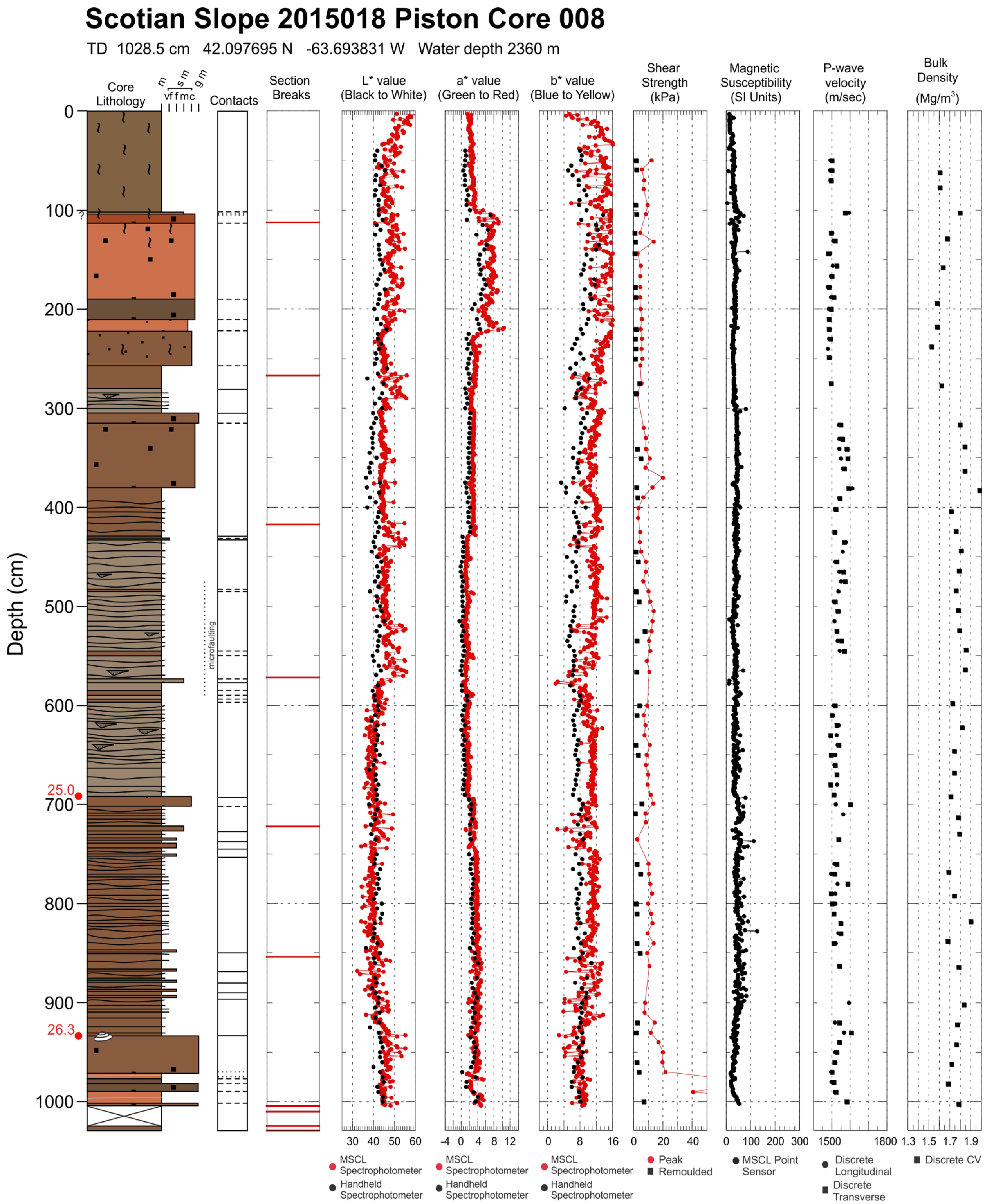

Figure 3.65a. Core plot summary for piston core 2015018 008.

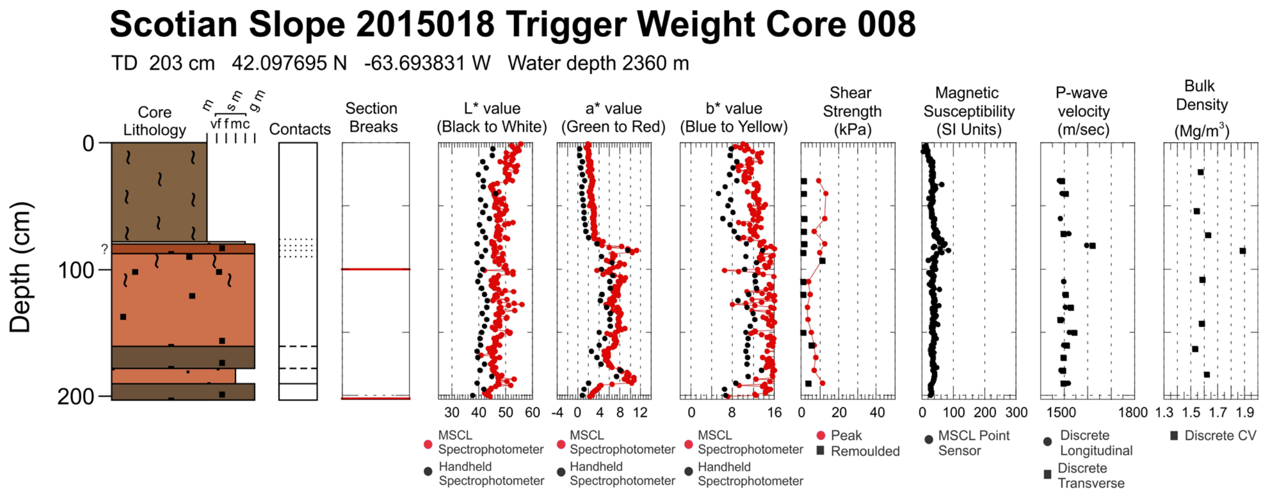

Figure 3.65b. Core plot summary for trigger weight core 2015018 008.

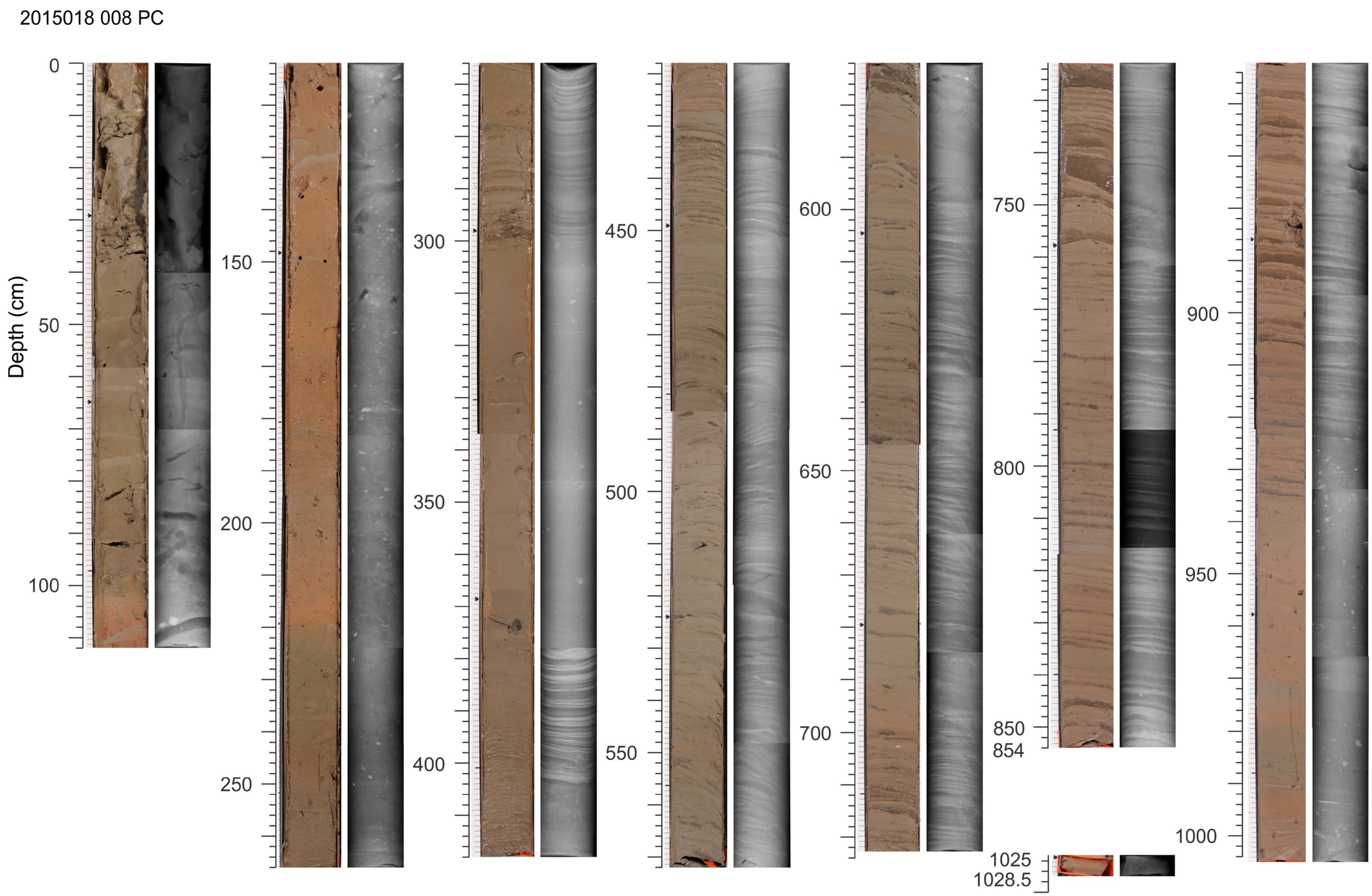

Figure 3.66a. Photography and X-radiography compilation for piston core 2015018 008.

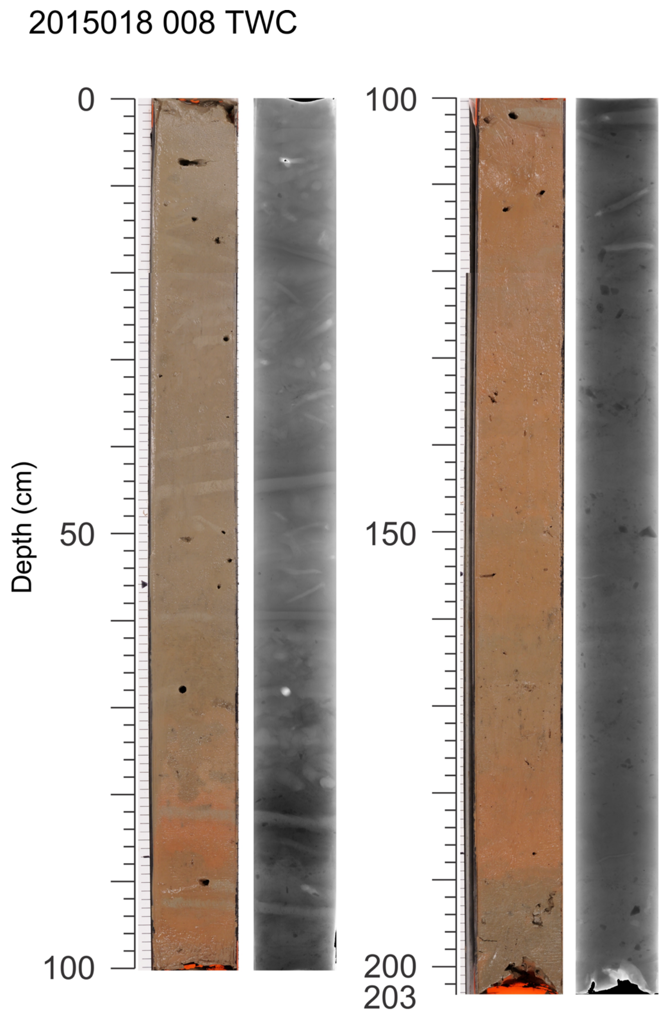

Figure 3.66b. Photography and X-radiography compilation for trigger weight core 2015018 008.

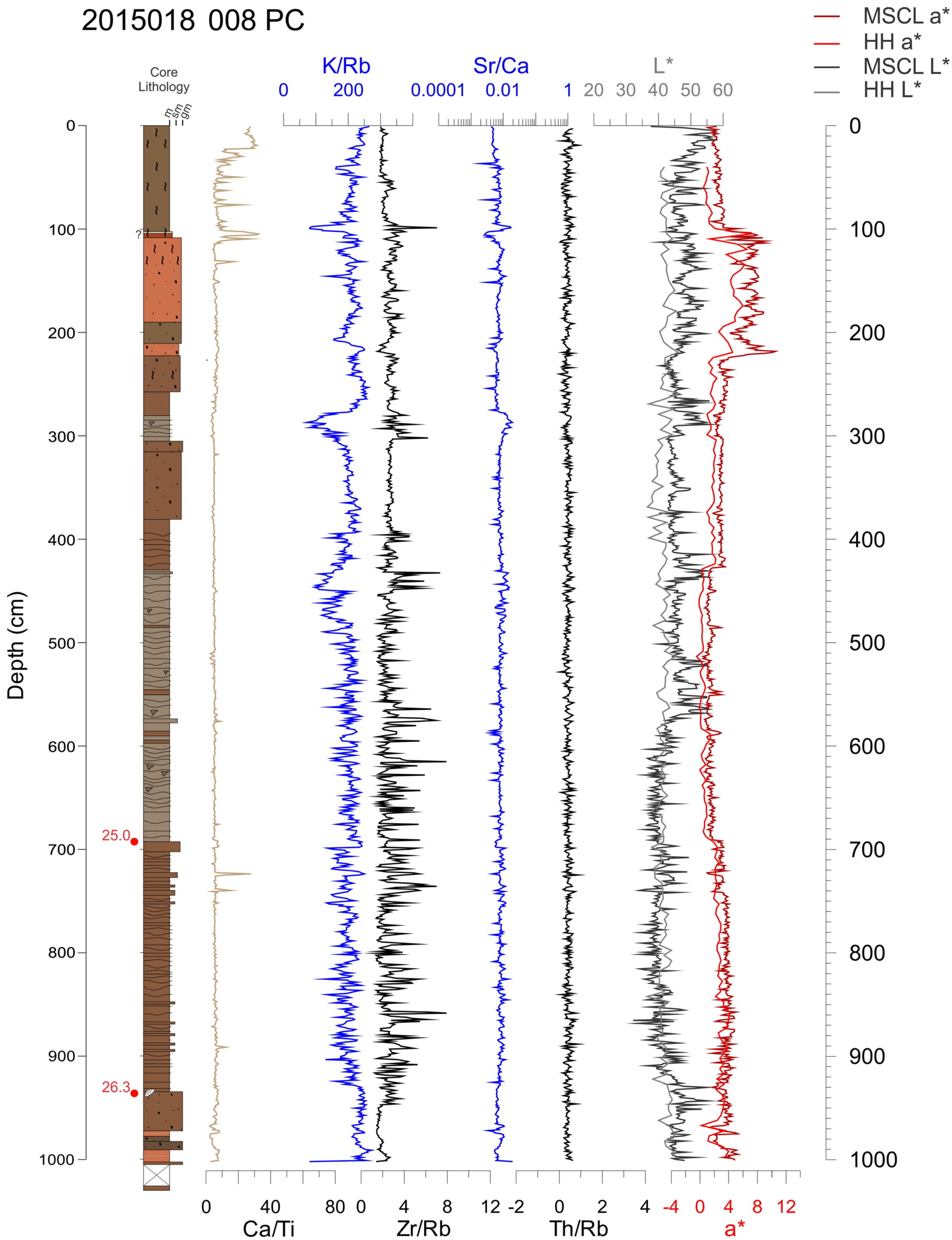

Figure 3.67. Down-core pXRF analyses for piston core 2015018 008. MSCL - Multi Sensor Core Logger; HH - handheld spectrophotometry.

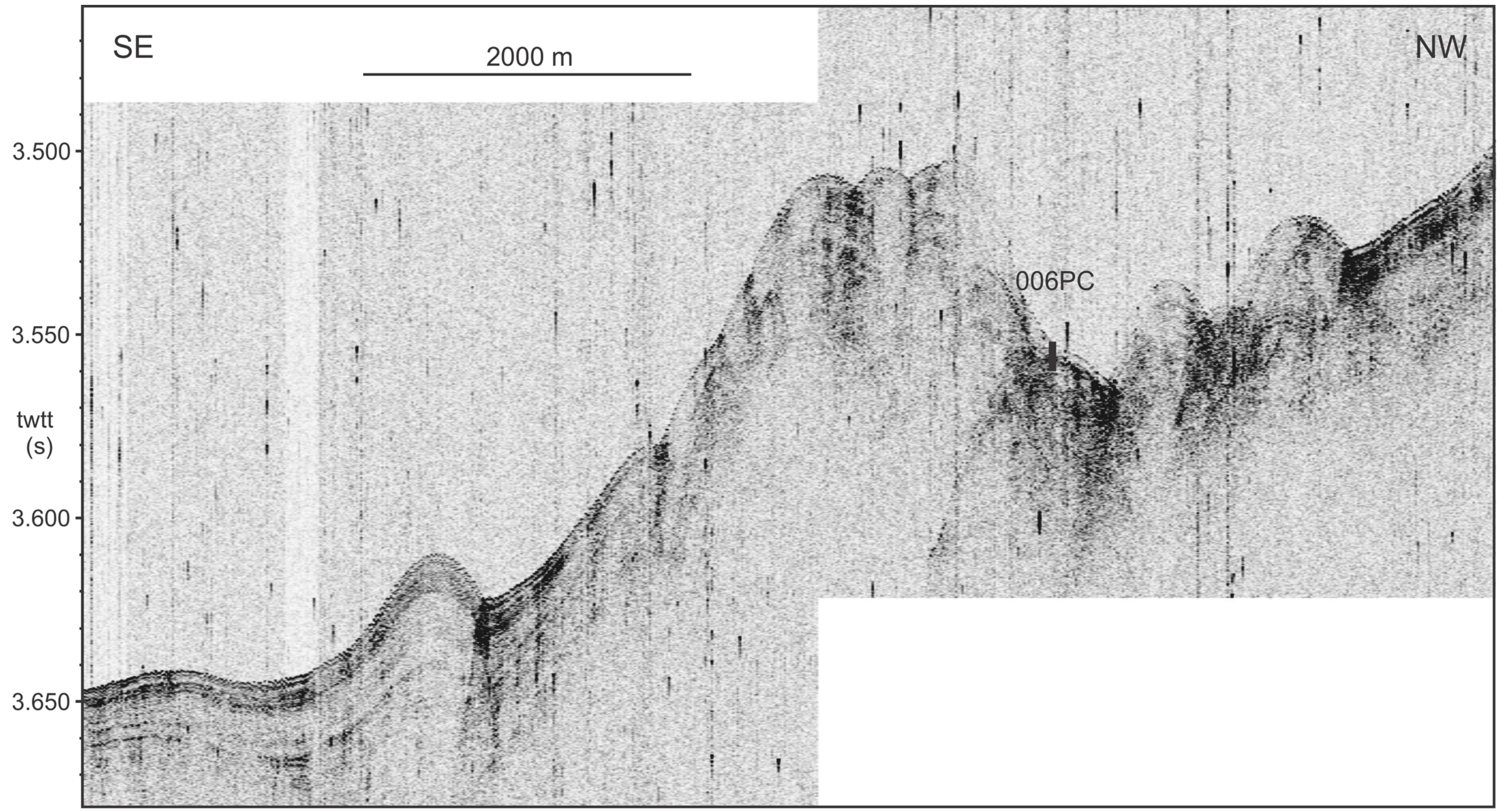

Figure 3.68. High resolution sub-bottom profile showing the acoustic stratigraphy and position of core 2015018 006 (Campbell and MacDonald, 2016).

Scotian Slope 2015018 Piston Core 006

TD 597 cm 41.92713 N -63.71642 W Water depth 2648 m

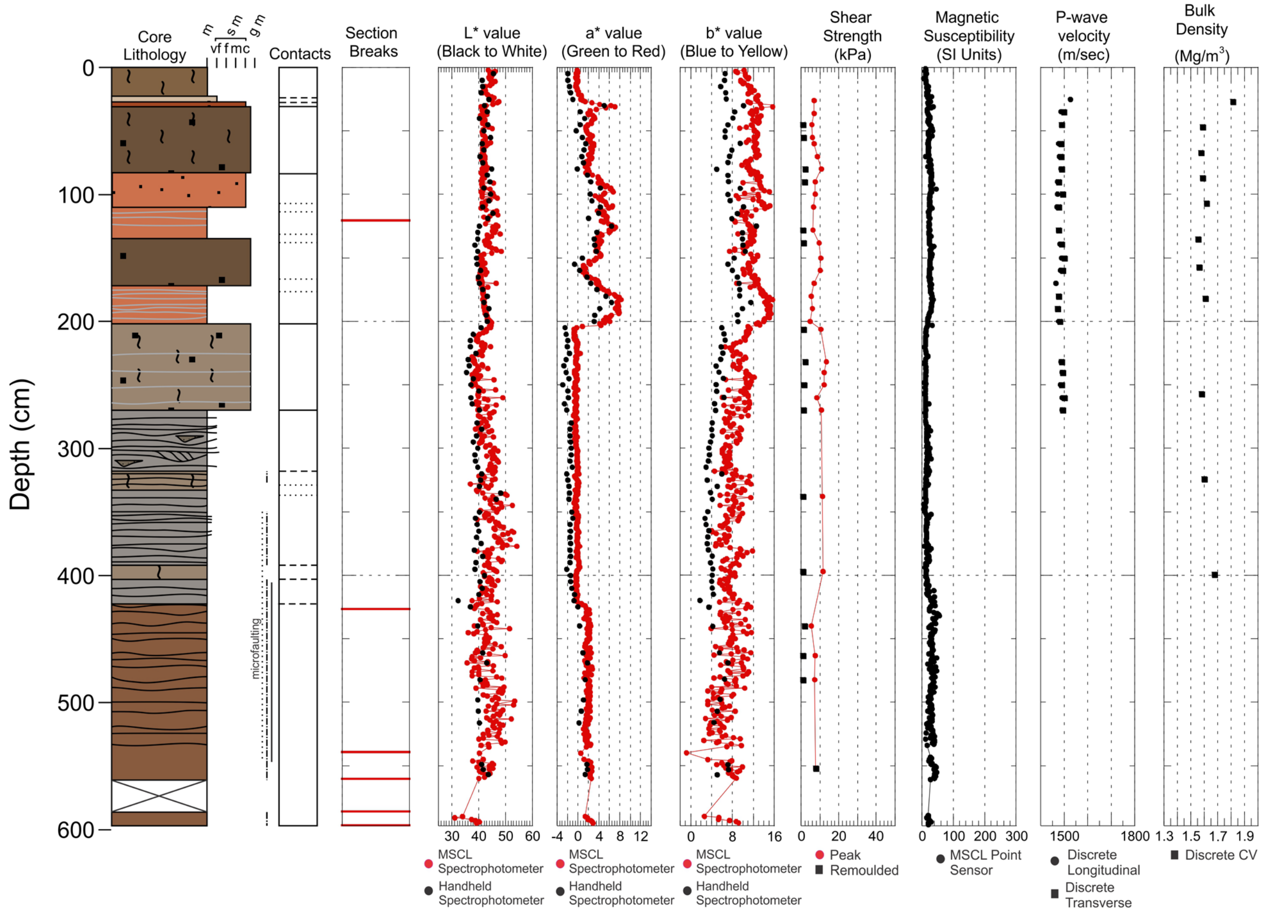

Figure 3.69a. Core plot summary for piston core 2015018 006.

Scotian Slope 2015018 Trigger Weight Core 006

TD 204 cm 41.92713 N -63.71642 W Water depth 2648 m

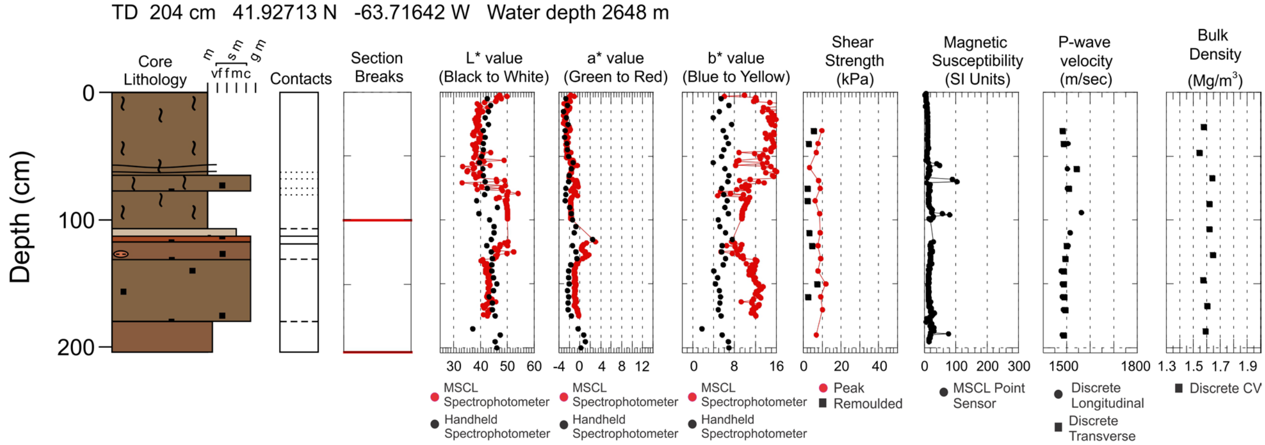

Figure 3.69b. Core plot summary for trigger weight core 2015018 006.

2015018 006 PC

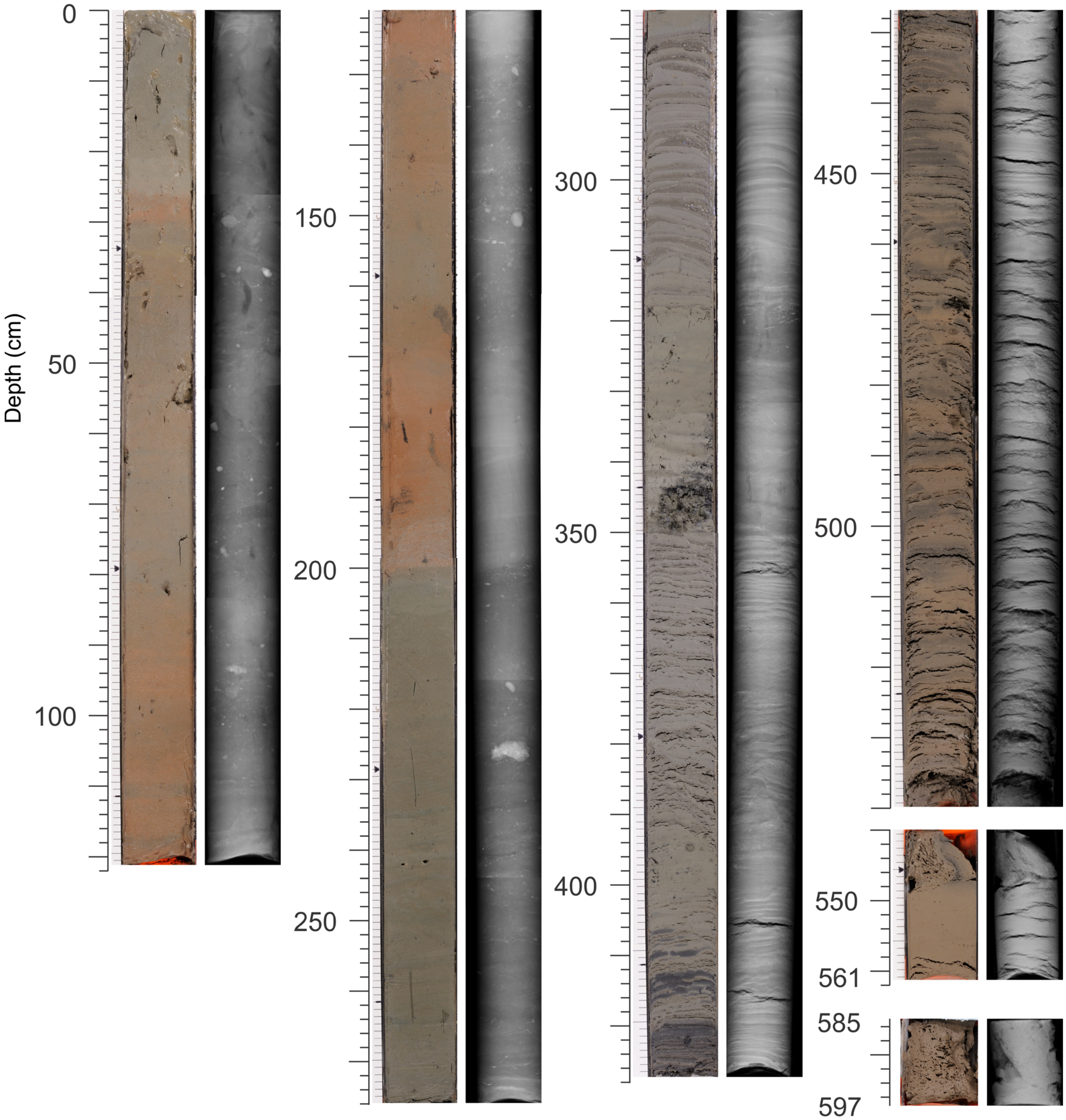

Figure 3.70a. Photography and X-radiography compilation for piston core 2015018 006.

2015018 006 TWC

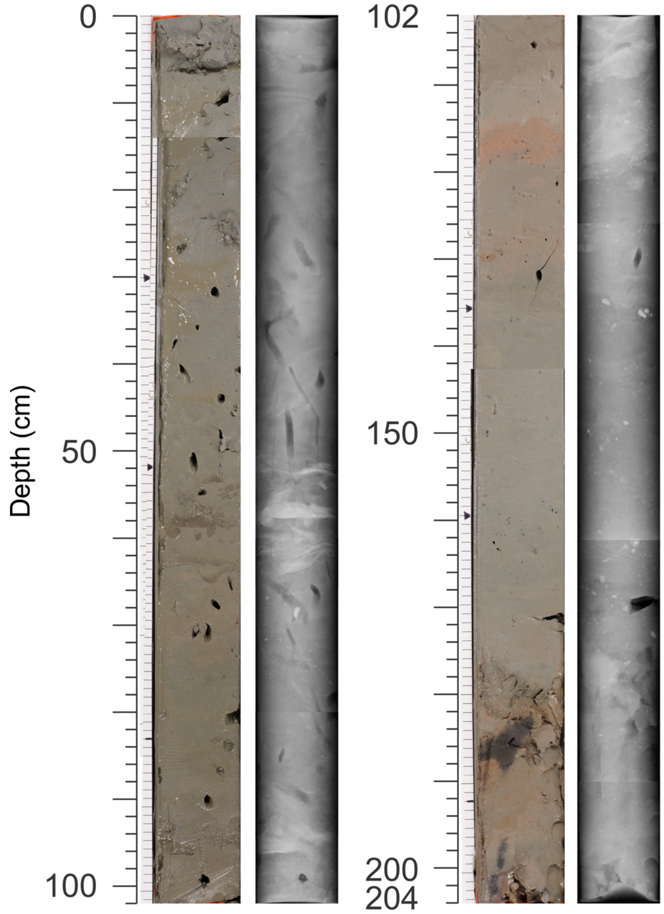

Figure 3.70b. Photography and X-radiography compilation for trigger weight core 2015018 006.

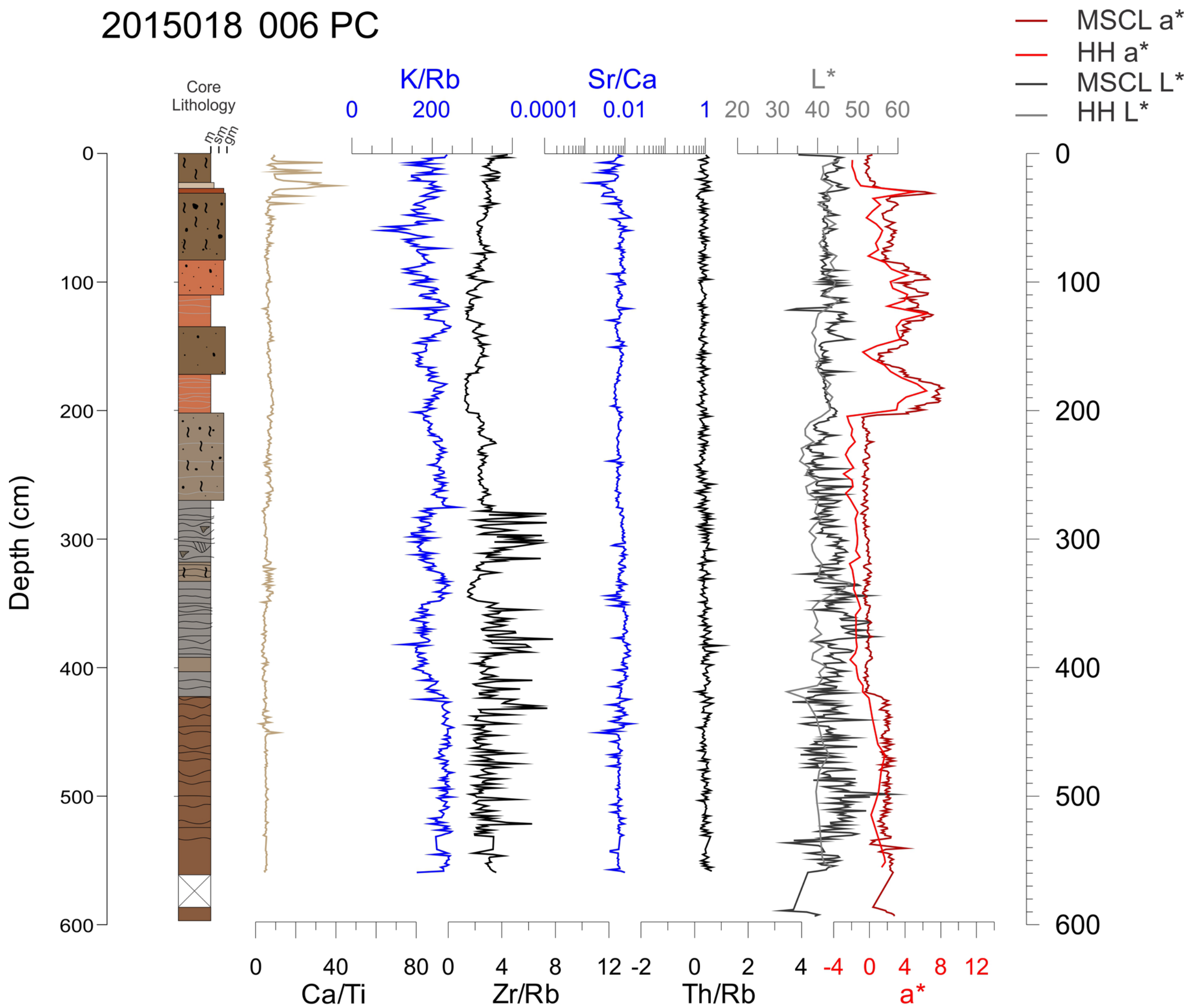

Figure 3.71. Down-core pXRF analyses for piston core 2015018 006. MSCL - Multi Sensor Core Logger; HH - handheld spectrophotometry.

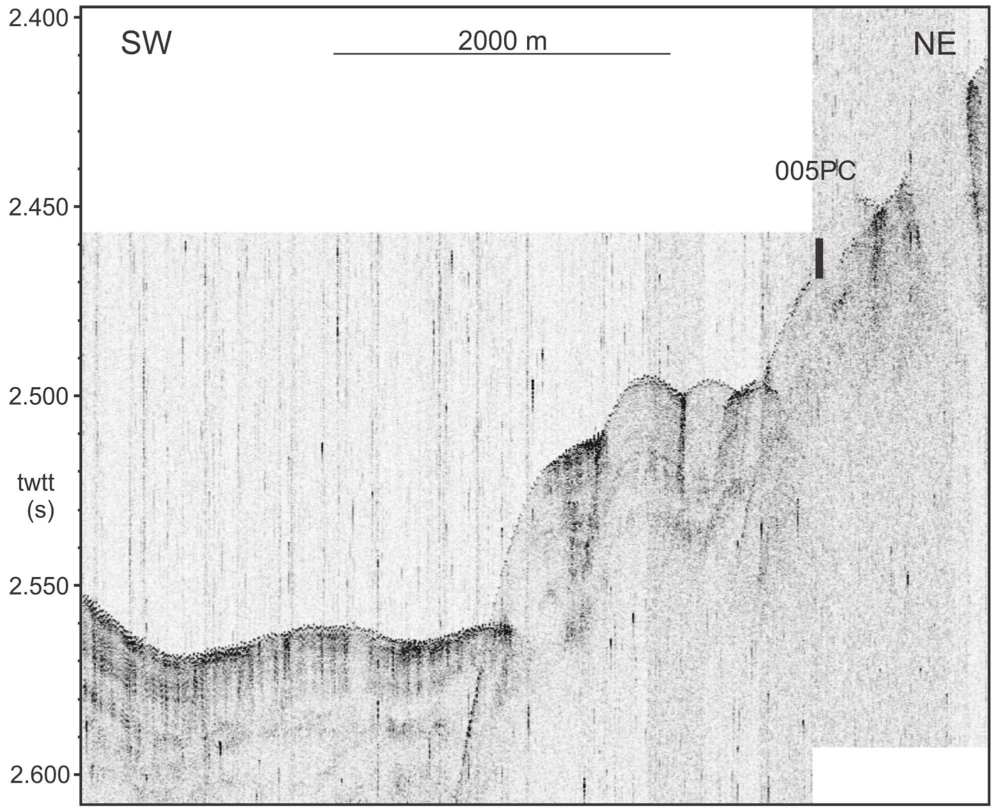

Figure 3.72. High resolution sub-bottom profile showing the acoustic stratigraphy and position of core 2015018 005 (Campbell and MacDonald, 2016).

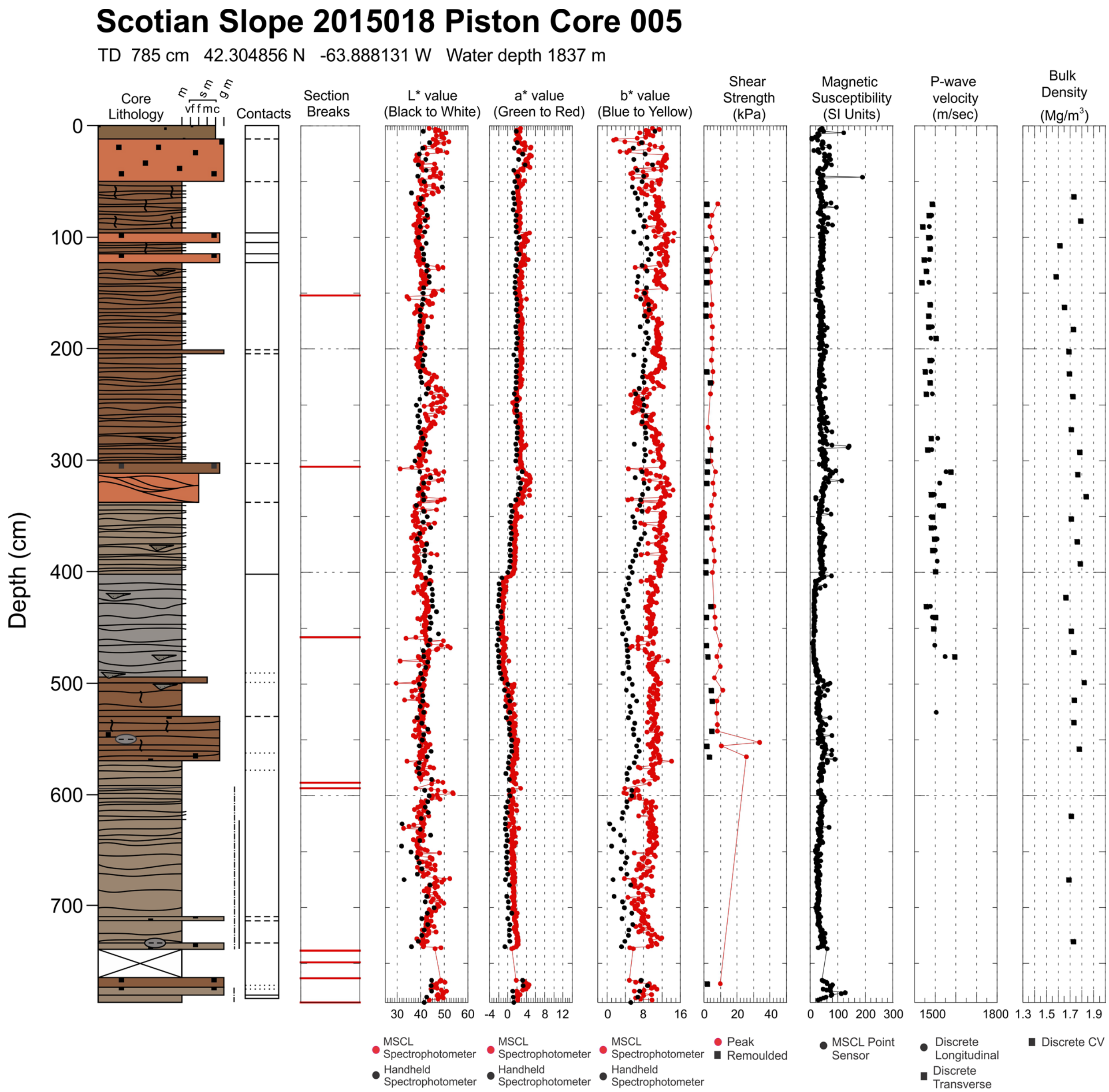

Figure 3.73a. Core plot summary for piston core 2015018 005.

Scotian Slope 2015018 Trigger Weight Core 005

TD 182 cm 42.304856 N -63.888131 W Water depth 1837 m

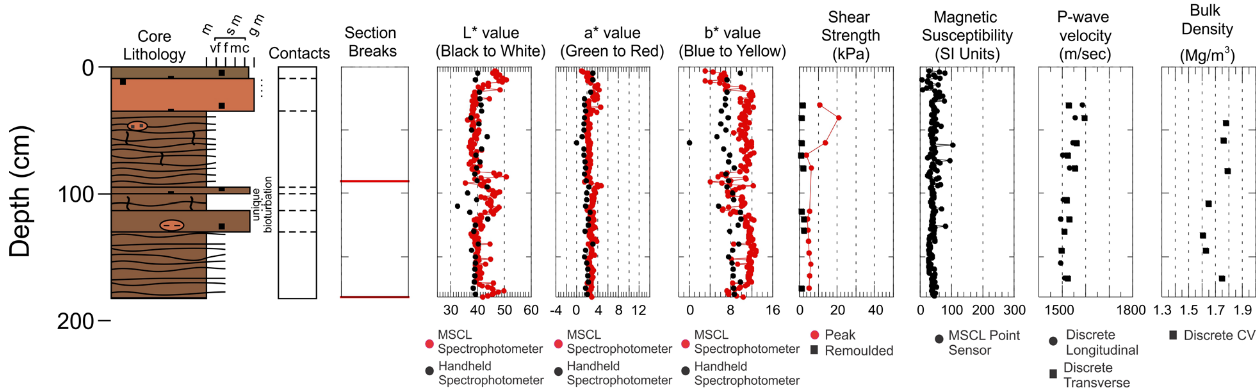

Figure 3.73b. Core plot summary for trigger weight core 2015018 005.

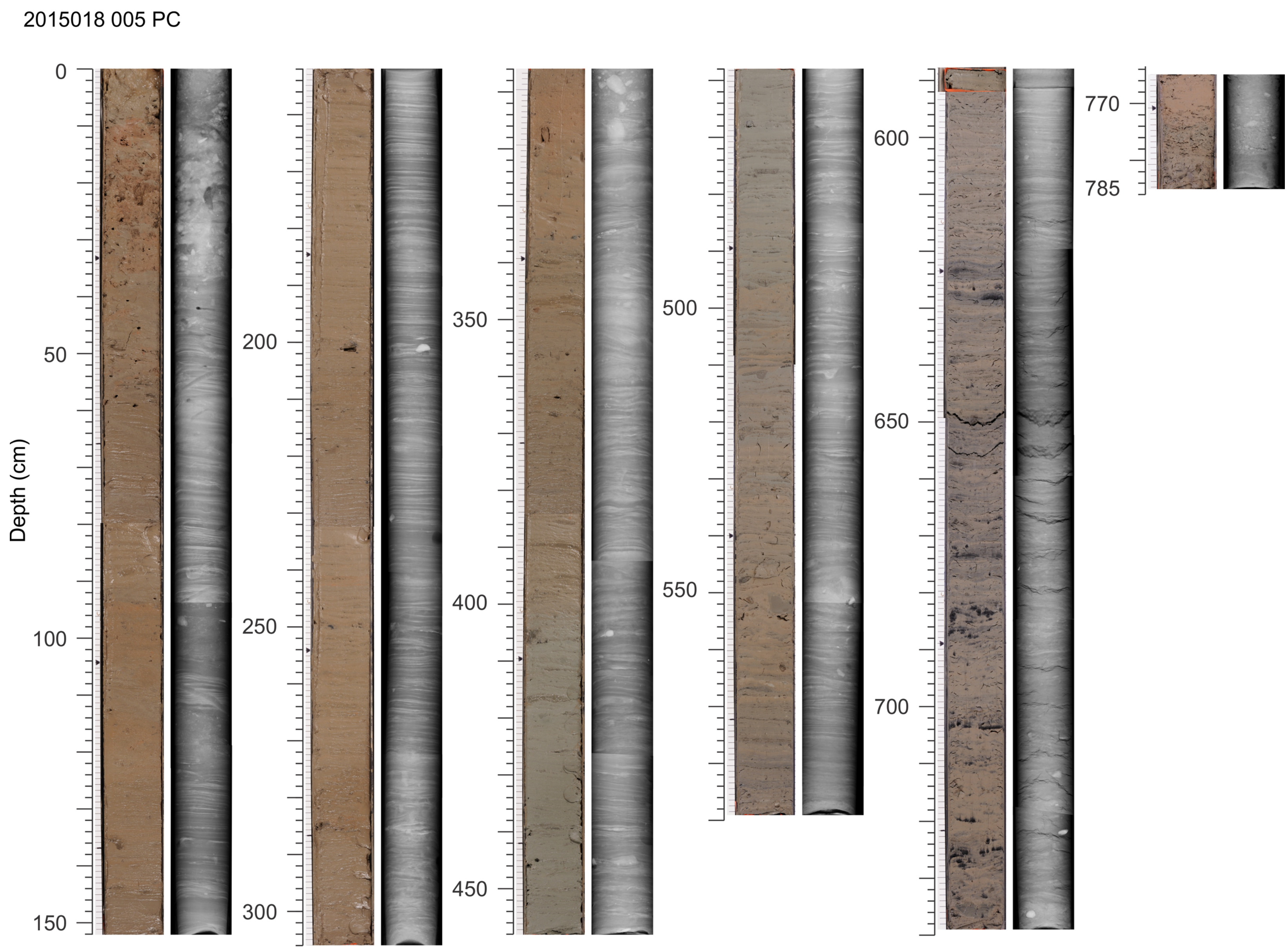

Figure 3.74a. Photography and X-radiography compilation for piston core 2015018 005.

2015018 005 TWC

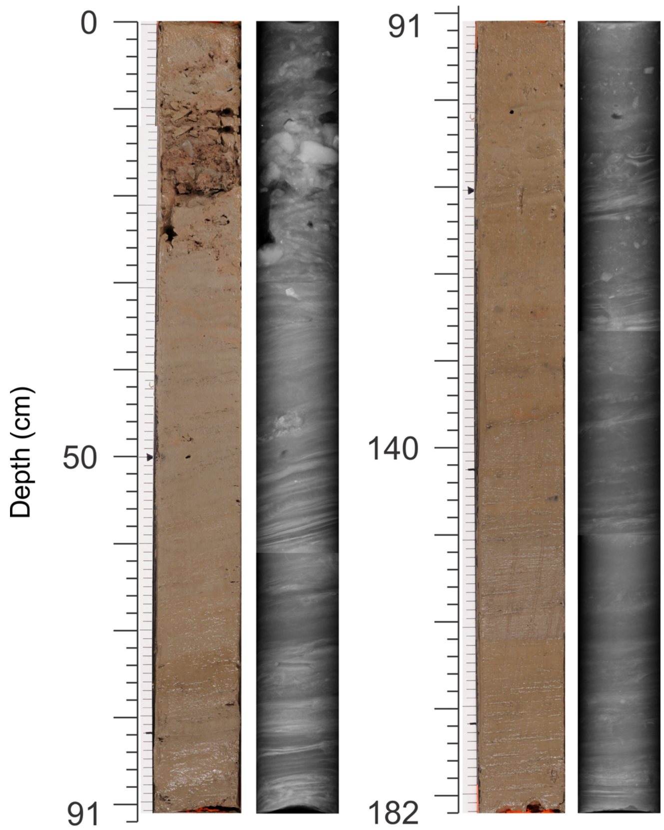

Figure 3.74b. Photography and X-radiography compilation for trigger weight core 2015018 005.

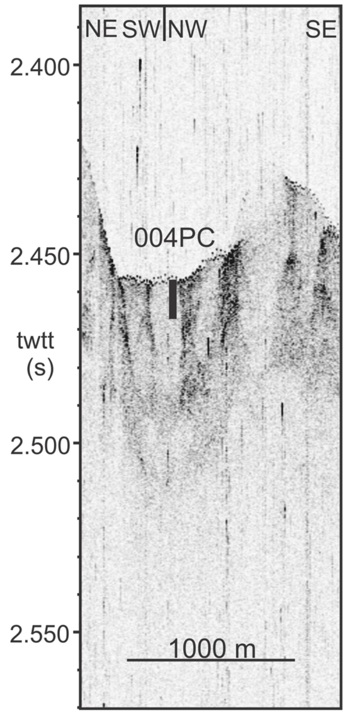

Figure 3.75. High resolution
sub-bottom profile showing
the acoustic stratigraphy and
position of core 2015018 004
(Campbell and MacDonald, 2016).

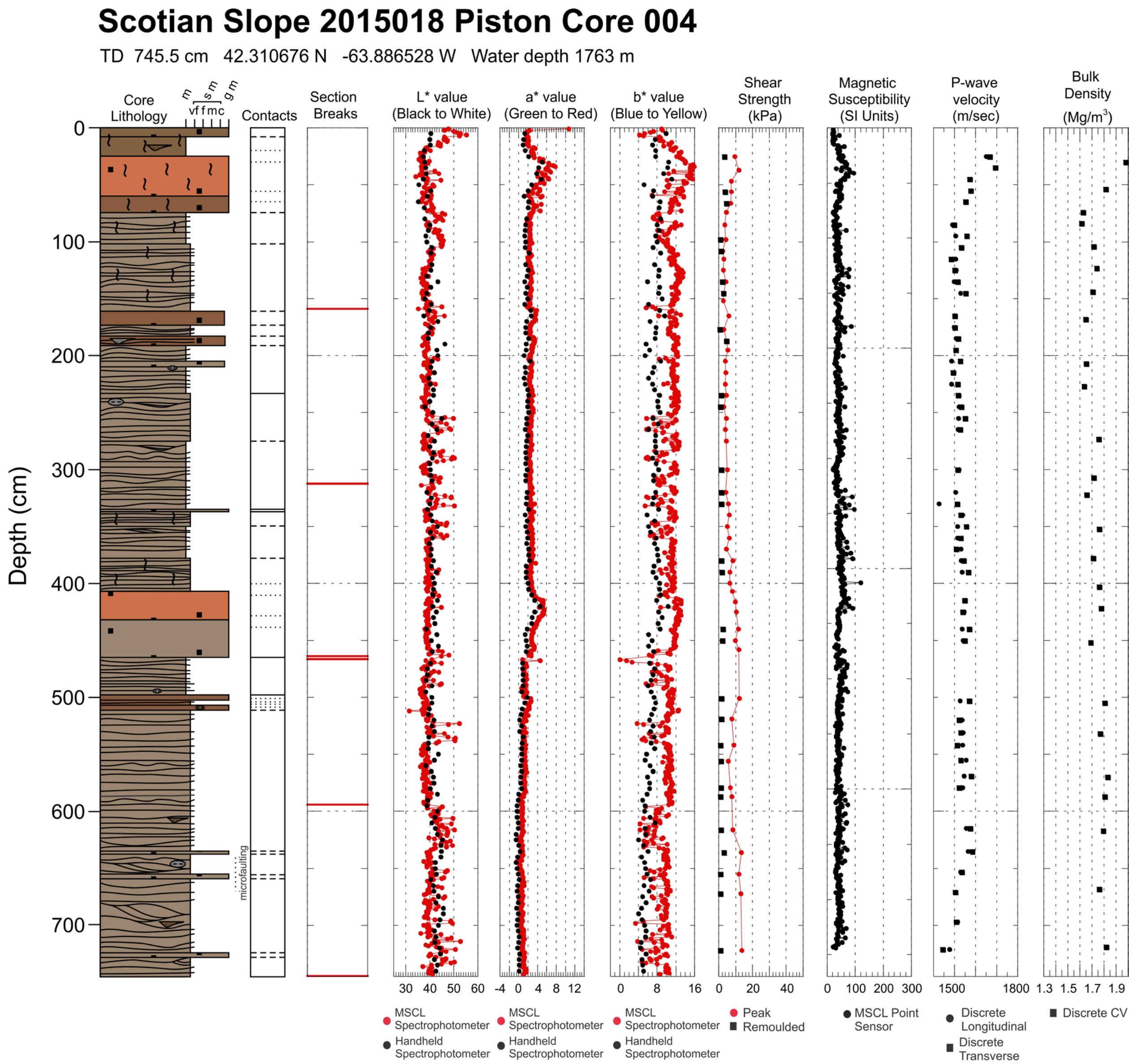

Figure 3.76a. Core plot summary for piston core 2015018 004.

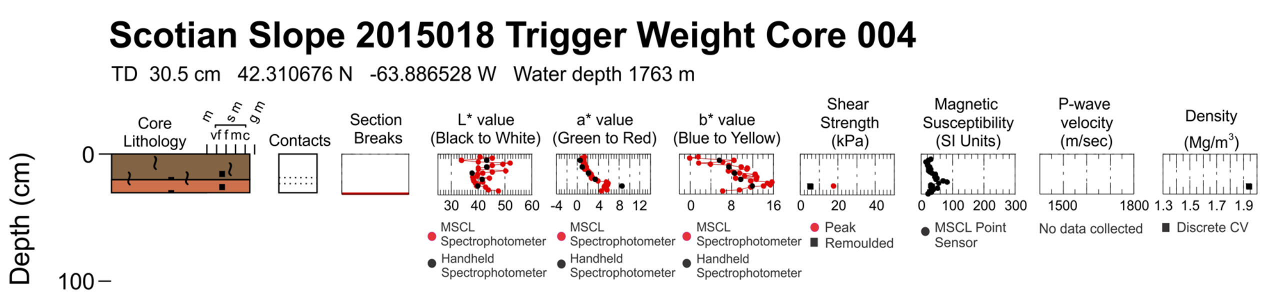

Figure 3.76b. Core plot summary for trigger weight core 2015018 004.

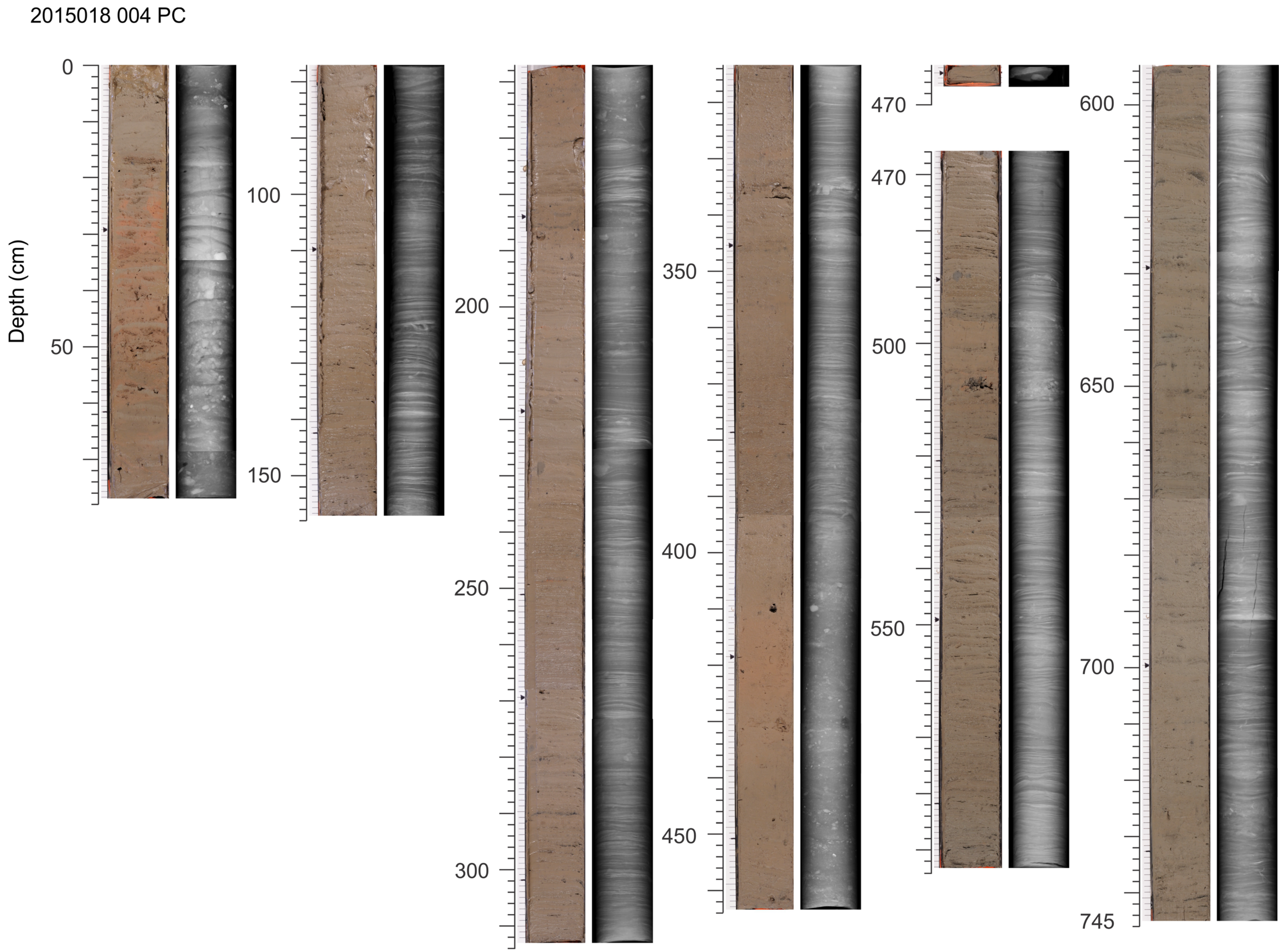

Figure 3.77a. Photography and X-radiography compilation for piston core 2015018 004.

2015018 004 TWC

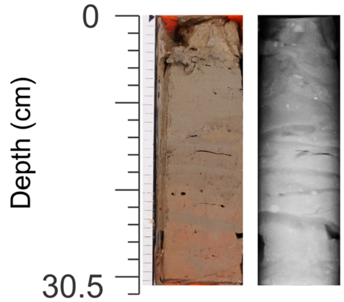

Figure 3.77b. Photography and X-radiography compilation for trigger weight core 2015018 004.

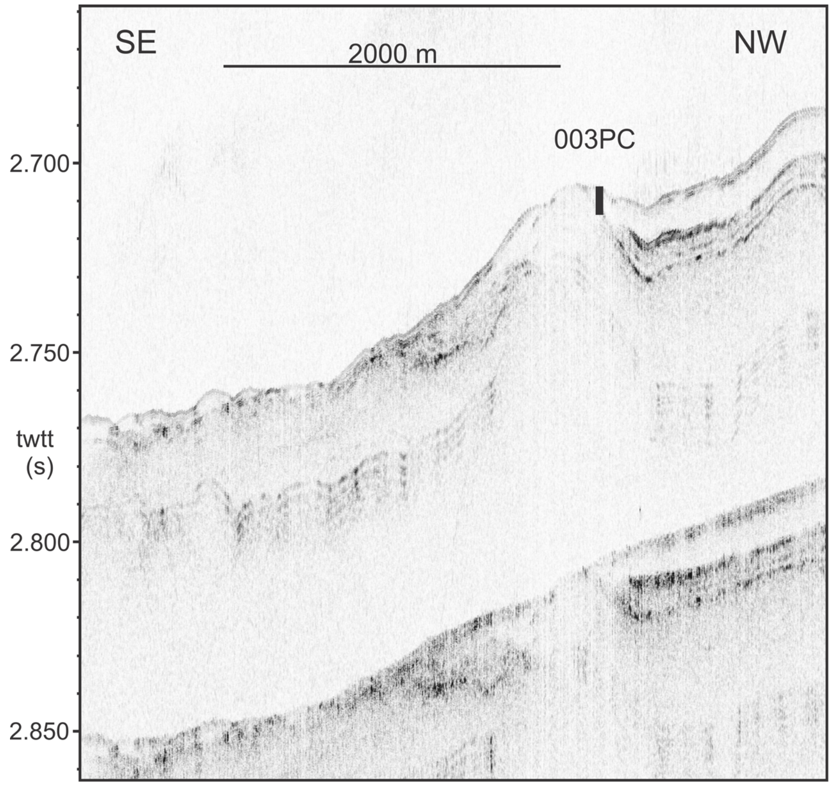

Figure 3.78. High resolution sub-bottom profile showing the acoustic stratigraphy and position of core 2015018 003 (Campbell and MacDonald, 2016).

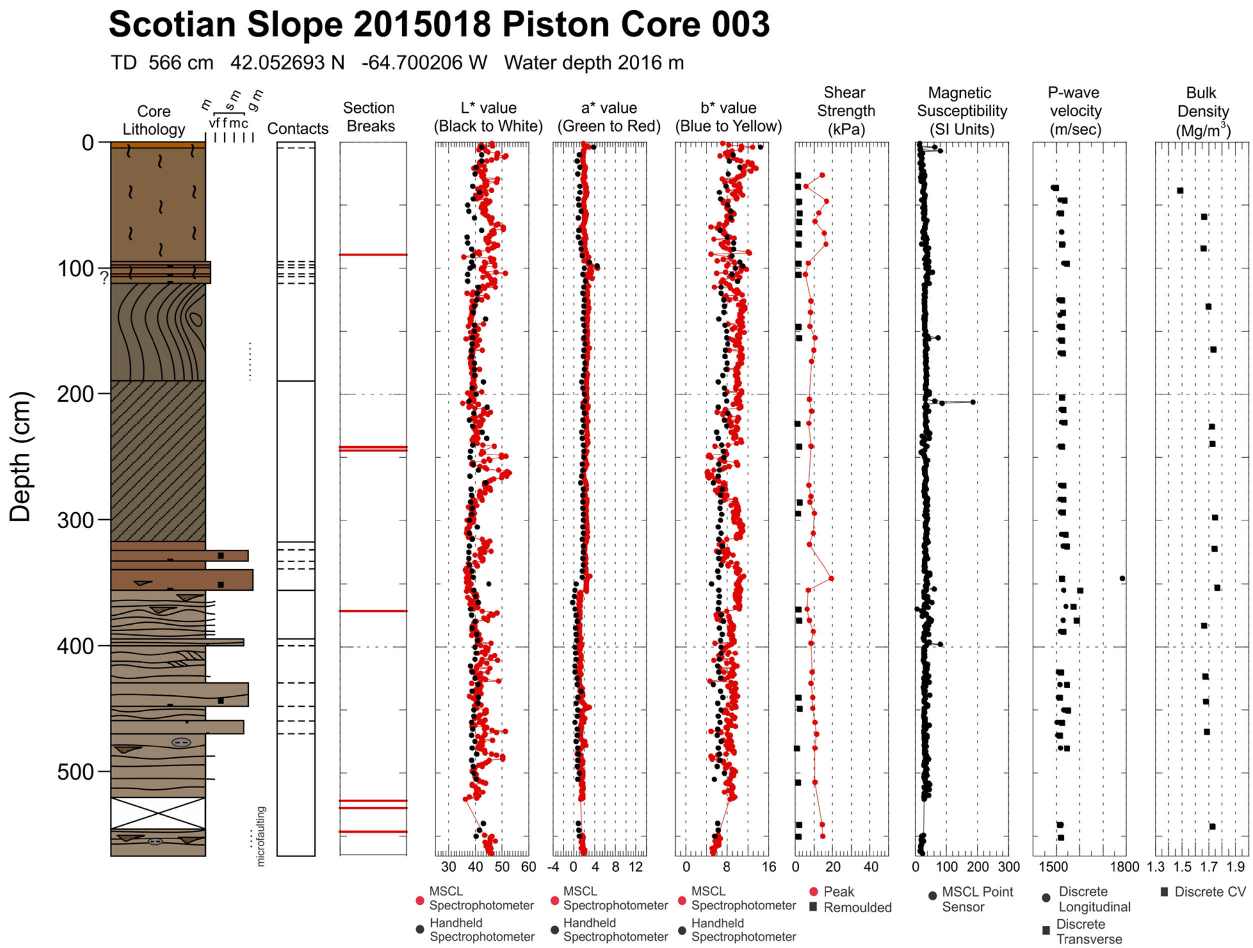

Figure 3.79a. Core plot summary for piston core 2015018 003.

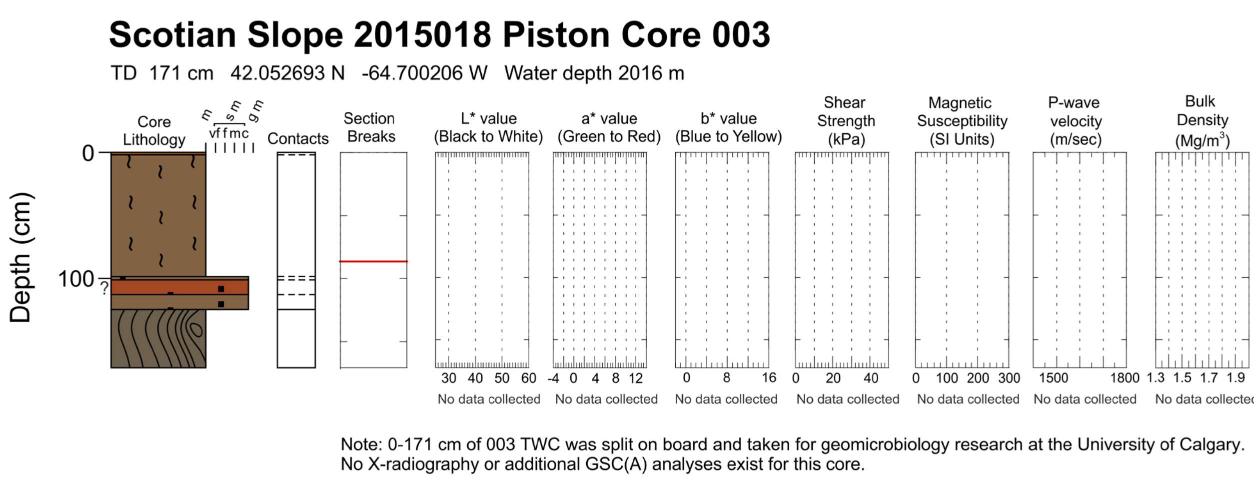

Figure 3.79b. Core plot summary for trigger weight core 2015018 003.

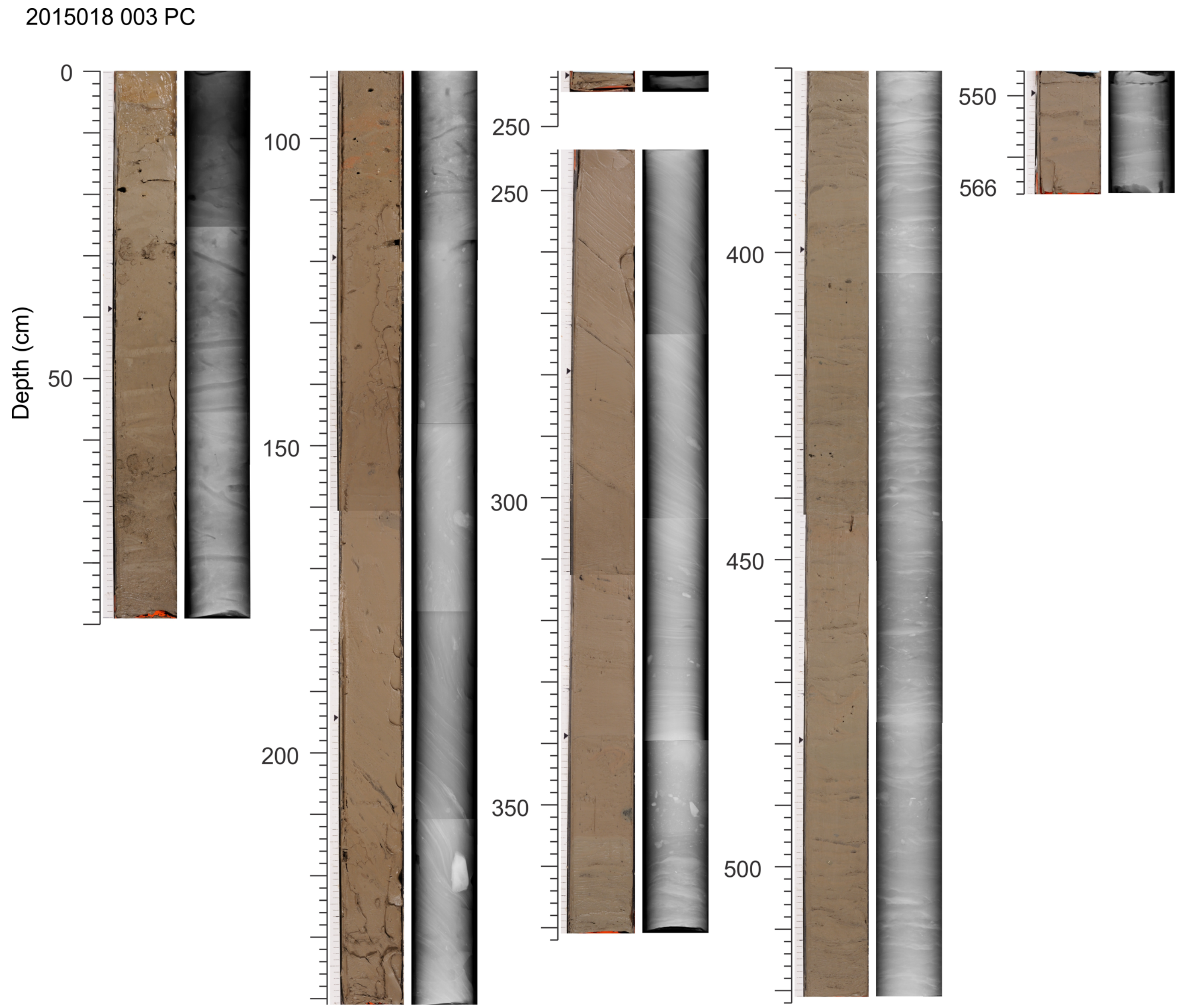

Figure 3.80a. Photography and X-radiography compilation for piston core 2015018 003.

2015018 003 TWC

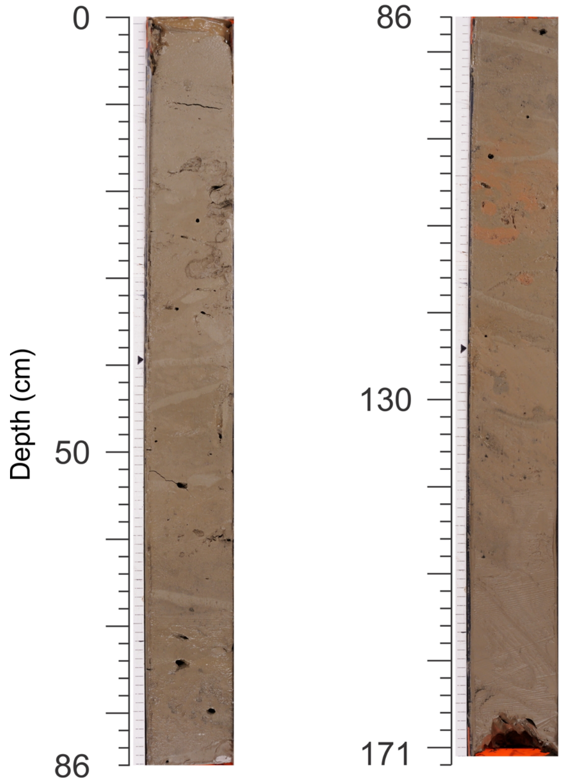

Note: 0-171 cm was taken for geomicrobiology research at the University of Calgary (no X-radiography).

Figure 3.80b. Photography compilation for trigger weight core 2015018 003.

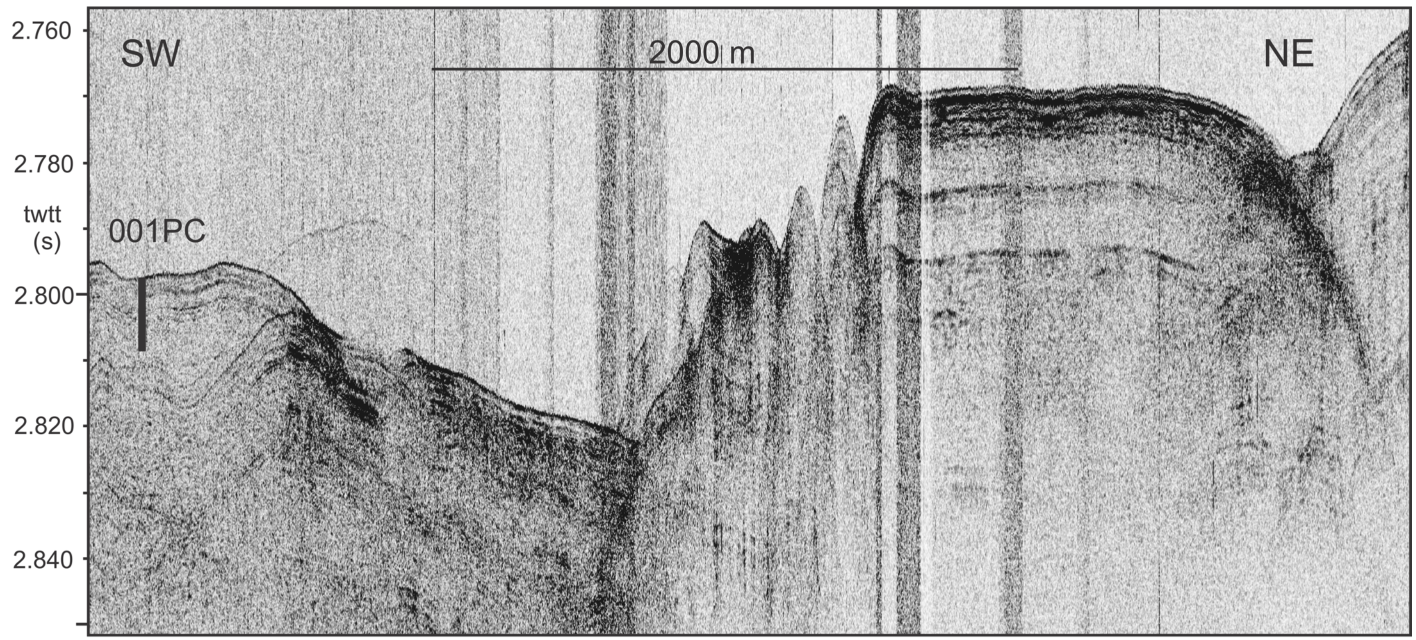

Figure 3.81. High resolution sub-bottom profile showing the acoustic stratigraphy and position of core 2015018 001 (Campbell and MacDonald, 2016).

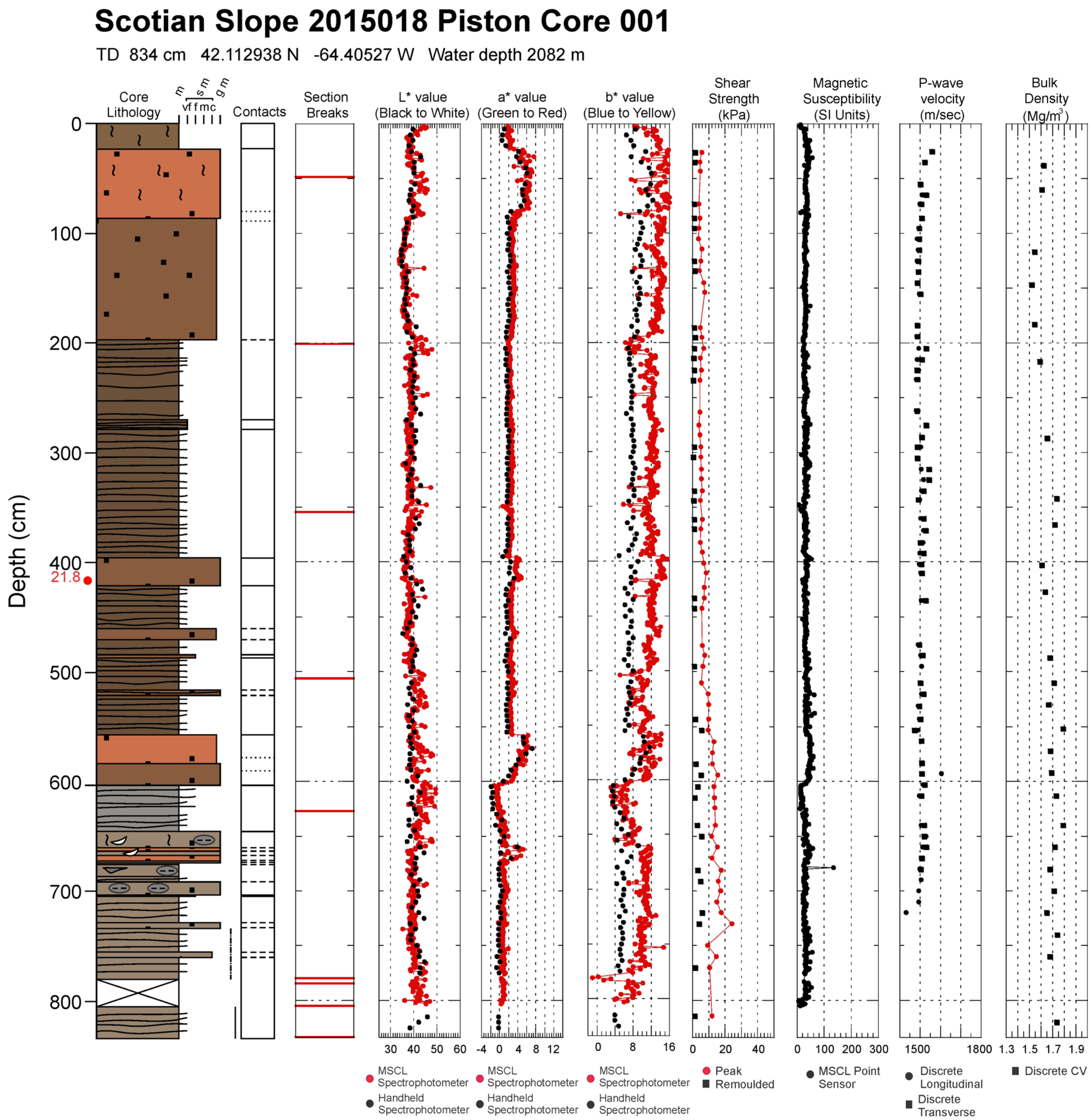

Figure 3.82a. Core plot summary for piston core 2015018 001.

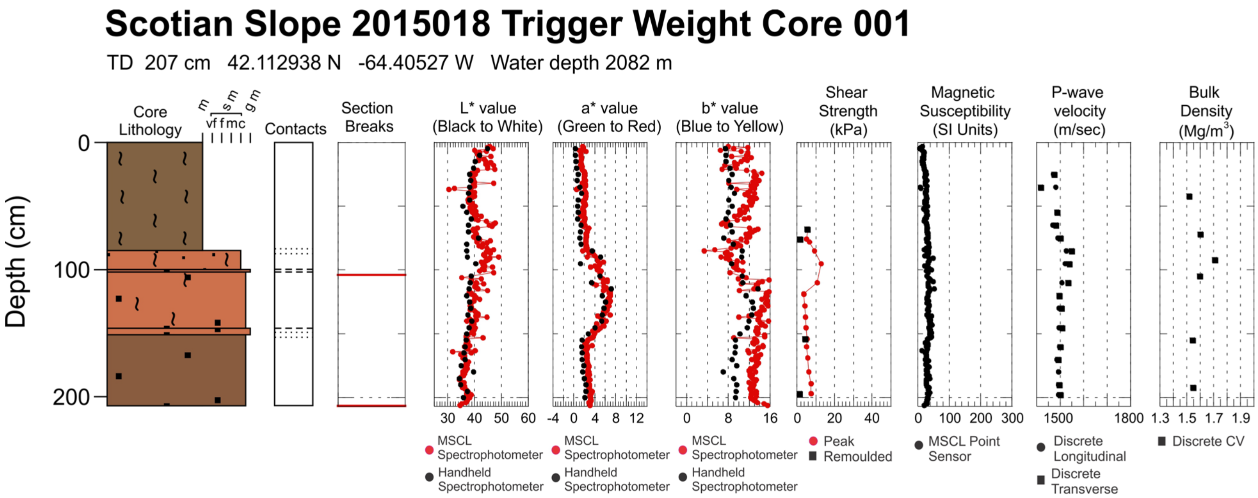

Figure 3.82b. Core plot summary for trigger weight core 2015018 001.

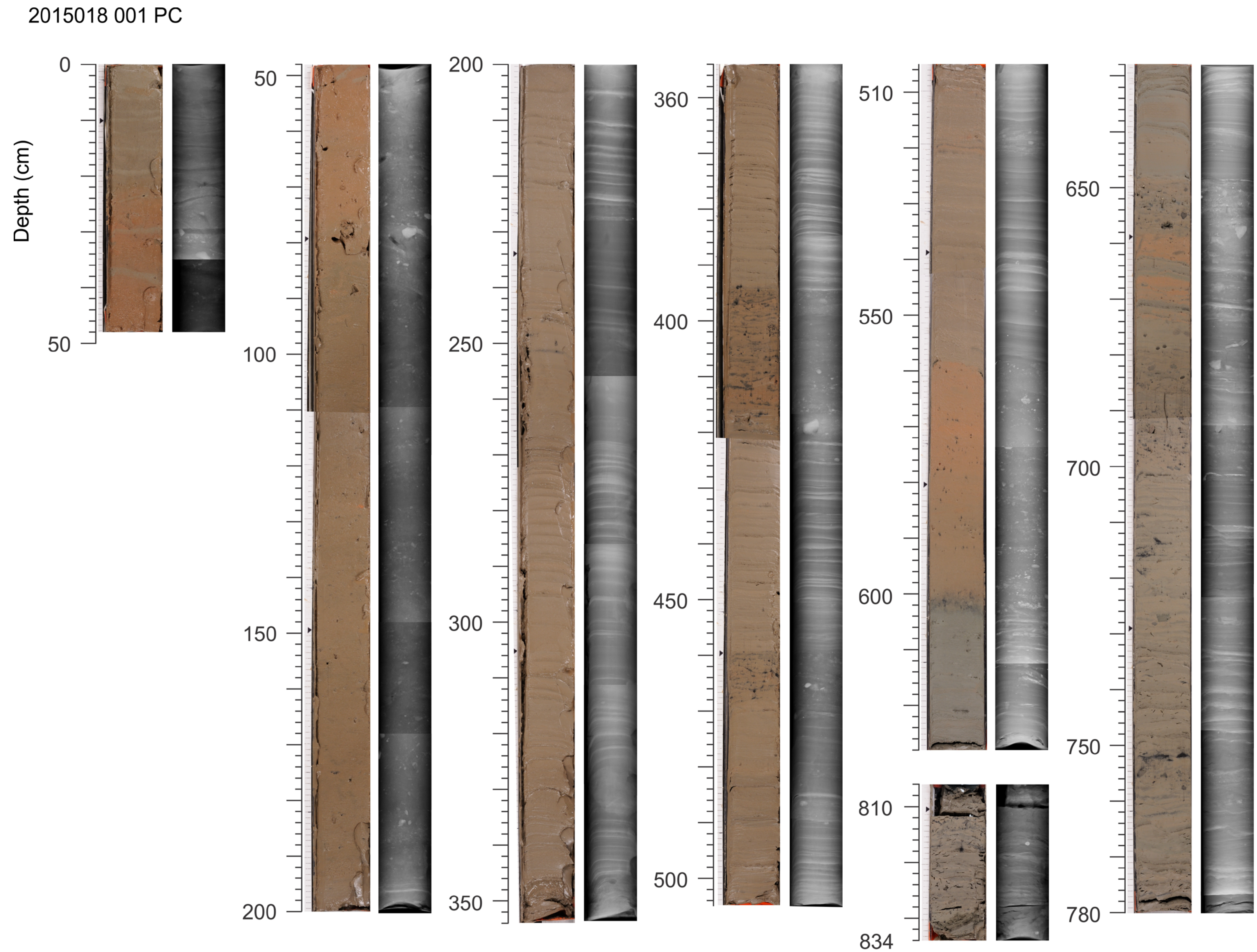

Figure 3.83a. Photography and X-radiography compilation for piston core 2015018 001.

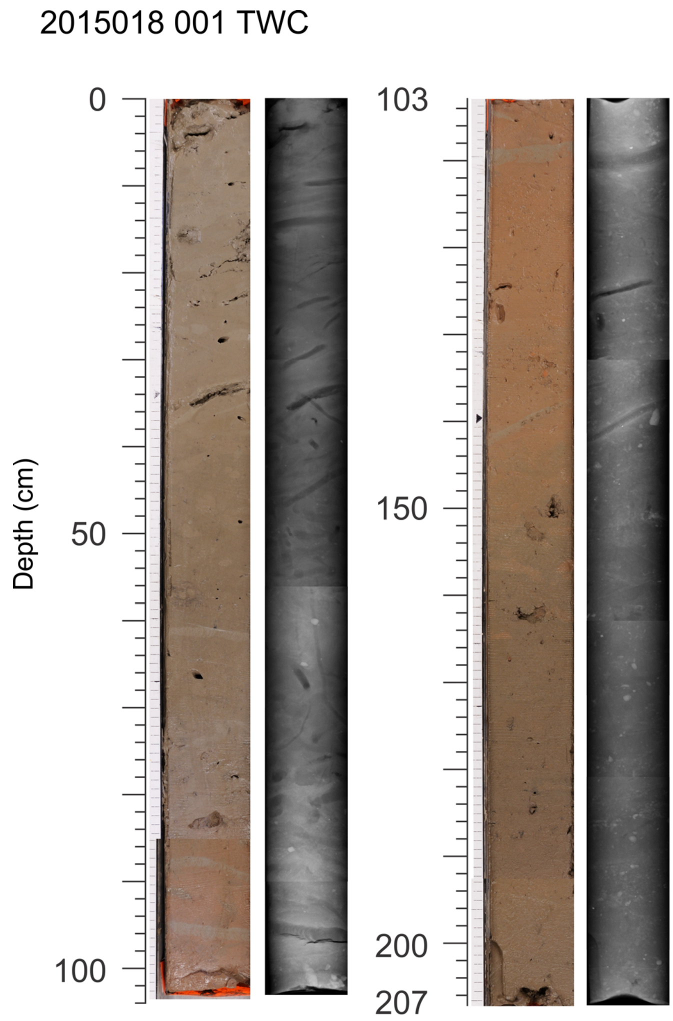

Figure 3.83b. Photography and X-radiography compilation trigger weight core 2015018 001.

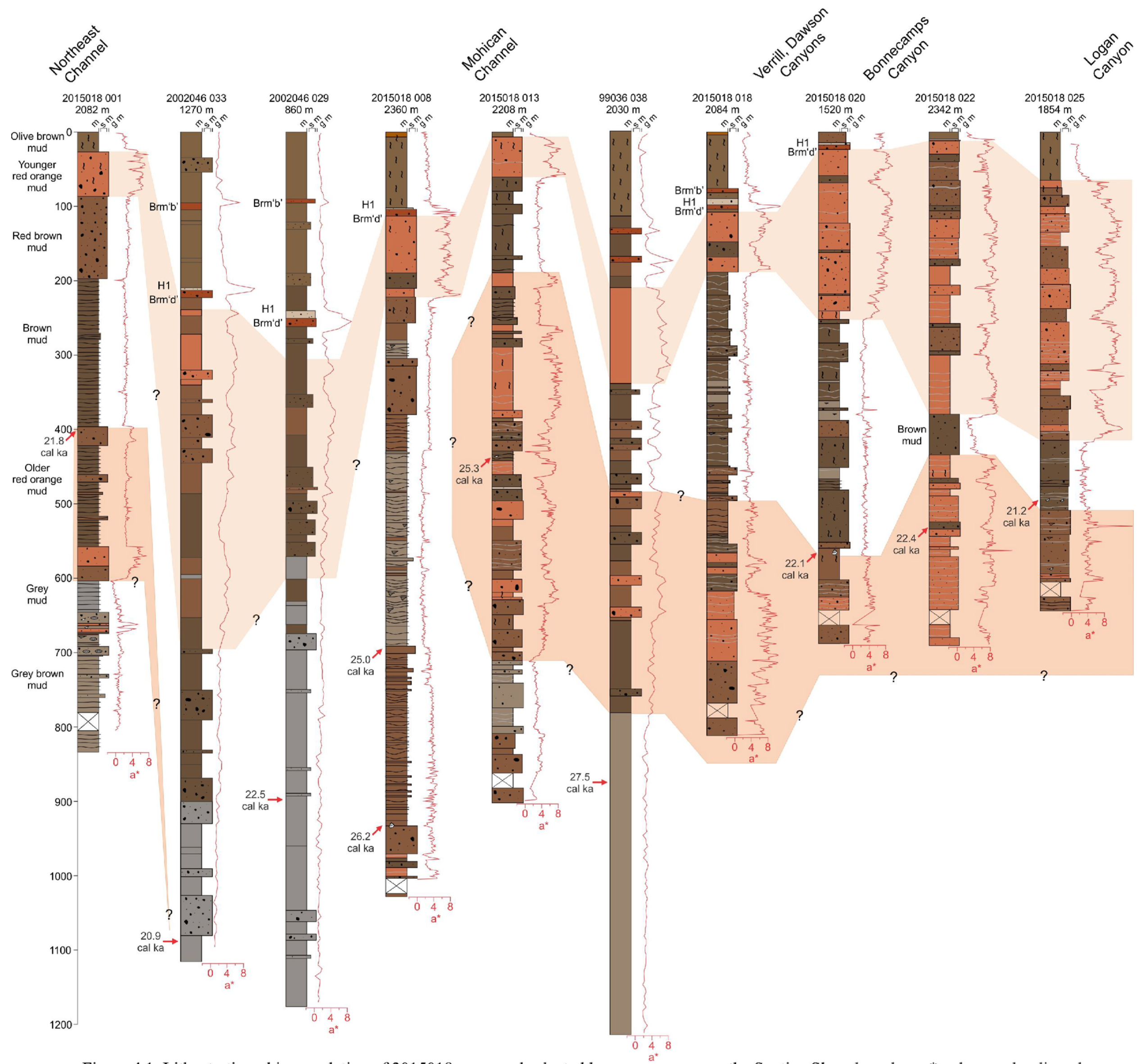

Figure 4.1. Lithostratigraphic correlation of 2015018 cores and selected legacy cores across the Scotian Slope based on a* values and radiocarbon dating (Table 2.1). Younger red orange mud correlation is shown in light orange. Older red orange mud correlation is shown in dark orange. Refer to Figure 3.2 for legend.

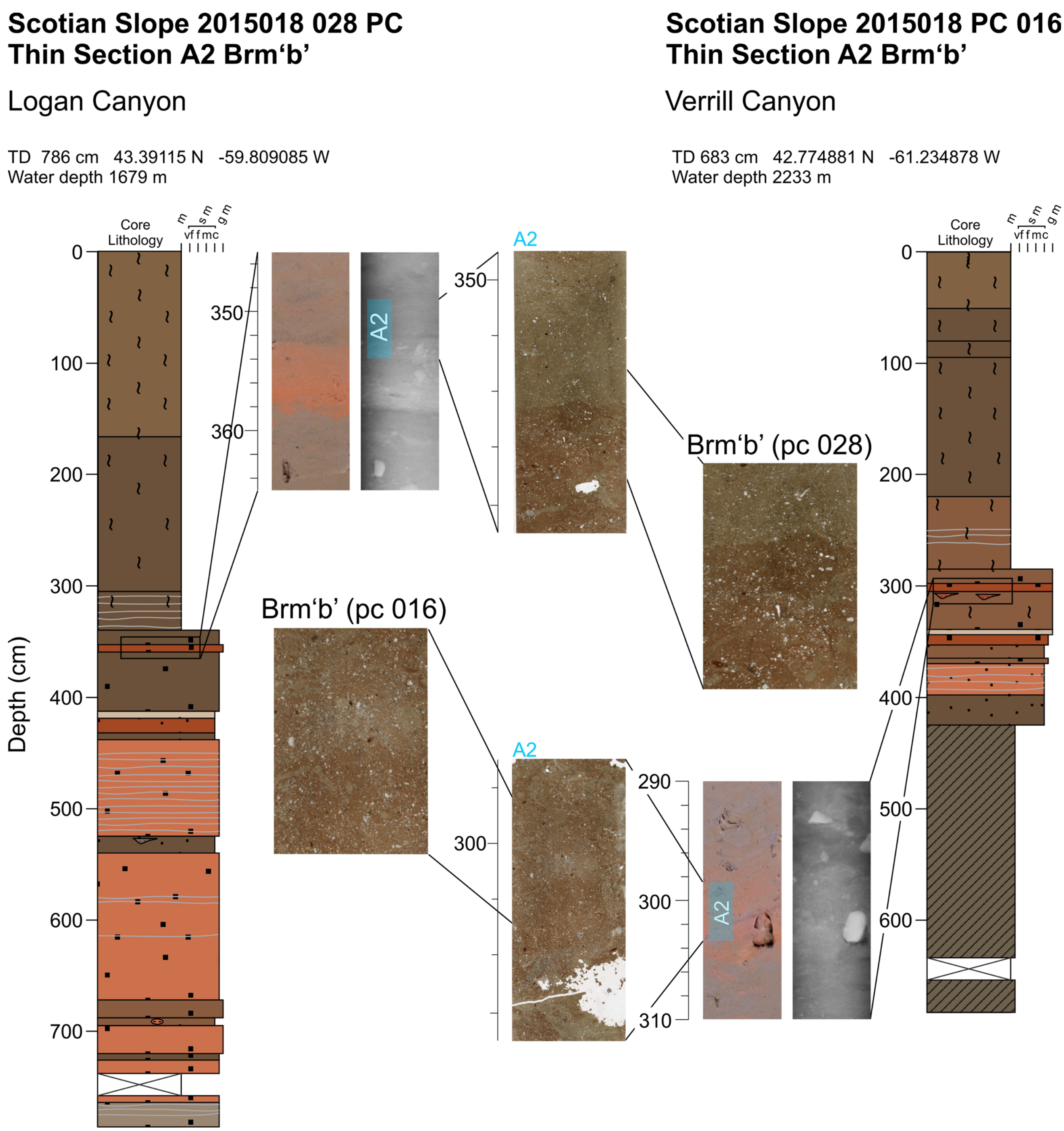

Figure 4.2. Brm‘b’ thin section comparison between Logan Canyon (piston core 2015018 028) and Verrill Canyon (piston core 2015018 016).